NONLINEAR OPTIMAL CONTROL OF INTERIOR PERMANENT MAGNET SYNCHRONOUS MOTORS FOR ELECTRIC VEHICLES

Merve ÖZTEKİN

A thesis submitted to the University of Warwick for

the degree of

Doctor of Philosophy in Engineering

Supervisors: Assoc. Prof Oleh KISELYCHNYK

Prof Jihong WANG

AUGUST 5, 2022

THE UNIVERSITY OF WARWICK
West Midlands, UK

NONLINEAR OPTIMAL CONTROL OF INTERIOR PERMANENT MAGNET SYNCHRONOUS MOTORS FOR ELECTRIC VEHICLES

A thesis submitted to the University of Warwick for the degree of

Doctor of Philosophy in Engineering

Merve ÖZTEKİN

Supervisors: Assoc. Prof Oleh KISELYCHNYK

Prof Jihong WANG

School of Engineering

Power and Control Systems Research Laboratory

The University of Warwick

August 2022

West Midlands-United Kingdom

NONLINEAR OPTIMAL CONTROL OF INTERIOR PERMANENT MAGNET SYNCHRONOUS MOTOR FOR ELECTRIC VEHICLES

ABSTRACT

At present time, research in the field of Electric Vehicles (EV) is significantly intensifying around the world due to the ambitious goals of many countries, including the UK, to prohibit the sale of new gasoline and diesel vehicles, as well as hybrid vehicles, in the near future around 2030-35. The primary goal of this Ph.D. research is to improve the propulsion system of electric vehicles' powertrains through improvements in the control of Interior Permanent Magnet Synchronous Motors (IPMSM), which are commonly used in EV applications. The proposed approaches are supported by simulations in Matlab, Matlab-Simulink and laboratory-based experiments.

The research initially proposes an analytical solution in implicit view for a combined Maximum Torque per Ampere (MTPA) and Maximum Efficiency (ME) control, allowing to determine the optimal d-axis current, based on the concept of minimisation of the fictitious electric power loss. With the exception of two parameters, the equation is identical to that of the ME control. Therefore, upgrading the ME control to the combined MTPA/ME control is relatively easy and doesn't require any change in hardware beyond a few minors of controller code in the software. The presented research demonstrates an easy-to-apply combined MTPA/ME control leading to the 'Transients Optimal and Energy-Efficient IPMSM Drive' providing smooth transitions to the MTPA control during transients and to the ME control during steady states.

A concept of 'Nonlinear Optimal Control of IPMSM Drives' is also introduced in this Ph.D. research. The velocity control loop develops nonlinearities when energy consumption optimisation methods like MTPA, ME, or combined MTPA/ME are added. In addition, the control system's parameters can be inaccurate and fluctuate depending on the operating point or possible uncertainties in real-time operation. In the proposed method, the control structure is the same as in the Field Oriented

Control (FOC), with the close velocity and two current loops, but the Proportional-Integral (PI) controllers are replaced by Nonlinear Optimal (NO) Controllers. The linear part of the controller is designed as a Linear Quadratic Regulator (LQR) with integral action for each loop separately. This is, in fact, a PI controller with optimal gain parameters for a specific operating point. The nonlinear part takes the required fluctuations of the control system's optimal gain parameters in real-time operation as new control actions to improve a robust control structure. The design procedure for the nonlinear part is similar to that of the LQR, but the criterion of A. Krasovsky's generalised work is used, and the analytical derivations lead to an explicit control solution for the nonlinear optimal part. The nonlinear part emulates the adjustments for updating the linear part's optimal LQR gains based on operating conditions, instead of employing extensive look-up tables or complicated estimation algorithms. The proposed control is robust in the allowed range of the system's parameters.

In conclusion, upgrading existing industrial IPMSM drives into a robust and optimal energy-efficient version that can be used for electric vehicle applications is the main advantage of the novel control concept described in this Ph.D. research. For this upgrade, only a small portion of the software that is related to the PI controllers needs to be changed; no new hardware is needed. Therefore, it is cost-effective and simple to transform existing industrial IPMSM drives into a better version with the proposed method. This feature also leads to the design of more adequate IPMSM drives to meet the demands of Electric Vehicle (EV) operating cycles.

Key Words: Interior Permanent Magnet Synchronous Motor, Field Oriented Control (FOC), Maximum Torque Per Ampere Control (MTPA), Maximum Efficiency Control (ME), combined MTPA/ME control, Linear Quadratic Regulator (LQR), Nonlinear Optimal Control, Optimal Control, Electric Vehicle (EV).

TABLE OF CONTENTS

LIST OF FIGURES

LIST OF TABLES

ABBREVIATIONS

EMF	Electromagnetic Force
EV	Electric Vehicle
FEM	Finite Element Analysis Method
FLC	Fuzzy Logic Controller
FOC	Field Oriented Control
IM	Induction Motor
IPMSM	Interior Permanent Magnet Synchronous Motor
LM	Loss Minimisation
LUT	Look-up Table
ME	Maximum Efficiency
MTPA	Maximum Torque Per Ampere
NO	Nonlinear Optimal
PWM	Pulse Width Modulation
RLS	Recursive Least Square Algorithm
SSFR	Standstill Frequency Response
VSD	Variable Speed Drive
ZDAC	Zero d-Axis Control

ACKNOWLEDGEMENTS

All of my efforts for this PhD research are dedicated to my very beloved ones that I lost within the last 5 years... I'm sure they'd be very proud of me if they knew I'd spent my time on such a worthwhile path…

I would like to express my gratitude to my supervisors *Assoc. Prof. Oleh KISELYCHNYK* and *Prof. Jihong WANG* for their endless patience and tremendous support in guiding my research path…

I would like to thank the Turkish Government for investing in those who work in such intellectual fields to advance the country's future through the "YLSL" Scholarship.

Yıkmak insanlara yapmak gibi kıymet mi verir?

Onu en çolpa herifler de emin ol becerir.

Sade sen gösteriver 'İşte budur kubbe diye'

İki ırgatla iner şimdi Süleymaniye!

Ama gel kaldıralım dendi mi, heyhat, o zaman

Bir Süleyman daha lazım yeniden bir de Sinan…

MEHMET AKIF ERSOY

Building requires qualification but destroying not

Of which even the most vulgar men are capable.

Take as an example the Great Mosque Süleymaniye,

Even just two hodmen can tear it all down!

But when it is needed to build it back again which is not that much easy

In fact, impossible…

Without such a magnificent as Suleyman and the architect like Sinan…

DECLARATION

I hereby declare that the material in this thesis has not been submitted for a higher degree at any other university. This thesis entirely contains research work carried out by Ms Merve ÖZTEKİN under the supervision of Associate Professor Oleh KISELYCHNYK and Professor Jihong WANG unless references are given.

Some parts of this thesis were included in the following publications:

M. Öztekin, O. Kiselychnyk and J. Wang, "Energy Efficient and Transients Optimal IPMSM Drive for Electric Vehicles," 2022 International Symposium on Power Electronics, Electrical Drives, Automation and Motion (SPEEDAM), 2022, pp. 832-837, doi: 10.1109/SPEEDAM53979.2022.9842114.

M. Öztekin, O. Kiselychnyk and J. Wang, "Nonlinear Optimal Control for Interior Permanent Magnet Synchronous Motor Drives," 2022 European Control Conference (ECC), 2022, pp. 590-595, doi: 10.23919/ECC55457.2022.9838314.

CHAPTER 1. INTRODUCTION

1.1. Background

The United Kingdom will outlaw the sale of new gasoline, diesel and hybrid vehicles by 2030 but only pure electric vehicles will be allowed for sales [1]. This goal motivates engineers and designers to continue improving electric vehicle technologies.

The propulsion system is the key component of electric vehicles, which is made up of electric motors, batteries, inverters, and controllers. At the moment, most electric vehicle propulsion systems use Interior Permanent Magnet Synchronous Motors (IPMSM) and squirrel cage Induction Motors (IM)[2]. The first has a higher power density and is easier to control due to its simpler dynamic mathematical description. The second may have been perceived as a better option because it is less expensive and more reliable (due to no magnet fixing required), and thus easier to protect (as no power generation occurs in case of any fault, related to a disconnected power supply while operating), only if it did not require a more complex control implementation due to its complicated dynamic mathematical description[3]. In conventional electric vehicle propulsion systems, the electric motor is fed by a DC power source (battery) through a power electronic converter, typically two-level full bridge inverter, which is driven by mostly Space Vector Pulse-Width-Modulation (PWM) signals [4]. In both cases (IPMSM or IM), a vector control algorithm is utilised to achieve either torque or velocity control targets.

For the IPMSMs, the vector control algorithm is designed in a rotating reference frame aligned with the rotor permanent magnet flux. For the induction motor, there are a lot of choices including the classical one with the reference frame alignment with the rotor flux linkage vector. As the two-phased rotating reference frame transformation (with Park Clarke transform) provides a less complex mathematical description of AC motors that is identical to applications for DC motors, vector control is preferred over alternative control methods[3], [4]. As a result, all control methods for controlling DC motors can be effectively used for ones of AC motors via vector control designs. However, there is still room for advancement in this research area due to the challenges in high-performance dynamic control of the velocity and the torque in presence of disturbances coming from vehicle side and the optimisation of energy consumption. This PhD study focuses on identifying control challenges of IPMSM drives, suggesting new control design approaches and their validation. The study is based on the two innovative approaches described below:

1. The majority of industrial IPMSM drive applications use the most basic energy-efficient control algorithm: the Zero D-Axis Current (ZDAC) control [4]. It makes the motor torque proportional to the q axis current and allows for a simple control implementation similar to DC motor control because the system is linear in the case of constant parameters. However, it is not a solution for optimising energy efficiency or providing fast torque response. Another widely used energy-efficient control solution is Maximum Torque Per Ampere (MTPA) control [5]. It allows to maximise the motor torque for a given motor current (or to minimise the motor current for a given torque). Thus, the fastest torque response is achieved. It also provides more efficient real-time operation than ZDAC control because the copper loss is inherently minimised; however, it introduces nonlinearity into the velocity loop because the optimal

relationship between the d and q axis currents is nonlinear. It has the benefit of being based on an explicit equation (no real-time iterative solutions of nonlinear equations are necessary) which includes typical IPMSM parameters (stator resistance, d and q axis inductances and permanent magnet flux). Maximum efficiency (ME) control is the last but not least energy efficient control solution [6]. It can be used to create a more energy-efficient control algorithm by minimizing total electric loss. The disadvantage is that it requires precise knowledge and modelling of the core loss. Although the approach is well presented in the research literature, it is not widely used in industrial AC drives to the best of our knowledge.

It is a constant dilemma to decide between the MTPA and the ME control solution for control designers [7]. Some recent studies suggest some switching algorithms for alternating between them based on the operating circumstances, such as using the MTPA during transients and the ME during steady states. However, additional transients are introduced by this switching algorithm. In this PhD research a new optimal energy-efficient control solution based on the concept of the fictitious electric power loss which consists of the copper loss and a fraction of the core (iron) loss is proposed [8]. The minimisation procedure is the same as for the ME approach and it yields the identical nonlinear implicit equation from which the optimal d-axis current is determined in real time. The aforementioned fraction of the core loss, called β parameter, appears in the equation in only two places. If β=0, then the MTPA is realised. If β=1, then the ME is realised. The value of β between 0 and 1 provides the optimal currents curve in-between the MTPA and ME approaches. Therefore, the method is called combined MTPA/ME control. In this case, the dilemma of which strategy to choose has been superseded by the problem of β parameter optimisation. In this PhD study, the combined MTPA/ME method is based on the iterative solution of

just one optimal equation, is applied in a very straightforward manner to create "the Transients Optimal and Energy Efficient IPMSM Drive," which provides MTPA control during transients and ME control during steady states without switching.

2. Industrial vector controlled IPMSM drives are usually implemented through Field Oriented Control (FOC), based on three close control loops: an external velocity loop with PI velocity controller and two internal d- and q-axis currents loops with PI current controllers. In ideal circumstances, the controller parameters are determined for a specific operating point and specific motor parameters. However, in real time operation, motor parameters variate due to any type of uncertainties [3]. Further to that, for variable velocity applications like electric vehicles, there is an infinite number of operating points. In addition, even (for example) the number of passengers in the vehicle effects control characteristics like the parameter of moment of inertia. The motor inductance parameters also variate with different motor loading due to magnetic saturation.

The proposed strategy is based on replacing three PI controllers with more sophisticated self-adjusting ones (referred to as Nonlinear Optimal (NO) Controllers in this study) in the exact same control structure (FOC) [9]. Thus, the effects of uncertainties in real-time operation like inaccurate motor parameter identification, motor parameter variations, or any nonlinearities brought on by optimal energy-efficient strategies are all eliminated to ensure precise torque control. The NO controllers, are designed based on the optimal control theory, consist of linear and nonlinear parts. The linear part for each control loop is designed independently using standard Linear Quadratic Regulators (LQR) with integral action for a specific operating point [10], [11] . The deviations in LQR controller’s gain parameters are then regarded as new control actions for the nonlinear part. A procedure similar to

LQR design is used for the nonlinear part, but this time with the criterion of A. Krasovskiy's generalised work. This process produces an explicit optimal control solution for the nonlinear part. In other words, the nonlinear parts do not require the LQR controller parameters to be modified in response to operating circumstances.

As a result, the Nonlinear Optimal Controller is a PI controller with optimal gains that also includes a nonlinear optimal component. It eliminates the need for extensive look-up tables or complicated estimation algorithms to adjust the LQR controllers for multiple operating points. No hardware changes are required to upgrade the industrial IPMSM drives; only the software directly related to the PI controllers must be updated. The proposed control is robust in the allowed range of the system's parameters and eliminates any uncertainties like parameter variations in the real time operation or the nonlinearities introduced by optimal energy-efficient algorithms.

1.2. Research Objectives and Methodology

The aforementioned goals of this PhD research are summarised belove:

The following objectives will be attained in order to reach the goals:

- Literature review of existing approaches for dynamic IPMSM velocity and torque control strategies including parameter identification methods, and also for optimal energy-efficient strategies.
- Development of the Matlab/Simulink models for simulation of the zero D-axis current control, MTPA control and ME control for IPMSM, in Field Oriented Control (FOC) with three PI controllers, for benchmarking with the new suggested approaches.

- Analytical derivations for the combined MTPA/ME control leading to the new optimal energy-efficient equation identical to the ME approach.
- Application of the combined MTPA/ME algorithm into existing FOC structure for designing 'The Transients Optimal and Energy Efficient IPMSM drive'.
- Development of the Matlab/Simulink models for the combined MTPA/ME approach and for 'transients optimal and energy efficient drive'. Comparison of the simulation results with existing approaches.
- Analytical redesign of the controllers with LQR gain parameters for all three loops in FOC structure of IPMSM drive, including the linearisation of the loops.
- Analytical design of the Nonlinear Optimal Controllers based on LQR design procedure combined with the criterion of the generalised work of A. Krasovskiy.
- Development of the Matlab/Simulink models with Nonlinear Optimal Controllers for zero D-axis current, MTPA, ME and combined MTPA/ME approaches. Comparison of the simulation results with the corresponding systems with PI controllers.
- Learning of the hardware and software of the existing test-rig and the real-time Hardware-In the Loop simulators, dSpace DS1104 and OPAL RT OP5600 for rapid control prototyping. Developing a procedure for safe testing and data recording.
- Laboratory-based experimental testing of some of the existing and suggested approaches.

Regarding the research objectives the research methodology is shaped as in Figure 1.1. An extensive literature review was completed in the first place. Dynamic

mathematical modelling of IPMSM, FOC structure with ZDAC control approach were analysed and the observations on the lab-based test rig were completed. The next level of the Ph.D. study consists of four steps, targeting to propose the transients optimal energy-efficient control method, inspired by existing MTPA and ME control methods. It is followed by another four-step level for the nonlinear optimal control approach for enhancing the robustness of the existing FOC structure of IPMSM drives.

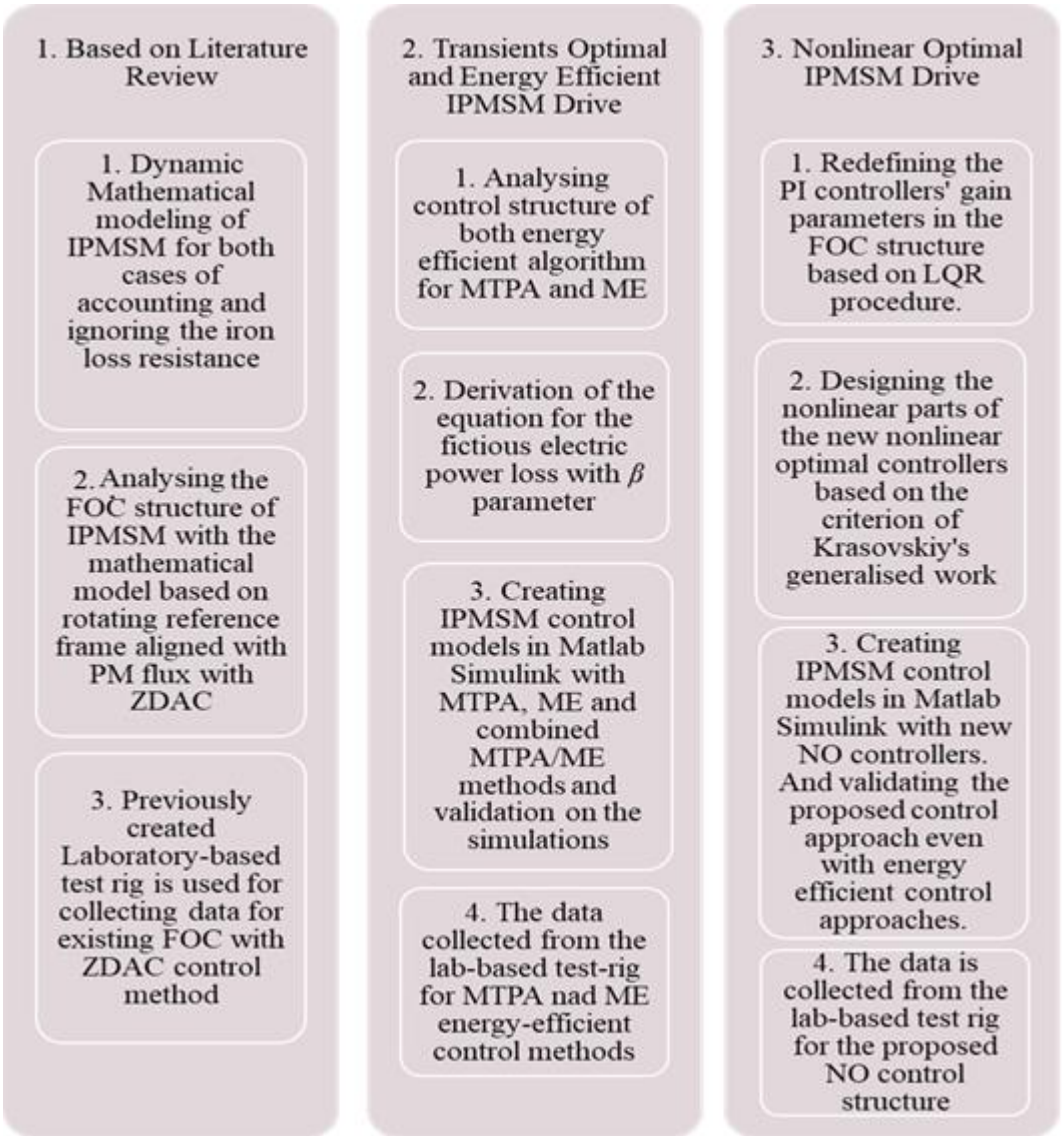

Figure 1.1 The Research Methodology

1.3. Novelty and Practical Value

The nonlinear optimal control methodology was developed allowing to keep the standard control structure used in industry and to cope with the nonlinearities of energy consumption optimisation algorithms, inaccuracy and varying of parameters by simple replacement of the PI controllers by the Nonlinear Optimal Controllers. Practical engineers do not need to have knowledge in optimal control theory since the replacement is straightforward and all parameters are computed using explicit equations. No hardware change is required. Only a piece of software related to the PI controllers needs to be modified.

The nonlinear optimal implicit equation for implementation of the combined MTPA/ME approach allows very easy to upgrade ME systems to the combined MTPA/ME systems. No hardware change is required. Only a piece of software related to the ME code must be modified. The proposed methodology is convenient for implementation of the 'transients optimal and energy efficient drive' and the algorithm execution time will be close to the ME approach since the optimal nonlinear equations to be solved in real time iteratively are identical except two parameters.

1.4. Structure

Chapter 1 *Introduction* is provided for the main motivation, challenges and outlines, explains the objective and followed methodology during whole PhD duration

Chapter 2 *Literature Review* The background of IPMSM drives, existing energy efficient and robust control approaches are explained.

Chapter 3 The design procedure behind *The Transients Optimal and Energy Efficient IPMSM Drive* is introduced, the method is verified via simulation results. The practical use of new energy efficient algorithm in EVs is explained.

Chapter 4 *Nonlinear Optimal Control Design for IPMSM Drive* is introduced. The standard IPMSM control structure (FOC) is redesigned via replacing the PI controllers with Nonlinear Optimal Controllers. The method is supported with simulation results. It is explained how the robustness of the conventional IPMSM drives is enhanced.

Chapter 5 *Verification of Energy Efficient Nonlinear Optimal Control for IPMSM Drives.* The proposed methods in chapter 3 and 4 are verified on a laboratory-based test-rig.

Chapter 6 *Conclusions* The outcomes of the PhD study are discussed, and foreseen future works are explained.

1.5. Publications

M. Oztekin, O. Kiselychnyk, and J. Wang, “Energy Efficient and Transients Optimal IPMSM Drive for Electric Vehicles,” in 2022 International Symposium on Power Electronics, Electrical Drives, Automation and Motion (SPEEDAM), Jun. 2022, pp. 832–837. doi: 10.1109/SPEEDAM53979.2022.9842114

M. Öztekin, O. Kiselychnyk and J. Wang, "Nonlinear Optimal Control for Interior Permanent Magnet Synchronous Motor Drives," 2022 European Control Conference (ECC), 2022, pp. 590-595, doi: 10.23919/ECC55457.2022.9838314.

The papers are attached in Appendix J.

CHAPTER 2. LITERATURE REVIEW

2.1. Interior Permanent Magnet Synchronous Motors (IPMSMs)

The concept of replacing excitation windings with permanent magnets first appeared in AC machines in the 1950s [3]. The cost of the rotor magnets in a hybrid electric vehicle -Prius 09, produced in 2012- is announced as 81% of all material cost used for the motor [12]. However, by excluding rotor current/windings, operational costs were reduced; less operation heat resulted in less stator current, and thus less copper loss. Overall cost analysis [4] shows that PM motors are more cost effective than their competitors.

There is no doubt that rotor winding exclusion leads to more compact motor designs. Compactness raises power density (power/weight), and thus torque to inertia ratio, resulting in better acceleration and peak torque performance. PM rotor designs offer constant excitation, allowing for the design of less complex braking systems than those for induction motors [13]–[15].

In the constant torque region, PM motors inherently attain high torque to ampere performance; nevertheless, the robustness of their performance is parameter-dependent, particularly beyond base speed. Cogging torque is produced by position-dependent torque response, which does not occur in induction motors [16], [17].

In terms of magnet location in the rotor, Permanent Magnet Synchronous Motors

(PMSM) are divided into Surface Mounted Permanent Magnet Synchronous Motors (SPMSM) and Interior Permanent Magnet Synchronous Motors (IPMSM). In SPMSM, magnets are adhered to the rotor surface and can be projected from the outside. The magnets in the IPMSM case are buried into the rotor, resulting in improved physical robustness in high-speed ranges and reluctance torque contribution to torque capability [18]–[20].

The investigation on efficiency maps created with Finite Element Analysis (FEA) in [20] reveals that IPMSM achieves less iron loss at high-speed levels, making it more efficient, whereas SPMSM achieves slightly higher peak torque due to less airgap flux linkage.

2.2. The Control Concept of IPMSM Drives

A typical converter-fed AC motor drive for electric vehicle applications is built around five main components, as shown in Figure 2.1.An IPMSM, for example, can be powered by a battery (a DC voltage source) via a three-phase, current-controlled Voltage-Sourced Inverter (VSI) led by Pulse Width Modulation (PWM) gate signals generated by a controller unit, the input signals of which are current and position feedback signals sampled from the IPMSM by sensors [3], [4], [19]

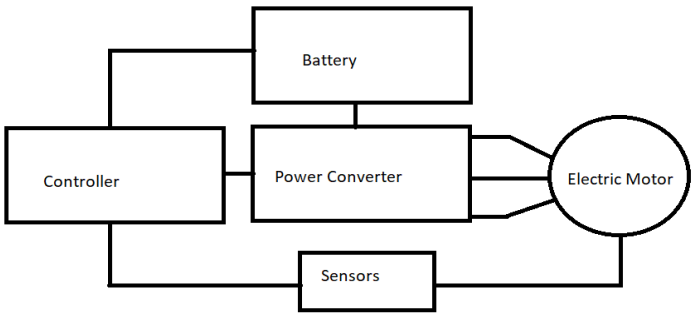

Figure 2.1 Typical Structure of a Converter-fed AC Motor Drive in Electric Vehicle Applications

A DC motor drive is controlled by two separate and independent DC currents called field current (flux-producing current) and armature current (electromagnetic torque producing current). However, because the armature current includes both air-gap flux and torque producing components, designing such a simple, linear, dynamic control for AC motor drives necessitates a reference frame transformation with the chosen control scheme. In order to convert any n-phase motor variable into an equivalent, orthogonal, two-phased, stationary reference frame, the Clarke transform is used. In order to eliminate position dependent components of the motor parameters, Park Transform, likewise, expresses motor variables in a two-phased reference frame, but this time, synchronously rotating with the electrical rotor speed [3], [4].

Due to the difficulty of separate and dynamic control of flux and electromagnetic torque producing currents, scalar control schemes are rarely used for IPMSM drives [3]. Field Oriented Control (FOC) and Direct Torque Control (DTC) are two vector control schemes that address the dynamic current control issue by processing an equivalent stator current phasor rather than the current amplitude, which is produced through a reference frame transformation using the input signals from the current and position sensors[3], [4].

Physical limitations such as maximum DC voltage of the converter, maximum phase current capability of the motor isolation material, air gap flux capability, and so on influence motor torque and velocity response, as illustrated symbolically in Figure 2.2. If the air-gap flux is kept constant as in the constant torque region, the DC voltage amplitude appears higher than inverter capability beyond the base speed. To maintain the velocity increase that reduces torque capability, flux-weakening operation is employed. However, once the critical speed is reached, both the current and the voltage

go over their safe limits. As a result, the power and flux are reduced to prevent the device from physical harm like PM demagnetization. Combining control algorithms for various velocity regions results in the creation of high performance IPMSM drives. As in [21], (energy efficient algorithm for constant torque region + flux weakening algorithm for constant power region).

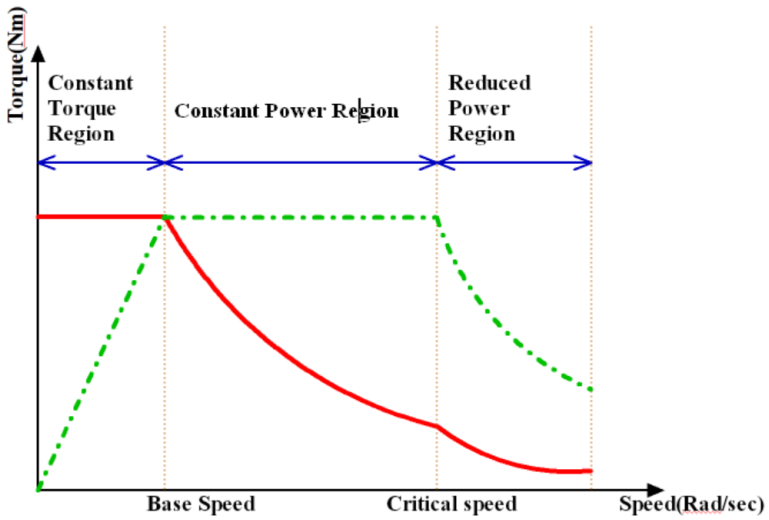

Figure 2.2 Symbolic Torque-Speed Characteristics of an electric motor [22]

2.3. Energy Efficient Control Strategies for IPMSMs

As the motor operates within its physical constraints, optimal performance goals are targeted in the constant torque region (below the base speed). As a result, energy-efficient control strategies are proposed to achieve various control goals [4].

Zero D-Axis Current Control (ZDAC - Constant torque angle control) is a straightforward, linear control algorithm which resembles DC motor control. It is the traditional control strategy that is primarily used in industrial AC motor driving applications, is used as a reference control approach to compare the novel control approaches [23]–[25]. The ZDAC control goal is to devote the entire stator current phasor to torque production, leaving only the magnet flux for excitation flux. It is

technically possible if the torque angle δ_r is set to 0° (Symbolic phasor diagram is demonstrated in Figure 2.3- d-axis current is zero in ZDAC control). Thus, a fast, simple, and linear AC motor control similar to DC motor control is possible, and irreversible demagnetisation of PMs is avoided. However, the reluctance torque caused by saliency is eliminated, so it does not fully utilize the torque capability of the IPMSM [3], [4], [23].

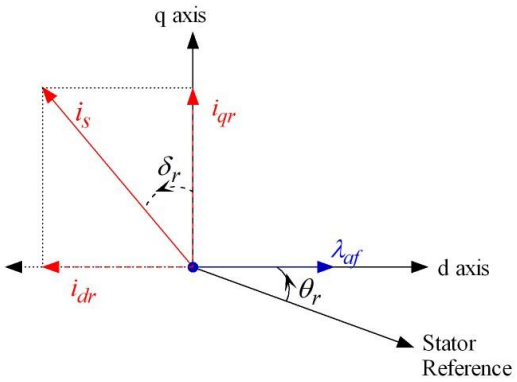

Figure 2.3 Phasor diagram of two reaction model [3]

Maximum Torque Per Ampere (MTPA) Control Approach

After it was determined that the ZDAC control strategy is the simplest but not the best control strategy for IPMSM in terms of performance measures, it was investigated which factors might influence torque production, energy efficiency, and power quality.

It is demonstrated in [23] that d, q-axis inductances, and saliency (the inherent difference in d, q-axis inductance due to the magnet configuration in the rotor) have a reluctance effect on torque production, which is referred to as reluctance torque. For the same speed and current amplitude, the motor with higher inductance and saliency has a higher torque response. It is also stated that inductance has an additive effect on magnetisation, reducing the torque response to current control. As a result, magnetic saturation should be considered while selecting a motor for a specific application. Another extensive analysis [26] revealed the relationship between torque capability

with saliency and magnet flux proportion in variable speed drive applications. Due to voltage constraints, the torque response drops to zero at around five times higher speed ranges. It is claimed that by maintaining a certain level of saliency and magnet flux proportion, the torque capability could be extended to infinite speeds. However, as the speed range is extended, the torque response at low-speed levels decreases. As a result, the proportion of the saliency and magnet flux should be optimised in relation to the application's targeted speed range. Figure 2.4 provides an illustration of the saliency effect on torque capability across torque angle at the rated current amplitude. (Compiled using the simulation in Appendix A and prepared in light of [23]).

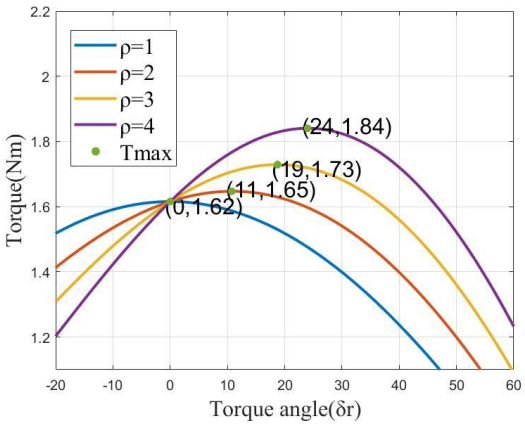

$T_{rated} = 1.67N$
$I_{rated} = 5A$
$\omega_{rated} = 2000$
$V_{rated} = 97V$
$R_s = 0.57\Omega$
$L_d = 8.72mH$
$\rho = L_q / L_d$
$\lambda_{af} = 0.1077Wb$
$n_p = 2$

Figure 2.4 Torque variation over torque angle regarding different saliency

In the paper, it is also given that the synchronous torque is greatest at a torque angle of 0° and the reluctance torque is greatest at 45° in any case, it is concluded in [27] that the maximum total torque can be obtained between these two angles ($0^\circ \le \delta_r \le 45^\circ$). Maximum torque response is also expressed as a function of torque angle δ_r. It is attained by partial derivative of total torque with respect to torque angle equals zero. According to the evaluations in the paper, the MTPA control helps to widen speed capability as it decreases the terminal voltage compared with ZDAC

control and the power factor is increased inherently as the current phasor converges to voltage phasor. Besides, a faster speed response is obtained in comparison with ZDAC control.

The same authors introduce the relationship between maximum torque and d axis current in [5] by equating the partial derivative of the torque equation to zero, but this time with respect to d-axis current. The MTPA control trajectory is introduced in the d, q-axes reference frame, as shown in Figure 2.5, and is obtained by using their equation in conjunction with the simulation in Appendix 2. With this advancement, real-time MTPA control is now possible. A feed-forward voltage compensator is also introduced in the same study in order to remove the cross-coupling effect of the d

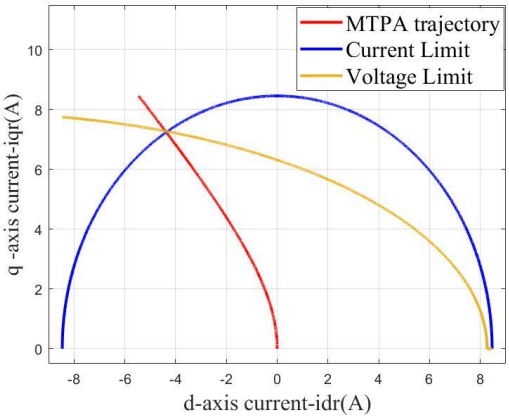

$T_{rated} = 1.67N$
$I_{\max} = 8.46A$
$\omega_{base} = 2400$
$V_{\max} = 50V$
$R_s = 0.57\Omega$
$L_d = 8.72mH$
$L_q = 22.78mH$
$\lambda_{af} = 0.1077Wb$
$n_p = 2$

Figure 2.5 Maximum Torque per Ampere (MTPA) trajectory on d, q-axes plane

and q-axis currents in the voltage equations illustrated in Figure 2.6. As in the ZDAC control strategy, the compensator decouples the flux and torque producing currents. An algorithm is proposed in [28] to achieve an accurate MTPA trajectory in the full speed range.

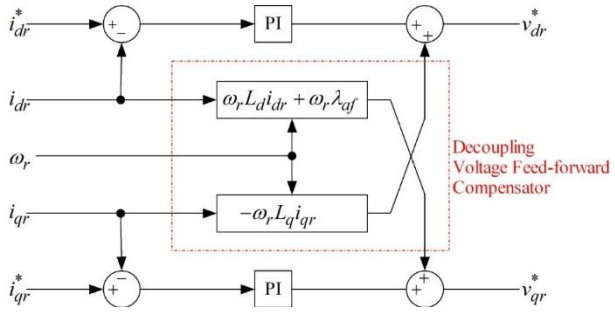

Figure 2.6 Decoupling Voltage Feed-forward Compensation for IPMSM Drives

Maximum Efficiency (ME-Loss Minimization) Control Approach

The losses, appear in IPMSM operation, are initially classified into two groups: electrical loss and mechanical loss. The mechanical loss is not controllable with electrical variables. However, the electrical losses are controllable and subdivided into three groups: copper loss, core loss and stray loss.

To maximize torque response for a specific current amplitude is the goal of MTPA control. From another angle, it reduces the stator current vector's amplitude for a specific torque demand. The copper loss is directly proportional to the square of the stator current. However, for high torque and high-speed operation, the core loss becomes larger than that of the copper loss, which indicates the efficiency will decline for high speed, high torque operation. The researchers discover a more effective method for decreasing overall power loss as a result of this variance in performance.

Efficiency maps (Loss Contour plots) are examined in [29] to determine "the best optimum operating position" for a given torque demand without saliency effect in constant power operation without voltage and frequency limits. The torque response typically declines while the velocity square (ω^2) grows in constant power operation. As a result, the stator current amplitude and, by extension, the copper loss, and the core loss are proportional to the velocity square. According to the paper, the copper

loss and core loss were eventually expected to be equal, and the total loss was minimized at the optimum speed. In light of this concept, the ratio of copper loss resistance to iron loss resistance (R_s / R_c) is defined as the 'loss parameter,' and efficiency maps are generated. However, because of great deal of the neglection and assumptions made, these efficiency maps can only contour the motor efficiency roughly, therefore, are useful for scalar control but not for precise torque control. (For instance, the efficiency diverges from these maps for motors with a higher Ld.) The core losses are caused by the eddy current and hysteresis effects, which are represented as a core resistance R_c in the IPMSM equivalent circuit.

Instead of offline efficiency maps, online numerical solutions for real-time operation are investigated in time. The total electric power loss regarding the core, copper and stray losses, is identified as a function of the speed, torque, d, q-axis current and saliency as in [30]. Similar to traditional MTPA control algorithm, this time the relationship between the minimum power loss point and d-axis current is identified by the derivative of overall electrical loss (W_E) with respect to d-axis current (i_{dr}) equal zero ($\partial W_E / \partial i_{dr} = 0$). As the derivative equation is a fourth-order function, polynomial fitting methods are proposed in [6] and [31] in the shape of $AB = T_e^2 C$ and $XT_e^2 + YT_e + Z = 0$, respectively, to simplify real time calculations and As a results, the total electrical loss (W_E) is identified as a function of the electromagnetic torque (T_e), the angular velocity (ω_r) and d-axis current (i_{dr}) $W_E = f(i_{dr}, \omega_r, T_e)$. the loss minimisation trajectory is introduced on d, q axes plane as in figure. Bernal et al proposed another solution for simplifying the fourth-order function in [32], [33]. They investigated copper and core losses, separately for IPMSMs, and claimed that the

minimum total loss point should be in between that of core and copper losses, called partial minima demonstrated in Figure 2.7 . In this approach, a weighting factor for motor parameters is identified. Cao suggested an online and iterative solution called Golden Section Method in [34] to find minimum loss point for a specific torque and speed operation with respect to the torque angle. Another iterative approach in [35] based on Newton's iteration method is explained and employed as an analytical solution of the fourth order equation.

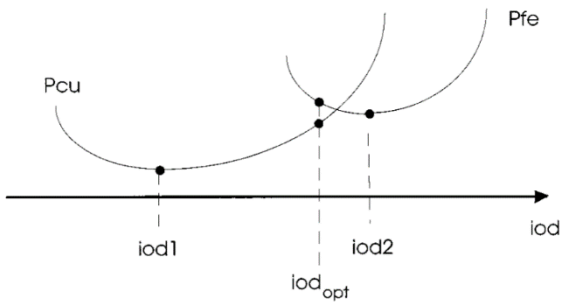

Figure 2.7 Explanation of partial minima

Comparison of MTPA and ME control methods and combined strategies

The efficiency of MTPA and ME control strategies for variable speed drives is compared in [36]. The MTPA and ME trajectories on the d, q axes current plane are generated by using FEM-based efficiency maps for copper loss, core loss, inverter loss, and PM loss. The performances of two methods are compared using standard electric vehicle drive cycle inputs. The results show that the loss minimization algorithm is around 10% more efficient than the MTPA control algorithm for high-speed low torque operation. Similar results demonstrating that the loss minimization (ME) algorithm outperforms MTPA are obtained in [37], [38] via simulations created with the fourth order loss minimization equation.

A fuzzy set with speed and torque error as fuzzy state variables is established in [38]. Seven overlapping fuzzy sets are created to categorize the fuzzy state variables. The predefined control variables, such as field current and estimated airgap-flux, are stored in a look-up table based on the combinations of the state variables.

Khan et al. introduced a combined energy efficient algorithm for IPMSM drives in [39]. The algorithm is built into a FOC scheme that follows the MTPA trajectory during transient operation and shifts to the ME trajectory during steady-state operation based on instantaneous angular speed error and estimated DC power. Similar combined method with the suggestions of ME in steady state operation and MTPA control in transient operation are put out in [40]. Both studies use speed error as a decision variable for the shift between two methods, but this one includes a switch in the middle, which introduces additional transients. Another comprehensive combined loss minimization strategy, known as the Gopinath-style loss minimizing method, is suggested in [41] regarding the efficacy fluctuations. The top and bottom margins of the proposed Loss minimisation control (LMC) method are assumed to be the traditional MTPA and ME trajectories on the d, q axis current reference frame. A cost function based on the error of a flux observer determines the instantaneous operation point. Another approach is suggested in [7], which uses a parameter to smoothly combine two methods. In terms of their solution, the MTPA control is active in low torque operation, while the ME method is active in high torque operation. The actual measured torque and rated torque are defined in [0,1].

2.4. Robust IPMSM Drive Solutions

The aforementioned strategies are developed under the assumption that the motor parameters are constant and that all disturbances are ignored. In real-time operation,

however, the motor parameters vary depending on environmental factors such as mostly temperature, magnetic saturation, cross saturation and also pressure, moisture, the aging factor and so on. Most control approaches also assume that the motor's three phases are distributed to produce sinusoidal magnetic flux and that the PM flux is also sinusoidal, but this is not the case precisely. Furthermore, electromagnetic harmonics can appear as a result of winding slots or converter nonlinearities. They are sources of torque pulsations and reduce the control method's accuracy [19].

Look-up Table (LUT) based solutions

Look-up Table (LUT) solutions are utilized to boost the precise control quality, particularly in industrial applications, to produce more robust real-time operation of IPMSM drive. In order to use them in real-time control algorithms, several studies suggested storing MTPA trajectory [42]–[48], ME trajectory [49], [50], or motor parameters [51]–[53] into LUTs.

The conventional MTPA control is expanded into the flux weakening region in [42], [43] by using two LUT in the d-axis current control loop to avoid real time analytical calculations to find the real time MTPA operation point. It is claimed that EVs can obtain a faster torque response with this framework. A similar strategy is used in [44]. For the purpose of illustrating the effects of motor constraints on the MTPA control trajectory, the entire operating region is separated into constant torque, flux weakening 1 and flux weakening 2. The conventional MTPA trajectory is implemented in a FOC-controlled IPMSM drive, and a voltage regulator updates the d-axis current reference in accordance with an LUT created regarding all three control regions.

A high-performance IPMSM drive for an electric scooter is created in [45]. First, using offline Finite Element Analysis (FEM) and experimental investigations, the typical

MTPA control trajectory in the d, q axes reference frame is derived. This trajectory is then expanded to include the flux weakening region. After that, a look-up table is created and utilized to store the MTPA trajectory for usage in real-time operations. As a result, magnetic saturation-related motor nonlinearities are reduced., A similar MTPA control design with LUT for IPMSM drives is recommended in [46] this time considering magnetic saturation and cross coupling as well. The experimental data gained through numerous constant velocity operations and offline calculations utilizing the Lagrange multiplier approach is used to update the standard MTPA trajectory, are saved into the LUT. Using a PI controller as a feed forward solution, the disparity between the d axis current in real-time operation and in the LUT is eliminated.

Kang et al. investigated the temperature dependence of magnetic saturation in IPMSM for Hybrid EVs in [47]. An LUT with temperature dependent stator current phasor data for MTPA control is embedded in a real time torque control scheme. Cao et al. investigated the MTPA trajectory using offline experimental tests for a wide load range to observe the effects of magnetic saturation, d-, q-axis inductance variations, and iron loss variations on the trajectory in [48]. The same author used the same procedure in [49] to create the maximum efficiency control trajectory for IPMSM drives. Both data were saved into LUTs and then incorporated into the d-axis current loop of the conventional FOC control of IPMSM in an electric motorcycle. [50] investigates the same goal, creating an LUT for maximum efficiency trajectory, but this time a more extensive investigation of cross saturation and iron loss variation is carried out. LUT for stator current phasor is created and implemented into FOC controlled IPMSM drive based on offline finite element analysis calculations.

Extensive research on the MTPA trajectory is done in [51]. When the flux weakening region is considered, the fourth order polynomial function turns into a complex construction. A large bulky look-up table solution with the magnetic saturation effect may result in slow torque response for EV applications. Therefore, it is suggested that the MTPA trajectory is calculated online using Ferrari's method, and the magnetic saturation effect is implemented using 3-D LUTs (on d- and q-axis currents and Torque plane) for d- and q-axis inductances. Another MTPA control method with a similar strategy for a wide velocity range is proposed in [52], [53]. Finite element analysis is used to create LUTs for d-, q-axis inductances and PM flux linkage (on 2-D d, q-axis currents plane) that are then implemented into the control algorithm via torque and flux regulators.

Additionally, LUT solutions are employed to reduce torque ripple [54] brought on by inverter nonlinearities, torque harmonics, etc. The real-time AC component of the q-axis current is regulated with a repetitive control block with the correct AC component q-axis current data fed by LUT in order to reduce torque ripple.

LUT solutions are useful for shortening online calculation times. However, because of the size of the LUT, real-time control processing becomes cumbersome. Furthermore, significant engineering time is required for a large number of offline experiments or pre-calculations to generate the LUT data [55]. Despite considerable engineering effort, each LUT is unique for a specific motor; that is, another LUT should be created for a different motor even if the same control method is used.

Parameter Identification Methods

LUT solutions for precise control, as previously stated, are frequently employed in industrial applications to eliminate uncertainties that arise during real-time operation. Determining precise motor parameters in real-time operation is a research area that addresses some of these uncertainties and has caught the attention of the motor control research community.

The International Electrotechnical Commission -IEC- [56] and the Institute of Electrical and Electronics Engineers-IEEE- [57], [58]. introduced testing standards to identify synchronous machine parameters through measurements with the intention of improving the robustness of synchronous motor drives. Additionally, a number of offline parameter identification methods for SMs based on observed data through current, voltage measurements are assessed. These methods include the dc-decay test [59], [60], load rejection test [61]–[63], Standstill Frequency Response Test (SSFR) [64], [65], and others.

The nonlinear magnetic behaviour of IPMSMs is investigated [66], [67], in which the flux versus current characteristics are well established in Figure 2.8. The blue line in Figure 2.8a indicates the PM flux linkage regarding rotor position may lead to magnetic saturation. Additionally, the red lines in both Figure 2.8a and b represent cross saturation effect on both d, q-axis flux linkages. Due to this nonlinear magnetic behaviour, it is clear that the magnetic saturation and cross saturation cause variations in d, q-axis inductances. Therefore, it is concluded that the d, q-axis inductances are stator current and rotor position dependant.

a.)

b.)

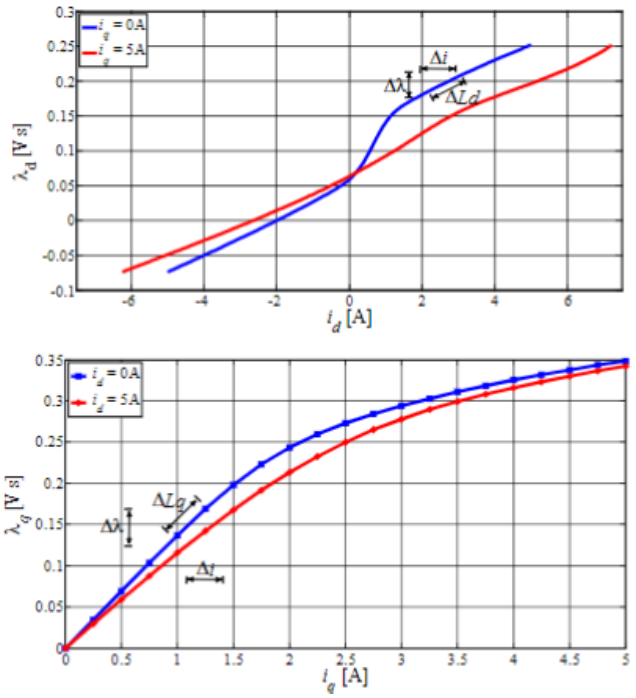

Figure 2.8 a.) d-axis b.) q-axis flux to current characteristics [67]

d, q-axis inductance variations of IPMSM due to magnetic saturation and cross coupling effect is also evaluated in [68]–[77]. The conventional IPMSM model is updated regarding magnetic saturation and cross coupling effect in [68] using offline maps created with Finite Element Analysis Method (FEM) and locked rotor magnetic flux observations. The method is for standstill parameter identification. Another experimental research is presented in [69] in order to determine the d, q axis impedances for high-speed, flux weakening operation. The paper demonstrates the variation of d, q-axis impedances to the torque angle for various velocity values. The research reveals that assuming d axis inductance as a constant does not result in an accurate control, especially for high-speed flux weakening operation. Because the reluctance torque cannot be fully utilised. El-Serafi et all compared four different analytical methods for both cross-coupling effect [70] and magnetic saturation [71]. The methods are based on calculation intermediate axis saturation [70] and q-axis

saturation characteristics [71] obtained via measured d-axis characteristics. A nonlinear IPMSM model is suggested to fully map the characteristics of magnetic saturation phenomenon in wide speed range and load conditions in [72]. Regarding d, q-axis inductances variate in high saturation levels, another nonlinear IPMSM model, consisting of dynamic and static components is introduced in [73]. The method suggests a d-axis equivalent circuit including a new K parameter representing q axis saturation into the conventional IPMSM model. Effects of magnetic saturation on sensorless control investigated in [74] and [75]. As the ill-defined inductance parameters worsens the accuracy of the IPMSM control, a q-axis inductance compensator is suggested for enhancing precise control quality especially in flux-weakening region to include magnetic saturation effect into the conventional control scheme [76], [77]. It is also stated that the effects of magnetic saturation due to armature reaction is more dominant in IPMSM as the effective airgap is shorter than that of other motors. q-axis inductance, particularly, varies depending on q axis current. Even a linear characteristic definition for q-axis inductance may lead the terminal voltage to exceed its available maximum value. Therefore, transient responses become unstable in the flux weakening region. In proposed method, q-axis inductance is modelled as a function of q-axis current. In [78], another d, q-axis compensator (self-commissioning method) is proposed to eliminate inverter nonlinearities while mapping the d, q- inductance variations. The method is for offline standstill parameter identification, the copper loss resistance is also identified with linear regression method.

The core loss resistance is assumed to be constant in conventional mathematical IPMSM model, however it variates in real time operation, which is evaluated in [79]–[81]. It is commonly calculated by subtracting mechanical loss from total no load loss.

In [79], it is shown that the core loss is linear proportional to the square of velocity-electromagnetic flux linkage product ($\omega^2\left(\lambda_d^2+\lambda_q^2\right)$). Therefore, the iron loss resistance has an almost linear proportional relation with velocity, test results shown in Figure 2.9. However, the exact relation can be worsening due to the copper loss resistance variation.

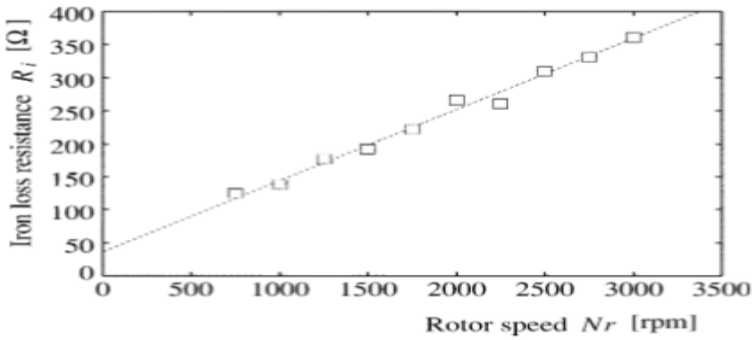

Figure 2.9 Iron Loss Resistance versus Rotor Speed [79]

In [80], it is proved that an extra core loss component appears when d axis current is different from zero. Therefore, the core loss resistance cannot be constant but variates as a function of PM flux and d, q-axis currents combinations. Thus, the paper proposes a novel method which combines conventional constant core loss resistance with a component which variates according to a function of d axis current. The method validated by FEM and experimental measurements. An extensive study [81] shows that electromagnetic flux linkage trajectories in rotating machines may be in shape of lines, circles, or etc depending on location. The core loss occurring in a rotational field is much more significant than that in an alternating field. Therefore, ignoring such contribution of rotational field to the core loss result in a high rate of error in control. In addition, saliency, slots, teeth, non-sinusoidal drive etc cause flux density with

harmonics in the core. In the paper, the core loss considering rotational field and flux harmonics is investigated by using 2-D FEM.

Online Solutions

Offline parameter identification methods are mostly utilised into control schemes with LUTs for real time operation. Alternatively, online parameter estimation methods are suggested in order to enhance the precise control quality.

In [82], a systematic procedure based on current, voltage and rotor position measurements is introduced for estimation all IPMSM parameters in steady state operation. The method is particularly useful when power and torque measurements are not available. The PM flux linkage can be calculated by measuring the terminal voltages while the stator current vector is zero in constant speed. Linear regression algorithm is suggested for the copper loss resistance estimation considering the temperature effect. The core loss resistance is identified as a function of angular speed and the core loss resistance at rated speed. This procedure is for online identification of conventional IPMSM model parameters. In order to increase accuracy of conventional MTPA control, polynomial fitting algorithms for real time MTPA control are proposed [83], [84] which introduces magnetic saturation and/or cross-coupling effect into the motor parameters. The input data, phase currents, rotor position and dc-link voltage, is used for online calculation of flux linkage to d, q-axis currents curves as explained in [85]. The methods do not exactly represent the real motor parameters but converges them according to calculated flux linkages through the polynomial fitting algorithm.

Some papers [86]–[89] suggested signal injection method for online full parameter estimation. In [86], a fast online parameter estimation algorithm for all parameters

based on sinusoidal signal injection on d-axis current. It is claimed that it has faster convergence time than the other methods and it is compatible with transient operation as well. The estimation technique is employed as recursive least square (RLS) algorithm to estimate four parameters of the IPMSM and an average sliding mode window to eliminate the effect of measurement noise. In [87], a signal injection method combined with EMF observer for fast online parameter estimation is suggested for sensorless control. Initial rotor position is identified at standstill with signal injection method. Regarding this, the resistances, including on-resistance of the IGBT, the voltage error caused dead time of inverter and d, q axes inductances are identified for standstill using estimated initial position based on RLS method. The magnet flux cannot be identified during standstill operation. Therefore, the EMF observer is implemented during medium and high speed. Affine Projection Algorithm (APA) is also proposed for online identification of the copper loss resistance and d, q-axis inductances for medium and high-speed operations in [90]. The method employs EMF observer, too. It is claimed that APA has lower computational burden and execution time, therefore guarantees high convergence rate and good tracking capability. A parameter is introduced for a trade-off between convergence rate and steady state error. The method shows good performance during temperature variations, magnetic saturation and transients. It is also stated that signal injection method is proper for standstill or low speed operations, however it introduces extra pulsations into torque response in high speeds. Later on, the method is improved based on two separate APA used for estimating all motor parameters [91].

Recursive Least Square (RLS) algorithm is commonly adopted especially for d, q-axis inductances identification. In [92] RLS algorithm is used to estimate q axis inductance via processing d, q-axis current error for a high performance (wide speed range) MTPA

control. In [93], an RLS method is adopted to estimate d, q-axis inductances using d, q axis voltage, current and velocity as input data. Updated parameters used for online calculation of torque and DC link voltage. Torque ripple, hence, vibration and noise in IPMSM drives, sourced by magnetic saturation is supposed to be eliminated by keeping output of the inverter linear, however ill-estimation can happen.

In [94], an online parameter estimation algorithm is proposed to improve the MTPA performance of IPMSM. It is shown that MTPA trajectory manipulated by the effect of both magnetic saturations along only q axis direction and d, q-axis directions together. The proposed method is for steady state algorithms, derivative terms are accepted to be zero. d, q-axis inductances are updated according to relationship with reference voltages and instantaneous current and speed data. The copper loss resistance and PM flux assumed to be constant. The saturation effect on MTPA control trajectory is well established via experimental data in Figure 2.10.

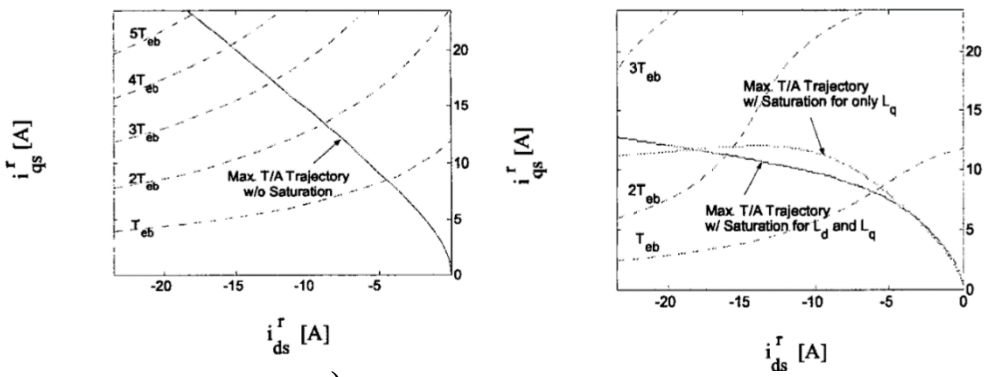

Figure 2.10 MTPA trajectory a.) using nominal parameters
b.) including magnetic saturation [94]

In [95], the motor parameters are updated similar to previous method. In this case, the harmonics of the back EMF due to magnetic circuit variations are also considered. Therefore, a Low Pass Filter utilized to eliminate higher harmonics. The method is improved for IPM assisted SynRMs in EV applications. Besides, the copper loss

resistance and PM flux variates with temperature. d, q-axis inductances are air-gap flux linkage dependant. As PM flux density variates with temperature, d, q-axis inductances are implicitly temperature dependant. The conventional steady state mathematical model and fifth harmonics of the back-EMF are used for updating d, q-axis inductances and PM flux linkage in an MTPA search algorithm.

The mechanical parameters effect the precise control quality. Therefore, sliding mode observers [96] and disturbance observers [97] are commonly employed for the mechanical parameter identification, the moment of inertia and the viscous friction coefficient.

Parameter Independent Methods

Online parameter estimation methods are improved to eliminate any uncertainties due to nonlinear relations. However, the suggested methods in literature are basically focus on one specific issue like temperature variation or magnetic saturation etc. for one or two parameters mostly and the other possibilities kept out of consideration. Therefore, in practical use, the methods should be combined in real time control algorithms to achieve precise control. This results in highly complicated and sensitive control algorithms and increases convergence time and computational cost. Instead, some parameter independent methods are suggested in literature. Those methods are improved based on fuzzy logic[98]–[101], signal injection algorithm[102]–[107], searching algorithm [108], [109], quasi real time adjusting algorithm[110], artificial neural networks [111], Lyapunov stability criterion [112]–[115] and so on. The common point all these methods that they do not require exact parameter identification and focuses on enhancing robustness of the IPMSM drives.

In[98], an adaptive fuzzy solution is proposed to overcome the inductance variations of the motor. The conventional Field Oriented Control under MTPA is updated with a Fuzzy Logic Speed Controller (FLC) to overcome any uncertainties sourced by any unknown parameter variations and load disturbances. It is evaluated via simulations in Matlab Simulink that the proposed FLC based IPMSM drive has enhanced robustness against d, q axis inductance and inertia variations. The scaling factors of FLC is identified according to normalised speed error and the normalised variation of the speed error as well. Fuzzy logic-based controllers can overcome any uncertainties caused by parameter variations, do not require exact mathematical model and created based on linguistic rules with an IF-THEN rule; however, it increases computational costs and complexity and therefore convergence time increases which is not feasible for VSDs. In[99], a Wavelet Fuzzy Neural Network (WFNN) Integral-Proportional Speed controller is adopted. Speed Controller parameters are updated based on four-layer, two input two output wavelet-fuzzy neural network system. Inputs of the WFNN are speed error and speed error derivative. The outputs are the PI parameters of the speed controller. Stator current amplitude is calculated through the sum of speed controller output and feedforward torque disturbance observer. The torque angle for MTPA control is identified based on small signal injection method which can work for even start-up and low speed operations. The proposed MTPA control method works well during standstill and low speed operation as it is based on small signal injection method. In [100], a Fuzzy Neural Network Speed Controller is adopted, and PI parameters of the speed controller are updated regarding speed and acceleration error. ZDAC control is adopted. The adaptive algorithm is derived with Lyapunov theorem. The uncertainties sourced by parameter variations, sudden load changes and nonlinear friction variations are investigated on simulations. In [101], a FOC scheme for IPMSM

both increasing torque capability and enhance robustness is suggested based on fuzzy logic speed controller. The controller parameters are identified mostly heuristic method. The method considers both efficiency and dynamic performance.

Real signal injection-based parameter independent methods [102]–[104] and virtual signal injection-based parameter independent methods [105]–[107] methods

In[111], a Model Referenced Adaptive Control is proposed for IPMSM. The conventional vector control concept under MTPA is redesigned with Artificial Neural Network (ANN) based speed controller to overcome parameter variations. A radial basis function ANN based speed controller is employed for enhancing robustness.

In [112], the conventional IPMSM model is replaced with an adaptive model which aims to eliminate errors sourced by dynamic variations. Therefore, a disturbance observer of which adaptation gain is updated using Lyapunov function, is adopted into the current loop in the VC scheme to enhance the robustness of precise torque control. Hence, fast torque response for transient operation is achieved. In [113], an adaptive speed controller is adopted to eliminate uncertainties by separating system into static and dynamic components. The static component includes conventional speed algorithm. The dynamic component is updated via the recursive equations defined for steady state speed error. The stability analysis is validated with Lyapunov function to show the convergence time is short. In [114], an adaptive nonlinear controller is proposed to enhance the robustness of IPMSM drives. The nonlinear controller is designed with Lyapunov Stability criterion of which conditions are supported by Barbalat's lemma. The q axis inductance, mechanical coefficients and load torque is estimated using adaptive backstepping derivations. Another adaptive solution is proposed based on Neural Network based Dynamic surface control is proposed in [115]. Radial Basis Neural Networks are used for approximation to the unknown

parameters and Lyapunov functions are used for stability analysis. The method is suggested to decrease complex computational work of the backstepping derivations.

2.5. Conclusions

In this chapter, an extensive, up to date overview for IPMSM Drives in control aspect is provided.

- Although the control of IPMSM drives is well established area with a lot of methods, the industrial applications still prefer simpler solutions like Zero D-axis Current Control and Maximum Torque per Ampere Control due to simple implementation and industrial requirements satisfaction.

- In energy efficient design applications, there is still a dilemma either to use Maximum Torque per Ampere or Maximum Efficiency Control algorithms since improving in efficiency depends on the accurate knowledge on the core losses. This dilemma can be replaced by a problem of switching or combining two methods depending on the motor's operating conditions and there is a space for a new research direction on the combining optimisation.

- Although there is a lot of papers on the motor's parameters determination and identification, the problem of their accurate determination still exists and potentially can be resolved by a robust control solution.

- The algorithms optimising motor's energy consumption introduce extra nonlinearities into the velocity loop of Field Oriented Control which requires corresponding addressing in control.

- The aim of the control design suitable for industry will be to design a control which has the same structure as used in industry (d and q axes current loops and

velocity loop) but to replace the used PI controller by sophisticated controllers coping with the nonlinearities introduced by the energy optimisation algorithms and parameters inaccuracy and allowing to achieve the dynamical performance comparable with the linear variant for D-axis current control in idealised conditions.

CHAPTER 3. ENERGY EFFICIENT AND TRANSIENTS OPTIMAL IPMSM DRIVE

3.1. Introduction

Compared to DC motor control applications, AC motor control is more challenging because of the inherent complicated structure that tends to include nonlinear features into the control algorithm. Therefore, dynamic AC motor model is commonly designed via using Clarke transform to convert n phase AC variables into an equivalent stator phasor in d, q-axis reference frame and Park transform to eliminate sinusoidal component in the stator phasor components [3]. Thus, linear control theory can be utilised for AC motor control applications. However, conventional Field Oriented Control (FOC) concept still requires some optimisation methods like Zero d-Axis Current (ZDAC) control to achieve linear control features which is possible in DC motor control [4].

IPMSM drives can be simply controlled with FOC optimised with ZDAC control, however, the total torque capability cannot be fully utilised as the inherent reluctance torque is disregarded. As alternative approaches to ZDAC control, Maximum Torque per Ampere (MTPA) Control is proposed [5] to extract maximum possible torque for a given stator current amplitude and Maximum Efficiency (ME) Control is suggested for achieving energy efficient operation through considering the core loss characteristics [6].

In EV applications, the designers face a dilemma which control approach to be selected since there is a trade-off between faster dynamics and higher efficiency which varies during corresponding driving cycles. Besides, the motor parameters are also subject to change during real time operation, worsens the control accuracy [7].

An energy efficient and transients optimal control for Interior Permanent Magnet Synchronous Motors [8] is introduced in this chapter based on the concept of the combined Maximum Torque per Ampere (MTPA) and Maximum Efficiency (ME) control approaches. The nonlinear optimal implicit equation of the combined MTPA/ME method is derived in a new compact form, the same as for the conventional ME approach explained in [6]. Then it is simply applied to activate the MTPA control during transients for fast dynamics and the ME control during steady states for maximum efficiency. Compared to the existing similar approaches, it allows smooth transition between the methods with smaller number of equations simplifying required control coding and reducing the control algorithm execution time.

This Chapter is organized as follows: Section **3.2** to Section **3.5** explain existing optimal control solutions - ZDAC, MTPA, and ME, respectively - with conventional FOC concept, then Section **3.6** introduces the proposed 'Energy efficient and transients optimal IPMSM drive' and the analytical results are verified by simulations, followed by conclusions.

3.2. Dynamic Mathematical IPMSM Model

Instantaneous variations of voltages/currents, stator frequency and torque demands are major inputs of the motor control concept. Due to the need of evaluating the transients caused by the variations, dynamic modelling is employed in a real-time control system design. Rotor reference framed two reaction (two phase) dynamic model is mostly

preferred approach for IPMSM. The idea of two-reaction motor modelling of any type of n phase machine is named as Clarke transform, depicted in Figure 3.1. The equivalence between real motor and its model in Clarke transform is provided by graphical observations and power invariance. The concept of modelling in rotational reference frame named as Park Transform eliminates rotor-position dependency of parameters in the model. A set of two fictional windings placed 90° phase shift in space, are represented in direct-quadrature (d, q) axes reference frame. The winding set is assumed to be instantaneously revolving around the rotor in electrical rotor speed. Rotor magnets are represented via a flux linkage source [3].

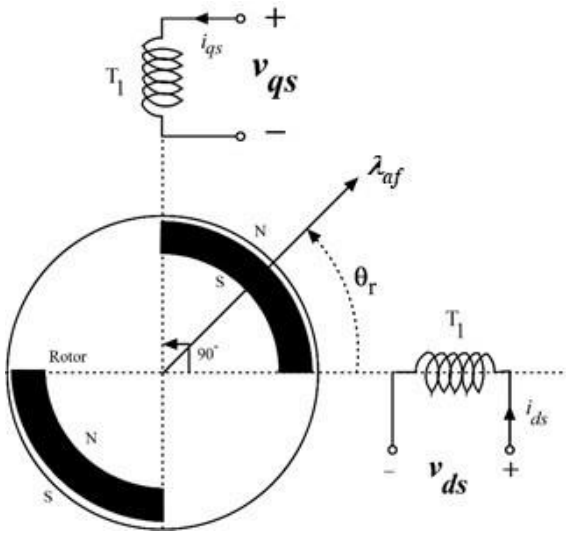

Figure 3.1 Two Reaction Model in Rotor Reference Frame for IPMSM [3]

Implementing such a dynamic model requires some assumptions as listed below [3]:

- The stator windings are balanced, results in rotational magnetomotive force to be sinusoidal. Thus, instantaneous variation of real winding inductances via rotor position is assumed to be sinusoidal.
- All parameter changes stem from saturation, harmonics and etc are neglected.

- The magnetic flux density of PMs is assumed to be sinusoidal even though it is trapezoidal in real machines [4].
- Stray losses are neglected, the core loss is neglected for ZDAC control research and MTPA control and then it is considered for ME investigation.

The very first and fundamental electromagnetic relations in the stator reference frame (represented with '$_s$' subscriptions in the equations) are seen in equations (3.1) and (3.2) transformed into (3.3) and (3.4) in a rotating reference frame (represented with '$_r$' subscription in the equations) after derivations, respectively.

$$v_{qs} = R_q i_{qs} + \left(d\lambda_{qs}/dt\right) \tag{3.1}$$

$$v_{ds} = R_d i_{ds} + \left(d\lambda_{ds}/dt\right) \tag{3.2}$$

v_{qs}, v_{ds} denote q and d axis stator voltages, respectively.

i_{qs}, i_{ds} denote stator q and d axis currents, respectively.

R_q, R_d denote stator q and d axis winding resistance, respectively.

λ_{qs}, λ_{ds} denote stator q and d axis flux linkages, respectively.

$$v_{qr} = R_s i_{qr} + L_q\left(di_{qr}/dt\right) + \omega_r L_d i_{dr} + \omega_r \lambda_{af} \tag{3.3}$$

$$v_{dr} = R_s i_{dr} + L_d\left(di_{dr}/dt\right) - \omega_r L_q i_{qr} \tag{3.4}$$

Figure 3.2 depicts the equivalent circuits for the sake of better understanding

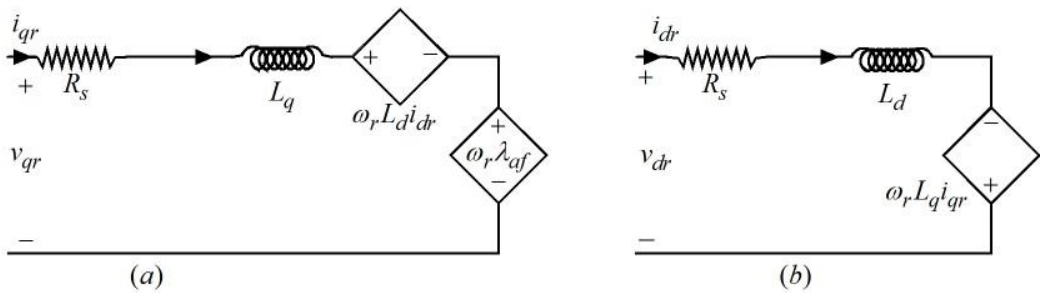

Figure 3.2 IPMSM (a) q-axis (b) d-axis Equivalent Circuit without Core Loss

v_{qr}, v_{dr} denote q, d axis voltages, respectively,

i_{qr}, i_{dr} denote q, d axis currents, respectively,

L_q, L_d denote q, d axis inductances, respectively,

λ_{af} denotes the magnet flux linkage,

ω_r denotes electrical rotor speed,

$R_s = R_q = R_d$ denotes the copper loss resistance.

The electrical torque in eqn. (3.6) is derived from the power equation in (3.5). Because of the power equivalence between the three-phase machine and its two-phase equivalent, the coefficient $(3/2)$ appears in the equations. The electromechanical dynamics are depicted in (3.7).

$$P_{in} = (3/2)\left(v_{qr} i_{qr} + v_{dr} i_{dr}\right) \tag{3.5}$$

$$T_e = \left(3n_p/2\right)\left[\lambda_{af} + (L_d - L_q) i_{dr}\right] i_{qr} \tag{3.6}$$

$$T_e - T_l = J\left(d\omega_m/dt\right) + B\omega_m \tag{3.7}$$

P_{in} denotes electrical input power,

T_e, T_l denote electrical and load torques, respectively,

J denotes the moment of inertia,

B denotes the friction coefficient,

ω_m denotes mechanical speed,

n_p denotes the number of pole pairs.

The core loss, which is proportional to the square of the electrical speed and appears as a nonlinear resistance (R_c) in the equivalent circuits depicted in Figure 3.3,

contributes significantly to the power loss, and the model equations can be updated as (3.8), (3.9), and (3.10).

$$v_{qr} = R_s i_{oqr} + \left(1+\left(R_s/R_c\right)\right)L_q\left(di_{oqr}/dt\right) + \left(1+\left(R_s/R_c\right)\right)\omega_r L_d i_{odr} + \left(1+\left(R_s/R_c\right)\right)\omega_r \lambda_{af} \tag{3.8}$$

$$v_{dr} = R_s i_{odr} + \left(1+\left(R_s/R_c\right)\right)L_d\left(di_{odr}/dt\right) - \left(1+\left(R_s/R_c\right)\right)\omega_r Li \tag{3.9}$$

$$T_e = \left(3n_p/2\right)\left[\lambda_{af} + (L_d - L_q)i_{odr}\right]i_{oqr} \tag{3.10}$$

Equivalent circuit with core loss can be seen in Figure 3.3

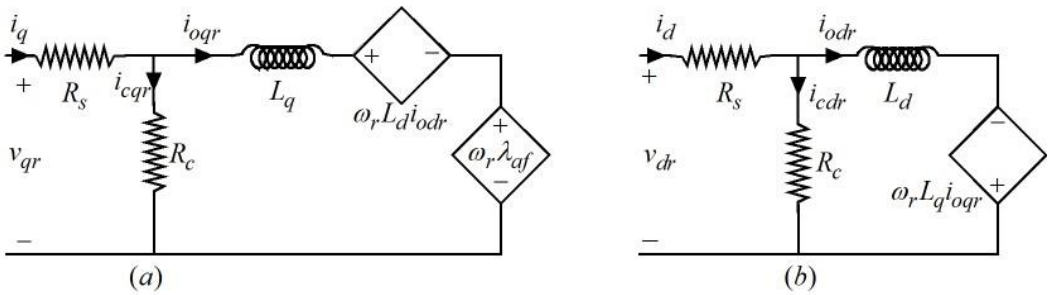

Figure 3.3 IPMSM (a) q-axis (b) d-axis equivalent circuit with core loss

3.3. Zero d-axis Current Control of IPMSM

The well-known IPMSM drive control structure, FOC, is composed of three linear PI control loops. Two internal loops for d- and q-axis currents are included in the exterior velocity control loop. Setting the reference value of the d axis current to zero and connecting the velocity controller output directly to the reference value of the q axis current yields the optimum dynamic velocity performance, as shown in Figure 3.4. (Zero d-axis Current- ZDAC Control). In this case, the torque producing current (equivalent stator current phasor) is perpendicular to and independent from the field producing current (PM flux linkage), hence the coupling found in voltage equations (3.3), (3.4) and the nonlinear component of the torque equation in (3.6) are eliminated.

As a result of the motor torque being directly proportional to the q axis current, the control system becomes linear, similar to DC motor control, resulting in an easy-to-implement control design. However, it does not optimise power loss and ignores the contribution of reluctance torque to torque capability.

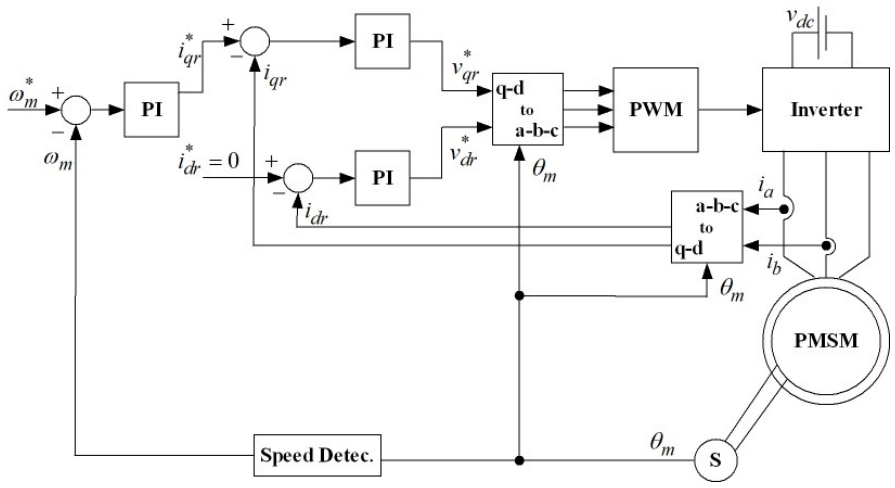

Figure 3.4 ZDAC Control Scheme for IPMSMs with PI controllers

ZDAC control model is created in Matlab Simulink regarding the block diagram in Figure 3.4. The Matlab Simulink Model views are attached in Appendix D. Nonlinear dynamics due to switching of the inverter and PWM modulation are not investigated in the simulations, the stator d and q axes voltages are assumed to be equal their references.

Table 3.1 shows the motor parameters utilized in the simulations, which are obtained from a previous article in [5]. The load torque steps follow no load start, while the velocity reference also changes with steps. Figure 3.5 depicts the velocity reference and load torque disturbance variations. The moment of inertia $J = 0.004\ Nm^2$ is considered to be default.

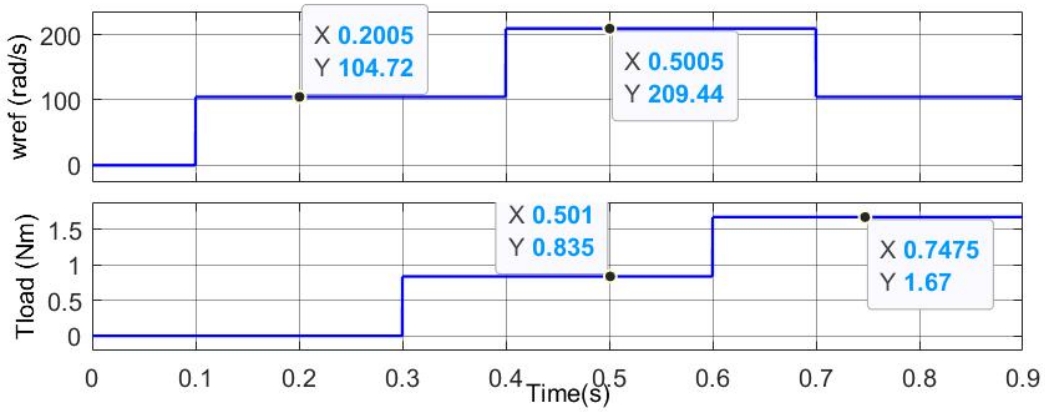

Figure 3.5 Speed and Load Torque Input References

Figure 3.7 shows the simulation results for ZDAC control using conventinal PI controllers. Because of the effect of the moment of inertia, the velocity response reaches the reference value in around 0.1 second. Figure 3.7c shows the d q axis currents for the model without the core loss, while Figure 3.7d shows the currents for the model with the core loss. The decoupling voltage feedforward compensation mentioned in Figure 3.6 makes the d and q-axis current loops independent in both circumstances. The d-axis current is kept constant at zero, and the torque is proportional to the q-axis current. Because an ideal condition is simulated, the quality of the velocity control is high. (These simulations exclude PWM dynamics.) The PI controller parameters demonstrated in Table 3.2, calculated in Appendix C The difference of Figure 3.7c and Figure 3.7d proves that even a constant core loss resistance may induce extra overshoots and fluctuations into d-axis current even in ideal conditions, will be discussed in Chapter 4 of this study.

Table 3.1 Specifications and Parameters for IPMSM in Simulations

Rated Torque T_{rt} (Nm)	1.67
Rated Current I_{rt} (A)	5
Rated Speed W_{rt} (rpm)	2000
Rated Voltage V_{rt} (V)	97
R_s (Ω)	0.57
R_c (Ω)	240
L_q (mH)	22.78
L_d (mH)	8.72
λ_{af} (Wb)	0.1077
n_p	2

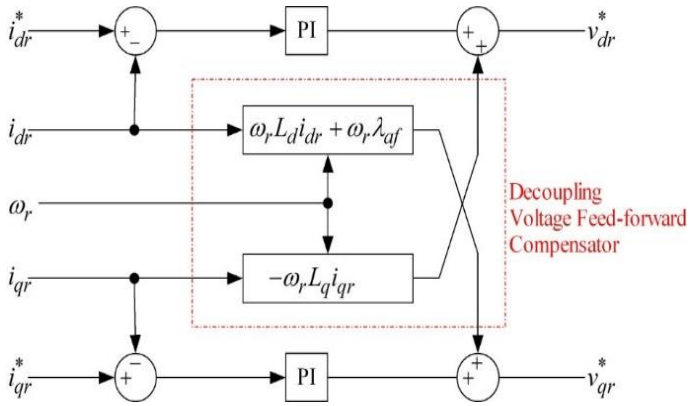

Figure 3.6 Decoupling Voltage Feed-forward Compensation for IPMSM Drives [5]

Table 3.2 PI Controller parameters

		ω_m Controller	i_d Controller	i_q Controller
PI	*ki*	125	285	285
	kp	1	4.36	11.4
	Saturation	5	150	150

3.4. MTPA Control of IPMSM

Two components of the torque equation in (3.6) are

Synchronous Torque $T_{sync} = (3/2) n_p \lambda_{af} i_{qr}$

Reluctance Torque $T = (3/2) n_p \left(L_d - L_q \right) i_{dr} i_{qr}$

In ZDAC control of surface-mounted PMSM, the bigger q-axis current means the bigger torque response. Because the reluctance torque converges to zero as d-, q-axis inductances are almost the same. However, for IPMSM drives, q-axis inductance is approximately 2.5-times bigger than d-axis inductance in nature, which may result in better torque capability for some d-, q-axis current combinations [3].

MTPA control approach is suggested to employ all motor torque capability sourced by both the synchronous and the reluctance torque for a specific operation point via adjusting the torque angle, consequently d-axis current. To derive MTPA algorithm, the steady state conditions should be regarded, that is, the stator current amplitude is assumed to be constant ($I_s = \sqrt{i_d^2 + i_q^2} = const$). Since the core (iron) loss is disregarded, the iron loss resistance is infinite. The explicit nonlinear relationship between d and q-axis currents, which maximizes the torque response for a given stator current or, in other words, minimizes stator current amplitude for a demanded torque, is produced by partial differentiating the torque equation in (3.6) with respect to the d axis current and equating the result to zero. Combining this optimal dependence with the torque equation allows to find q axis current reference and then to compute d-axis current reference as in (3.11) [5].

MTPA algorithm, meanwhile, minimises the copper loss implicitly.

$$i_{dr} = \left(\lambda_{af} \Big/ \left(2\left(L_q - L_d \right) \right) \right) - \sqrt{\left(\left(\lambda_{af}^2 \Big/ \left(4\left(L_q - L_d \right)^2 \right) \right) + i_{qr}^2 \right)} \qquad (3.11)$$

ZDAC Control Scheme depicted in Figure 3.4 can be transformed into MTPA control scheme only by adding an MTPA optimisation block between the velocity controller and d-, q-axis current controllers. Thus, d-, q- axis current references are defined according to the MTPA block output and the input of the MTPA block is the output of the velocity controller, represents the torque demand (T_e). The simulations carried out with MTPA control, Figure 3.8, show more nonlinear behaviour in d, q-axis current compared to ZDAC control results in Figure 3.7, as expected. However, a larger torque capability is produced with a lower current demand, which leads to a faster dynamic response.

3.5. Maximum Efficiency (Loss Minimization) Control for IPMSM

Especially for speed ranges beyond base speed, the iron loss becomes significant compared to the copper loss. Maximum Efficiency (ME) control approach is mainly search for an optimal operation point to minimise total electrical loss including both the copper loss and the iron loss. The three equations in (3.13) for the copper loss, the iron loss and the electromagnetic torque, respectively, are utilised to express total electrical loss in (3.12) as a function of d-axis current.

$$W_e = W_{Cu} + W_{Fe} \qquad (3.12)$$

$$W_{cu} = \frac{3}{2} R_s \left(\left(i_{odr} - \frac{\omega_r L_q i_{oqr}}{R_c} \right)^2 + \left(i_{oqr} + \frac{\omega_r \left(\lambda_{af} + L_d i_{odr} \right)}{R_c} \right)^2 \right)$$

$$W_{Fe} = \frac{3}{2} \left(\frac{\omega_r^2 \left(L_q i_{oq} \right)^2}{R_c} + \frac{\omega_r^2 \left(\lambda_{af} + L_d i_{od} \right)^2}{R_c} \right) \tag{3.13}$$

$$T = \frac{3}{2} n_p \left(\lambda_{af} i_{oqr} + \left(L_d - L_q \right) i_{odr} i_{oqr} \right)$$

The partial differentiation of the total electrical loss with respect to d axis current and equating the result to zero ($\delta W_e / \delta i_{odr} = 0$) ends up to a fourth order polynomial equation in the form of (3.14). To implement the ME control, this polynomial equation of d-axis current (i_{odr}) must be solved iteratively in real time. Then q axis current reference (i_{oqr}^*) is determined from the torque equation. Finally, the d and q axis references (i_{odr}^* *and* i_{oqr}^*) must be mapped into i_{dr}^* *and* i_{qr}^* references [6].

$$AB = T_e^2 C \tag{3.14}$$

where,

$$\begin{aligned} A &= \left(9 n_p^2 / 4 \right) \left(R_s {R_c}^2 i_{odr} + \left(\omega_r^2 L_d \left(R_s + R_c \right) \left(L_d i_{odr} + \lambda af \right) \right) \right) \\ B &= \{ \lambda_{af} + (L_d - L_q) i_{odr} \}^3 \\ C &= \{ R_s {R_c}^2 + (R_s + R_c)(\omega_r L_q)^2 \} (L_d - L_q) \} \end{aligned} \tag{3.15}$$

The simulation results for IPMSM drive with ME control approach is depicted in Figure 3.9. Similar pattern for d, q-axis currents with MTPA control approach in Figure 3.8 is observed but with different current amplitude. Therefore, higher efficiency is achieved.

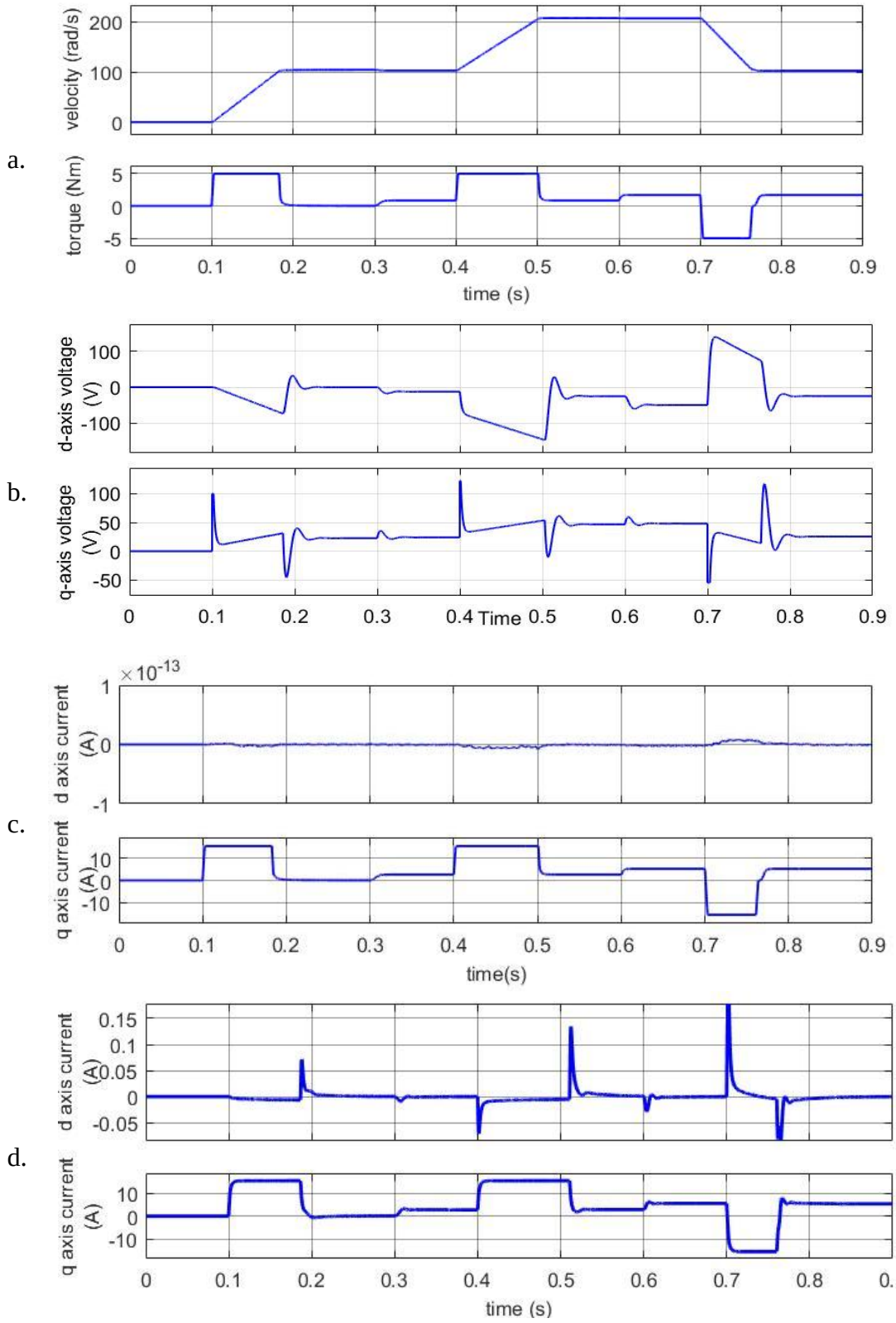

Figure 3.7 ZDAC Control

a. Velocity and torque response
b. d, q axes voltages
c. d, q axes currents (ignoring core resistance)
d. d, q axes currents (regarding core resistance)

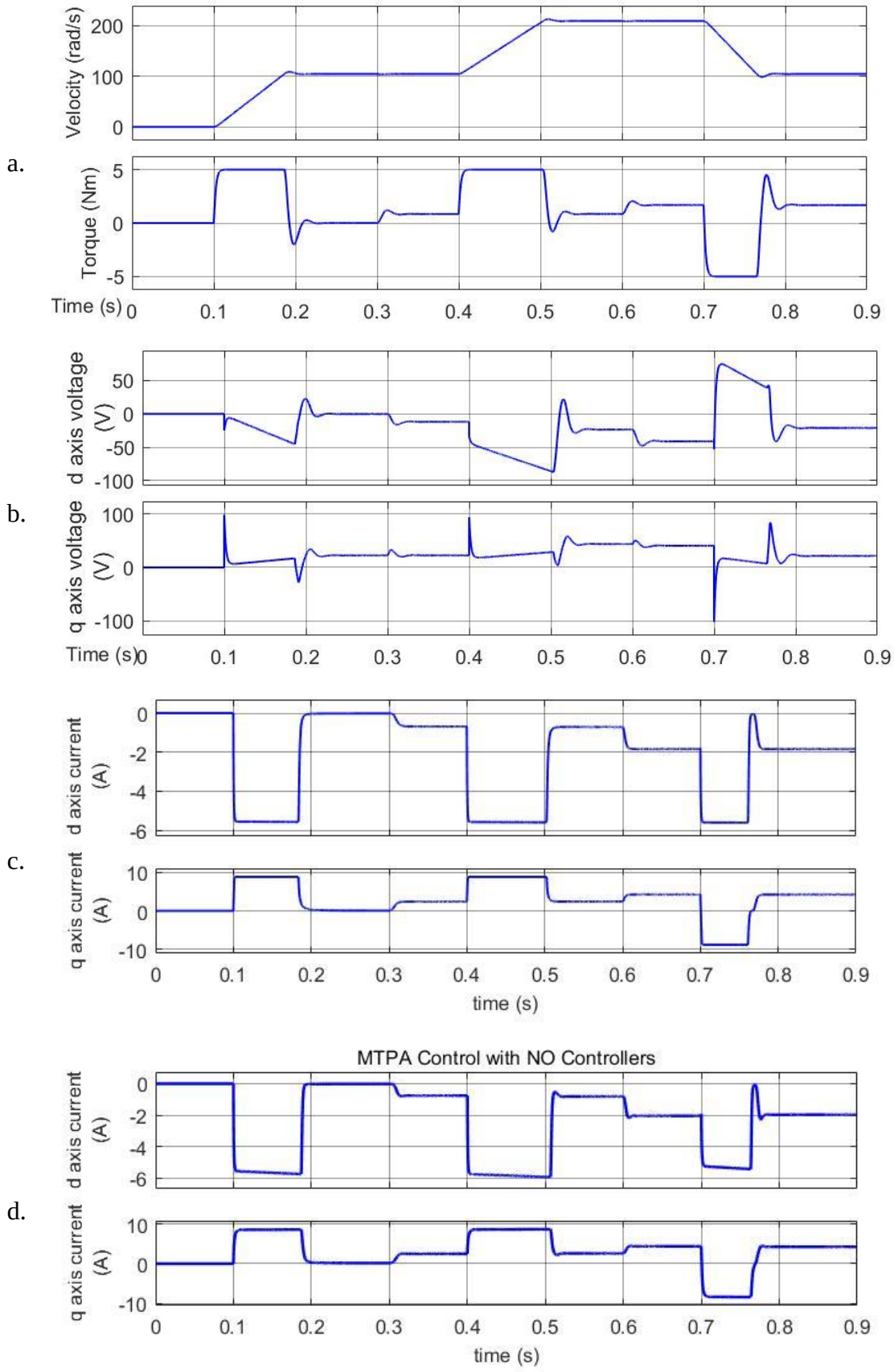

Figure 3.8 MTPA Control

a. Velocity and torque response
b. d, q axes voltages
c. d, q axes currents (ignoring core resistance)
d. d, q axes currents (regarding core resistance)

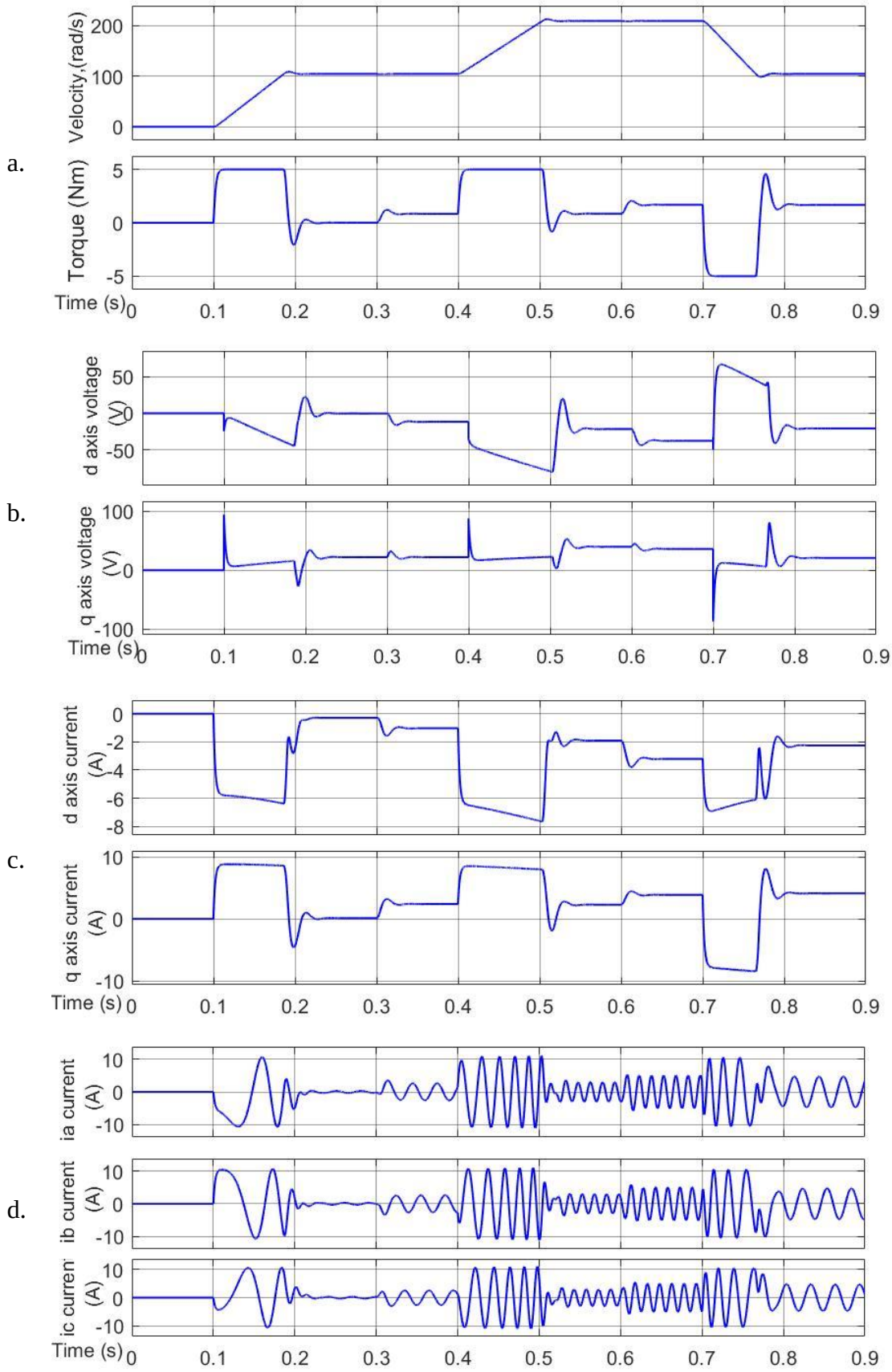

Figure 3.9 ME Control

a. Velocity and torque response
b. d, q axes voltages
c. d, q axes currents
d. a, b, c phase currents

3.6. Combined MTPA/ ME Approach

The performance requirements for electric motors used in variable speed applications, particularly those used in electric vehicles (EVs), may change instantly. Therefore, it follows that the control objectives of a variable speed drive should alter in relation to the current operating circumstances.

Among the existing optimal control approaches, it is very well-known fact that MTPA control approach is the solution for the best dynamic torque response particularly for IPMSM drives, while ME control approach is employed to achieve an energy efficient operation. Instead of deciding which strategy to use when designing the variable speed IPMSM drive, adding an "adaptive optimal decision algorithm" may lead to a new control solution that offers the benefits of both approaches depending on the operating conditions. In the spirit of this perspective, the combined MTPA/ME control approach is demonstrated in Figure 3.10. The conventional FOC concept is updated by adding an optimisation block between the velocity controller and the current controllers which defines d-, q- axis current references with respect to velocity controller output (torque demand), similar to ME or MTPA control approaches but with the 'β Generator'.

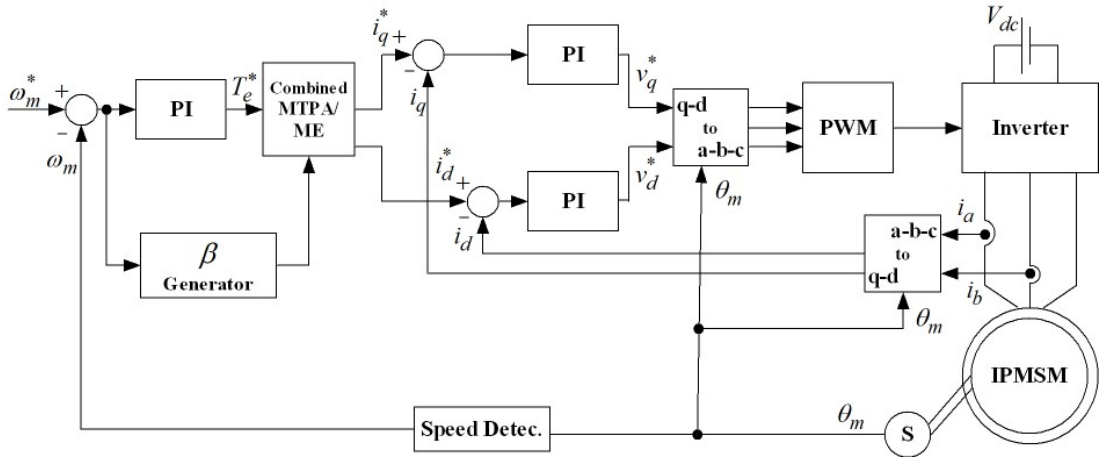

Figure 3.10 The Block Diagram of the proposed Combined MPTPA/ME Control

'β Generator' is a type of decision block that specifies which control approach will be used. It could be as simple as a switch [40] or as complex as a fuzzy algorithm with a look-up table [39]. One disadvantage of using a switch is that it introduces additional nonlinearities and transients owing to switching behaviour. A fuzzy look-up table approach may result in bulky control solutions and increase real-time computing cost.

The proposed approach in this study is influenced by the findings of a previously presented paper in [7], which introduces a so-called combined MTPA/ME control approach with β generator described as an 'adaptive optimisation parameter' that varies with torque demand. The optimisation block compels the control algorithm to converge to ME control for higher torque commands, and vice versa to MTPA for lower torque commands. A fictitious electric power loss is introduced as in (3.16) for a smooth combination of two procedures in real time. The copper loss and the core loss are obtained as in (3.19) by substituting (3.18) into (3.17). Electromagnetic torque equation in (3.20) can be rewritten as in (3.21) to state q-axis current as a function of d axis current, torque, and velocity ($i_{oqr} = f(i_{odr}, T_e, \omega_r)$). Final expression of the copper and core losses are obtained as in (3.22) by substituting (3.21) into (3.19).This allows to eliminate i_{oqr} from (3.19).

$$W_f = W_{cu} + \beta W_{fe} \qquad \text{for } 0 \le \beta \le 1 \tag{3.16}$$

$$\begin{aligned} W_{cu} &= 3R_s(i_{dr}^2 + i_{qr}^2)/2 \\ W_{fe} &= 3R_c(i_{cdr}^2 + i_{cqr}^2)/2 \end{aligned} \tag{3.17}$$

$$i_{cdr} = \left(-\omega_r L_q i_{oqr}/R_c\right) \text{ and } i_{cqr} = \left(\left(\omega_r \lambda_{af} + \omega_r L_d i_{odr}\right)/R_c\right) \tag{3.18}$$

$$W_{cu} = (3/2) R_s \left[\left(i_{odr} + \left(-\omega_r L_q \, i_{oqr} / R_c \right) \right)^2 + \left(i_{oqr} + \left(\omega_r \left(\lambda_{af} + L_d \, i_{odr} \right) / R_c \right) \right)^2 \right]$$
$$W_{fe} = (3/2) R_c \left[\left(\omega_r L_q \, i_{oqr} / R_c \right)^2 + \left(\left(\omega_r \lambda_{af} + \omega_r L_d \, i_{odr} \right) / R_c \right)^2 \right] \quad (3.19)$$

$$T_e = n_p \left(\lambda_{af} + \left(L_d - L_q \right) i_{odr} \right) i_{oqr} \quad (3.20)$$

Then

$$i_{oqr} = \left(T_e \Big/ \left(n_p \left(\lambda_{af} + \left(L_d - L_q \right) i_{odr} \right) \right) \right) \quad (3.21)$$

Then

$$W_{cu} = (3/2) R_s \left[\left(i_{odr} + \frac{-\omega_r L_q}{R_c} \frac{T_e}{n_p \left(\lambda_{af} + \left(L_d - L_q \right) i_{odr} \right)} \right)^2 + \left(\frac{T_e}{n_p \left(\lambda_{af} + \left(L_d - L_q \right) i_{odr} \right)} + \frac{\omega_r (\lambda_{af} + L_d \, i_{odr})}{R_c} \right)^2 \right]$$
$$W_{fe} = (3/2) R_c \left[\left(\frac{\omega_r L_q}{R_c} \frac{T_e}{n_p \left(\lambda_{af} + \left(L_d - L_q \right) i_{odr} \right)} \right)^2 + \left(\frac{\omega_r \lambda_{af} + \omega_r L_d \, i_{odr}}{R_c} \right)^2 \right] \quad (3.22)$$

The fourth order polynomial equation for loss minimisation algorithm in section 3.5 is updated as in (3.24) in the paper [7] by the partial differentiation of the fictious electric power loss with respect to d axis current and equating the result to zero ($\delta W_f / \delta i_{odr} = 0$). The fourth order polynomial equation is a nonlinear implicit equation therefore it can be rewritten in a nonlinear but more explicit form of $P_1 + P_2 + P_3 + P_4 = 0$ for iterative computation of i_{odr} in real time. After the derivations from (3.23) to (3.37), the very last polynomial equation is obtained in (3.38).

$$\frac{\delta W_f}{\delta i_{odr}} = \frac{\delta W_{cu}}{\delta i_{odr}} + \frac{\delta \beta W_{fe}}{\delta i_{odr}} = 0$$

$$\Rightarrow \frac{\delta W_{cu}}{\delta i_{odr}} = 2R_s \left[\left(i_{odr} + \frac{-\omega_r L_q}{R_c} \frac{T_e}{n_p\left(\lambda_{af} + \left(L_d - L_q\right) i_{odr}\right)} \right) \left(1 + \frac{-\omega_r L_q}{R_c} \frac{-T_e n_p \left(L_d - L_q\right)}{\left(n_p\left(\lambda_{af} + \left(L_d - L_q\right) i_{odr}\right)\right)^2} \right) + \left(\frac{T_e}{n_p\left(\lambda_{af} + \left(L_d - L_q\right) i_{odr}\right)} + \frac{\omega_r (\lambda_{af} + L_d\, i_{odr})}{R_c} \right) \left(\frac{-T_e n_p \left(L_d - L_q\right)}{\left(n_p\left(\lambda_{af} + \left(L_d - L_q\right) i_{odr}\right)\right)^2} + \frac{\omega_r L_d}{R_c} \right) \right]$$

and

$$\Rightarrow \frac{\delta \beta W_{fe}}{\delta i_{odr}} = 2\beta R_c \left[\left(\frac{\omega_r L_q}{R_c} \frac{T_e}{n_p\left(\lambda_{af} + \left(L_d - L_q\right) i_{odr}\right)} \right) \left(\frac{\omega_r L_q}{R_c} \frac{-T_e n_p \left(L_d - L_q\right)}{\left(n_p\left(\lambda_{af} + \left(L_d - L_q\right) i_{odr}\right)\right)^2} \right) + \left(\frac{\omega_r \lambda_{af} + \omega_r L_d\, i_{odr}}{R_c} \right) \left(\frac{\omega_r L_d}{R_c} \right) \right]$$

(3.24)

where,

$$P_1 = 2R_s \left[\frac{2L_q T_e \omega_m \left(L_d - L_q\right)}{3R_c \left(\lambda_m + i_{odr}(L_d - L_q)\right)^2} + 1 \right] \left[i_{od} - \frac{2L_q T_e \omega_m}{3R_c \left(\lambda_m + i_{odr}(L_d - L_q)\right)} \right]$$

$$P_2 = 2R_s \left[\frac{L_d n_p \omega_m}{R_c} - \frac{2T_e \left(L_d - L_q\right)}{3n_p \left(\lambda_{af} + i_{odr}(L_d - L_q)\right)^2} \right] \left[\frac{2T_e}{3n_p \left(\lambda_{af} + i_{odr}(L_d - L_q)\right)} + \frac{n_p \omega_m \left(\lambda_{af} + i_{odr} L_d\right)}{R_c} \right]$$

(3.25)

$$P_3 = -\frac{8\beta L_q^2 \omega_m^2 (L_d - L_q)}{9R_c \left(\lambda_{af} + i_{odr}(L_d - L_q)\right)^3} T_e^2$$

$$P_4 = \frac{2\beta L_d n_p^2 \omega_m^2 \left(\lambda_{af} + L_d i_{odr}\right)}{R_c}$$

(3.26)

First simplify the expression for P1

$$P_1 = 2R_s \frac{2L_q T_e \omega_m \left(L_d - L_q\right)}{3R_c \left(\lambda_m + i_{odr}(L_d - L_q)\right)^2} i_{od}$$
$$-2R_s \frac{2L_q T_e \omega_m \left(L_d - L_q\right)}{3R_c \left(\lambda_m + i_{odr}(L_d - L_q)\right)^2} \frac{2L_q T_e \omega_m}{3R_c \left(\lambda_m + i_{odr}(L_d - L_q)\right)} \tag{3.27}$$
$$+2R_s i_{odr} - 2R_s \frac{2L_q T_e \omega_m}{3R_c \left(\lambda_m + i_{odr}(L_d - L_q)\right)}$$

Then

$$P_1 = \frac{4R_s L_q T_e \omega_m \left(L_d - L_q\right) i_{odr}}{3R_c \left(\lambda_m + i_{odr}(L_d - L_q)\right)^2} - \frac{8R_s L_q^2 T_e^2 \omega_m^2 \left(L_d - L_q\right)}{9R_c^2 \left(\lambda_m + i_{odr}(L_d - L_q)\right)^3}$$
$$+2R_s i_{od} - \frac{4R_S L_q T_e \omega_m}{3R_c \left(\lambda_m + i_{odr}(L_d - L_q)\right)} \tag{3.28}$$

Now simplify expression for P2

$$P_2 = 2R_S \left[\frac{L_d n_p \omega_m}{R_C} - \frac{2T_e \left(L_d - L_q\right)}{3n_p \left(\lambda_m + i_{odr}(L_d - L_q)\right)^2}\right]\left[\frac{2T_e}{3n_p \left(\lambda_m + i_{odr}(L_d - L_q)\right)} + \frac{n_p \omega_m \left(\lambda_m + i_{odr} L_d\right)}{R_C}\right] \tag{3.29}$$

$$P_2 = 2R_s \frac{L_d n_p \omega_m}{R_c} \frac{2T_e}{3n_p \left(\lambda_m + i_{odr}(L_d - L_q)\right)} + 2R_s \frac{L_d n_p \omega_m}{R_c} \frac{n_p \omega_m \left(\lambda_m + i_{odr} L_d\right)}{R_c}$$
$$-2R_s \frac{2T_e \left(L_d - L_q\right)}{3n_p \left(\lambda_m + i_{odr}(L_d - L_q)\right)^2} \frac{2T_e}{3n_p \left(\lambda_m + i_{odr}(L_d - L_q)\right)}$$
$$-2R_s \frac{2T_e \left(L_d - L_q\right)}{3n_p \left(\lambda_m + i_{odr}(L_d - L_q)\right)^2} \frac{n_p \omega_m \left(\lambda_m + i_{odr} L_d\right)}{R_c} \tag{3.30}$$

Then

$$P_2 = \frac{4R_s L_d \omega_m}{3R_c} \frac{T_e}{\left(\lambda_m + i_{odr}(L_d - L_q)\right)} + \frac{2R_s L_d n_p^2 \omega_m^2}{R_c^2}\left(\lambda_m + i_{odr} L_d\right) - \frac{8R_s\left(L_d - L_q\right)}{9n_p^2\left(\lambda_m + i_{odr}(L_d - L_q)\right)^3} T_e^2 - \frac{4R_s T_e\left(L_d - L_q\right)\omega_m\left(\lambda_m + i_{odr} L_d\right)}{3R_c\left(\lambda_m + i_{odr}(L_d - L_q)\right)^2} \tag{3.31}$$

Then the sum of P1 and P2 is

$$\begin{aligned} P_1 + P_2 = {} & \frac{4R_s L_q \omega_m\left(L_d - L_q\right) i_{odr}}{3R_c\left(\lambda_m + i_{odr}(L_d - L_q)\right)^2} T_e - \frac{8R_s L_q^2 \omega_m^2\left(L_d - L_q\right)}{9R_c^2\left(\lambda_m + i_{odr}(L_d - L_q)\right)^3} T_e^2 \\ & + 2R_s i_{odr} - \frac{4R_S L_q \omega_m}{3R_c\left(\lambda_m + i_{odr}(L_d - L_q)\right)} T_e \\ & + \frac{4R_s L_d \omega_m}{3R_c\left(\lambda_m + i_{odr}(L_d - L_q)\right)} T_e + \frac{2R_s L_d n_p^2 \omega_m^2}{R_c^2}\left(\lambda_m + i_{odr} L_d\right) \\ & - \frac{8R_s\left(L_d - L_q\right)}{9n_p^2\left(\lambda_m + i_{odr}(L_d - L_q)\right)^3} T_e^2 - \frac{4R_s\left(L_d - L_q\right)\omega_m\left(\lambda_m + i_{odr} L_d\right)}{3R_c\left(\lambda_m + i_{odr}(L_d - L_q)\right)^2} T_e \end{aligned} \tag{3.32}$$

Then

$$\begin{aligned} P_1 + P_2 = {} & -\frac{8R_s L_q^2 \omega_m^2\left(L_d - L_q\right)}{9R_c^2\left(\lambda_m + i_{odr}(L_d - L_q)\right)^3} T_e^2 - \frac{8R_s\left(L_d - L_q\right)}{9n_p^2\left(\lambda_m + i_{odr}(L_d - L_q)\right)^3} T_e^2 \\ & + \frac{4R_s L_q \omega_m\left(L_d - L_q\right) i_{odr}}{3R_c\left(\lambda_m + i_{odr}(L_d - L_q)\right)^2} T_e - \frac{4R_s L_q \omega_m}{3R_c\left(\lambda_m + i_{odr}(L_d - L_q)\right)} T_e \\ & + \frac{4R_s L_d \omega_m}{3R_c\left(\lambda_m + i_{odr}(L_d - L_q)\right)} T_e - \frac{4R_s\left(L_d - L_q\right)\omega_m\left(\lambda_m + i_{odr} L_d\right)}{3R_c\left(\lambda_m + i_{odr}(L_d - L_q)\right)^2} T_e \\ & + 2R_s i_{odr} + \frac{2R_s L_d n_p^2 \omega_m^2}{R_c^2}\left(\lambda_m + i_{odr} L_d\right) \end{aligned} \tag{3.33}$$

Then

$$P_1+P_2=-T_e^2\frac{8R_s\left(L_d-L_q\right)}{9\left(\lambda_m+i_{odr}(L_d-L_q)\right)^3}\left[\frac{L_q^2\omega_m^2}{R_c^2}+\frac{1}{n_p^2}\right]+2R_si_{odr}+\frac{2R_sL_dn_p^2\omega_m^2}{R_c^2}\left(\lambda_m+i_{odr}L_d\right)$$
$$+T_e\frac{4R_s}{3R_c}\left[\frac{L_q\omega_m\left(L_d-L_q\right)i_{odr}}{\left(\lambda_m+i_{odr}(L_d-L_q)\right)^2}+\frac{\left(L_d-L_q\right)\omega_m}{\left(\lambda_m+i_{odr}(L_d-L_q)\right)}-\frac{\left(L_d-L_q\right)\omega_m\left(\lambda_m+i_{odr}L_d\right)}{\left(\lambda_m+i_{odr}(L_d-L_q)\right)^2}\right] \tag{3.34}$$

Now show that the second term disappear due to

$$\Rightarrow\frac{L_q\omega_m\left(L_d-L_q\right)i_{od}}{\left(\lambda_m+i_{od}(L_d-L_q)\right)^2}+\frac{\left(L_d-L_q\right)\omega_m}{\left(\lambda_m+i_{od}(L_d-L_q)\right)}-\frac{\left(L_d-L_q\right)\omega_m\left(\lambda_m+i_{od}L_d\right)}{\left(\lambda_m+i_{od}(L_d-L_q)\right)^2}$$
$$=\frac{L_q\omega_m\left(L_d-L_q\right)i_{od}+\left(L_d-L_q\right)\omega_m\left(\lambda_m+i_{od}(L_d-L_q)\right)-\left(L_d-L_q\right)\omega_m\left(\lambda_m+i_{od}L_d\right)}{\left(\lambda_m+i_{od}(L_d-L_q)\right)^2}$$
$$=\frac{\omega_m\left(L_d-L_q\right)\left(L_qi_{od}+\lambda_m+i_{od}(L_d-L_q)-\lambda_m-i_{od}L_d\right)}{\left(\lambda_m+i_{od}(L_d-L_q)\right)^2}$$
$$=\frac{\omega_m\left(L_d-L_q\right)\left(L_qi_{od}+i_{od}(L_d-L_q)-i_{od}L_d\right)}{\left(\lambda_m+i_{od}(L_d-L_q)\right)^2}=0 \tag{3.35}$$

Then

$$P_1+P_2=-T_e^2\frac{8R_s\left(L_d-L_q\right)}{9\left(\lambda_m+i_{od}(L_d-L_q)\right)^3}\left[\frac{L_q^2\omega_m^2}{R_c^2}+\frac{1}{n_p^2}\right]$$
$$+2R_si_{od}+\frac{2R_sL_dn_p^2\omega_m^2}{R_c^2}\left(\lambda_m+i_{od}L_d\right) \tag{3.36}$$

and

$$P_3+P_4=-\frac{8\beta L_q^2\omega_m^2(L_d-L_q)}{9R_c\left(\lambda_m+i_{odr}(L_d-L_q)\right)^3}T_e^2+\frac{2\beta L_dn_p^2\omega_m^2\left(\lambda_m+L_di_{odr}\right)}{R_c} \tag{3.37}$$

Finally

$$P_1+P_2+P_3+P_4 = -T_e^2\frac{8R_s\left(L_d-L_q\right)}{9\left(\lambda_m+i_{odr}(L_d-L_q)\right)^3}\left(\frac{L_q^2\omega_m^2}{R_c^2}+\frac{1}{n_p^2}\right)-\frac{8\beta L_q^2\omega_m^2(L_d-L_q)}{9R_c\left(\lambda_m+i_{odr}(L_d-L_q)\right)^3}T_e^2 +2R_S i_{od}+\frac{2R_s L_d n_p^2\omega_m^2}{R_c^2}\left(\lambda_m+i_{odr}L_d\right)+\frac{2\beta L_d n_p^2\omega_m^2\left(\lambda_m+L_d i_{od}\right)}{R_C} = 0 \quad (3.38)$$

AB-T²C=0 format is used for the novel method in this study

The abovementioned combined MTPA/ME control method is complex and offers no indication of how it relates to the ME control method for real-time implementation, in fact, it appears to be a totally different strategy. However, this equation can be brought to a similar view to that of (3.15) via a subsequent derivation of traditional ME algorithm by slightly modifying A and C. This makes upgrading ME control algorithm to combined MTPA/ME in a simple way, is explained belove.

For the derivations in the proposed method, the copper loss and the core loss equations are recalled in (3.39). The fictious electrical power loss in (3.16) can be expressed as in (3.40) by substituting (3.39). In order to achieve the correct equation form to determine the minimum power loss point, the partial differentiation of the fictitious power loss with respect to the d axis current in (3.41) can be equated to zero as in (3.42). The final version of this equation is the AB-T^2C=0 form (3.43).

$$W_{cu} = \frac{3}{2} R_s \left[\begin{array}{l} i_{odr}^2 + 2 i_{odr} \dfrac{-\omega_r L_q}{R_c} \dfrac{T_e}{n_p \left(\lambda_{af} + \left(L_d - L_q \right) i_{odr} \right)} \\ + \left(\left(\dfrac{-\omega_r L_q}{R_c} \right)^2 + 1 \right) \dfrac{T_e^2}{n_p^2 \left(\lambda_{af} + \left(L_d - L_q \right) i_{odr} \right)^2} \\ + 2 \dfrac{T_e}{n_p \left(\lambda_{af} + \left(L_d - L_q \right) i_{odr} \right)} \dfrac{\omega_r (\lambda_{af} + L_d \, i_{odr})}{R_c} + \dfrac{\omega_r^2 (\lambda_{af} + L_d \, i_{odr})^2}{R_c^2} \end{array} \right]$$

$$W_{fe} = (3/2) R_c \left[\left(\frac{\omega_r L_q}{R_c} \right)^2 \left(\frac{T_e}{n_p \left(\lambda_{af} + \left(L_d - L_q \right) i_{odr} \right)} \right)^2 + \left(\frac{\omega_r \left(\lambda_{af} + L_d \, i_{odr} \right)}{R_c} \right)^2 \right]$$

(3.39)

$$W_f = \left(\frac{3}{2} \right) \left[\begin{array}{l} R_s \left(i_{odr} \right)^2 + \left(\left(R_s + \beta R_c \right) \left(\dfrac{\omega_r L_q}{R_c} \right)^2 + R_s \right) \left(\dfrac{T_e}{n_p \left(\lambda_{af} + \left(L_d - L_q \right) i_{odr} \right)} \right)^2 \\ + 2 R_s \dfrac{\omega_r T_e}{R_c n_p} + \left(R_s + \beta R_c \right) \left(\dfrac{\omega_r (\lambda_{af} + L_d \, i_{odr})}{R_c} \right)^2 \end{array} \right]$$

(3.40)

$$\frac{\delta W_f}{\delta i_{odr}} = \frac{3}{2} \left[\begin{array}{l} 2 R_s \left(i_{odr} \right) + \left(\left(R_s + \beta R_c \right) \left(\dfrac{\omega_r L_q}{R_c} \right)^2 + R_s \right) \left(\dfrac{T_e}{n_p} \right)^2 \left(\dfrac{-2 \left(L_d - L_q \right)}{\left(\lambda_{af} + \left(L_d - L_q \right) i_{odr} \right)^3} \right) \\ + \left(R_s + \beta R_c \right) \dfrac{\omega_r^2}{R_c^2} 2 L_d \left(\lambda_{af} + L_d \, i_{odr} \right) \end{array} \right]$$

(3.41)

Then

$$\begin{array}{l} n_p^2 \left(R_s R_c^2 \left(i_{odr} \right) + \left(R_s + \beta R_c \right) \omega_r^2 L_d \left(\lambda_{af} + L_d \, i_{odr} \right) \right) \left(\lambda_{af} + \left(L_d - L_q \right) i_{odr} \right)^3 \\ = \left(\left(R_s + \beta R_c \right) \left(\omega_r L_q \right)^2 + R_s R_c^2 \right) \left(L_d - L_q \right) T_e^2 \end{array}$$

(3.42)

Writing the equation in the format of $AB = CT^2$,then

$$A = (9/4)n_p^2\left(R_s {R_c}^2\left(i_{odr}\right) + \left(R_s + \beta R_c\right){\omega_r}^2 L_d\left(\lambda_{af} + L_d\, i_{odr}\right)\right)$$
$$B = \left(\lambda_{af} + \left(L_d - L_q\right) i_{odr}\right)^3 \qquad (3.43)$$
$$C = \left(\left(R_s + \beta R_c\right)\left(\omega_r L_q\right)^2 + R_s {R_c}^2\right)\left(L_d - L_q\right)$$

Figure 3.11 illustrates the substantial differences between reformatting of the fourth order polynomial equation of the fictitious power loss differentiation based on P1+P2+P3+P4=0 proposed in [7] and based on AB-T²C=0 in this study [8]. The fictitious power loss differentiation curve is shown in Figure 3.11a, which is produced using the Matlab coding in Appendix E, and Figure 3.11b, which was produced using the Matlab coding in Appendix F, for P1+P2+P3+P4=0. As shown in Figure 3.11a, the broken curve will result in some robustness issues during real-time operation. However, the proposed method's curve in Figure 3.11b is continuous, providing linear control features not only in ideal but also in unknown settings, and hence it is favoured in this study.

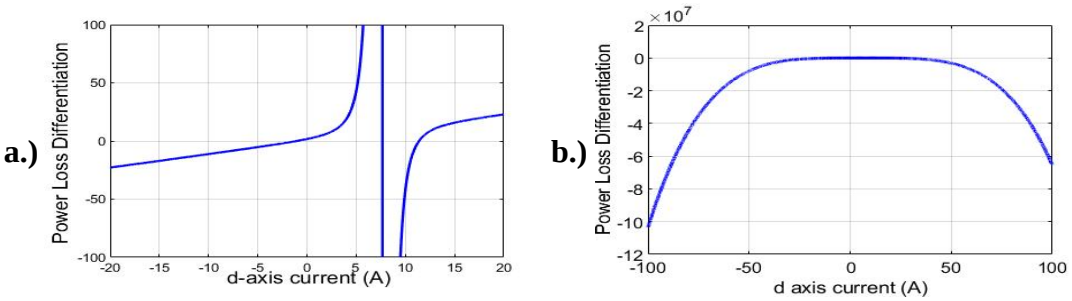

Figure 3.11 The Power loss differentiation curve of the fictious power loss
a.) Based on $P_1+P_2+P_3+P_4$ formatting
b.) Based on $AB= T^2C$ formatting

The suggested combined MTPA/ME control strategy with AB-T²C=0 formatting and the method provided in [7] in P1+P2+P3+P4=0 formatting are simulated using Matlab Simulink control models based on the FOC control concept (Figure 3.10) Appendix G

contains the views of Matlab Simulink models. Figure 3.13 shows the results of the model developed with AB-T²C=0, whereas Figure 3.14 shows the results of the model created with P1+P2+P3+P4=0. Figure 3.5 shows the velocity and load torque references for both models. The moment of inertia is defined as what it is in ideal conditions $J = 0.004\ Nm^2$. As shown in Figure 3.12, β parameter is defined as a constant value of 0.5, which provides an optimal operating solution in the middle of the MTPA and ME control trajectories. Table 3.1 describes the IPMSM parameters.

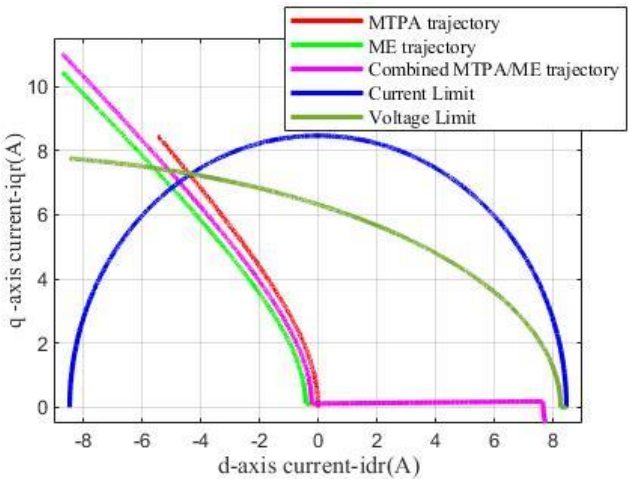

Figure 3.12 MTPA, ME and β=0.5 trajectories

In both Figure 3.13 and Figure 3.14, it is clear that both methods exhibit the identical behaviour in ideal conditions for torque, velocity, d and q-axis voltage/current responses. The results reveal a similar pattern with different values to the results shown in Figure 3.8 and Figure 3.9, which exhibit MTPA and ME simulation results, respectively. As a result, the suggested combination technique is easily adaptable to existing industrial IPMSM drives.

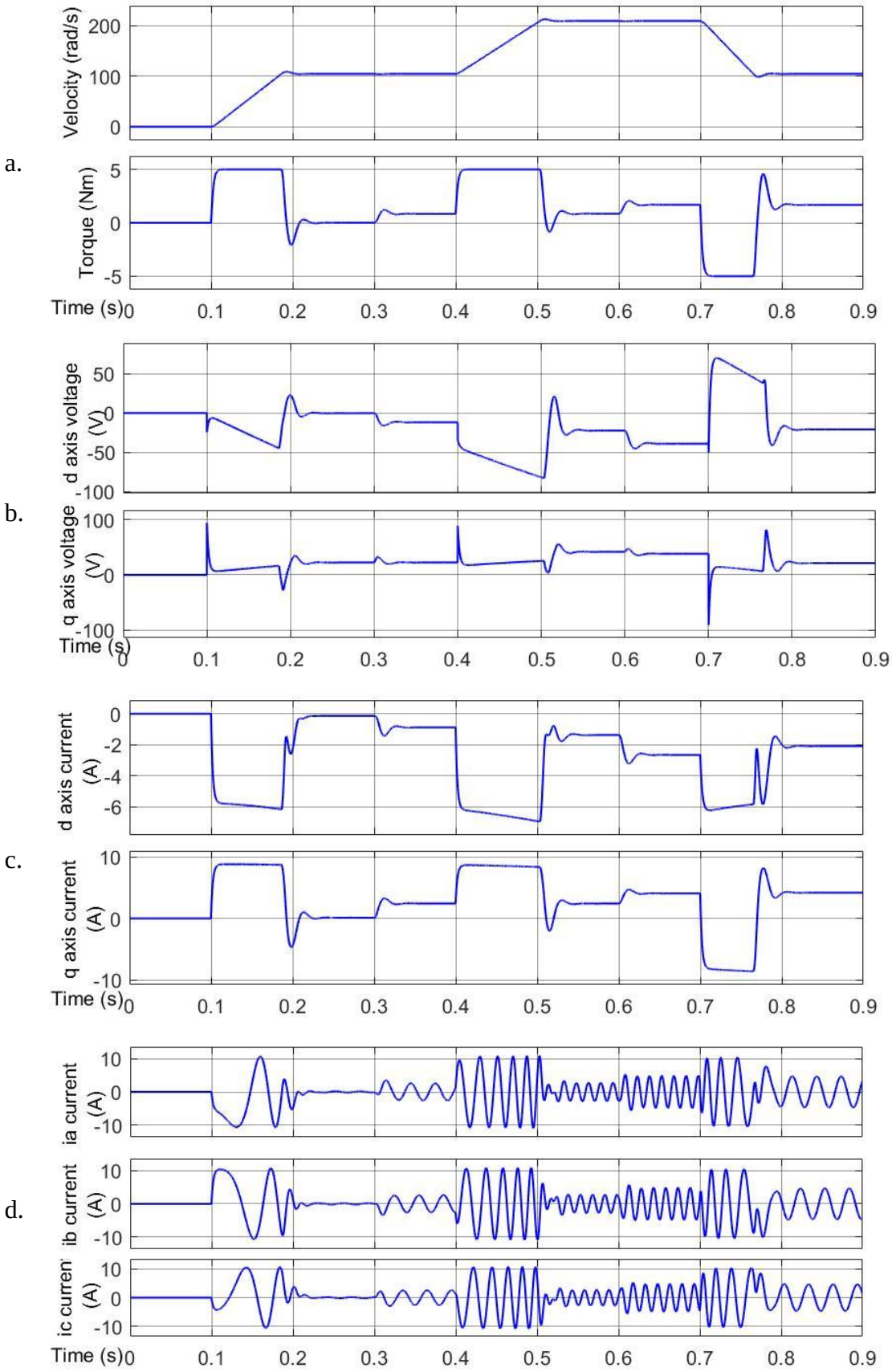

Figure 3.13 Combined MTPA/ME control first method

a. Velocity and torque response
b. d, q axes voltages
c. d, q axes currents
d. a, b, c phase currents

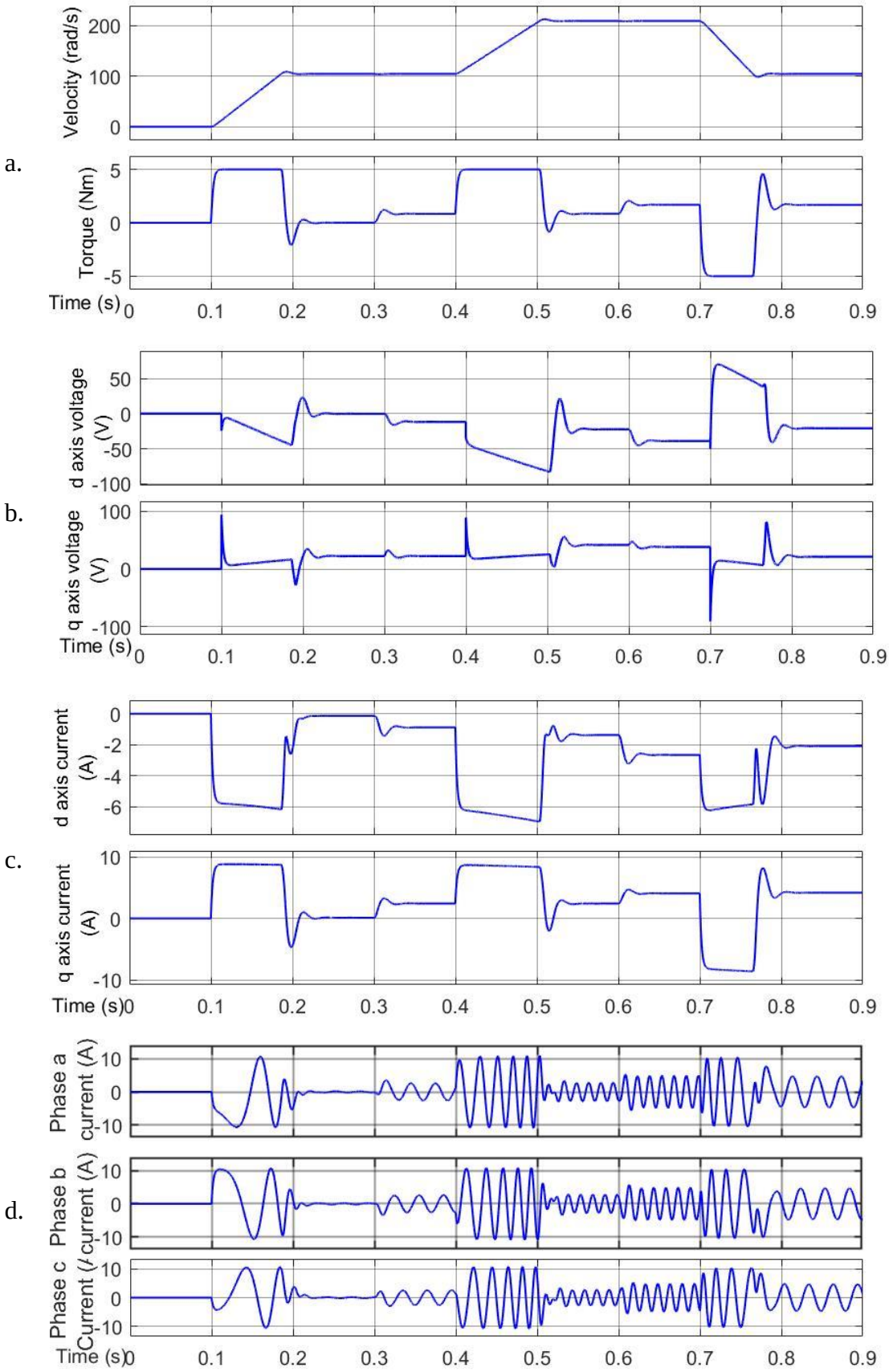

Figure 3.14 Combined MTPA/ME Control second method

a. Velocity and torque response
b. d, q axes voltages
c. d, q axes currents
d. a, b, c phase currents

3.6.1. Combined Steady-State ME and Dynamic MTPA Control Implementation

Figure 3.15 shows interior view of the decision algorithm in the β generator block. During transients, the dynamic velocity error $\left(\omega_m^* - \omega_m\right)$ is greater than zero. The k_p proportional gain parameter is used to magnify the velocity error, which acts to adjust the algorithm's sensitivity. The absolute value of the k_p gain block output is subtracted from the maximum value of the β parameter, which is defined as 1 in this study. k_p should be chosen so that the saturation block has a value of zero for transients and one for steady-state operations. Since the β generator output is zero, β =0, during transients, MTPA control will be activated; however, during steady states ($\omega_m^* = \omega_m$), β =1 and the ME control strategy will be utilised. Because of an inherent feature of the PI controller's integral component, β changes smoothly in [0,1] ($0 \leq \beta \leq 1$). Hence, a smooth transition between MTPA and ME control approaches is given. The nonlinear characteristics of switching between two algorithms, as seen in [40], are avoided.

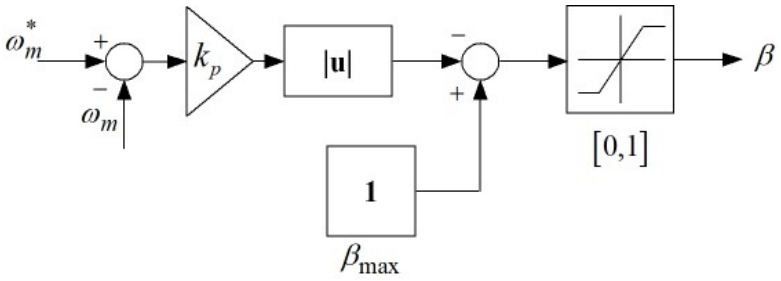

Figure 3.15 Decision algorithm in the β generator

The results of the control model designed in Matlab Simulink (Appendix G) for the proposed technique and those for the combined method provided in [7] are shown in Figure 3.13 and Figure 3.14, respectively, for constant $\beta = 0.5$. Figure 3.16 shows the results for the updated model with proposed β generator demonstrated in Figure 3.15. The most noticeable difference can be seen graphically in the d- and q- axis current, the combined method adapts to the MTPA algorithm during torque and velocity transients and to ME during steady states.

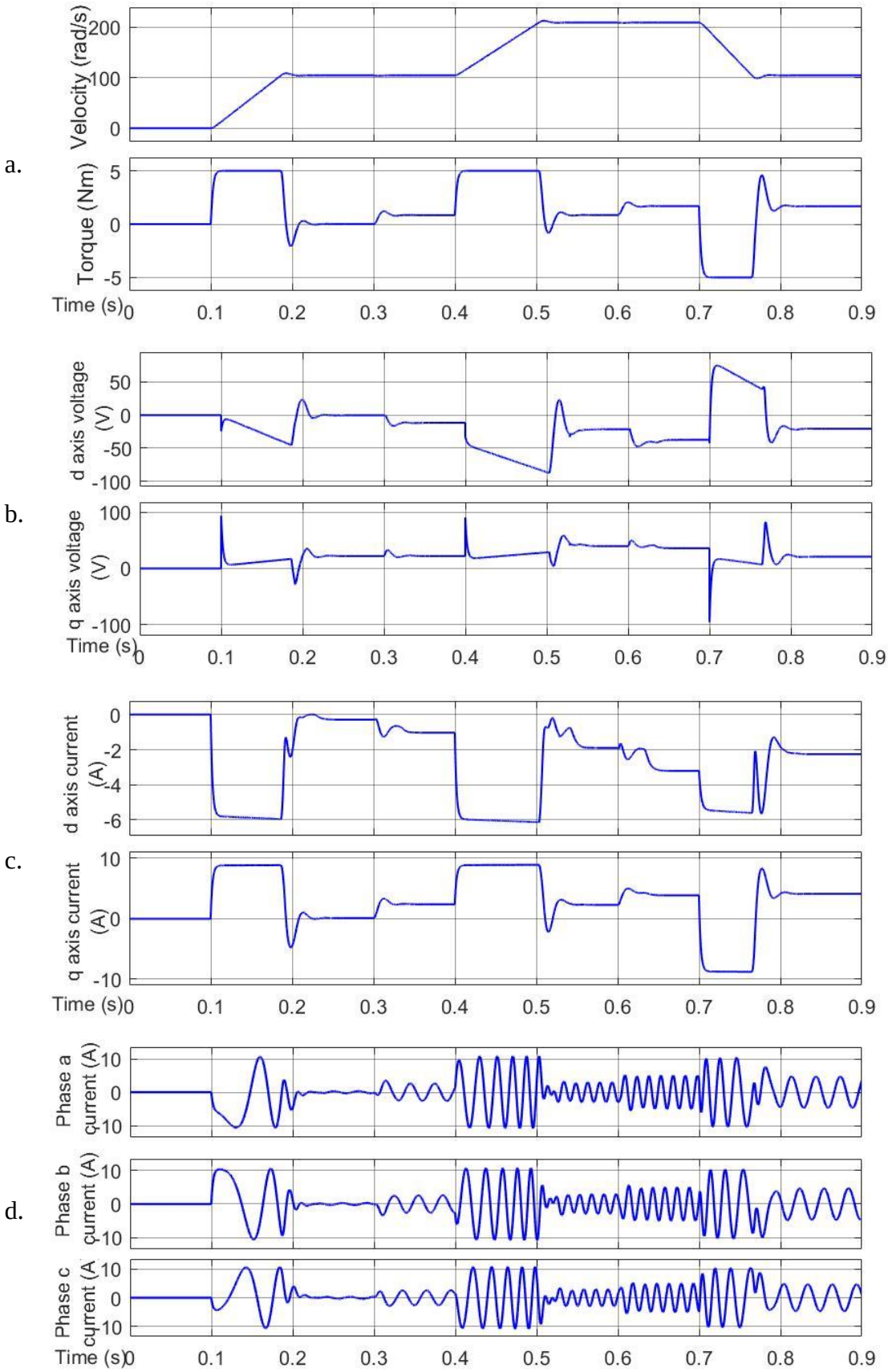

Figure 3.16 Combined MTPA/ME Control third method

a. Velocity and torque response
b. d, q axes voltages
c. d, q axes currents
d. a, b, c phase currents

3.7. Conclusions

The purpose of this chapter is to build a control concept for IPMSM drives to satisfy the performance requirements of an EV propulsion system. The proposed method is enhanced considering the terms used in EV marketing like 'time for 0 to 60 miles' and 'long cruise distance per charge'.

The control algorithms used in industrial IPMSM drives today are mostly based on the ZDAC control approach, which is simple to develop and more robust due to its linear control features. However, the reluctance torque is disregarded, hence it does not deliver the entire torque capabilities of IPMSM. Furthermore, since it is unable to adapt to the nonlinear characteristics of electrical power loss, ZDAC control cannot deliver an energy efficient control performance. To maximize the torque capabilities of the motor, MTPA control strategy was presented, and ME control was proposed to minimize electrical power loss. These approaches provide improved performance measures, particularly for their intended objectives. However, due to the instantaneous variation in operating circumstances in an application like EV, they are still insufficient.

The proposed algorithm in this chapter is based on combining MTPA and ME control approaches by introducing the fictious electrical power loss based on β optimisation parameter into ME algorithm. Therefore, the proposed algorithm has completely same flow with ME control, that is to say, the proposed algorithm can be easily implemented into the current industrial IPMSM drives by simply introducing the fictious electrical power loss into the software, no hardware changes and additional computational costs

are required. Thus, the dilemma which control approach to choose is replaced by how to optimise the combined approach.

β optimisation parameter is set to vary between 0 and 1 ($0 \le \beta \le 1$): 0 during transient operations (such as EV acceleration or deceleration) and 1 during steady state operations (to increase cruise distance per charge). The smooth transition between two approaches is made possible by the comparatively modest variation of angular velocity due to the moment of inertia (as the β generator's input is connected to the dynamic angular velocity error) and k_p proportional gain parameter used in β generator. As a result, any additional nonlinearities and transients may appear due to the combined algorithm are removed.

The simulation results for ZDAC (Figure 3.7), MTPA (Figure 3.8), ME (Figure 3.9), combined MTPA/ME with constant β=0.5 (Figure 3.13 and Figure 3.14) and energy efficient and transients optimal control method for IPMSM drives (combined MTPA/ME with β generator in Figure 3.16) shows similar pattern in ideal conditions, demonstrating that the proposed method can be considered as an alternative to existing energy efficient control methods, especially for variating operating circumstances. The proposed method is also superior to existing combined methods. Because it does not introduce any nonlinearities due to switching behaviour, any extra computational burden or does not cause any possible unstable operation.

.

CHAPTER 4. NONLINEAR OPTIMAL CONTROL DESIGN FOR IPMSM DRIVES

4.1. Introduction

Despite the universe's nonlinear structure, man-made applications are typically created on the basis of linear aspects due to the necessity for simple and robust instruments to ease human living. From the same perspective, the AC motor control area is frequently built on linearized motor models. Nonlinear aspects of the environment or the motor, on the other hand, degrade precision motor control quality, particularly in variable speed applications.

The dynamic mathematical IPMSM model described in Section 3.2 of Chapter 3 is a conventional motor model based on linearized motor features with constant parameters. As a result, any nonlinear characteristics sourced by the motor, or the environment are classed as 'uncertainty' or 'disturbance'. A research area in the field of motor control is explaining these uncertainties one by one and providing solutions to eliminate the disturbances.

Many studies are focused to determining precise motor parameters and updating motor models on the fly in order to improve motor control accuracy. The majority of these proposed identifying the parameters offline and updating the motor model with LUTs. These methods result in time-consuming and one-of-a-kind solutions for individual motors. Even though the motor type and control model are same, the engineering

efforts should be redone for any other motor. Others propose using online parameter identification methods to eliminate the disturbances. The online methods for parameter identification result in extra computing cost and complex control structure due to a number of elements such as temperature variation, magnetic saturation, aging factor, and so on. This may increase sensitivity but decrease robustness.

To enhance the robustness of traditional motor control systems without increasing the details of the model parameters in the control structure, parameter independent methods are proposed. These methods primarily focus on the variation and derivation of the velocity error and eliminate any uncertainties by maintaining these errors within a previously determined margin. As a result, the approach provides intrinsic stability without the need for any additional motor parameter updates.

This chapter introduces a nonlinear optimal IPMSM drive based on the Linear Quadratic Regulator (LQR) with integral actions and Krasovskiy's criterion to improve the robustness of the traditional FOC with energy efficient optimisation methods (ZDAC, MTPA, ME, and Combined MTPA/ME optimisation approaches). The proposed nonlinear optimal control method is considered as parameter independent. The conventional FOC has three control loops, including two internal d, q-axis current control loops and one external velocity loop, as was discussed in Chapter 3. The method suggests replacing PI controllers in each loop with Linear Quadratic Regulators (LQR). This results in PI velocity and currents controllers with optimal gain parameters. However, the LQR gain parameters should be updated whenever the operating point variates. In the literature, adaptive solutions based on LUTs are proposed for updating the controller parameters. In this study, the deviations of the controllers' gain parameters are considered as new control inputs. Then the LQR design procedure is repeated but with generalised work of Krasovkiy's criterion which

is integrated into the controllers as nonlinear parts. Krasovskiy's criterion offers an automated optimisation without adjusting default gain parameters. As a result, the nonlinear optimal velocity and currents controllers consisting of linear and nonlinear parts provide a robust motor control in a specified control range. Thus, industrial IPMSM drives' robustness can be improved without any hardware modifications but simply updating the controller-related component of the software.

The chapter progresses from Section 4.2's explanation for the details of the nonlinear optimal controller design to Section 4.3 and Section 4.4's evaluation of the proposed IPMSM drive with consideration to energy-efficient optimisation methods in simulations on Matlab Simulink and conclusions.

4.2. Nonlinear Optimal Controller Design

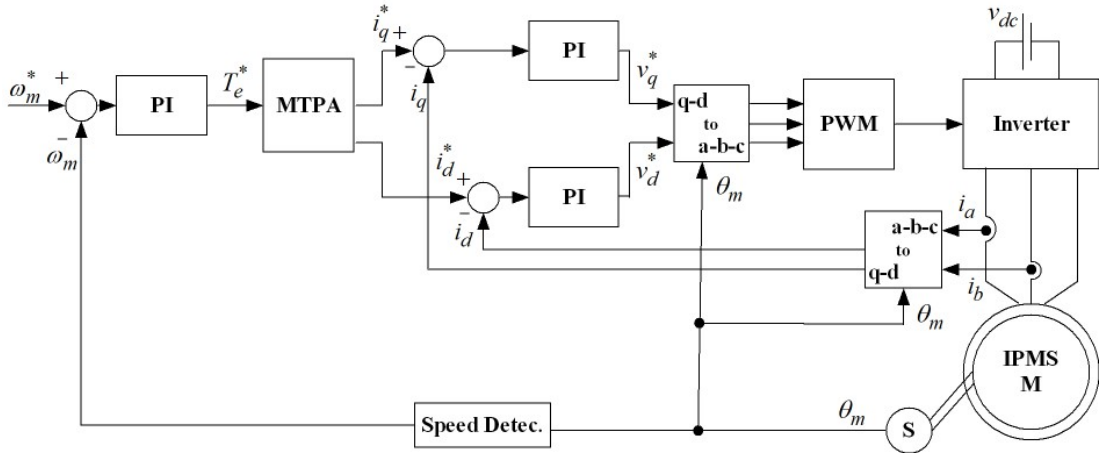

Figure 4.1 Conventional FOC control scheme with MTPA energy-efficient optimisation method

Figure 4.1 recalls the traditional FOC block diagram for IPMSM drives. A PI controller with constant gain parameters is used in each control loop (one external velocity and two internal d, q-axis current control loops). This linear control technique performs well under ideal circumstances, but it falls short in real-time operations with random uncertainty. Each PI controller is thus replaced with a nonlinear optimal

controller. As a result, it aims to improve the robustness of industrial IPMSM drives without modifying the hardware. The conventional FOC is used for benchmarking. The motor parameters remained as in Chapter 3. The gain parameters of the controllers are recalled in Table 4.1.

Table 4.1 The parameters for traditional PI controllers

	ki	***kp***
d-axis controller	285	4.36
q-axis controller	285	11.4
velocity controller (ω_m)	125	1

For better understanding, a symbolic internal view of the classical PI controllers are also demonstrated in Figure 4.2. k_i *and* k_p demonstrate the gain parameters for integral and proportional actions, respectively.

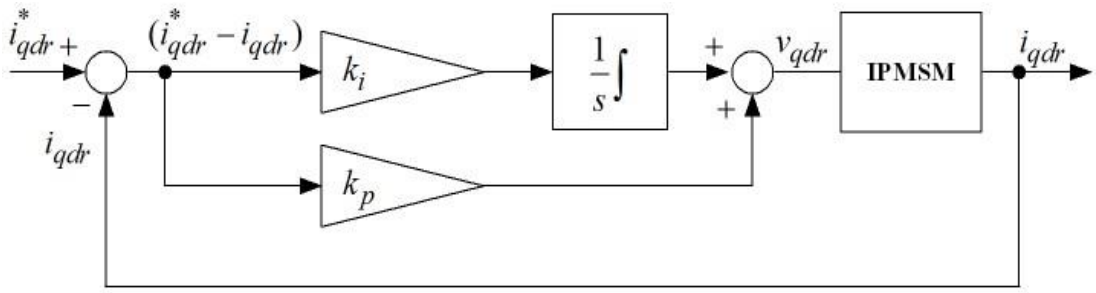

Figure 4.2 The Block Diagram of the PI Controller for d- q-axis currents

PI controllers in traditional FOC control scheme are replaced with nonlinear optimal controllers depicted in Figure 4.3. The proposed controllers consist of linear and nonlinear components.

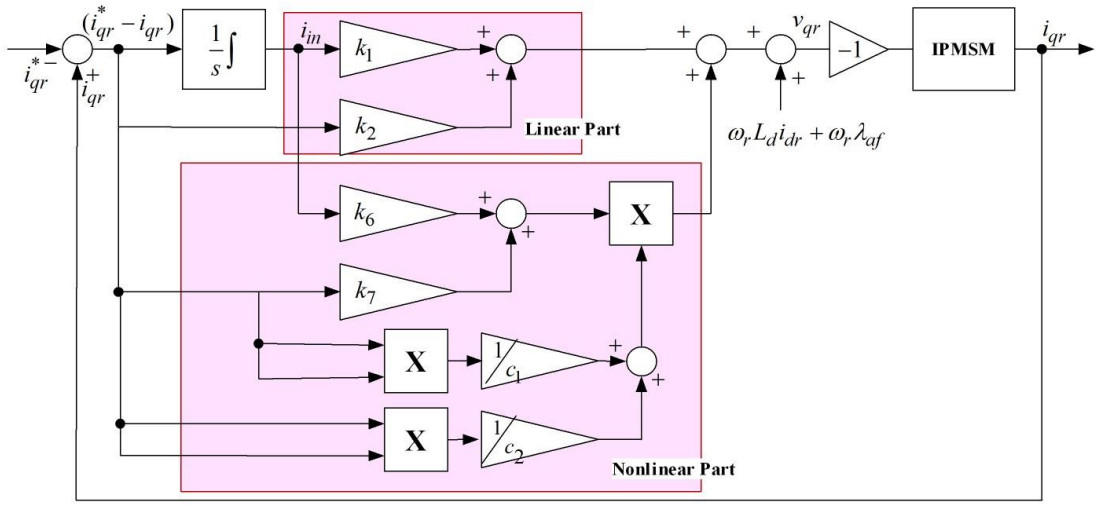

Figure 4.3 The nonlinear optimal controller block diagram for q-axis current

The linear component is basically a PI controller with optimal gain parameters, which actually has linear characteristics. The optimal gain parameters are obtained with well-known Linear Quadratic Regulator procedure, which also can be easily yielded with 'lqr' command in Matlab. Since the gain parameters should be updated according to operating circumstances, extensive LUTs or complicated adaptive solutions should be included into the real time control scheme. Instead, it is suggested to integrate a nonlinear component based on generalised work of Krasovskiy's criterion. Thus, the controller outputs are optimised without any update in motor or controller parameters. Same procedure is carried out for all three controllers.

4.2.1. Linear Component Design of Nonlinear Optimal Controller

Well-known Linear Quadratic Regulator Procedure is carried out for obtaining the optimal gain parameters shown as below

Step 1. Define the state space form of IPMSM

Step 2. Operate the functional Bellman equation on LQR cost function

Step 3. Include Hamilton-Jacobi-Bellman equation in closed form and solve Algebraic Riccati equations

Step 4. Define proper optimal gain parameters via iterative calculations with different Q and R matrices

The standard state space form is shown below

$$\dot{\mathbf{X}} = \mathbf{A}\mathbf{X} + \mathbf{B}u + \mathbf{F} \tag{4.1}$$

X denotes the vector of state variables,

u denotes the corresponding control input

F denotes the vector of disturbances

The equivalent differential equations in the dynamic mathematical IPMSM model for all three control loops are recalled in the eqn. (4.2)

$$\begin{cases} L_d\left(di_d/dt\right) + R_s i_d = v_d + n_p \omega_m L_q i_q \\ L_q\left(di_q/dt\right) + R_s i_q = v_q - n_p \omega_m L_d i_d - n_p \omega_R \lambda_{af} \\ \left(d\omega_m/dt\right) = \left(T_e - T_f - B\omega_m - T_l\right)/J \end{cases} \tag{4.2}$$

(It is worth to indicate that the subscript 'r' for d-, q- axis currents/voltages denoting rotational reference frame will be dropped hereafter for the sake of the simplicity of the formulations. All d-, q- axis currents/voltages are defined in rotational reference frame in this chapter.)

Introducing the time constants as $T_{d,q} = L_{d,q} / R_s$, and $T_m = J / B$ then

$$\begin{cases} T_d \left(di_d / dt \right) + i_d = \left(v_d + n_p \omega_m L_q i_q \right) \Big/ R_s \\ T_q \left(di_q / dt \right) + i_q = \left(v_q - n_p \omega_m L_d i_d - n_p \omega_m \lambda_{af} \right) \Big/ R_s \\ T_m \left(d\omega_m / dt \right) + \omega_m = \left(\left(T_e - T_f - T_l \right) \Big/ B \right) \end{cases} \tag{4.3}$$

For a steady state operation, '01' denotes operating point 1 then

$$\begin{cases} i_{d01} = \left(v_{d01} + n_p \omega_{m01} L_{q01} i_{q01} \right) \Big/ R_s \\ i_{q01} = \left(v_{q01} - n_p \omega_{m01} L_{d01} i_{d01} - n_p \omega_{m01} \lambda_{af} \right) \Big/ R_s \\ \omega_{m01} = \left(T^*_{e01} - T_{f01} - T_{l01} \right) \Big/ B \end{cases} \tag{4.4}$$

However, transients may appear due to uncertainties in steady state operations. Transients are introduced into the steady state operation in eqn. (4.4) via perturbations as below

$$\begin{cases} \left(T_{d01} + \delta T_d \right) \dfrac{d\left(i_{d01} + \delta i_d \right)}{dt} + i_{d01} + \delta i_d = \dfrac{1}{R_S} \left(v_{d01} + \delta v_d + n_p \omega_{m01} \left(L_{q01} + \delta L_q \right) \left(i_{q01} + \delta i_q \right) \right) \\ \left(T_{q01} + \delta T_q \right) \dfrac{d\left(i_{q01} + \delta i_q \right)}{dt} + i_{q01} + \delta i_q = \dfrac{1}{R_S} \left(v_{q01} + \delta v_q - n_p \omega_{m01} \left(L_{d01} + \delta L_d \right) \left(i_{d01} + \delta i_d \right) - n_p \omega_{m01} \lambda_{af} \right) \\ \left(T_{l01} + \delta T_l \right) \dfrac{d\left(\omega_{m01} + \delta \omega_m \right)}{dt} + \omega_{m01} + \delta \omega_m = \dfrac{1}{F} \left(\left(T^*_{e01} + \delta T^*_e \right) - T_{f01} - \delta T_f - T_{l01} - \delta T_l \right) \end{cases} \tag{4.5}$$

Subtracting eqn.(4.4) from eqn.(4.5) and neglecting second order small variables then

$$\begin{cases} T_{d01}\dfrac{d\left(\delta i_d\right)}{dt}+\delta i_d=\dfrac{1}{R_s}\left(\delta v_d+n_p\omega_{m01}L_{q01}\delta i_q+n_p\omega_{m01}i_{q01}\delta L_q\right) \\ T_{q01}\dfrac{d\left(\delta i_q\right)}{dt}+\delta i_q=\dfrac{1}{R_s}\left(\delta v_q-n_p\omega_{m01}L_{d01}\delta i_d-n_p\omega_{m01}i_{d01}\delta L_d\right) \\ T_{m01}\dfrac{d\left(\delta\omega_m\right)}{dt}+\delta\omega_m=\dfrac{1}{B}\left(-\delta T_f-\delta T_l\right) \end{cases} \tag{4.6}$$

The time integrals of dynamic errors in each loop are shown in eqn. (4.7) it is for adding integral action to the control dynamics to process steady state error as in Figure 4.3.

$$\begin{cases} i_{ind,q}=\int\left(i_{d,q}-i^*_{d,q}\right)dt \\ \omega_{in}=\int\left(\omega_m-\omega^*_m\right)dt \end{cases} \tag{4.7}$$

where "*" denotes the corresponding reference value. The derivative form of the steady state error in (4.7) is below

$$\begin{cases} di_{ind,q}/dt=i_{d,q}-i^*_{d,q} \\ d\omega_{in}/dt=\omega_m-\omega^*_m \end{cases} \tag{4.8}$$

If the perturbations are included into the differentiation of the steady state error in eqn. (4.8) then

$$\begin{cases} \left(d\delta i_{ind,q}/dt\right)=\delta i_{d,q}-\delta i^*_{d,q} \\ \left(d\delta\omega_{in}/dt\right)=\delta\omega_m-\delta\omega^*_m \end{cases} \tag{4.9}$$

The standard state space description in the form of eqn. (4.1) is defined in eqns. (4.10)-(4.13)

$$\mathbf{X} = \begin{bmatrix} x_1 & x_2 \end{bmatrix}^T = \begin{cases} \begin{bmatrix} \delta i_{ind} & \delta i_d \end{bmatrix}^T \\ \begin{bmatrix} \delta i_{inq} & \delta i_q \end{bmatrix}^T \\ \begin{bmatrix} \delta \omega_{in} & \delta \omega_m \end{bmatrix}^T \end{cases} \tag{4.10}$$

$$u = \begin{cases} \delta v_d \\ \delta v_q \\ \delta T_e^* \end{cases} \tag{4.11}$$

$$\mathbf{A} = \begin{bmatrix} 0 & 1 \\ 0 & a_1 \end{bmatrix} \rightarrow a_1 = \begin{cases} -1/T_{d01} \\ -1/T_{q01} \\ -1/T_{m01} \end{cases} \tag{4.12}$$

$$\mathbf{B} = \begin{bmatrix} 0 & b_1 \end{bmatrix}^T \rightarrow b_1 = \begin{cases} 1/(T_{d01} R_s) \\ 1/(T_{q01} R_s) \\ 1/(T_{m01} B) \end{cases} \tag{4.13}$$

$$\mathbf{F} = \begin{cases} \begin{bmatrix} -\delta i_d^* & n_p \omega_{m01} \left(L_{q01} \delta i_q + i_{q01} \delta L_q \right) \Big/ \left(T_{d01} R_s \right) \end{bmatrix}^T \\ \begin{bmatrix} -\delta i_q^* & -n_p \omega_{m01} \left(L_{d01} \delta i_d + i_{d01} \delta L_d \right) \Big/ \left(T_{q01} R_s \right) \end{bmatrix}^T \\ \begin{bmatrix} -\delta \omega_m^* & \left(-\delta T_f - \delta T_m \right) \Big/ \left(T_{m01} B \right) \end{bmatrix}^T \end{cases} \tag{4.14}$$

The cost function with two state space and one input variable is written as in eqn. (4.15) for step 2 of LQR procedure.

$$\min_{u} J = \int_{0}^{\infty} \left(\alpha_1 x_1^2 + \alpha_2 x_2^2 + cu^2 \right) dt \tag{4.15}$$

α_1, α_2, c are positive weighting parameters. According to functional Bellman equation for the linearised system based on eqns. (4.10)- (4.13), the cost function in eqn. (4.15) is written in eqn. (4.16) where 'V' represents Lyapunov function. Performing the minimisation procedure gives the optimal control solution in eqn. (4.18).

$$\min_{u} \left[\alpha_1 x_1^2 + \alpha_2 x_2^2 + cu^2 + \frac{\partial V}{\partial x_1}\left(0 \cdot x_1 + x_2 + 0 \cdot u\right) + \frac{\partial V}{\partial x_2}\left(0 \cdot x_1 + a_1 x_2 + b_1 u\right) \right] = 0 \tag{4.16}$$

$$\rightarrow 2cu + \left(\partial V / \partial x_2\right) b_1 = 0 \tag{4.17}$$

$$\rightarrow u = -\left(b_1 / 2c\right)\left(\partial V / \partial x_2\right) \tag{4.18}$$

As step 3 of LQR procedure, eqn. (4.18) is substituted into eqn. (4.16) then the equation of Hamilton-Jacobi-Bellman in closed form is obtained as below

$$\begin{aligned} &\alpha_1 x_1^2 + \alpha_2 x_2^2 + c\frac{b_1^2}{4c^2}\left(\frac{\partial V}{\partial x_2}\right)^2 + \frac{\partial V}{\partial x_1} x_2 + \frac{\partial V}{\partial x_2}\left(a_1 x_2 - \frac{b_1^2}{2c}\frac{\partial V}{\partial x_2}\right) = 0 \\ &\rightarrow \alpha_1 x_1^2 + \alpha_2 x_2^2 + \frac{\partial V}{\partial x_1} x_2 + \frac{\partial V}{\partial x_2} a_1 x_2 = -\frac{b_1^2}{4c}\left(\frac{\partial V}{\partial x_2}\right)^2 + \frac{\partial V}{\partial x_2}\frac{b_1^2}{2c}\frac{\partial V}{\partial x_2} \end{aligned} \tag{4.19}$$

$$\rightarrow \alpha_1 x_1^2 + \alpha_2 x_2^2 + \frac{\partial V}{\partial x_1} x_2 + \frac{\partial V}{\partial x_2} a_1 x_2 = \frac{b_1^2}{4c}\left(\frac{\partial V}{\partial x_2}\right)^2 \tag{4.20}$$

Selecting Lyapunov function in full quadratic form

$$V = k_{11}x_1^2 + 2k_{12}x_1x_2 + k_{22}x_2^2 \tag{4.21}$$

$k_{11},\ k_{12},\ k_{22}$ can be found via substitution of eqn. (4.21) into eqn. (4.20) or from the algebraic Riccati equation shown below

$$\mathbf{A}^T\mathbf{K} + \mathbf{K}\mathbf{A} - \mathbf{K}\mathbf{B}\mathbf{R}^{-1}\mathbf{B}^T\mathbf{K} + \mathbf{Q} = 0 \tag{4.22}$$

The components of algebraic Riccati equation in (4.22) are defined as

$$\mathbf{K} = \begin{bmatrix} k_{11} & k_{12} \\ k_{12} & k_{22} \end{bmatrix}, \mathbf{Q} = \begin{bmatrix} \alpha_1 & 0 \\ 0 & \alpha_2 \end{bmatrix}, \mathbf{R} = c \tag{4.23}$$

Now the derivations for solving the algebraic Riccati equation shown below

$$\rightarrow \begin{bmatrix} 0 & 0 \\ 1 & a_1 \end{bmatrix}\begin{bmatrix} k_{11} & k_{12} \\ k_{12} & k_{22} \end{bmatrix} + \begin{bmatrix} k_{11} & k_{12} \\ k_{12} & k_{22} \end{bmatrix}\begin{bmatrix} 0 & 1 \\ 0 & a_1 \end{bmatrix} - \begin{bmatrix} k_{11} & k_{12} \\ k_{12} & k_{22} \end{bmatrix}\begin{bmatrix} 0 \\ b_1 \end{bmatrix} c^{-1}\begin{bmatrix} 0 & b_1 \end{bmatrix}\begin{bmatrix} k_{11} & k_{12} \\ k_{12} & k_{22} \end{bmatrix} + \begin{bmatrix} \alpha_1 & 0 \\ 0 & \alpha_2 \end{bmatrix} = 0$$

$$\rightarrow \begin{bmatrix} 0 & 0 \\ k_{11} + a_1k_{12} & k_{12} + a_1k_{22} \end{bmatrix} + \begin{bmatrix} 0 & k_{11} + a_1k_{12} \\ 0 & k_{12} + a_1k_{22} \end{bmatrix} - \begin{bmatrix} k_{11} & k_{12} \\ k_{12} & k_{22} \end{bmatrix}\begin{bmatrix} 0 \\ b_1 \end{bmatrix} c^{-1}\begin{bmatrix} b_1k_{12} & b_1k_{22} \end{bmatrix} + \begin{bmatrix} \alpha_1 & 0 \\ 0 & \alpha_2 \end{bmatrix} = 0$$

$$\rightarrow \begin{bmatrix} 0 & k_{11} + a_1k_{12} \\ k_{11} + a_1k_{12} & k_{12} + a_1k_{22} + k_{12} + a_1k_{22} \end{bmatrix} - \begin{bmatrix} k_{11} & k_{12} \\ k_{12} & k_{22} \end{bmatrix}\begin{bmatrix} 0 \\ b_1 \end{bmatrix}\begin{bmatrix} \frac{b_1}{c}k_{12} & \frac{b_1}{c}k_{22} \end{bmatrix} + \begin{bmatrix} \alpha_1 & 0 \\ 0 & \alpha_2 \end{bmatrix} = 0$$

(4.24)

$$\rightarrow \begin{bmatrix} \alpha_1 & k_{11}+a_1k_{12} \\ k_{11}+a_1k_{12} & 2k_{12}+2a_1k_{22}+\alpha_2 \end{bmatrix} - \begin{bmatrix} k_{11} & k_{12} \\ k_{12} & k_{22} \end{bmatrix} \begin{bmatrix} 0 & 0 \\ \frac{b_1^2}{c}k_{12} & \frac{b_1^2}{c}k_{22} \end{bmatrix} = 0$$

$$\rightarrow \begin{bmatrix} \alpha_1 & k_{11}+a_1k_{12} \\ k_{11}+a_1k_{12} & 2k_{12}+2a_1k_{22}+\alpha_2 \end{bmatrix} = \begin{bmatrix} k_{11} & k_{12} \\ k_{12} & k_{22} \end{bmatrix} \begin{bmatrix} 0 & 0 \\ \frac{b_1^2}{c}k_{12} & \frac{b_1^2}{c}k_{22} \end{bmatrix} \tag{4.25}$$

$$\rightarrow \begin{bmatrix} \alpha_1 & k_{11}+a_1k_{12} \\ k_{11}+a_1k_{12} & 2k_{12}+2a_1k_{22}+\alpha_2 \end{bmatrix} = \begin{bmatrix} \frac{b_1^2}{c}k_{12}^2 & \frac{b_1^2}{c}k_{12}k_{22} \\ \frac{b_1^2}{c}k_{12}k_{22} & \frac{b_1^2}{c}k_{22}^2 \end{bmatrix}$$

$$\begin{cases} \alpha_1 = \dfrac{b_1^2}{c}k_{12}^2 \\ k_{11}+a_1k_{12} = \dfrac{b_1^2}{c}k_{12}k_{22} \\ 2k_{12}+2a_1k_{22}+\alpha_2 = \dfrac{b_1^2}{c}k_{22}^2 \end{cases} \tag{4.26}$$

Then

$$\begin{aligned} &\rightarrow k_{12} = \left(\sqrt{\alpha_1 c}\,/\,b_1\right) \\ &\rightarrow k_{22} = \left(a_1 + \sqrt{a_1^2 + \left(b_1^2/c\right)\left(\left(2\sqrt{\alpha_1 c}\,/\,b_1\right)+\alpha_2\right)}\,\Big/\left(b_1^2/c\right)\right) \end{aligned} \tag{4.27}$$

The LQR controller parameters k_1 *and* k_2 are obtained by solving Riccati Equation regarding $\begin{bmatrix} k_1 & k_2 \end{bmatrix}^T = \mathbf{R}^{-1}\mathbf{B}^T\mathbf{K}$ then

$$\begin{aligned} u &= -\left(b_1/c\right)\left(k_{12}x_1 + k_{22}x_2\right) \\ &= -\left(b_1/c\right)k_{12}x_1 - \left(b_1/c\right)k_{22}x_2 \\ &= -k_1x_1 - k_2x_2 \end{aligned} \tag{4.28}$$

4.2.2. Nonlinear Component Design of Nonlinear Optimal Controller

The state space form is briefly recalled in Table 4.2, represents the linearised form of the control system with optimal gain parameters k_1 *and* k_2.

Table 4.2 The State Space Variables

	Velocity Loop	**Current Loops,** $(i)=\{q,d\}$
Input Vector	$u=\left[\delta T_e\right]$	$u=\left[\delta v_{(i)r}\right]$
State Space Vector	$X=\left[\delta\omega_{in} \quad \delta\omega_m\right]^T$	$X=\left[\delta i_{(i)r_{in}} \quad \delta i_{(i)r}\right]^T$
Motor Parameters	J, F, T_f, T_L	L_q, L_d, R_s, R_c
Cost Function	$\min_u J=\int_0^\infty (X^TQX+U^TRU)\,dt$	$\min_u J=\int_0^\infty (X^TQX+U^TRU)\,dt$

The optimal gain parameters should be updated whenever operating point changes. The nonlinear component based on generalised work of Krasovskiy's criterion is introduced into the control structure to achieve an automated optimisation without changing default values of the controller and motor parameters. Thus, the robustness of the control scheme is improved without bulky LUT solutions or complicated adaptive solutions with high computational costs.

The procedure starts with assuming that the gain parameters in eqn. (4.28) are obtained for minimum values of time constants in (4.12) and (4.13). The eqns. are rewritten as in eqns. (4.29) and (4.30) by replacing a_1 *and* b_1 with possible maximum values $a_2=\left|a_{\max}\right|$ and $b_2=\left|b_{\max}\right|$.

$$\mathbf{A}=\begin{bmatrix}0 & 1\\ 0 & a_2\end{bmatrix}\rightarrow a_2=\begin{cases}-1/T_{d02}\\ -1/T_{q02}\\ -1/T_{m02}\end{cases} \tag{4.29}$$

$$\mathbf{B}=\begin{bmatrix}0 & b_2\end{bmatrix}^T\rightarrow b_2=\begin{cases}1/(T_{d02}R_s)\\ 1/(T_{q02}R_s)\\ 1/(T_{m02}B)\end{cases} \tag{4.30}$$

Similar derivations to yield eqn. (4.28) for steady state 1 results in eqn. (4.31) for steady state 2.

$$u'=-\left(b_2/c\right)k'_{12}x_1-\left(b_2/c\right)k'_{22}x_2=-k'_1x_1-k'_2x_2 \tag{4.31}$$

The gain parameters of the controllers should be updated between k_i *and* k_i' while the time constants are variating in $T_{d,q,m0\min}\le T_{d,q,m0}\le T_{d,q,m0\max}$. Therefore, the gain parameters look as below for an arbitrary time constant within the allowed range controller

$$\begin{aligned}u'&=-\left(k'_1x_1+k'_2x_2\right)=-\left(\left(k_1+\delta k_1\right)x_1+\left(k_2+\delta k_2\right)x_2\right)\\ &=-\left(k_1x_1+k_2x_2+\delta k_1x_1+\delta k_2x_2\right)\end{aligned} \tag{4.32}$$

If δk_1 *and* δk_2 are considered as new control inputs of the nonlinear component and the differential equations of the IPMSM model updated by considering the steady state 2, then

$$\begin{aligned}\dot{x}_1&=x_2\\ \dot{x}_2&=a_2x_2+b_2u=a_2x_2-b_2\left(k_1x_1+k_2x_2+\delta k_1x_1+\delta k_2x_2\right)\end{aligned} \tag{4.33}$$

And the cost function is updated as below considering the Krasovskiy's criterion

$$\min_{\delta k_1,\, \delta k_2} J = \int_0^{\infty} \left(\alpha_1 x_1^2 + \alpha_2 x_2^2 + c_1 \delta k_1^2 + c_2 \delta k_2^2 + \frac{b_2^2}{4c_1} \left(x_1 \frac{\partial V}{\partial x_2} \right)^2 + \frac{b_2^2}{4c_2} \left(x_2 \frac{\partial V}{\partial x_2} \right)^2 \right) dt \tag{4.34}$$

c_1 *and* c_2 appear as new positive weighting coefficients for new control inputs δk_1 *and* δk_2. It is obvious that first four terms of eqn. (4.34) are similar as for LQR, and the last two terms introduces the Bellman equation to obtain the explicit control solution. Then

$$\min_{\delta k_1,\, \delta k_2} \left[\begin{array}{l} \alpha_1 x_1^2 + \alpha_2 x_2^2 + c_1 \delta k_1^2 + c_2 \delta k_2^2 + \frac{b_2^2}{4c_1} \left(x_1 \frac{\partial V}{\partial x_2} \right)^2 + \frac{b_2^2}{4c_2} \left(x_2 \frac{\partial V}{\partial x_2} \right)^2 + \frac{\partial V}{\partial x_1} x_2 + \\ \frac{\partial V}{\partial x_2} \left(a_2 x_2 - b_2 \left(k_1 x_1 + k_2 x_2 + \delta k_1 x_1 + \delta k_2 x_2 \right) \right) \end{array} \right] = 0 \tag{4.35}$$

Each control variable should be equated zero for the closed form of the Bellman equation then

$$\begin{aligned} \delta k_1 &= \frac{b_2}{2c_1} x_1 \frac{\partial V}{\partial x_2} \\ \delta k_2 &= \frac{b_2}{2c_2} x_2 \frac{\partial V}{\partial x_2} \end{aligned} \tag{4.36}$$

The derivations by substituting eqn. (4.36) into eqn.(4.35)

$$\begin{aligned} &\alpha_1 x_1^2 + \alpha_2 x_2^2 + c_1 \left(\frac{b_2}{2c_1} x_1 \frac{\partial V}{\partial x_2} \right)^2 + c_2 \left(\frac{b_2}{2c_2} x_2 \frac{\partial V}{\partial x_2} \right)^2 + \frac{b_2^2}{4c_1} \left(x_1 \frac{\partial V}{\partial x_2} \right)^2 + \frac{b_2^2}{4c_2} \left(x_2 \frac{\partial V}{\partial x_2} \right)^2 \\ &+ \frac{\partial V}{\partial x_1} x_2 + \frac{\partial V}{\partial x_2} \left(a_2 x_2 - b_2 \left(k_1 x_1 + k_2 x_2 + \left(\frac{b_2}{2c_1} x_1 \frac{\partial V}{\partial x_2} \right) x_1 + \left(\frac{b_2}{2c_2} x_2 \frac{\partial V}{\partial x_2} \right) x_2 \right) \right) = 0 \end{aligned} \tag{4.37}$$

Then

$$\alpha_1 x_1^2 + \alpha_2 x_2^2 + \frac{\partial V}{\partial x_1} x_2 + \frac{\partial V}{\partial x_2}\left(a_2 x_2 - b_2\left(k_1 x_1 + k_2 x_2\right)\right) = 0 \tag{4.38}$$

$$V = k_3 x_1^2 + k_4 x_1 x_2 + k_5 x_2^2 \tag{4.39}$$

Updating eqn. (4.38) with the quadratic form of the Lyapunov function in eqn. (4.39) then

$$\begin{aligned} &\rightarrow \left(\partial V / \partial x_2\right) = 2k_4 x_1 + 2k_5 x_2 \\ &\rightarrow \left(\partial V / \partial x_1\right) = 2k_3 x_1 + 2k_4 x_2 \end{aligned} \tag{4.40}$$

By substituting (4.40) into eqn. (4.38) then

$$\alpha_1 x_1^2 + \alpha_2 x_2^2 + \left(2k_3 x_1 + 2k_4 x_2\right) x_2 + \left(2k_4 x_1 + 2k_5 x_2\right)\left(a_2 x_2 - b_2\left(k_1 x_1 + k_2 x_2\right)\right) = 0 \tag{4.41}$$

$$\rightarrow \left(\alpha_1 - 2k_4 b_2 k_1\right) x_1^2 + \left(\alpha_2 + 2k_4 + 2k_5\left(a_2 - b_2 k_2\right)\right) x_2^2 + \left(2k_3 + 2k_4\left(a_2 - b_2 k_2\right) - 2k_5 b_2 k_1\right) x_1 x_2 = 0 \tag{4.42}$$

The equation above can be split into following equations

$$\begin{cases} x_1^2: \quad \alpha_1 - 2k_4 b_2 k_1 = 0 \\ x_2^2: \quad \alpha_2 + 2k_4 + 2k_5\left(a_2 - b_2 k_2\right) = 0 \\ x_1 x_2: \quad 2k_3 + 2k_4\left(a_2 - b_2 k_2\right) - 2k_5 b_2 k_1 = 0 \end{cases} \tag{4.43}$$

the parameters of the controllers can be defined as follows

$$\begin{aligned} k_3 &= k_5 b_2 k_1 - k_4\left(a_2 - b_2 k_2\right) \\ k_4 &= \left(\alpha_1 / 2b_2 k_1\right) \\ k_5 &= \left(\alpha_2 + 2k_4\right) / \left(2\left(b_2 k_2 - a_2\right)\right) \end{aligned} \tag{4.44}$$

Returning back to the controller form based on eqn. (4.32) and regarding eqn. (4.36) then

$$\begin{aligned}\delta k_1 &= \frac{b_2}{2c_1} x_1 \frac{\partial V}{\partial x_2} = \frac{b_2}{2c_1} x_1 \left(2k_4 x_1 + 2k_5 x_2\right) \\ \delta k_2 &= \frac{b_2}{2c_2} x_2 \frac{\partial V}{\partial x_2} = \frac{b_2}{2c_2} x_2 \left(2k_4 x_1 + 2k_5 x_2\right)\end{aligned} \tag{4.45}$$

Finally, the equation of the nonlinear optimal controller is defined as

$$\begin{aligned}u' &= -\left(k_1 x_1 + k_2 x_2 + \delta k_1 x_1 + \delta k_2 x_2\right) \\ &= -\left(k_1 x_1 + k_2 x_2 + \frac{b_2}{2c_1}\left(2k_4 x_1 + 2k_5 x_2\right) x_1^2 + \frac{b_2}{2c_2}\left(2k_4 x_1 + 2k_5 x_2\right) x_2^2\right) = \\ &= -\left(k_1 x_1 + k_2 x_2 + \frac{b_2}{2c_1}\left(2k_4 x_1 + 2k_5 x_2\right) x_1^2 + \frac{b_2}{2c_2}\left(2k_4 x_1 + 2k_5 x_2\right) x_2^2\right) = \\ &= -\left(k_1 x_1 + k_2 x_2 + \left(k_4 x_1 + k_5 x_2\right)\left(\frac{b_2}{c_1} x_1^2 + \frac{b_2}{c_2} x_2^2\right)\right)\end{aligned} \tag{4.46}$$

Finally, the equation above can be transformed into

$$u' = -\left(k_1 x_1 + k_2 x_2 + \left(k_4 x_1 + k_5 x_2\right)\left(\frac{b_2}{c_1} x_1^2 + \frac{b_2}{c_2} x_2^2\right)\right) = u'_{lp} + u'_{np} \tag{4.47}$$

Of which the linear component represented as

$$u'_{lp} = -\left(k_1 x_1 + k_2 x_2\right)$$

And the nonlinear component represented as

$$u'_{np} = -\left(k_4 x_1 + k_5 x_2\right)\left(\left(b_2/c_1\right) x_1^2 + \left(b_2/c_2\right) x_2^2\right)$$

It is worth to repeat that

$$\text{for steady states } \begin{cases} i_{d,q01} = i^*_{d,q} \\ \omega_{m01} = \omega^*_m \end{cases} \text{ then } \begin{cases} x_1 = \begin{cases} \int \left(i_{d,q} - i^*_{d,q} \right) dt \\ \int \left(\omega_m - \omega^*_m \right) dt \end{cases} \\ x_2 = \begin{cases} \delta i_{d,q} = i_{d,q} - i^*_{d,q} \\ \delta \omega_m = \omega_m - \omega^*_m \end{cases} \end{cases}$$

finally full view of the nonlinear optimal controller is

$$\begin{aligned} u'_{lp} &= -\left(k_1 x_1 + k_2 x_2 \right) \\ u'_{np} &= -\left(b_2 k_4 x_1 + b_2 k_5 x_2 \right) \left(\frac{1}{c_1} x_1^2 + \frac{1}{c_2} x_2^2 \right) \\ &= -\left(k_6 x_1 + k_7 x_2 \right) \left(\frac{1}{c_1} x_1^2 + \frac{1}{c_2} x_2^2 \right) \end{aligned} \tag{4.48}$$

4.2.3. Parameter Identification for Nonlinear Optimal Controller

The state space variables, the input variables and typical form of the cost function are recalled in eqns. (4.49), (4.50) and (4.51), respectively.

$$\mathbf{X} = \begin{bmatrix} x_1 & x_2 \end{bmatrix}^T = \begin{cases} \begin{bmatrix} \delta i_{ind} & \delta i_d \end{bmatrix}^T \\ \begin{bmatrix} \delta i_{inq} & \delta i_q \end{bmatrix}^T \\ \begin{bmatrix} \delta \omega_{in} & \delta \omega_m \end{bmatrix}^T \end{cases} \tag{4.49}$$

$$u = \begin{cases} \delta v_d \\ \delta v_q \\ \delta T^*_e \end{cases} \tag{4.50}$$

$$\min_{u} J = \int_{0}^{\infty} \left(\mathbf{XQX^T} + \mathbf{URU^T} \right) dt \tag{4.51}$$

$\mathbf{Q}$ and $\mathbf{R}$ represent the matrices for positive weighting coefficients. Sizes of the matrices are defined according to the number of the state space and input variables shown as below

$$\min_{u} J = \int_{0}^{\infty} \left(\alpha_1 x_1^2 + \alpha_2 x_2^2 + cu^2 \right) dt \tag{4.52}$$

$$\mathbf{Q} = \begin{bmatrix} \alpha_1 & 0 \\ 0 & \alpha_2 \end{bmatrix} \text{ and } \mathbf{R} = [c] \tag{4.53}$$

In these circumstances,

α_1	denotes the weighting coefficient for variation of the integral value of corresponding state space variable
α_2	denotes the weighting coefficient for the error of corresponding state space variable
c	the weighting coefficient for variation of the input variable

Conventional PI controllers in the simulations in Chapter 3 are replaced with proposed nonlinear optimal controllers. The controller parameters are initially calculated as in Table 4.3 in Appendix H regarding the weighting coefficients in eqns. (4.54) and (4.55). Heuristic approach is then applied for adjusting the controller parameters to achieve the best IPMSM drive response.

$$\alpha_1 = \alpha_2 = \begin{cases} 1/\omega_{rated}^2 & \textit{(For velocity controller } \omega_{rated} = 2000 \textit{ rpm)} \\ 1/I_{\max}^2 & \textit{(For current controllers } I_{\max} = 10 \textit{ A)} \end{cases} \tag{4.54}$$

$$c = \begin{cases} 1/T_{e\max}^2 & \textit{(For velocity controller } T_{e\max} = 5\ Nm\textit{)} \\ 1/v_{\max}^2 & \textit{(For current controllers } v_{\max} = 150\ V\textit{)} \end{cases} \tag{4.55}$$

Table 4.3 Nonlinear optimal controller parameters (first attempt)

	k_1	k_2	k_6	k_7	c_1	c_2
d-axis current controller	15	14.4495	3.33e-4	3.33e-4	0.001	0.001
q-axis current controller	15	14.4636	3.33e-4	3.32e-4	0.001	0.001
Velocity controller	0.0080	0.0112	0.0014	0.0013	0.01	0.01

Conventional IPMSM drive with MTPA control approach is simulated with the controller parameters in Table 4.1, the simulation results shown in Figure 4.4. The results for nonlinear optimal IPMSM drive with the parameters in Table 4.3 is shown in Figure 4.5. It is obvious both in torque, velocity and d, q-axis currents responses of the nonlinear optimal IPMSM drive are more robust. The results show less oscillations and overshoots during transients. Besides, the inherent nonlinearities sourced by MTPA control algorithm are eliminated (Best seen in between 0.75 and 0.8 seconds). Overshoot in the torque line is overdamped and the oscillations in d-axis current line are eliminated. This proves that the nonlinear optimal IPMSM drive supersedes the conventional one even in ideal circumstances.

a.

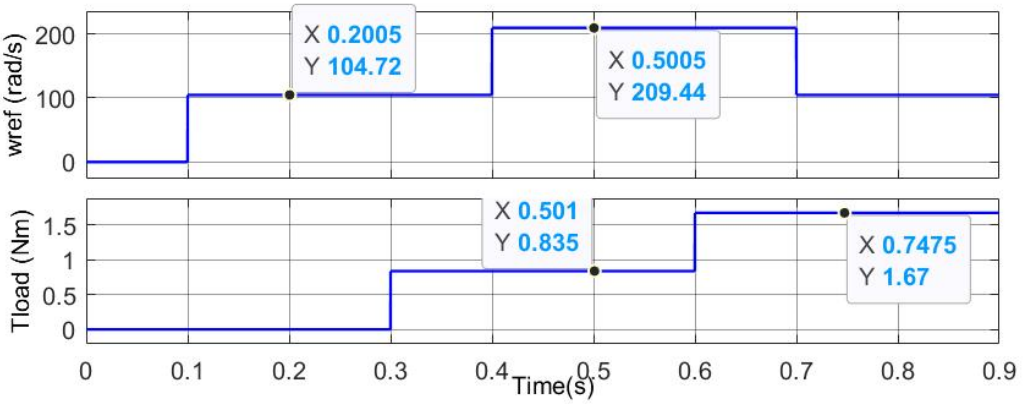

b.

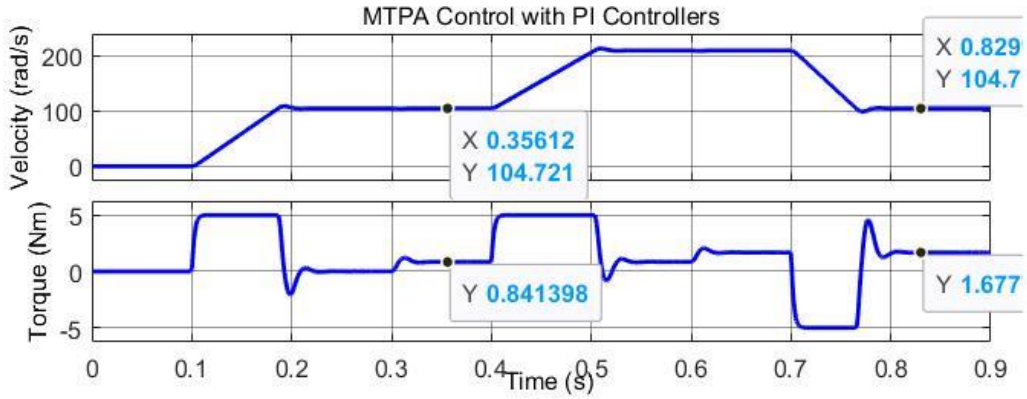

c.

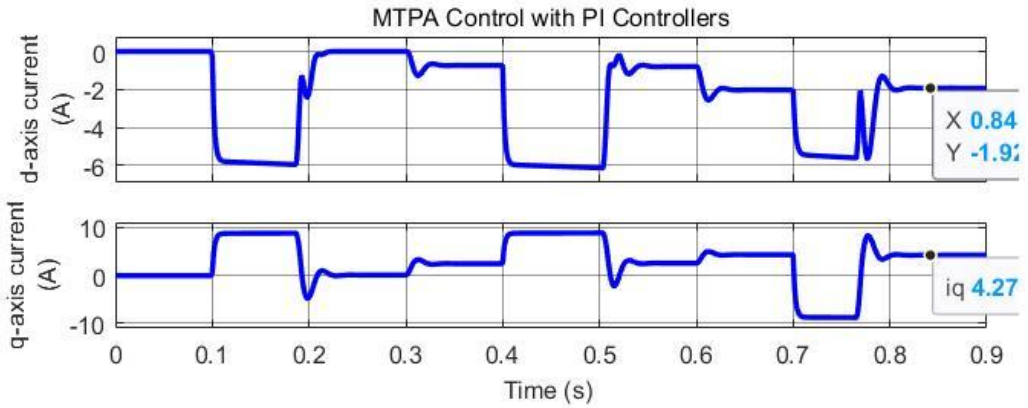

Figure 4.4 MTPA Control with PI

a. Input velocity and torque references
b. IPMSM velocity and torque responses
c. d, q-axis currents (regarding core resistance)

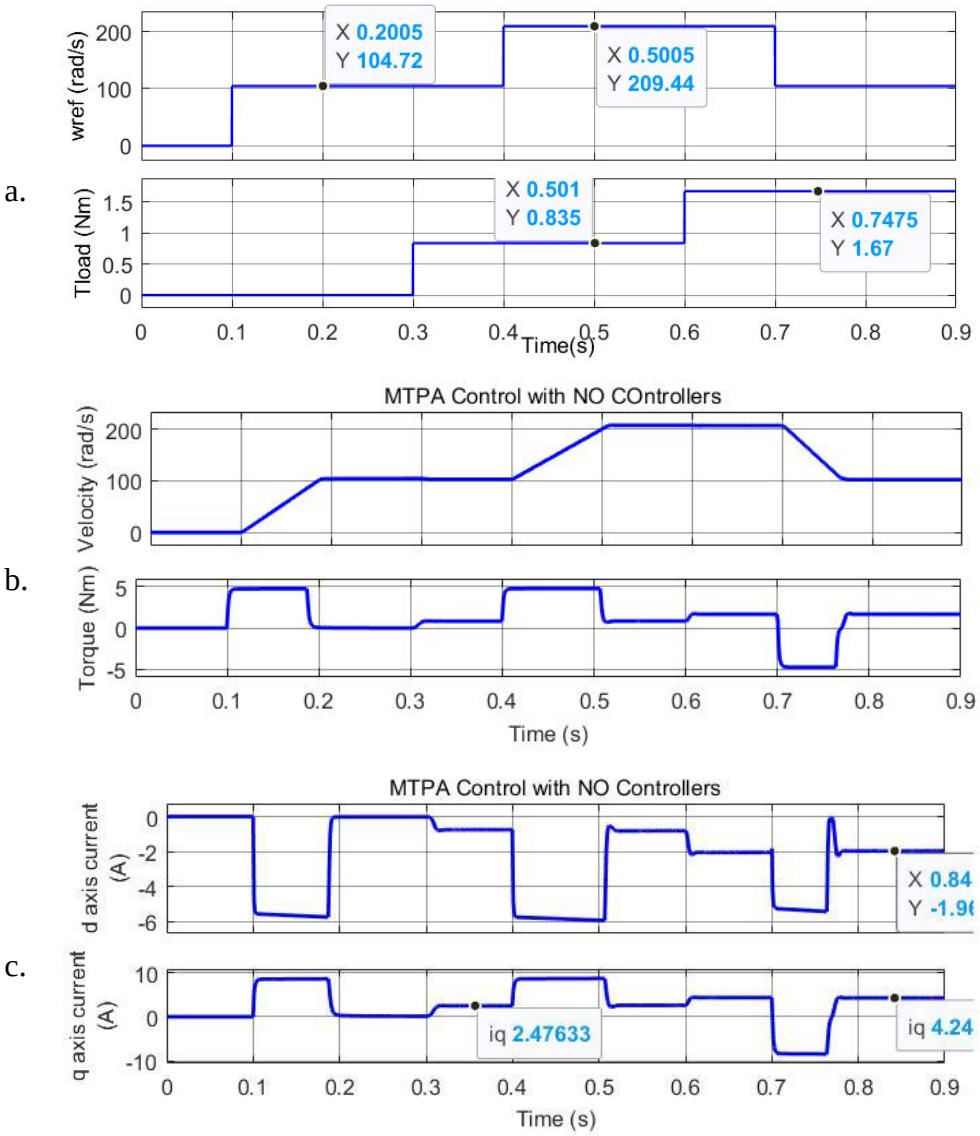

Figure 4.5 MTPA Control with NO
a. Input velocity and torque references
b. IPMSM velocity and torque responses
c. d, q-axis currents (regarding core resistance)

The heuristic method is carried out for optimising the velocity controller parameters, as illustrated in Table 4.4. Firstly, 'c' weighting coefficient is defined as 100 larger in the first case scenario and then 100 smaller in the second case scenario than the default value in eqn. (4.55). Results shown in Figure 4.6. Smaller c weighting coefficient for velocity controller ends up with less oscillations and overshoots than one with larger c. Compared to the results with default values in Figure 4.5, transitions are worsened.

Table 4.4 Nonlinear Optimal controller parameters with various c weighting coefficient for the velocity controller

	k_1	k_2	k_6	k_7	c_1	c_2	
d-axis current controller	15	14.4495	3.33e-4	3.33e-4	0.001	0.001	
q-axis current controller	15	14.4636	3.33e-4	3.32e-4	0.001	0.001	
Velocity controller	7.97e-4 0.0797	0.0026 0.0836	0.0143 1.42e-4	0.0151 1.39e-4	0.01 0.01	0.01 0.01	1st case 2nd case

α_1 weighting coefficient of the velocity controller has then been changed to its 100 larger (1st case) and 100 smaller values (2nd case) in Table 4.5, the simulation results shown in Figure 4.7. Same pattern has been carried out for α_2 , the velocity controller parameters are updated as in Table 4.6 and simulation results depicted in Figure 4.8.

Table 4.5 Nonlinear Optimal controller parameters with various α_1 weighting coefficient for the velocity controller

	k_1	k_2	k_6	k_7	c_1	c_2	
d-axis current controller	15	14.4495	3.33e-4	3.33e-4	0.001	0.001	
q-axis current controller	15	14.4636	3.33e-4	3.32e-4	0.001	0.001	
Velocity controller	0.07974 7.9737e-4	0.0264 0.0083	0.0143 1.4295e-4	0.0015 0.0014	0.01 0.01	0.01 0.01	1st case 2nd case

Table 4.6 Nonlinear Optimal controller parameters with various α_2 weighting coefficient for the velocity controller

	k_1	k_2	k_6	k_7	c_1	c_2	
d-axis current controller	15	14.4495	3.33e-4	3.33e-4	0.001	0.001	
q-axis current controller	15	14.4636	3.33e-4	3.32e-4	0.001	0.001	
Velocity controller	0.0080 0.0080	0.0801 0.0079	0.0014 0.0014	0.0143 3.7039e-4	0.01 0.01	0.01 0.01	1st case 2nd case

a.

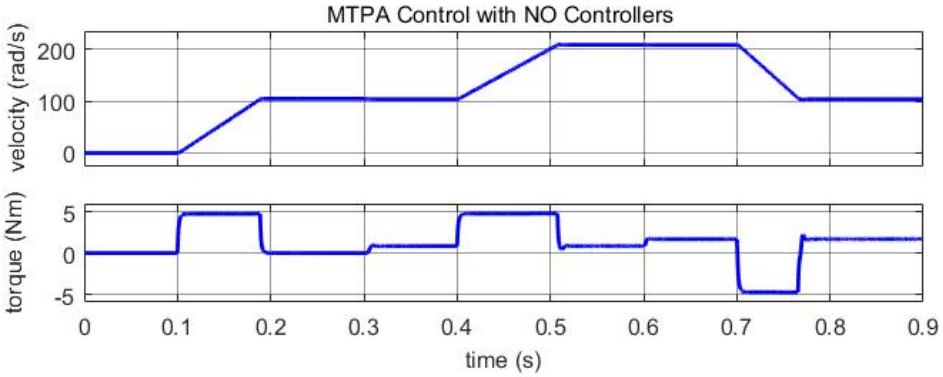

b.

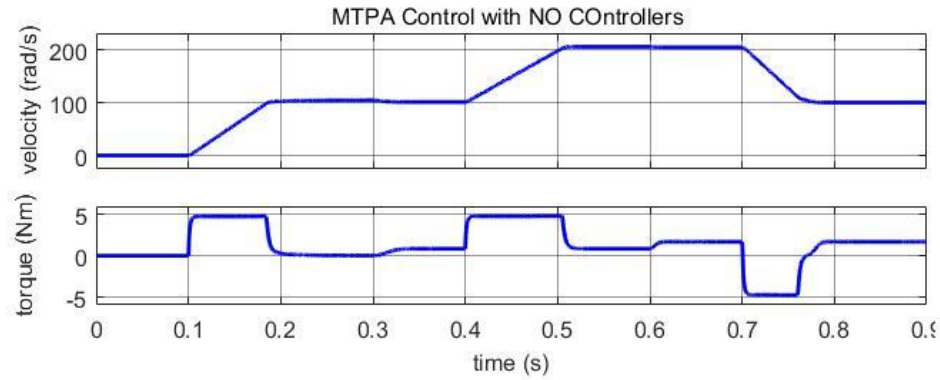

c.

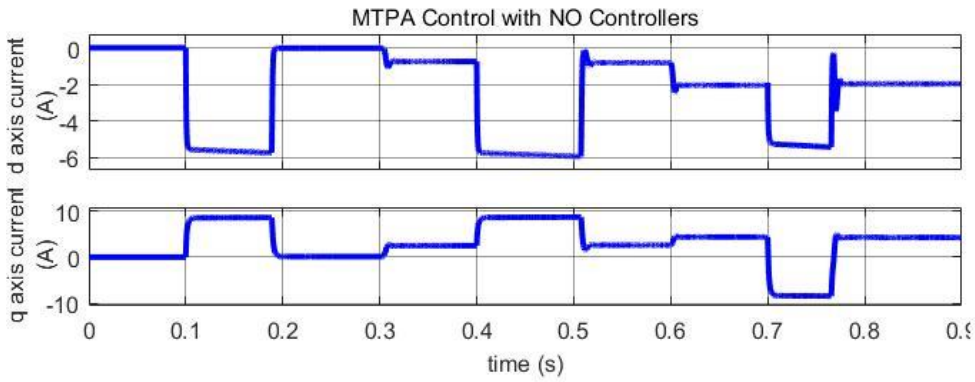

d.

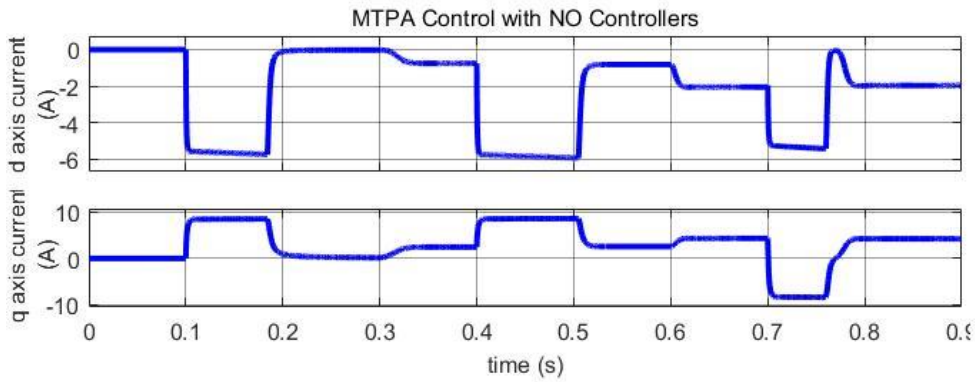

Figure 4.6 ‘c’ weighting coefficient variation of the velocity controller

a. velocity and torque response for c=100c
b. velocity and torque response for c=0.01c
c. d, q axes currents responses for c=100c
d. d, q axes currents responses for c=0.01c

a.

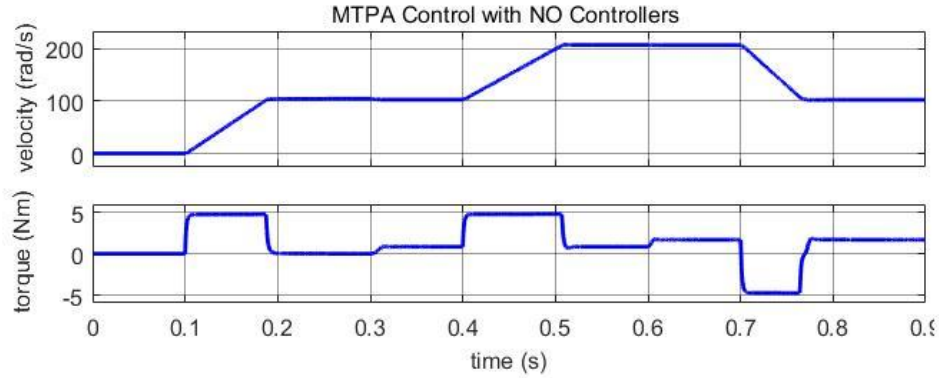

b.

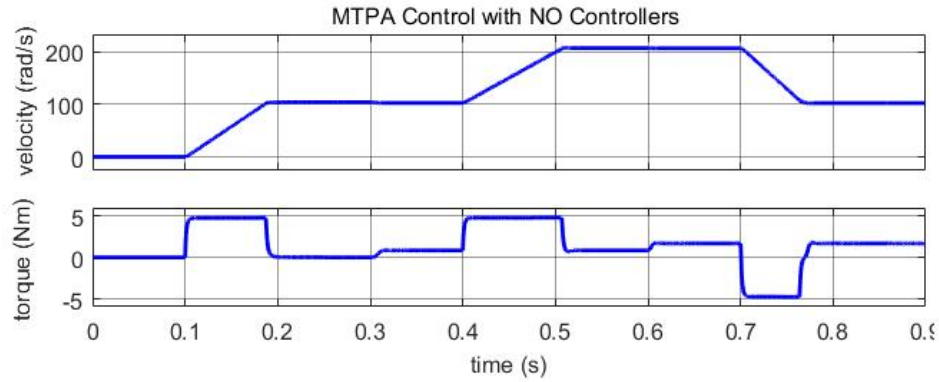

c.

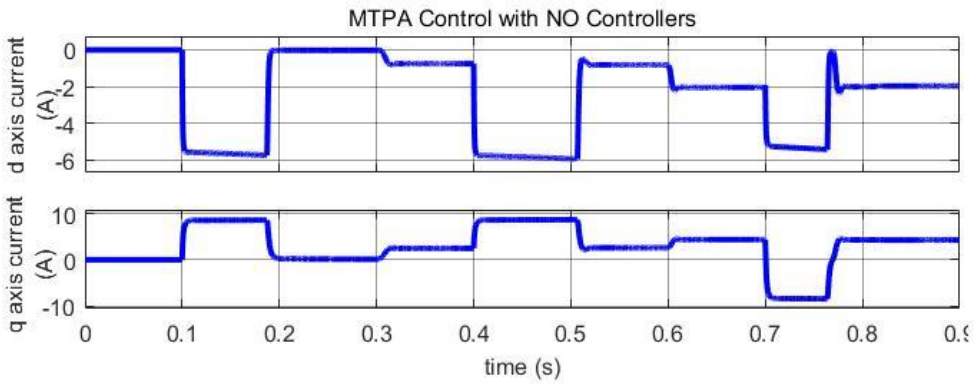

d.

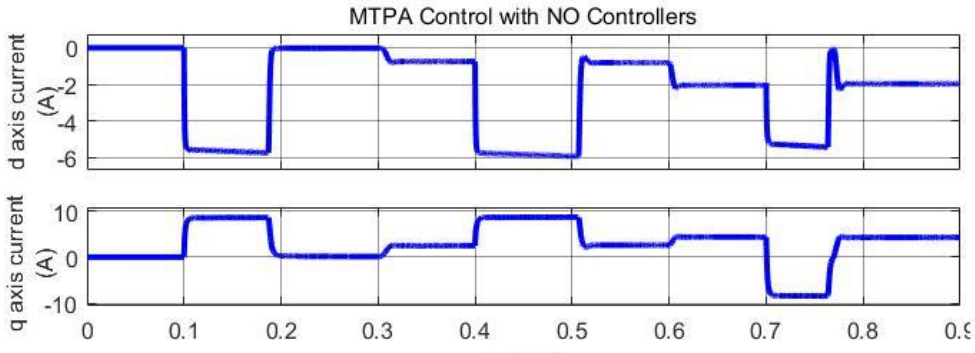

Figure 4.7 'α_1' weighting coefficient variation of the velocity controller

a. velocity and torque response for $\alpha_1 = 100\alpha_1$

b. velocity and torque response with $\alpha_1 = 0.01\alpha_1$

c. d, q axes currents response for $\alpha_1 = 100\alpha_1$

d. d, q axes currents response for $\alpha_1 = 0.01\alpha_1$

a.

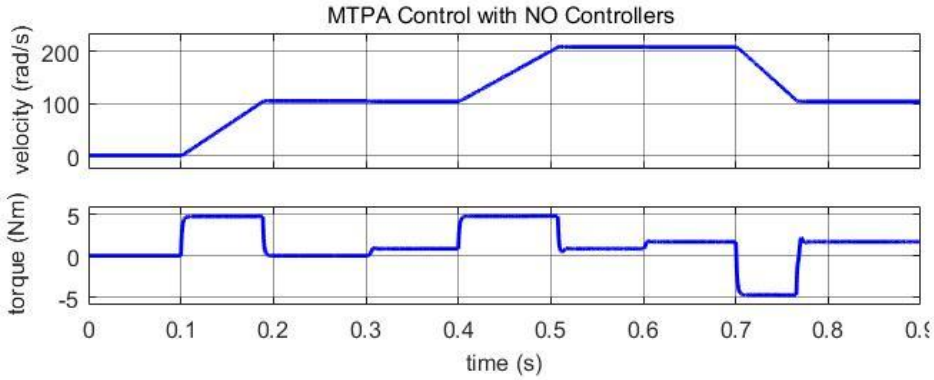

b.

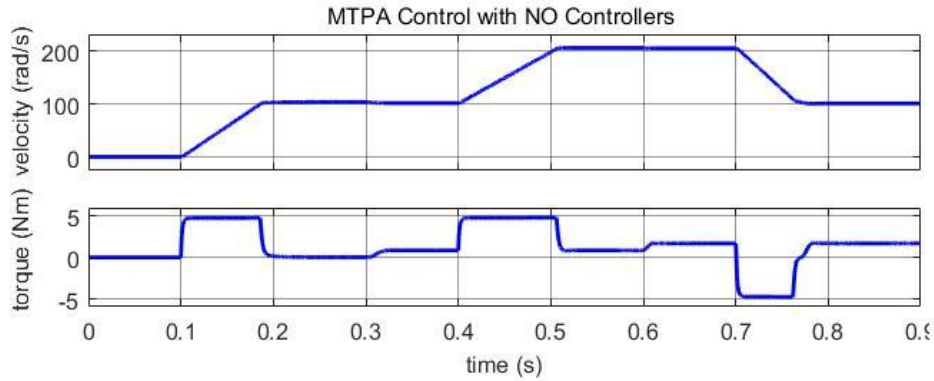

c.

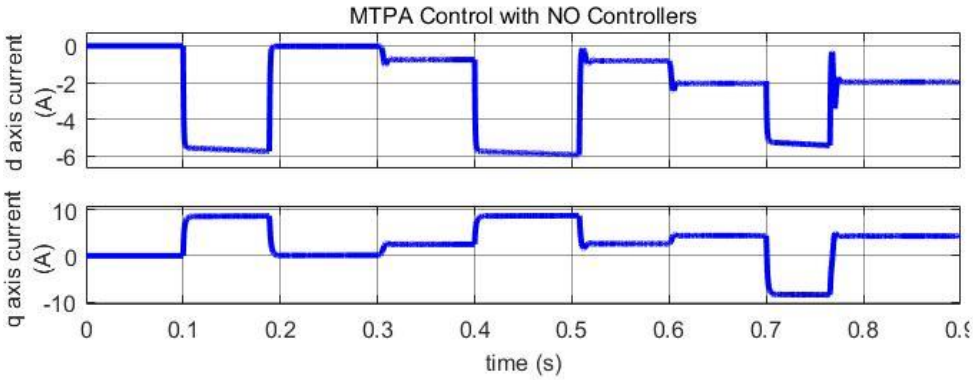

d.

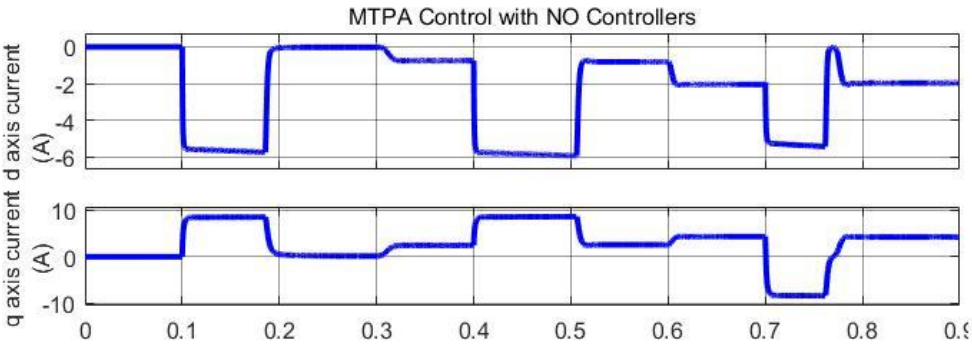

Figure 4.8 ' α_2 ' weighting coefficient variation of the velocity controller

a. velocity and torque response for α_2 =100c

b. velocity and torque response for α_2 =0.01c

c. d, q axes currents for α_2 =100c

d. d, q axes currents for α_2 =0.01c

The heuristic method then applied for d-axis current controller parameters with same pattern. The controller parameters are updated as in Table 4.7, Table 4.8 and Table 4.9 and the results are obtained shown as in Figure 4.9, Figure 4.10 and Figure 4.11, respectively.

Table 4.7 Nonlinear Optimal controller parameters with various c weighting coefficient for the d-axis current controller

	k_1	k_2	k_6	k_7	c_1	c_2	
d-axis current controller	1.5	1.0428	0.0033	0.0031	0.001	0.001	1st case
	150	149.4398	3.33e-5	3.33e-5	0.001	0.001	2nd case
q-axis current controller	15	14.4636	3.33e-4	3.32e-4	0.001	0.001	
Velocity controller	0.0080	0.0112	0.0014	0.0013	0.01	0.01	

Table 4.8 Nonlinear Optimal controller parameters with various α_1 weighting coefficient for the d-axis current controller

	k_1	k_2	k_6	k_7	c_1	c_2	
d-axis current controller	150	14.5277	0.0033	3.32e-4	0.001	0.001	1st case
	1.5	14.4417	3.33e-5	3.33e-4	0.001	0.001	2nd case
q-axis current controller	15	14.4636	3.33e-4	3.32e-4	0.001	0.001	
Velocity controller	0.0080	0.0112	0.0014	0.0013	0.01	0.01	

Table 4.9 Nonlinear Optimal controller parameters with various α_2 weighting coefficient for the d-axis current controller

	k_1	k_2	k_6	k_7	c_1	c_2	
d-axis current controller	15	149.4320	3.33e-4	0.0033	0.001	0.001	1st case
	15	1.1142	3.33e-4	3.055e-5	0.001	0.001	2nd case
q-axis current controller	15	14.4636	3.33e-4	3.32e-4	0.001	0.001	
Velocity controller	0.0080	0.0112	0.0014	0.0013	0.01	0.01	

a.

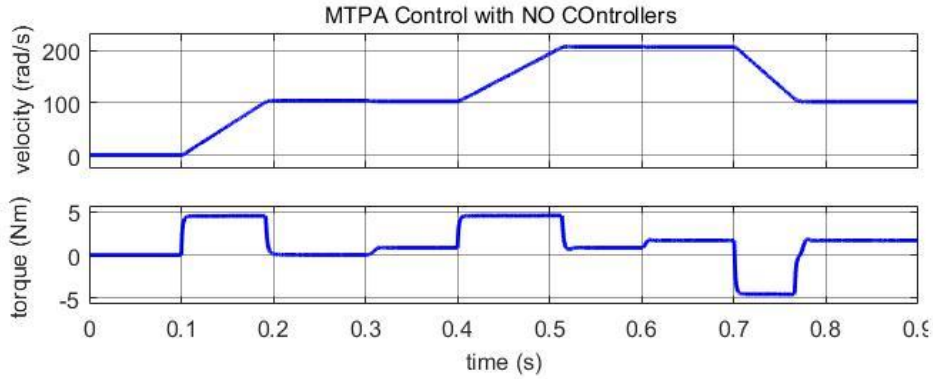

b.

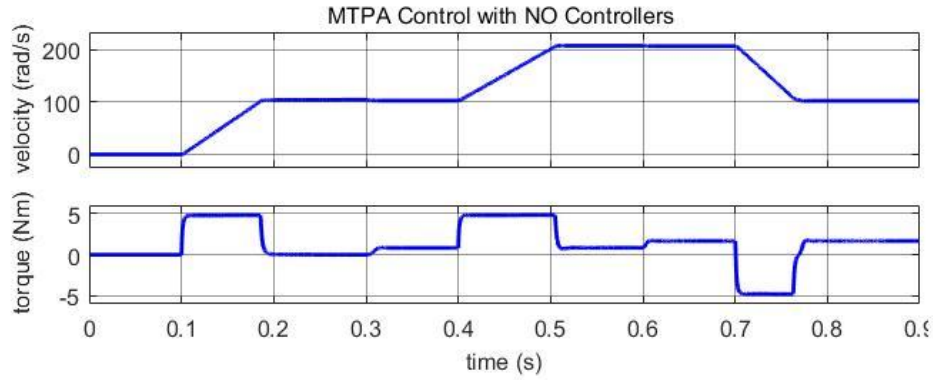

c.

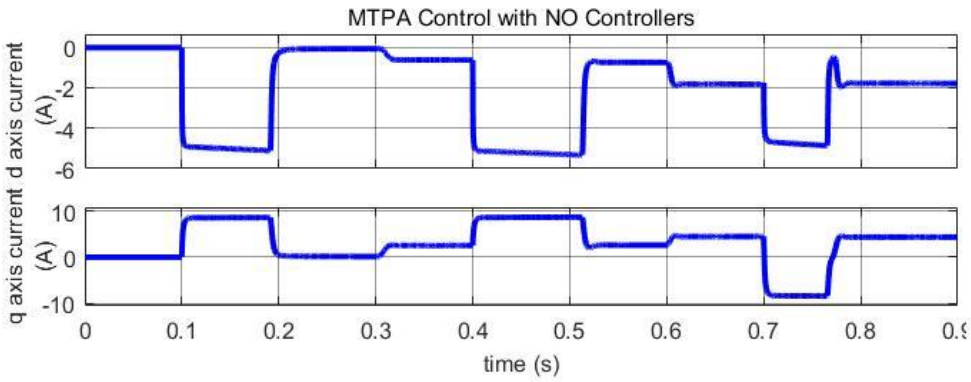

d.

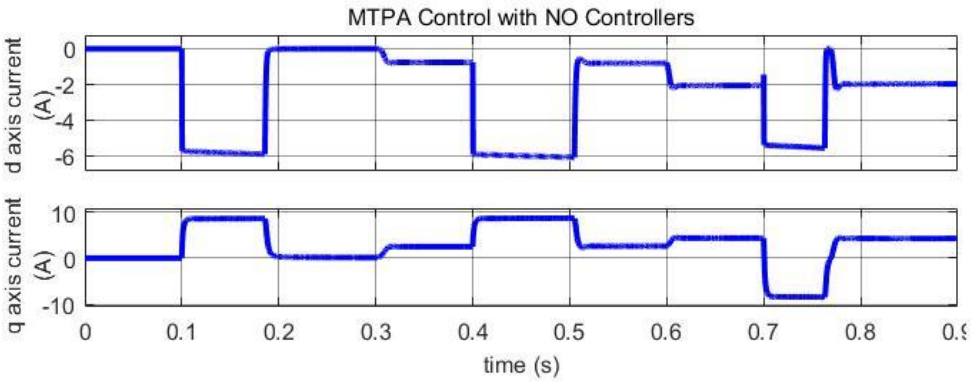

Figure 4.9 ‘c’ weighting coefficient variation of the d-axis controller

a. velocity and torque response for c=100c
b. velocity and torque response for c=0.01c
c. d, q axes currents responses for c=100c
d. d, q axes currents responses for c=0.01c

a.

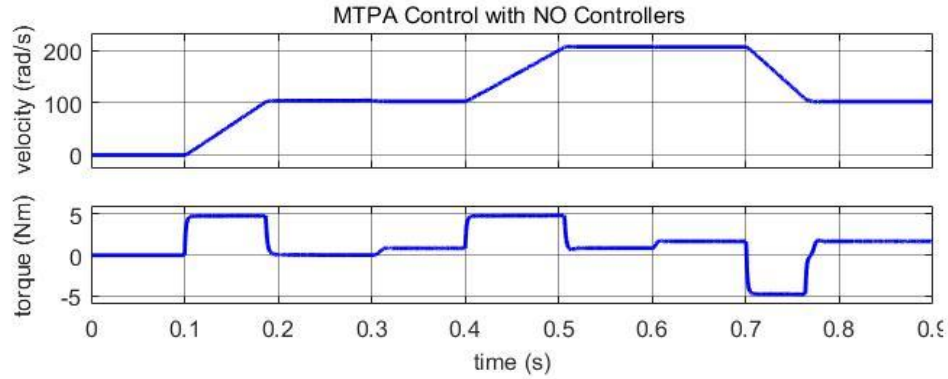

b.

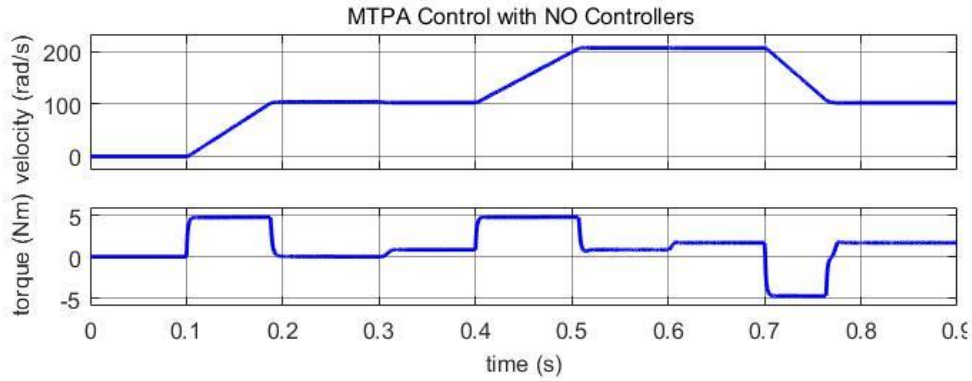

c.

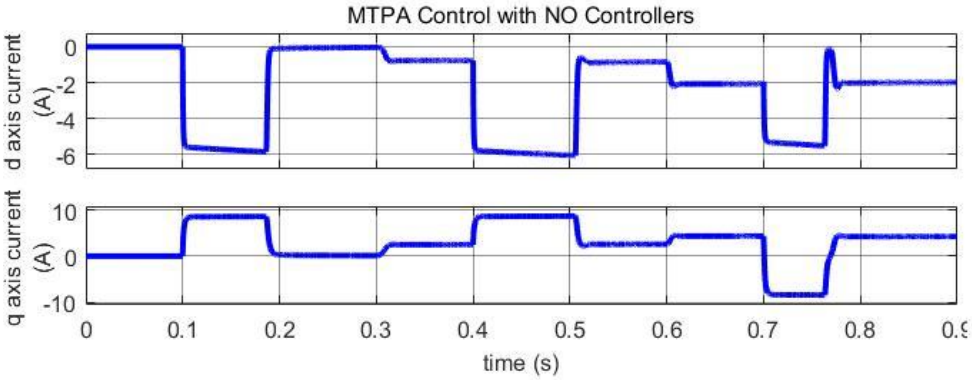

d.

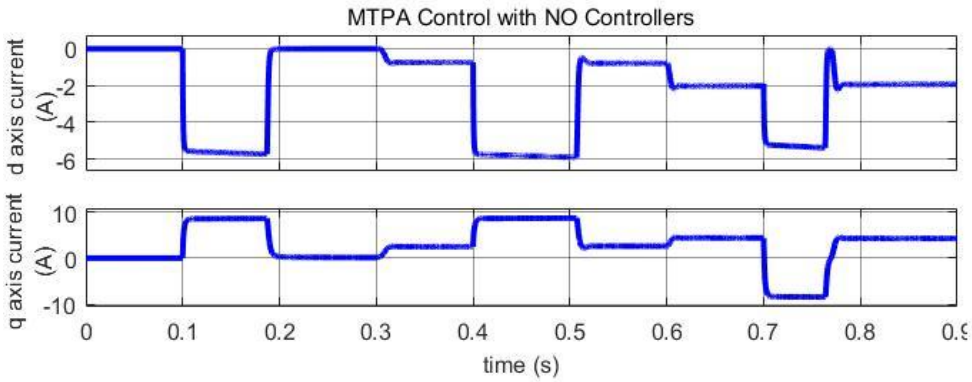

Figure 4.10 ' α_1 ' weighting coefficient variation of the d-axis controller

a. velocity and torque response for $\alpha_1 = 100\alpha_1$

b. velocity and torque response for $\alpha_1 = 0.01\alpha_1$

c. d, q axes currents responses for $\alpha_1 = 100\alpha_1$

d. d, q axes currents responses for $\alpha_1 = 0.01\alpha_1$

a.

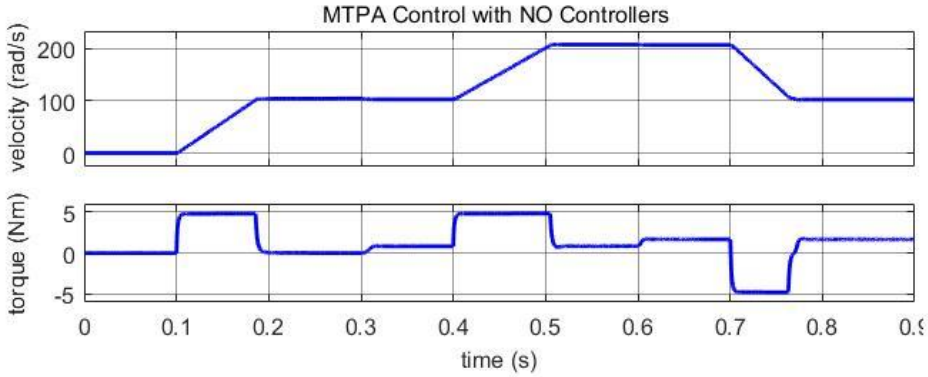

b.

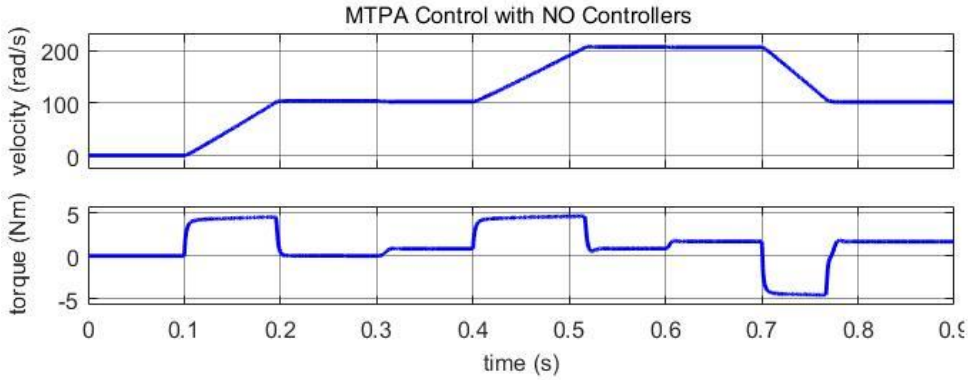

c.

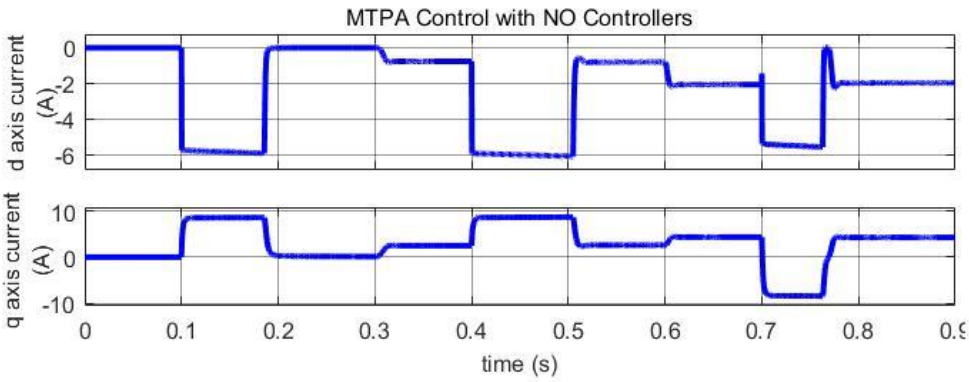

d.

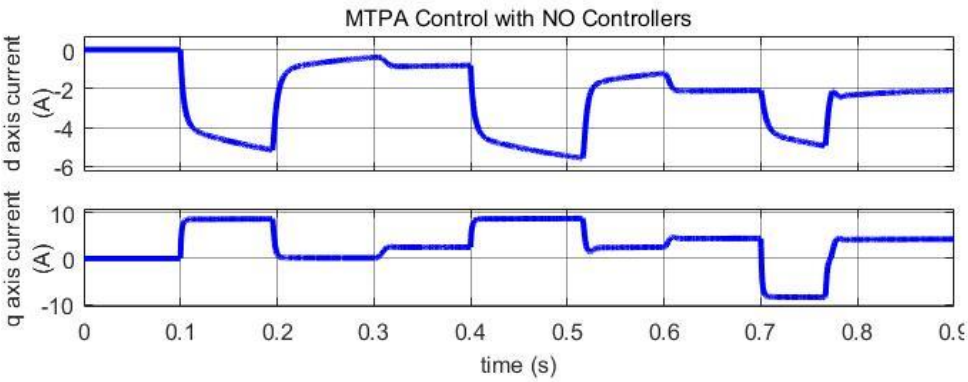

Figure 4.11 ' α_2 ' weighting coefficient variation of the d-axis controller

a. velocity and torque response for $\alpha_2 = 100\alpha_2$

b. velocity and torque response for $\alpha_2 = 0.01\alpha_2$

c. d, q axes currents responses for $\alpha_2 = 100\alpha_2$

d. d, q axes currents responses for $\alpha_2 = 0.01\alpha_2$

Exact same pattern is also carried out for q-axis current controller. The parameter are presented in Table 4.10, Table 4.11 and Table 4.12, the results as shown in Figure 4.12, Figure 4.13 and Figure 4.14, respectively.

Table 4.10 Nonlinear Optimal controller parameters with various c weighting coefficient for the q-axis current controller

	k_1	k_2	k_6	k_7	c_1	c_2	
d-axis current controller	15	14.4495	3.33e-4	3.33e-4	0.001	0.001	
q-axis current controller	1.5	1.0558	0.0033	0.0031	0.001	0.001	1st case
	150	149.4539	3.33e-5	3.33e-5	0.001	0.001	2nd case
Velocity controller	0.0080	0.0112	0.0014	0.0013	0.01	0.01	

Table 4.11 Nonlinear Optimal controller parameters with various α_1 weighting coefficient for the q-axis current controller

	k_1	k_2	k_6	k_7	c_1	c_2	
d-axis current controller	15	14.4495	3.33e-4	3.33e-4	0.001	0.001	
q-axis current controller	150	14.6668	0.0033	3.3065e-4	0.001	0.001	1st case
	1.5	14.4431	3.33e-5	3.33e-4	0.001	0.001	2nd case
Velocity controller	0.0080	0.0112	0.0014	0.0013	0.01	0.01	

Table 4.12 Nonlinear Optimal controller parameters with various α_2 weighting coefficient for the q-axis current controller

	k_1	k_2	k_6	k_7	c_1	c_2	
d-axis current controller	15	14.4495	3.33e-4	3.33e-4	0.001	0.001	
q-axis current controller	15	149.4334	3.33e-4	0.0033	0.001	0.001	1st case
	15	1.2351	3.33e-4	2.9803e-5	0.001	0.001	2nd case
Velocity controller	0.0080	0.0112	0.0014	0.0013	0.01	0.01	

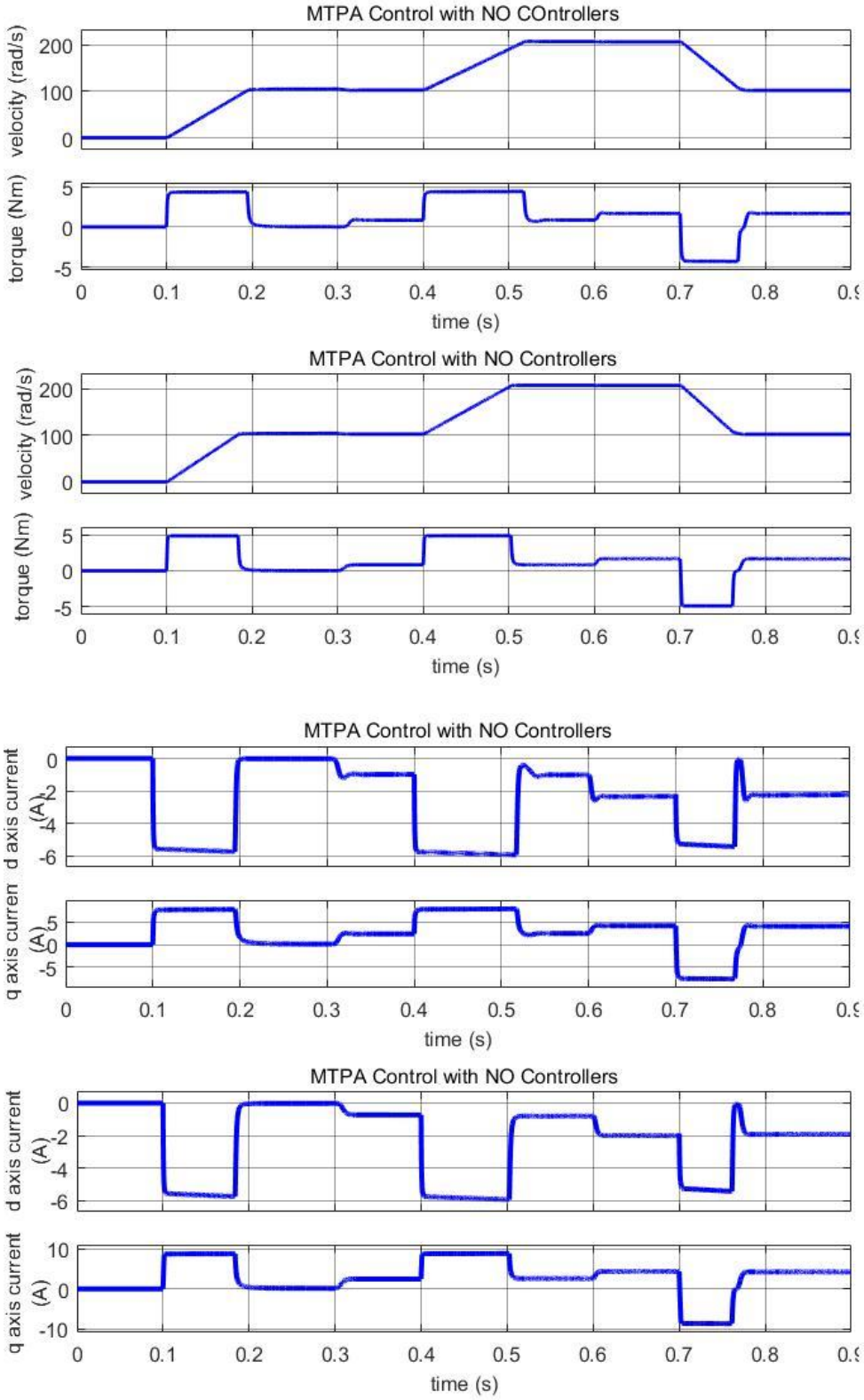

Figure 4.12 ‘c’ weighting coefficient variation of the q-axis controller

a. velocity and torque response for c=100c
b. velocity and torque response for c=0.01c
c. d, q axes currents responses for c=100c
d. d, q axes currents responses for c=0.01c

a.

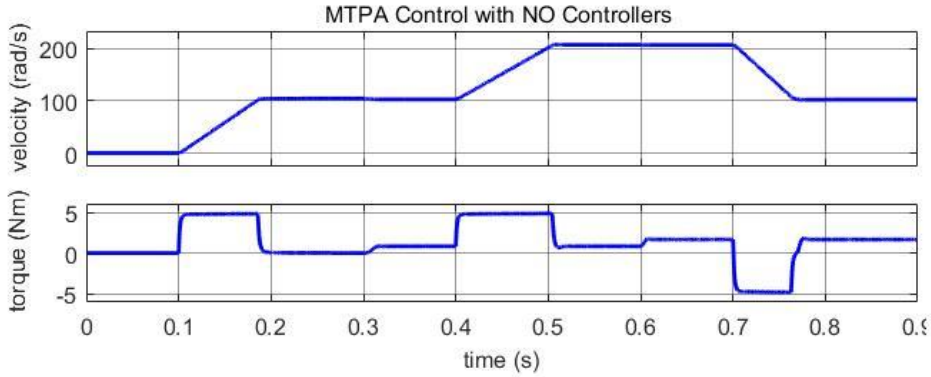

b.

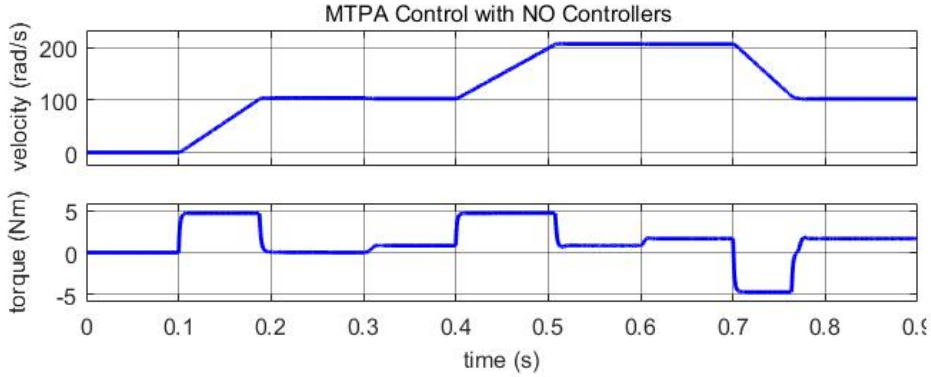

c.

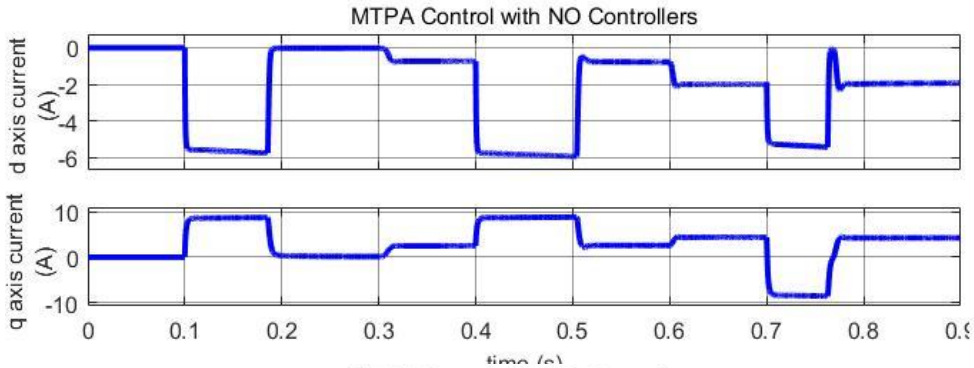

d.

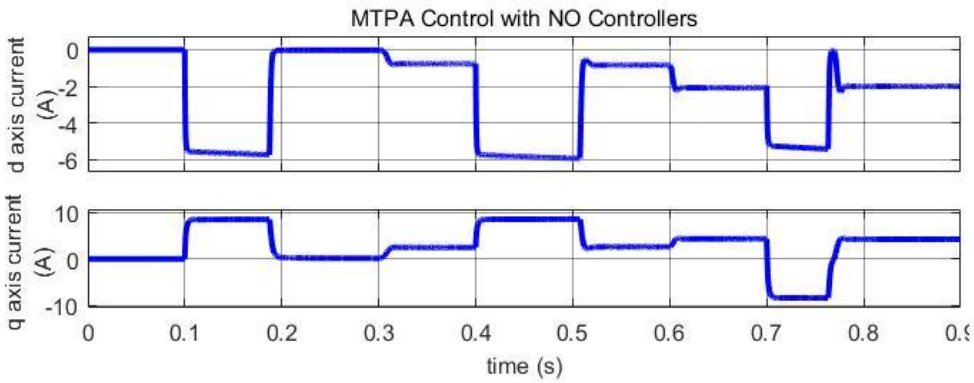

Figure 4.13 ' α_1 ' weighting coefficient variation of the q-axis controller

a. velocity and torque response for $\alpha_1 = 100\alpha_1$

b. velocity and torque response for $\alpha_1 = 0.01\alpha_1$

c. d, q axes currents responses for $\alpha_1 = 100\alpha_1$

d. d, q axes currents responses for $\alpha_1 = 0.01\alpha_1$

a.

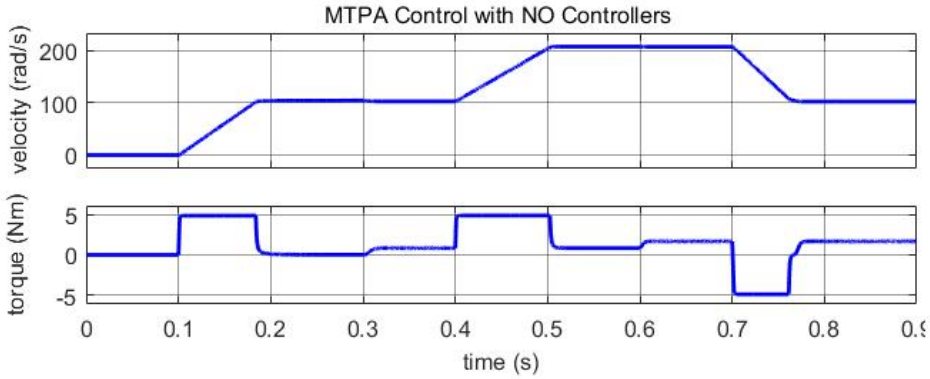

b.

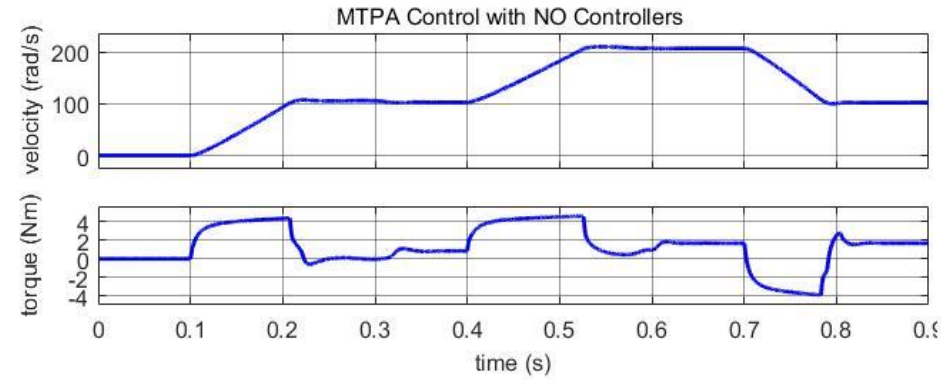

c.

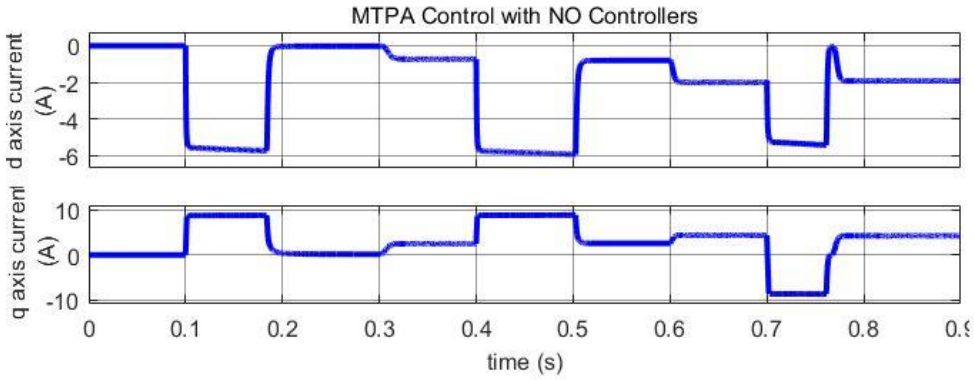

d.

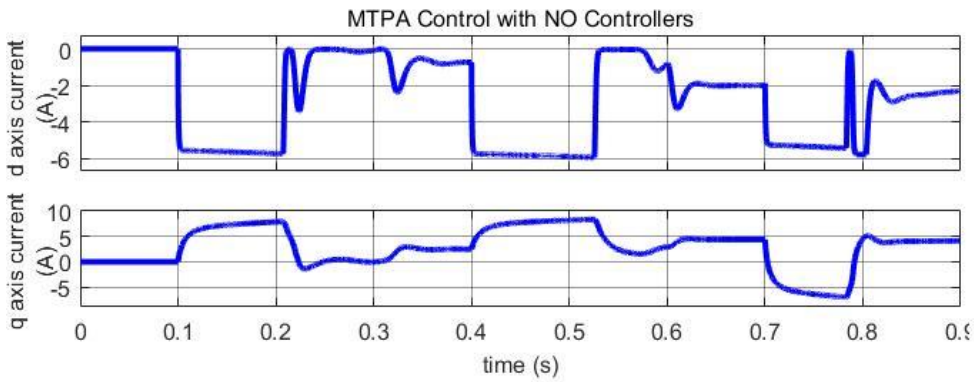

Figure 4.14 ‘ α_2 ’ weighting coefficient variation of the q-axis controller

a. velocity and torque response for $\alpha_2 = 100\alpha_2$

b. velocity and torque response for $\alpha_2 = 0.01\alpha_2$

c. d, q axes currents responses for $\alpha_2 = 100\alpha_2$

d. d, q axes currents responses for $\alpha_2 = 0.01\alpha_2$

Regarding parameter variations from Table 4.4 to Table 4.12, it can be seen that the square of c weighting coefficient is proportional to k_6 *and* k_7 and inversely proportional to k_1 *and* k_2; the square of α_1 is proportional with k_1 *and* k_6; and the square of α_2 is proportional with k_2 *and* k_7. Regarding demonstrated results in from Figure 4.6 to Figure 4.14, For the velocity controller, larger c and α_2 coefficients result in increase in oscillations and overshoots, however smaller ones cause increase in transition time; for q-axis current controller, smaller c and larger α_2 result in better responses; for d-axis current controller, larger c slightly overdamps the overshoots. α_1 does not significantly affect the responses for all three controllers. As a result, 10 times smaller c and 10 times larger α_2 weighting coefficients for q-axis current controller, 100 times larger c for d-axis current controller results in less overshoot, oscillations and transient time in total responses as seen in Figure 4.15 (Final controller parameters shown in Table 4.13)

Table 4.13 Nonlinear optimal controller parameters (final attempt)

	k_1	k_2	k_6	k_7	c_1	c_2
d-axis current controller	1.5	1.0428	0.0033	0.0031	0.001	0.001
q-axis current controller	47.43	149.4	1.05e-4	3.33e-4	0.001	0.001
Velocity controller	0.0080	0.0112	0.0014	0.0013	0.01	0.01

a.

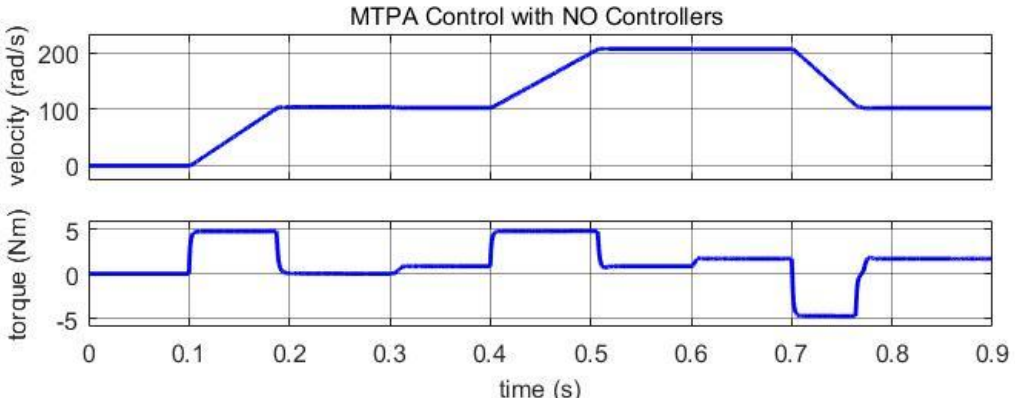

b.

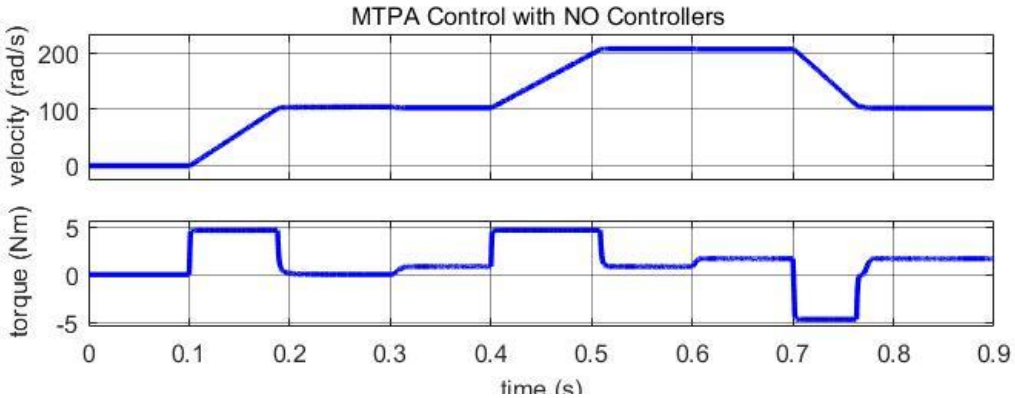

c.

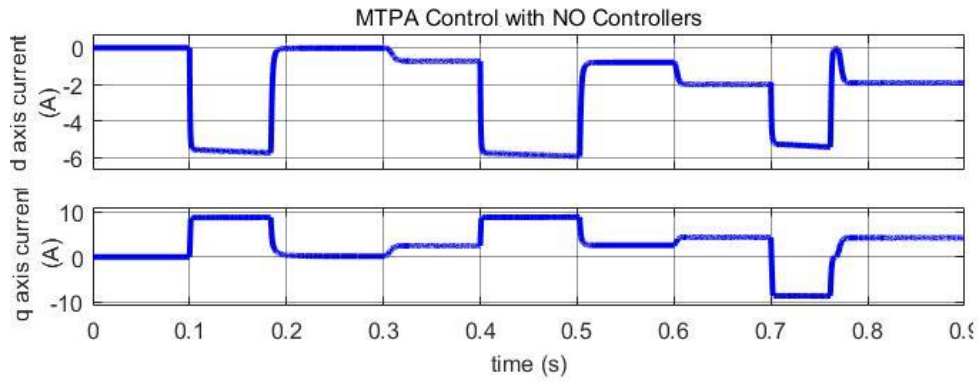

d.

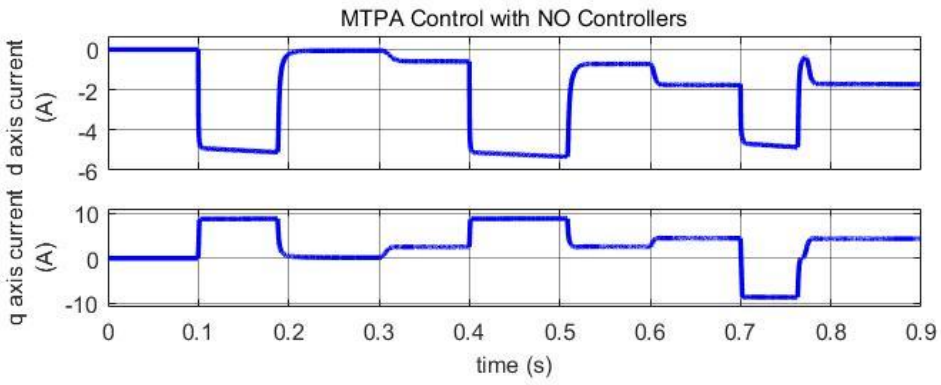

Figure 4.15 First and final responses

a. velocity and torque response for parameters in Table 4.3
b. velocity and torque response for parameters in Table 4.13
c. d, q axes currents responses for parameters in Table 4.3
d. d, q axes currents responses for parameters in Table 4.13

4.3. Application of Conventional Energy Efficient Control Approaches to Nonlinear Optimal IPMSM Drive

Figure 4.16 presents the results of simulation of ZDAC control structure of IPMSM when the PI controllers are replaced by the nonlinear optimal controllers. Please note that similar with PI controllers the outputs of the nonlinear optimal controllers and their integrators were saturated. The comparison of operation of both structures is only possible when the controllers are not saturated (close to steady state values). Compared to result with PI controllers in Figure 3.7 the velocity overshoots and undershoots are smaller and the same applies to the torque. The control modelling was performed based on IPMSM models ignoring and accounting for core loss.

Figure 4.17 depicts the results of simulation of MTPA control structure of IPMSM when the PI controllers are replaced by the nonlinear optimal controllers. Please note that similar with PI controllers the outputs of the nonlinear optimal controllers and their integrators were saturated. The comparison of operation of both structures is only possible when the controllers are not saturated (close to steady state values). Compared to the PI controllers case in Figure 3.8 the velocity overshoots and undershoots are smaller and the same applies to the torque. The modelling of the control was performed based on IPMSM models ignoring and accounting for core loss.

Figure 4.18 demonstrates the results of simulation of ME control structure of IPMSM when the PI controllers are replaced by the nonlinear optimal controllers. Please note that similar with PI controllers the outputs of the nonlinear optimal controllers and their integrators were saturated. The comparison of operation of both structures is only possible when the controllers are not saturated (close to steady state values). Compared to the PI controllers case in Figure 3.9 the velocity overshoots and undershoots are smaller and the same applies to the torque.

a.

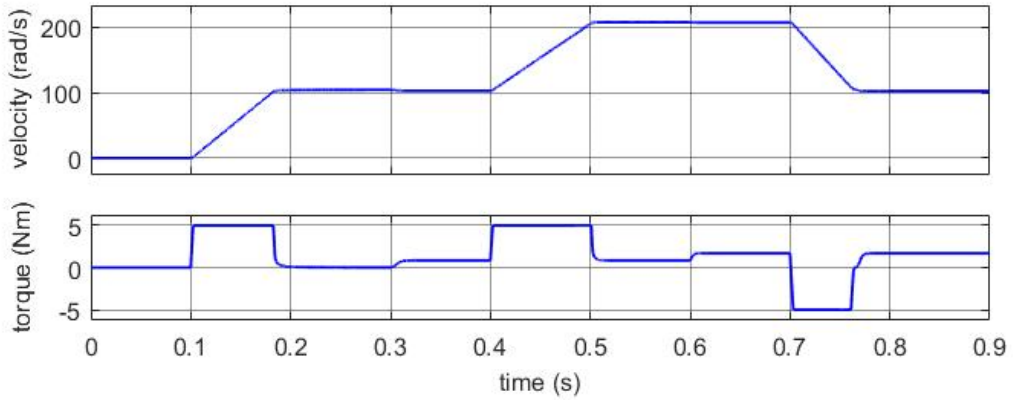

b.

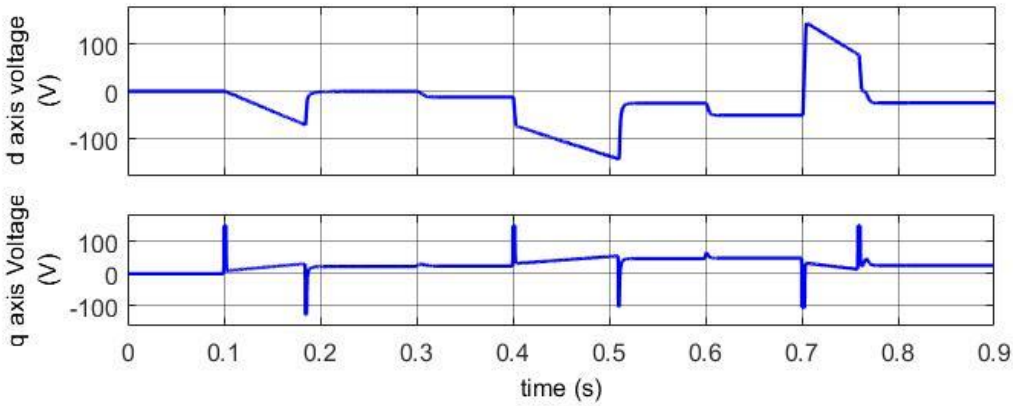

c.

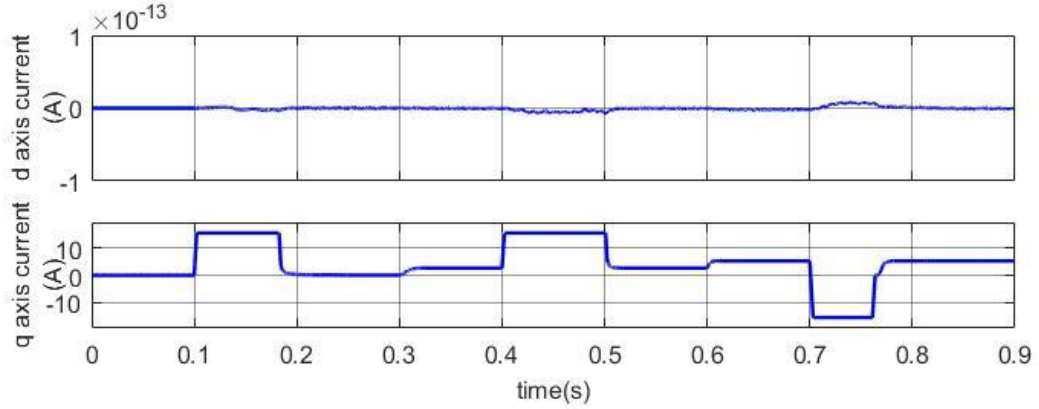

d.

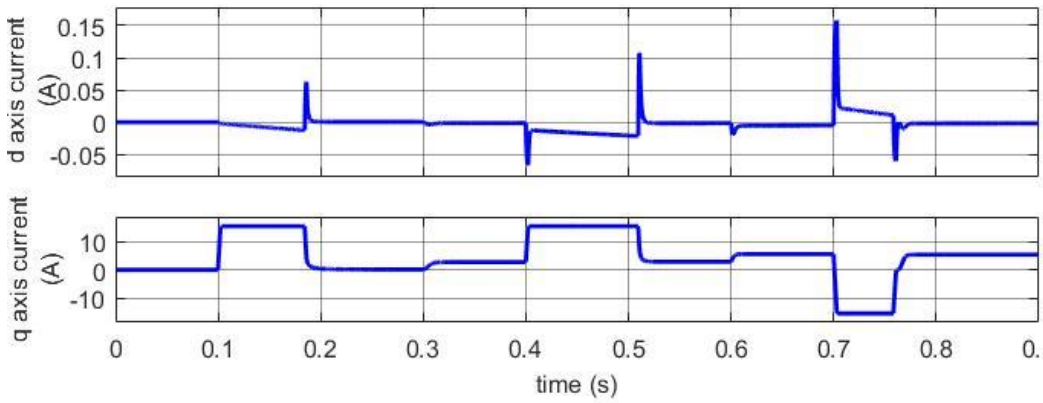

Figure 4.16 ZDAC Control with NO a. Velocity and torque response
b. d,q axes voltages
c. d,q axes currents (Ignoring core resistance)
d. d,q axes currents (Regarding core resistance

a.

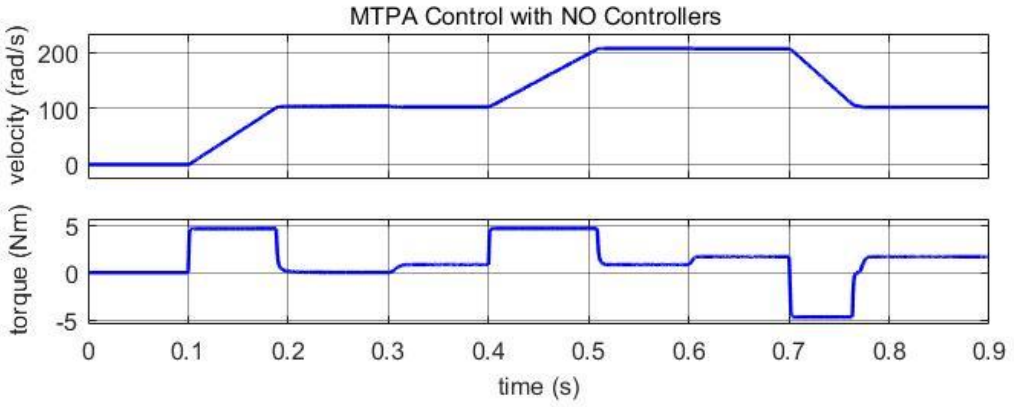

b.

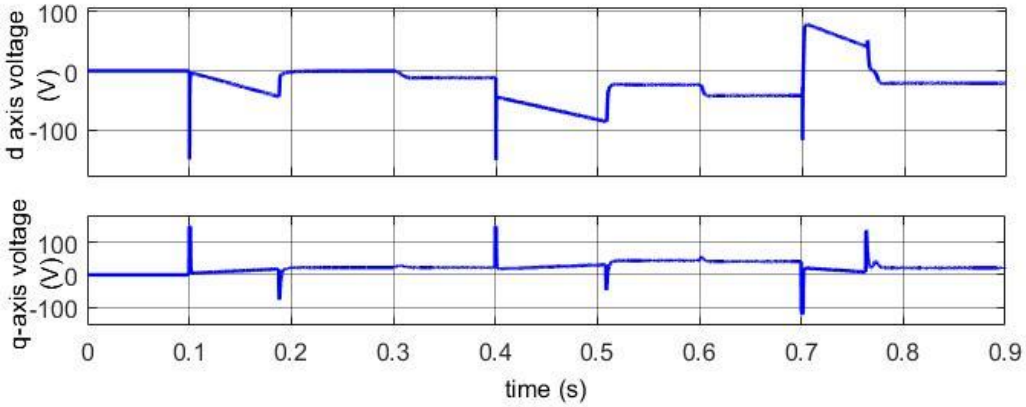

c.

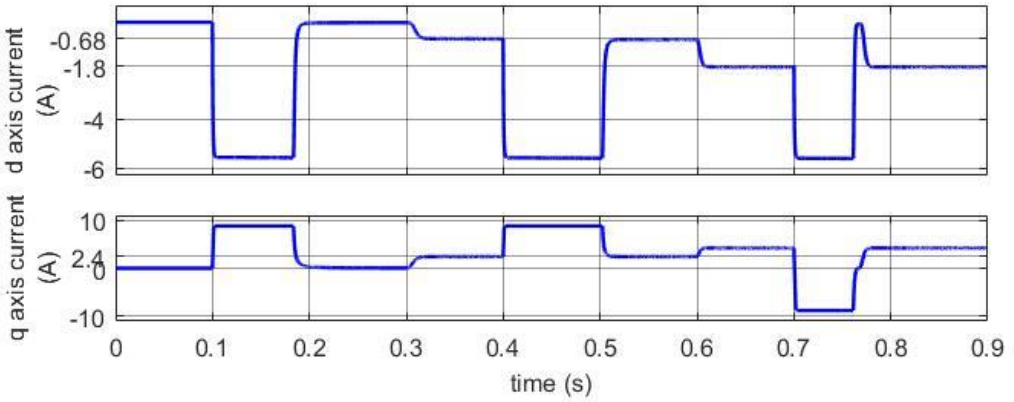

d.

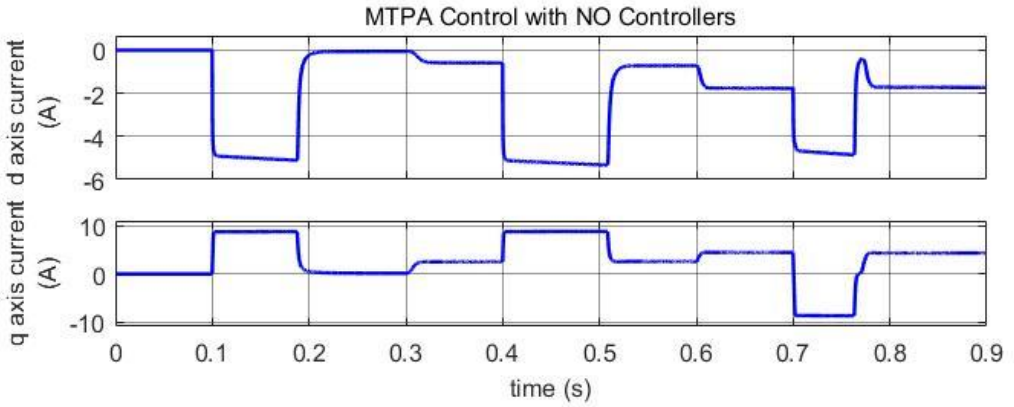

Figure 4.17 MTPA Control with NO
a. velocity and torque response
b. d,q axes voltages
c. d,q axes currents (Ignoring core resistance)
d. d,q axes currents (Regarding core resistance)

a.

b.

c.

d.

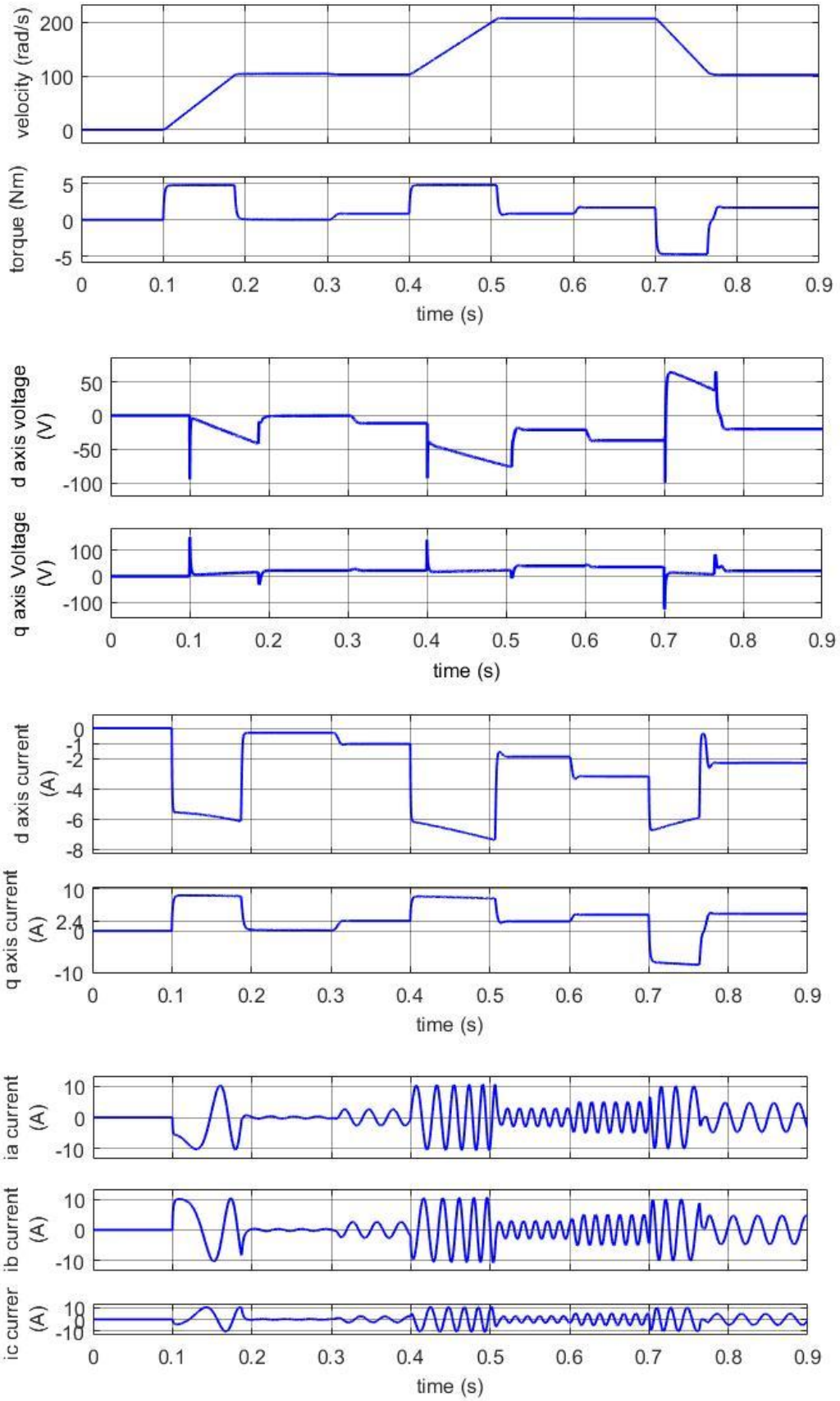

Figure 4.18 ME Control with NO

a. velocity and torque response
b. d,q-axis voltages
c. d,q axes currents
d. Phase a,b,c currents

4.4. Application of Energy Efficient and Transients Optimal Control Approach in Nonlinear Optimal IPMSM Drive

Figure 4.19 and Figure 4.20 present the simulation results of combined MTPA/ME control structure of IPMSM drive with $P_1 + P_2 + P_3 + P_4 = 0$ and $AB - T^2C = 0$ derivations respectively with nonlinear optimal IPMSM drive. It is worth to bear in mind that the outputs of the nonlinear optimal controllers and their integrators, similar with PI controllers, are saturated. Compared to the PI controllers case in Figure 3.13 and Figure 3.14 the velocity overshoots and undershoots are smaller and the same applies to the torque. The modelling of the control was performed based on IPMSM models ignoring and accounting for core loss. ($\beta = 0.5$)

Figure 4.21 demonstrates the results of simulation of energy efficient and transients optimal control structure of IPMSM with $AB - T^2C = 0$ derivations when the PI controllers are replaced by the nonlinear optimal controllers. Please note that similar with PI controllers the outputs of the nonlinear optimal controllers and their integrators were saturated. The comparison of operation of both structures is only possible when the controllers are not saturated (close to steady state values). Compared to the PI controllers case in Figure 3.15 the velocity overshoots and undershoots are smaller and the same applies to the torque. (β variates according to dynamic velocity error.). It is obvious in d-axis current characteristics in Figure 4.21c, a new control trajectory is traced between the MTPA and ME control trajectories according to β variations.

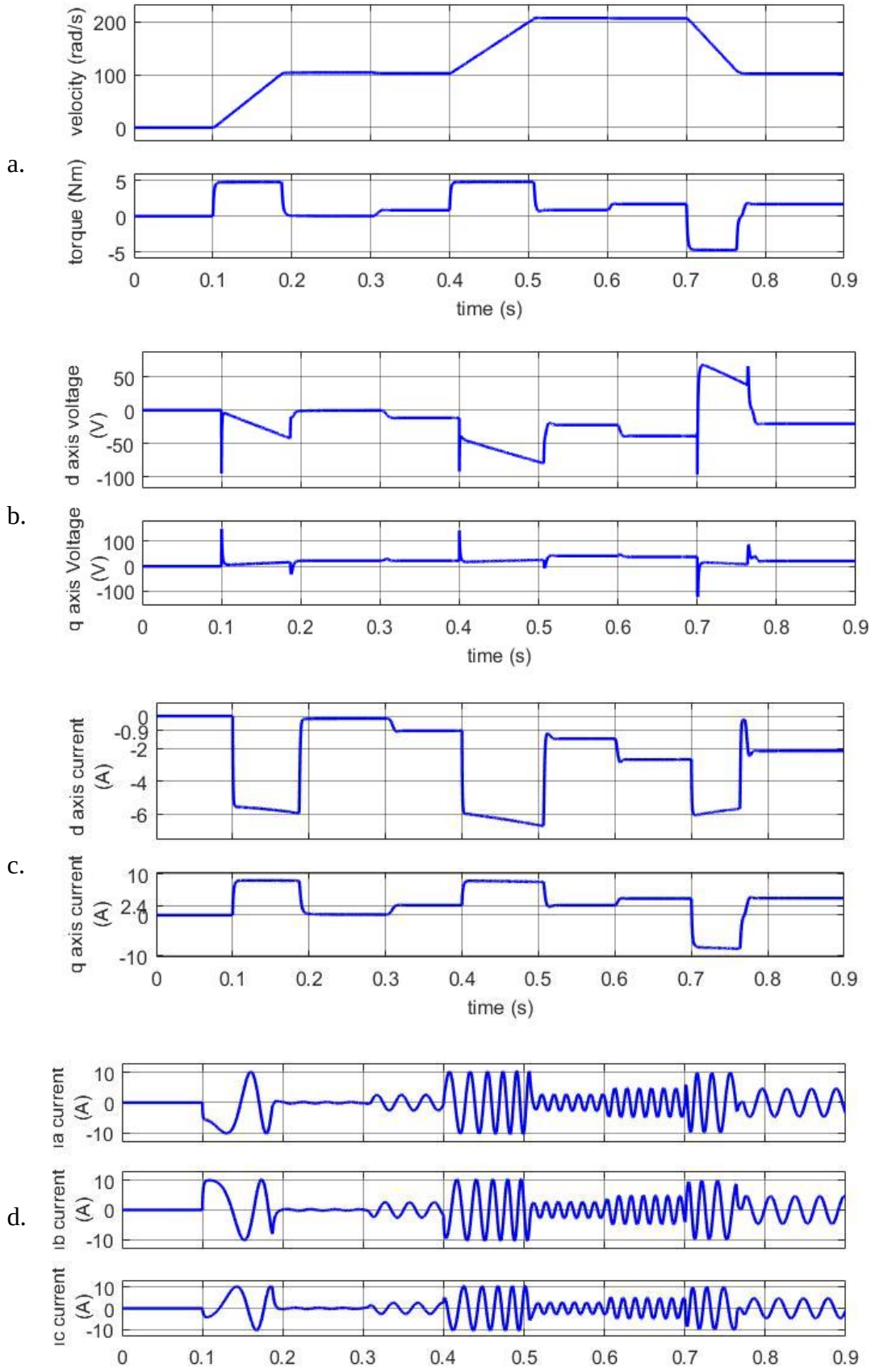

Figure 4.19 Combined MTPA/ME Control with NO first method

a. Velocity and torque response
b. d,q axes voltages
c. d,q axes currents
d. a,b,c phase currents

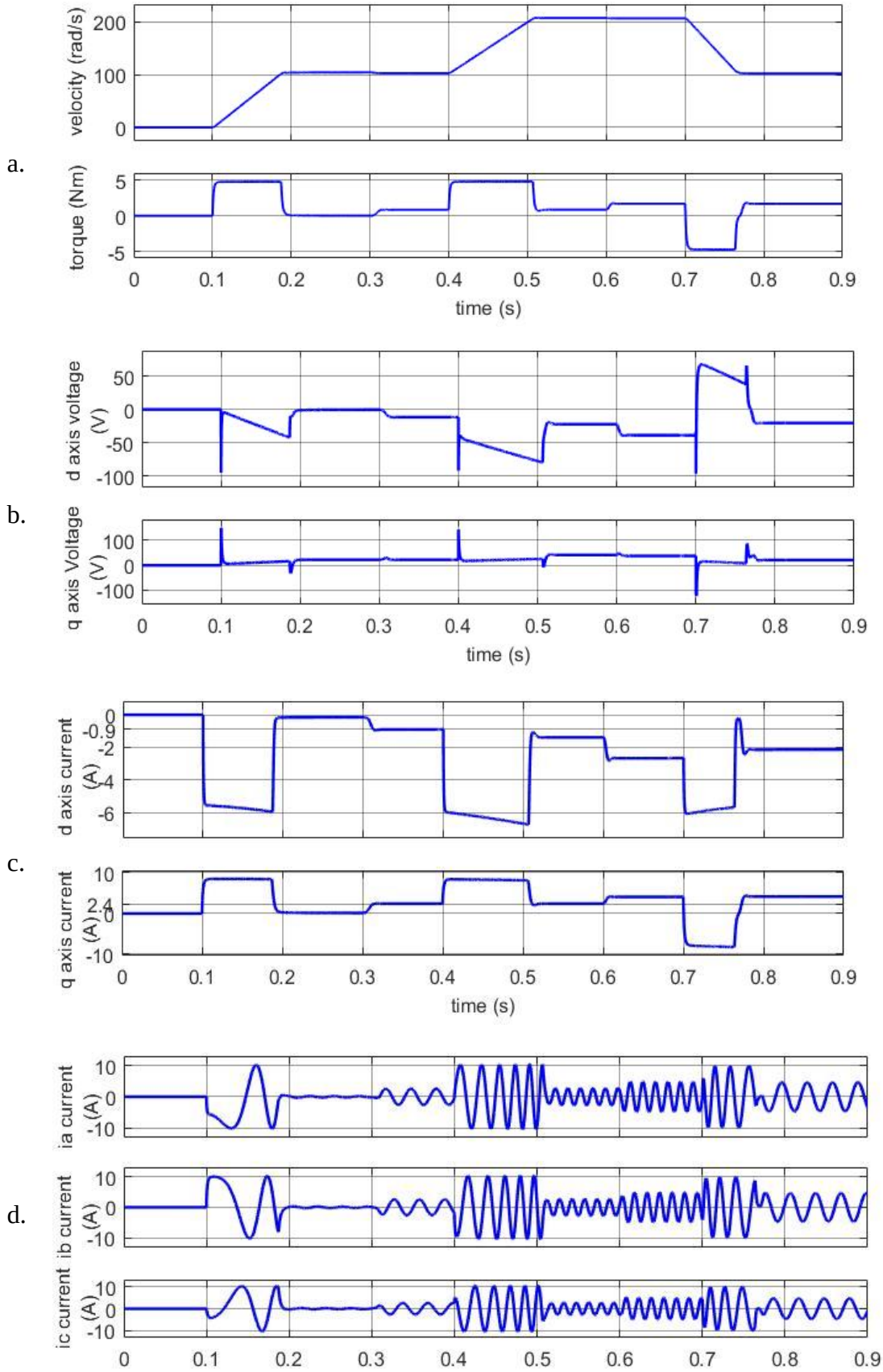

Figure 4.20 Combined MTPA/ME Control with NO second method

a. Velocity and torque response
b. d, q axis voltages
c. d, q-axis currents
d. a, b, c phase currents

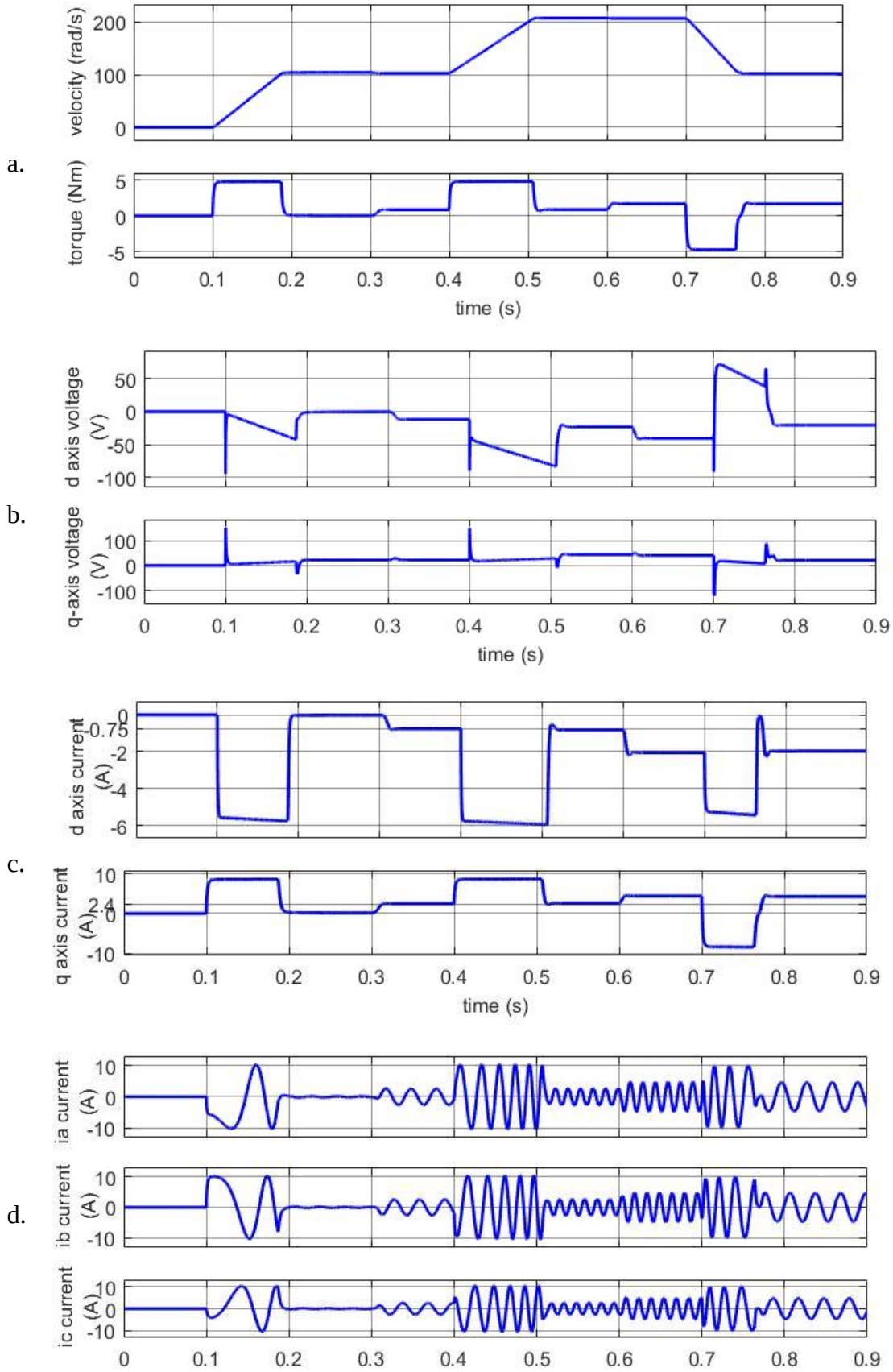

Figure 4.21 Combined MTPA/ME Control with NO third method

a. Velocity and torque response
b. d, q axes voltages
c. d, q axes currents
d. a, b, c phase currents

4.5. Robustness Assessment of Nonlinear Optimal IPMSM Drive

The simulation results for IPMSM drive under MTPA control approach are also investigated with both conventional PI (Figure 4.22) and NO controllers (Figure 4.23) to visually observe robustness of the methods against motor parameter variations. The default motor parameters and specifications are recalled in Table 4.14. The controllers are tuned with the gain parameters shown in Table 4.15.

In simulations, the velocity reference is linearly increased to the rated value (2000 rpm) starting at 0.1 s and without load. After the system reaches the reference velocity, the load torque is applied as the rated torque value $T_{rated} = 1,67$ Nm.

The simulations are performed with various moment of inertia values J= (0.004, 0.04, 0.0004) kgm² for both PI and NO controllers. As expected, the conventional method is more sensitive to the variations of moment of inertia than the proposed method. It is worth to remind that the initial start happens when both NO and PI velocity controllers are saturated, so the difference will be not seen. More overshoots appear with PI controllers when the velocity is close to its reference value and the region corresponding to the step load applying, even with the default parameters. The oscillations happens due to the parameter variations (the moment of inertia). However, it is obvious IPMSM drive with nonlinear optimal controllers overdamped the overshoots and oscillations. Thus, the proposed method helps to increase robustness without any hardware change.

Table 4.14 IPMSM parameters and specifications used in simulations

Rated Torque T_{rt} (Nm)	1.67
Rated Current I_{rt} (A)	5
Rated Speed W_{rt} (rpm)	2000
Rated Voltage V_{rt} (V)	97
DC link Voltage V_{dc} (V)	150
R_s (Ω)	0.57
L_q (mH)	22.78
L_d (mH)	8.72
λ_{af} (Wb)	0.1077
n_p	2

Table 4.15 The controller parameters of IPMSM drive used in simulations

		i_d Controller	i_q Controller	ω_m Controller
PI	ki	125	285	285
	kp	1	4.36	4.36
NO	K1	15	15	0.0080
	K2	14.44	14.4636	0.0112
	K6	3.33e-4	3.33e-4	0.0014
	K7	3.33e-4	3.32e-4	0,0013
	C1	0.001	0.001	0.01
	C2	0.001	0.001	0.01
	Saturation	10	10	0.05

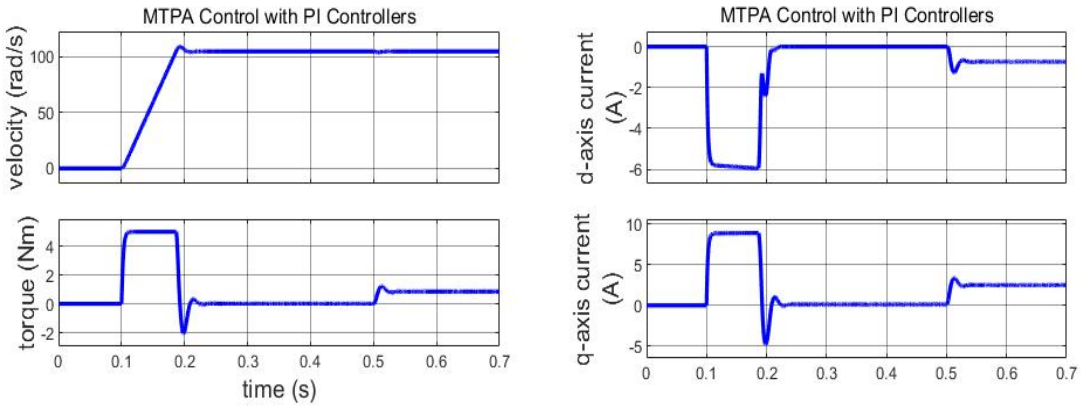

a. b.

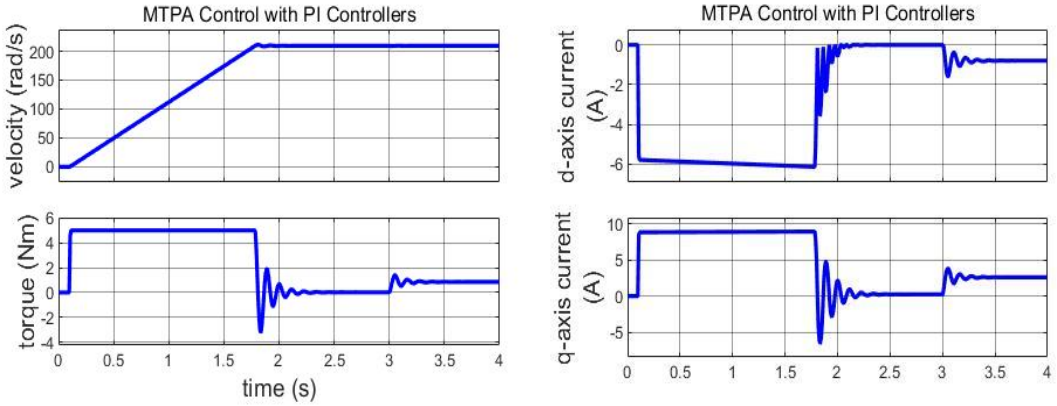

c. d.

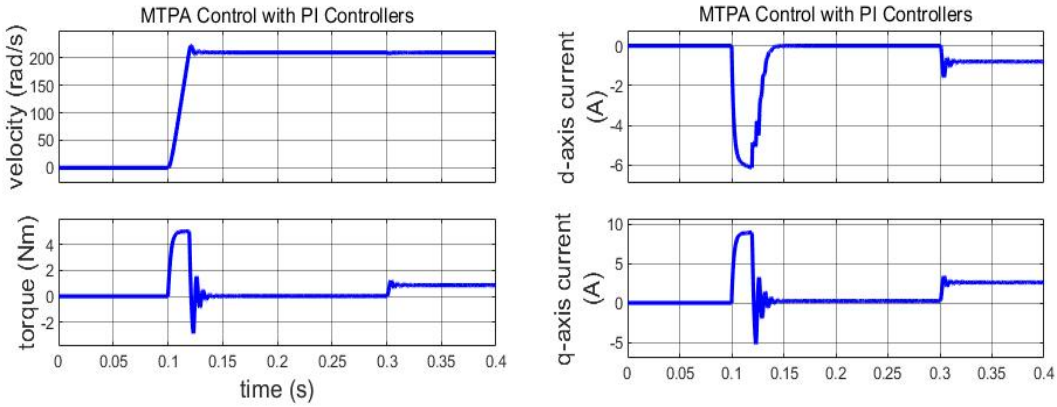

e. f.

Figure 4.22 IPMSM drive under MTPA control with PI controllers

a.) Velocity and torque responses for $J = 0.004\ Nm^2$

b.) d, q-axis current responses for $J = 0.004\ Nm^2$

c.) Velocity and torque responses for $J = 0.04\ Nm^2$

d.) d, q-axis current responses for $J = 0.04\ Nm^2$

e.) Velocity and torque responses for $J = 0.0004\ Nm^2$

f.) d, q-axis current responses for $J = 0.0004\ Nm^2$

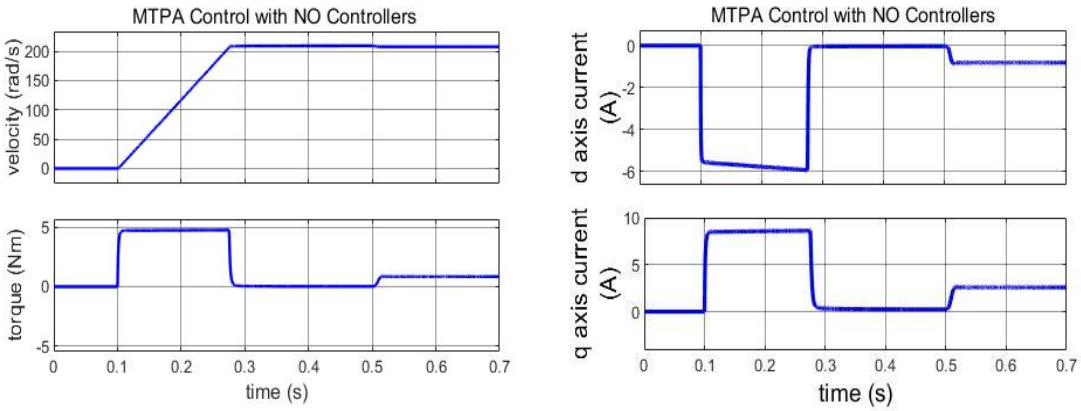

a. b.

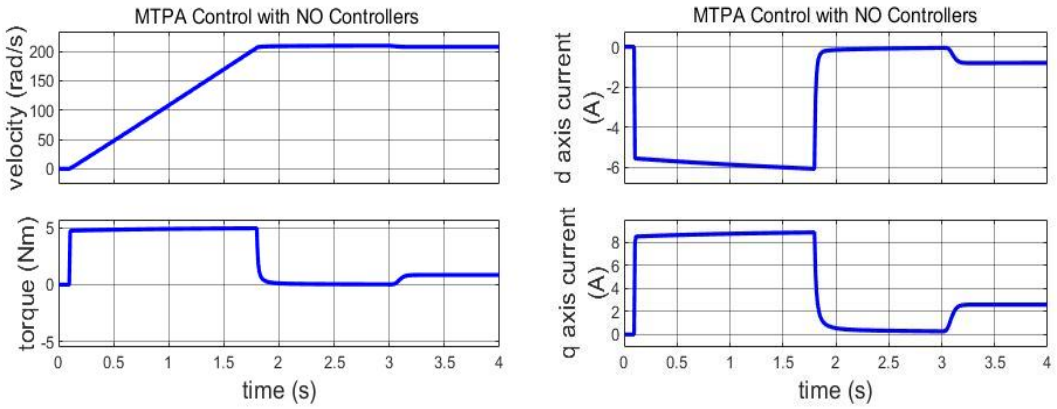

c. d.

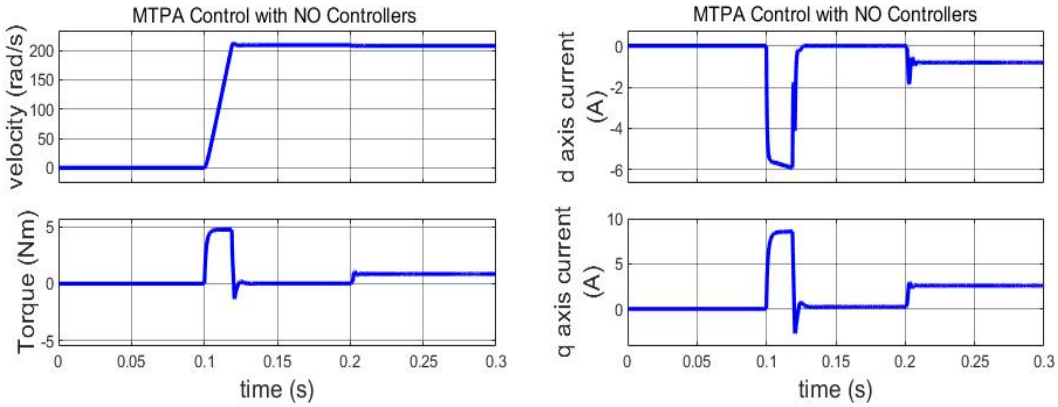

e. f.

Figure 4.23 IPMSM drive under MTPA control with NO controllers

a.) Velocity and torque responses for $J = 0.004\ Nm^2$

b.) d, q-axis current responses for $J = 0.004\ Nm^2$

c.) Velocity and torque responses for $J = 0.04\ Nm^2$

d.) d, q-axis current responses for $J = 0.04\ Nm^2$

e.) Velocity and torque responses for $J = 0.0004\ Nm^2$

f.) d, q-axis current responses for $J = 0.0004\ Nm^2$

4.6. Conclusions

The purpose of this chapter to enhance robustness of the conventional IPMSM drives. The PI controllers in conventional IPMSM drives are replaced with nonlinear optimal controllers to accomplish this objective. LQR procedure with integral actions is first employed to identify the optimal control parameters, which is linear part of the NO controllers. The very well-known reality is that if the operating point in real-time operation changes, the optimal control parameters should be adjusted, too. In order to prevent parameter updates, which forms the nonlinear part of the NO controllers, Krasovskiy's optimality criterion is applied. Consequently, a real-time automatic control action is provided instead of updating LQR gain parameters.

The optimal gain parameters are identified based on a cost function in LQR procedure which can be adjusted based on operation requirements. In this study, the **Q** and **R** matrices in the cost function, represents the weighting coefficient of the state space and input variables, are identified based on heuristic method.

The robustness of the proposed IPMSM drive is assessed with the simulations in created Matlab Simulink via changing the moment of inertia (to observe the reaction to parameter variations.)

The proposed method offers improved performance due to its robustness in the presence of uncertainties and parameter variations during real-time operation. Being based on conventional control structure and requiring just software adjustments rather than changes in hardware. This feature allows to upgrade existing industrial IPMSM drives to a more robust version.

CHAPTER 5. VERIFICATION OF ENERGY-EFFICIENT NONLINEAR OPTIMAL CONTROL FOR IPMSM DRIVES

5.1. Introduction

This chapter is designed to

- explain the main hardware scheme of the laboratory-based test rig
- explain the main software scheme of the test rig
- evaluate MTPA and ME control approaches in IPMSM drives with conventional FOC concept to see how feasible it is to implement the combined MTPA/ME control approach into existing industrial IPMSM drives
- evaluate the proposed nonlinear optimal control approach embedded in FOC control concept for IPMSM drives and validate how feasible it is to implement the proposed control concept and its robustness in real time operation

5.2. Overview of the Laboratory-based Test Rig

The real time experimental verification of this study was carried out on a pre-set test rig in the laboratory facilities of the Power and Control Systems Research (PCSR) Group of the School of Engineering of the University of Warwick. It is demonstrated in Figure 5.1.

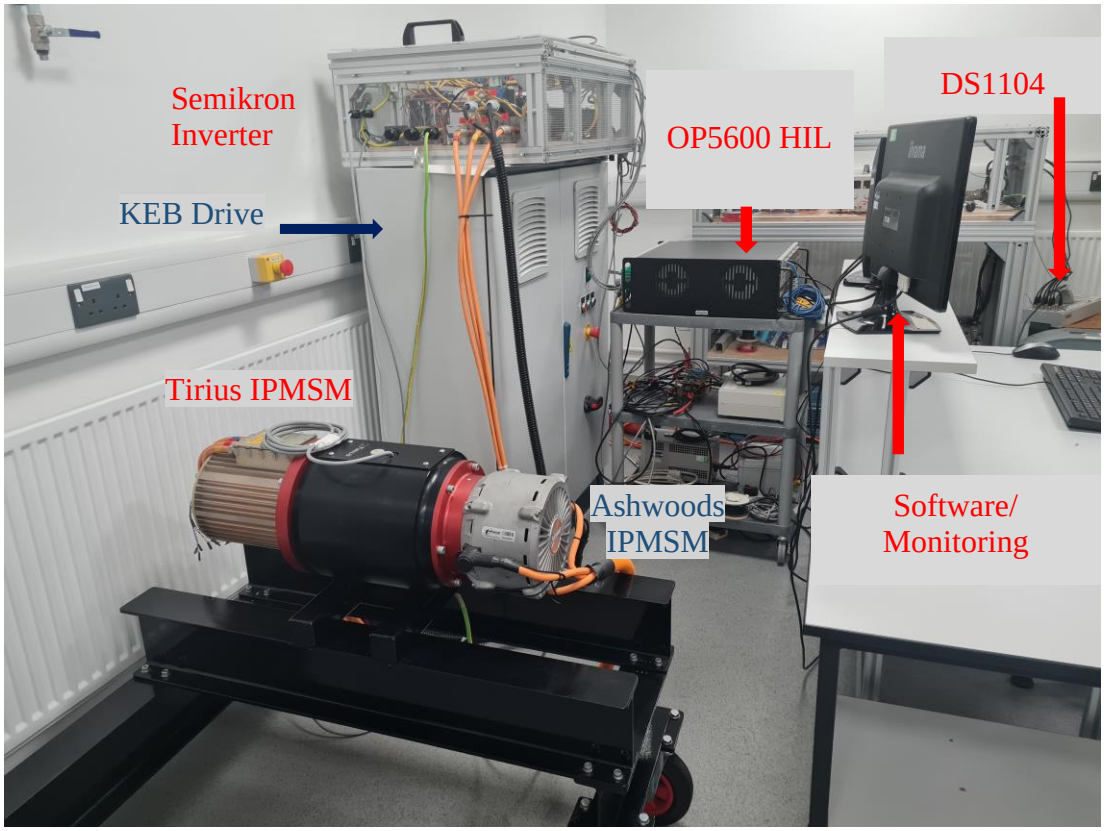

Figure 5.1 Test Rig

The test rig is built around two mechanically coupled IPMSMs of approximately the same rated power of 12 kW. Either of the motors can be used as under test motor or the load motor. The load motor is connected to the industrial AC drive from KEB with imbedded vector torque or velocity control. In this research the load motor was torque controlled. The KEB cabinet contains an inverter and a regenerative unit allowing to return the power from the DC link to return to the grid. The torque

reference and parameters of the load motor are set and monitored using a special KEB software - KEB Combivis 6. The motor under test is connected to a two-level three-phase inverter designed in the PCSR Group based on Semikron power modules. The control of the inverter is implemented OPAL RT OP5600 and dSpace DS1104 rapid control prototyping systems. Each of the motor is equipped by a resolver. The resolver of the load machine is connected to the corresponding interface of the KEN inverter. The signals from the under-test motor resolver are processed by the DS1104 and imbedded their velocity and position observer and finally the instantaneous values of velocity and position are transferred to OPAL RT OP5600. The OPAL RT implements corresponding control algorithms for the under-test motor including space vector PWM and protections: overcurrent and overvoltage. There are a DC link voltage sensor and a current sensor in each phase of the underload moto interfaced with the analog inputs of the OPAL-RT. Digital outputs of the OPAL-RT used for PWM modulation are galvanically isolated. The DC link of the inverter can be connected to the DC link of the KEB inverter but in this research, it was connected to a Magna DC supply to eliminate influence of the inverters on each other. The test rig was set up before this PhD research. In this PhD research only software part was modified to implement required control approaches.

The block diagram of the Test Rig to show the connections between the unites is demonstrated in Figure 5.2. And the control design created in Matlab Simulink with RT-Lab-platform to be carried out on the embedded FPGA unite in Opal-RT OP5600 Hardware in the loop (HIL) shown in

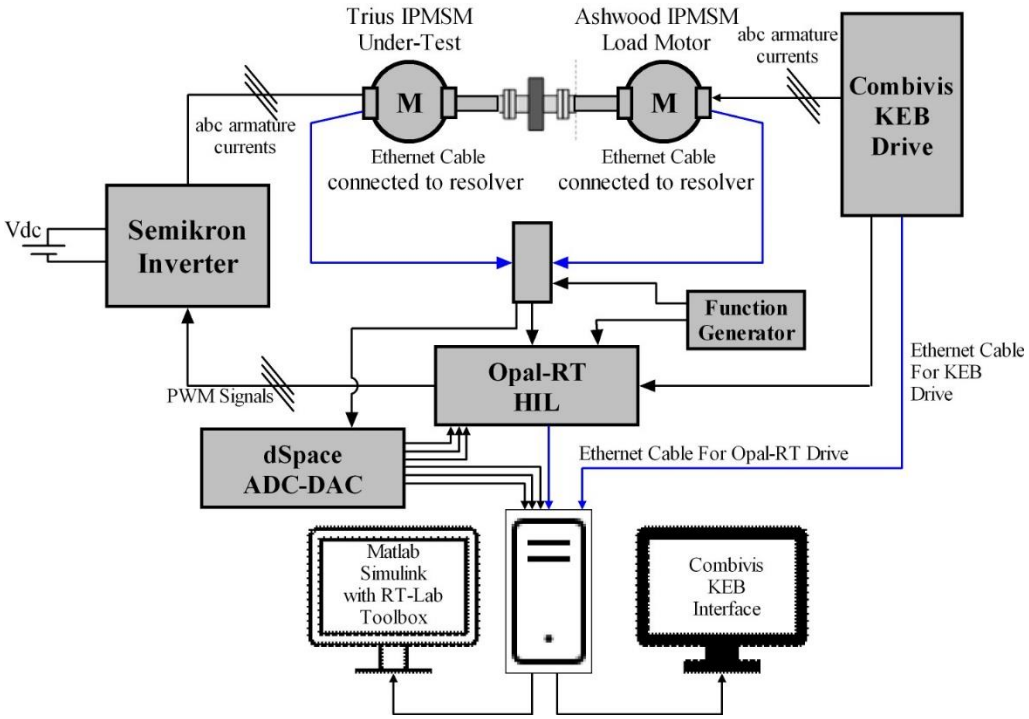

Figure 5.2 Connections of the test rig hardware

The test rig is an air-cooled system and compatible with standalone DC electric power supplies and standard 3-phase industrial grid. All hardware units and software required are specified in Table 5.1 The detailed explanations for both load and under-test motors is illustrated in **Appendix I**

Table 5.1 The hardware Unites of the Test Rig

No:	Identification	Explanation
1	Under Test Motor	Tirius JEM02 IPMSM, three-phase, 5 pole, 12kW, 28 Nm, 3700 rpm, 560 Vdc
2	Under Test Motor Drive	Semikron 3 power modules based three-phase IGBT inverter with 600 VDC
3	Load Motor	Ashwoods dual core IPMSM, three-phase, 4 pole, 10kW,43Nm, 3250 rpm 560 Vdc
4	Load Motor Drive	KEB COMBIVERT F5 AC motor controller and drive unit, 30kW, 305-500V,2-16kHz
5	Real Time Simulator	OPAL-RT OP5600 HIL
6	Real Time Simulator	dSPACE DS1104
7	Signal Generator	Any signal generator to produce 10kHz sin wave is acceptable
8	Software	Matlab Simulink with RT-Lab platform
9	Software	KEB Combivis 6 interface
10	Resolver	
11	High Power DC Supply	For Semikron İnverter

The Combivert F6 KEB Cabinet, which is particularly utilised for the load motor control, is a control cabinet designed as a 3-phase 415 V motor drive and regenerative unite. It mainly consists of two Combivis R6 AC-DC converters, one Combivis F5 3-phase DC-AC inverter and a DC busbar link among them. The cabinet represents the behaviours of the conventional industrial IPMSM drives controlled by traditional PWM signals produced by Combivis KEB 6 software created with CODESYS Automation Platform.

The function generator is used to supply 10 kHz sinusoidal signal for the resolver carrier signals for velocity estimation through dSpace DS1104.

The Semikron 3 phase inverter is designed based on three one-leg IGBT-modules with 600 VDC, which is implemented into modifiable power box to be able to verify various hardware architecture.

5.3. Validation of conventional MTPA and ME Control Approaches in FOC for industrial IPMSM drives

The results of experimental testing of standard MTPA and ME approaches are presented in Fig. 5.3. The no load start of the motor with linear reference increase till 3000 rpm was explored following by the gradual 2 Nm step increases in the load torque (and decreases at the end). As it can be observed in the figure, the torque overshoots are always higher for the MTPA case. During the no load start the torque is higher for the MTPA and this reduces the transients time.

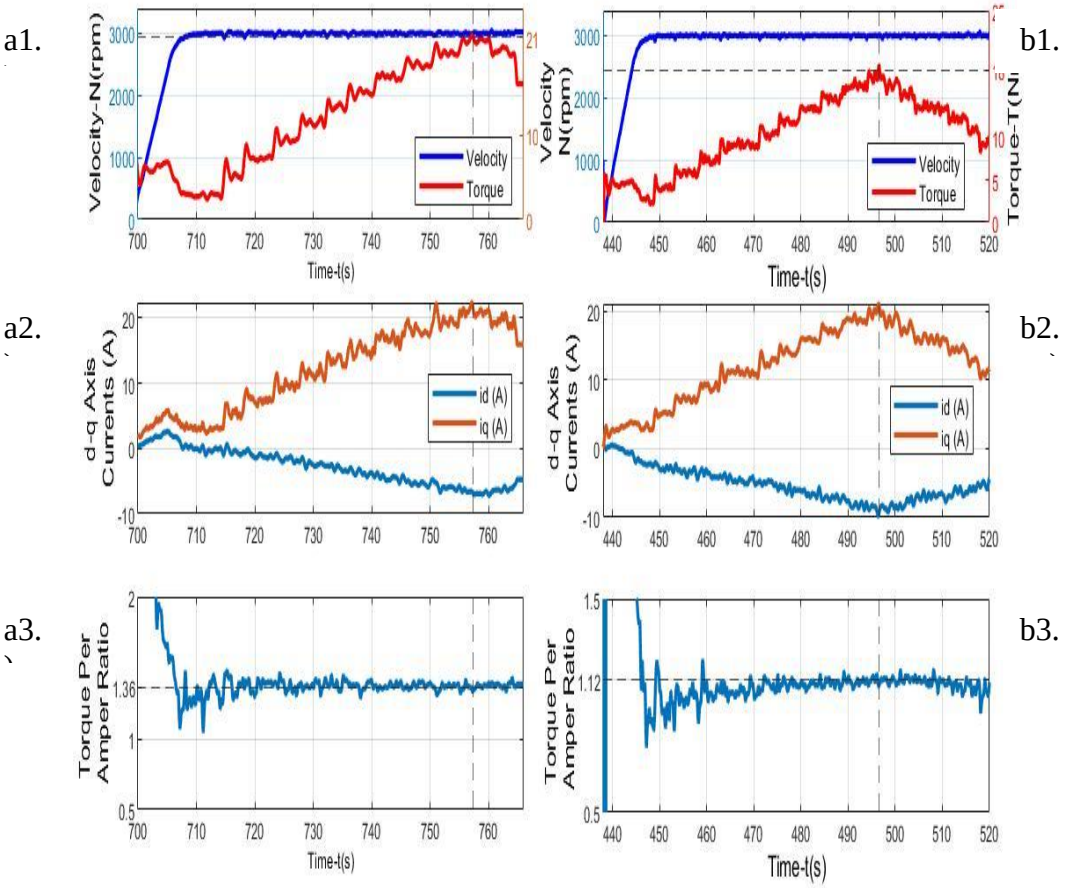

Figure 5.3
a.) MTPA Control
b.) ME Control

1.) Velocity and Torque Response
2.) d, q axis currents
3.) Torque to Current Ratio

As expected, the torque per Ampere ratio is higher for the MTPA case. The analysis proves the sense of combining the MTPA and ME approaches in 'transients optimal and energy efficient drive'. The parameters of the motors used in the control algorithms were provided by the motors manufacturers. The parameters of the PI controllers are shown in Table 5.2.

Table 5.2 PI Controller Parameters

		i_{dr} Controller	i_{qr} Controller	ω_m Controller
PI	k_i	8	8	1.2
	k_p	6	6	0.2

5.4. Nonlinear Optimal Control with MTPA

Fig. 5.4 shows the results of the experimental testing of the system with Nonlinear Optimal Controllers and MTPA. The no load motor start till 2000 rpm following the linear reference increase is explored. It is followed by a gradual loading increase with 2 Nm load torque steps.

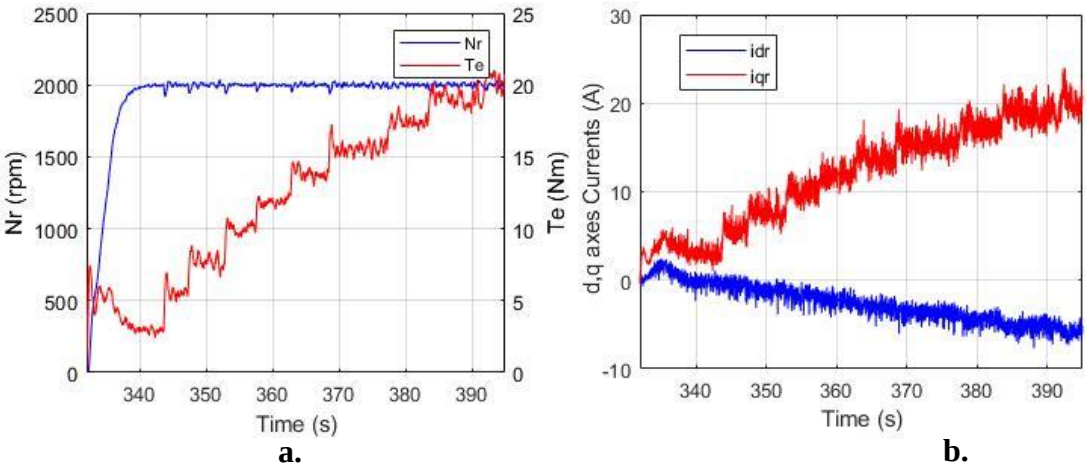

Figure 5.4. Experimental Data a.) Torque and velocity response b.) *d*, *q*-axis currents

Table 5.3 The Parameters in the Nonlinear Optimal Controllers

		i_d Controller	i_q Controller	ω_m Controller
	K1	8	8	1,2
	K2	6	6	0,2
	K6	0,4	0,8	0,12
NO	K7	0,3	0,6	0,02
	C1	15,6	15,6	694,45
	C2	27	27	25000
	Sat	35	175	29,167

It is worth to bearing in mind that the torque overshoots in this case with respect to the steady state step values are lower than in the case of the ordinary MTPA with PI controllers in Fig. 5.3. And they are approximately the same for different temporary operating points. This means less influence on the corresponding velocity deviations from the steady state value. The control implementation is feasible and demonstrates some dynamics improvement. The parameters of the Nonlinear Optimal Controllers are presented in Table 5.3.

5.5. Conclusions

The purpose of this chapter is to support energy efficient and transients optimal control structure proposed in Chapter 3 and nonlinear optimal IPMSM drive proposed in Chapter 4 with experiments. An extensive lab-based experiment rig is used to test existing and proposed control methods.

The experiment results for energy efficient and transients optimal control method show that conventional MTPA control provides better torque capability than the ME control method. The proposed energy efficient and transients optimal control method can provide energy efficient operation during steady states and better torque response is achieved during transients.

The experimental testing of Nonlinear Optimal IPMSM drive under MTPA control showed that overshoots in torque response were reduced compared to the case with PI controllers.

CHAPTER 6. CONCLUSIONS

The literature review has shown that the control of IPMSMs includes the high-performance torque or velocity control to meet the dynamical demands of the application and the energy consumption optimisation algorithms which improve the efficiency of the motor operation. Zero D-axis current, MTPA and ME approaches are utilised. Zero D-axis control is usually used in industrial drives. There are no established routes to make a choice between the MTPA and ME approaches. ME control can provide higher efficiency, but the accurate modelling of the core loss is required, and iterative real time solution of the implicit optimal equation is necessary. MTPA control is simpler in implementation since it does not require the core loss modelling and can provide faster dynamics. Therefore, there is a research space in solving this dilemma which this thesis addresses via combining both methods based on operating conditions. The torque and velocity control should cope with the inaccuracy of parameters and their variations along with the nonlinearities introduced by the nonlinear energy efficient algorithms. The new control approaches to be accepted by industry should require no significant hardware changes and should be straightforward in upgrading the existing industrial drives and simple in attenuation.

The research succeeded in analytical derivations of the nonlinear implicit optimal equation for the combined MTPA/ME method from which the optimal d-axis current can be computed iteratively in real time and the equation is identical to the

corresponding optimal equation of the ME method except two parameters which are scaled. It means only minor control code update when upgrading ME to the combined MTPA/ME. The derivations are based on the concept of the fictitious total electric loss which consists of the copper loss and a fraction of the core (iron) loss. The dilemma of the choice between the MTPA and ME is transformed into the problem of the optimisation of the fraction parameter. Moving this parameter between zero and one allows approaching either MTPA or ME control depending on operation conditions. This PhD research demonstrates very easy and straightforward application of the combined MTPA/ME method to implement 'transients optimal and energy efficient drive' providing the MTPA control during transients for faster dynamics and the ME control during steady states for higher efficiency and the transitions between the methods are smooth and simple.

This PhD research introduces the concept of Nonlinear Optimal Control of IPMSM. The control structure is the same as in industrial drives with the close velocity loop and two currents loops, but three PI controllers are replaced by three Nonlinear Optimal Controllers. The linear parts of the controllers are designed as LQR controllers with integral actions for a specific operating point based on the linearised model of the IPMSM. In fact, these are PI controllers with the optimal LQR gains for this point. Then the models of the loops are updated considering the deviations of the LQR gains from the designed values as new control inputs. Application of the LQR control design procedure combined with the criterion of the generalised work of A. Krasovskiy allows to yield the control solution in explicit view. The nonlinear optimal parts emulate the adjustments of the LQR gains of the linear parts based on operating conditions. It allows to cope with inaccuracy of parameters and their varying in permitted ranges and with nonlinearities of the energy consumption optimisation

algorithms. It allows to avoid using extensive look up tables for updating the LQR gains for various operating points. Although the theory behind is quite complicated, the upgrading of industrial drives with PI controllers is straightforward and simple: no hardware change is required and only software related to the PI controllers must be modified. Practical engineers making the upgrade do not need to have knowledge in optimal control theory since there are explicit formulae for all parameters of the controllers.

Simulation of the proposed control approaches and comparison with existing methods proved the analytical derivations and expected advantages. The feasibility of the Nonlinear Optimal Control was proved using an experimental test rig with rapid control prototyping using OPAL RT OP5600 and dSpace DS1104 systems. The dSpace was used for the velocity and position estimations only based on the signals from a resolver. The rest of the control was implemented in OPAL RT and squeezed into 100 μs execution time.

6.1. Foreseen Future Work

This study stands for investigating more energy efficient and robust control structures for IPMSM drives than the conventional industrial ones. An energy efficient and transients optimal IPMSM drive is first introduced. The main purpose of this method to specialise the conventional IPMSM drives to electric vehicle applications. The method is supported with extensive simulations created in Matlab Simulink. The simulation results show that the combining MTPA and ME control approaches according to operating circumstances may provide more energy efficient during steady state and faster torque dynamics during transients. However, the energy efficient and transients optimal control method is not validated according to specific operating conditions for electric vehicles. Developing a Simulink model consisting of IPMSM drive under energy efficient and transients optimal control method combined with electric vehicle model is a foreseen future work. Consequently, the effects of the proposed control method on battery, efficiency characteristics in standard driving cycles introduced in literature may be validated.

Main advantage of the nonlinear optimal IPMSM drive introduced in Chapter 4 is enhancing robustness against any uncertainties and parameter variations. The control structure is extensively introduced in the study. The method is validated with simulations in Matlab Simulink. It is assessed with various energy efficient control approaches. The method does not require any LUTs or updates during real-time operation, therefore it is advantageous. However, the optimal control parameters are investigated with heuristic method. This is time-consuming and should be repeated for each IPMSM from the beginning. This control parameter identification method can be replaced with an offline method based on stability analysis and can be coded in Matlab to shorten engineering time spent on optimal control parameter identification.

Both control methods proposed in this Ph.D. study are extensively validated in simulations created in Matlab Simulink. However, the experimental results need to be extended especially for operation in flux weakening region. Therefore, it is planned to combine proposed methods with a flux weakening solution in simulation at first. Then this new control approach for a wide speed range will be validated on the lab-based experiment rig introduced in this study.

REFERENCES

[1] F. Knobloch *et al.*, "Net emission reductions from electric cars and heat pumps in 59 world regions over time," *Nat Sustain*, vol. 3, no. 6, pp. 437–447, Jun. 2020, doi: 10.1038/S41893-020-0488-7.

[2] C. C. Chan and K. T. Chau, *Modern electric vehicle technology*, vol. 47. Oxford: Oxford University Press, 2001. [Online]. Available: https://go.exlibris.link/hv75ln6R

[3] R. Krishnan, *Permanent Magnet Synchronous and Brushless DC Motor Drives*. CRC Press, 2017. doi: 10.1201/9781420014235.

[4] S. Vaez-Zadeh, *Control of Permanent Magnet Synchronous Motors*. Oxford University Press, 2018. doi: 10.1093/OSO/9780198742968.001.0001.

[5] S. Morimoto, M. Sanada, and Y. Takeda, "Wide-Speed Operation of Interior Permanent Magnet Synchronous Motors with High-Performance Current Regulator," *IEEE Trans Ind Appl*, vol. 30, no. 4, pp. 920–926, 1994, doi: 10.1109/28.297908.

[6] S. Morimoto, Y. Tong, and T. Hirasa, "Loss Minimization Control of Permanent Magnet Synchronous Motor Drives," *IEEE Transactions on Industrial Electronics*, vol. 41, no. 5, pp. 511–517, 1994, doi: 10.1109/41.315269.

[7] S. Amornwongpeeti, O. Kiselychnyk, J. Wang, C. Antaloae, M. Soumelidis, and N. Shah, "A combined MTPA and maximum efficiency control strategy for IPMSM motor drive systems," in *2016 International Conference on Electrical Systems for Aircraft, Railway, Ship Propulsion and Road Vehicles and*

International Transportation Electrification Conference, ESARS-ITEC 2016, Feb. 2017. doi: 10.1109/ESARS-ITEC.2016.7841412.

[8] M. Oztekin, O. Kiselychnyk, and J. Wang, "Energy Efficient and Transients Optimal IPMSM Drive for Electric Vehicles," in *2022 International Symposium on Power Electronics, Electrical Drives, Automation and Motion (SPEEDAM)*, Jun. 2022, pp. 832–837. doi: 10.1109/SPEEDAM53979.2022.9842114.

[9] M. Oztekin, O. Kiselychnyk, and J. Wang, "Nonlinear Optimal Control for Interior Permanent Magnet Synchronous Motor Drives," in *2022 European Control Conference (ECC)*, Jul. 2022, pp. 590–595. doi: 10.23919/ECC55457.2022.9838314.

[10] V. Kudin, J. Koláčný, and O. Kiselychnyk, "Suboptimal two-zone automatic control system of separately excited direct current motor velocity," *Mendel*, vol. 2005-Janua, no. January, pp. 196–201, 2005.

[11] V. Kudin, J. Kolacny, O. Kiselychnyk, and H. Metelskaya, "Robust Controller Analytical Design of Electrical Drive by Using Bellman- Lyapunov Method," in *7th International Conference on Soft Computing.* , Jun. 2001, pp. 1–7.

[12] M. A. Rahman, "Status Review of Advances in Hybrid Electric Vehicles." https://www.ieee-pes.org/presentations/gm2014/PESGM2014P-002604.pdf (accessed Aug. 15, 2022).

[13] R. Krishnan, "Criteria for the comparison of motor drive systems in motion control," in *Singapore International Conference on Intelligent Control and Instrumentation - Proceedings*, 1992, vol. 1, pp. 127–133. doi: 10.1109/SICICI.1992.641659.

[14] R. Krishnan, “Selection Criteria for Servo Motor Drives,” *IEEE Trans Ind Appl*, vol. IA-23, no. 2, pp. 270–275, 1987, doi: 10.1109/TIA.1987.4504902.

[15] P. Pillay and R. Krishnan, “Modeling, Simulation, and Analysis of Permanent-Magnet Motor Drives,Part I: The Permanent-Magnet Synchronous Motor Drive,” *IEEE Trans Ind Appl*, vol. 25, no. 2, pp. 265–273, 1989, doi: 10.1109/28.25541.

[16] T. Sebastian and G. R. Slemon, “Operating limits of inverter-driven permanent magnet motor drives,” *IEEE Trans Ind Appl*, vol. IA-23, no. 2, pp. 327–333, 1987, doi: 10.1109/TIA.1987.4504909.

[17] R. Krishnan, “Application Characteristics of Permanent Magnet Synchronous and Brushless dc Motors for Servo Drives,” *IEEE Trans Ind Appl*, vol. 27, no. 5, pp. 986–996, 1991, doi: 10.1109/28.90357.

[18] B. K. Bose, “A High-Performance Inverter-Fed Drive System of an Interior Permanent Magnet Synchronous Machine,” *IEEE Trans Ind Appl*, vol. 24, no. 6, pp. 987–997, 1988, doi: 10.1109/28.17470.

[19] T. M. Jahns, G. B. Kliman, and T. W. Neumann, “Interior Permanent-Magnet Synchronous Motors for Adjustable-Speed Drives,” *IEEE Trans Ind Appl*, vol. IA-22, no. 4, pp. 738–747, 1986, doi: 10.1109/TIA.1986.4504786.

[20] H. M. Flieh, R. D. Lorenz, E. Totoki, S. Yamaguchi, and Y. Nakamura, “Investigation of Different Servo Motor Designs for Servo Cycle Operations and Loss Minimizing Control Performance,” *IEEE Trans Ind Appl*, vol. 54, no. 6, pp. 5791–5801, 2018, doi: 10.1109/TIA.2018.2849725.

[21] S. Morimoto, Y. Takeda, T. Hirasa, and K. Taniguchi, “Expansion of Operating Limits for Permanent Magnet Motor by Current Vector Control Considering

Inverter Capacity," *IEEE Trans Ind Appl*, vol. 26, no. 5, pp. 866–871, 1990, doi: 10.1109/28.60058.

[22] S. Morimoto, Y. Tong, Y. Takeda, T. Hirasa, and K. Hatanaka, "Servo Drive System and Control Characteristics of Salient Pole Permanent Magnet Synchronous Motor," *IEEE Trans Ind Appl*, vol. 29, no. 2, pp. 338–343, 1993, doi: 10.1109/28.216541.

[23] S. Morimoto, T. Hirasa, Y. Takeda, K. Hatanaka, and Y. Tong, "Design and control system of inverter-driven permanent magnet synchronous motors for high torque operation," *IEEE Trans Ind Appl*, vol. 29, no. 6, pp. 1150–1155, 1993, doi: 10.1109/28.259726.

[24] A. Purwadi, R. Hutahaean, A. Rizqiawan, N. Heryana, N. A. Heryanto, and H. Hindersah, "Comparison of maximum torque per Ampere and Constant Torque Angle control for 30kw Interior Interior Permanent Magnet Synchronous Motor," *Proceedings - Joint International Conference on Electric Vehicular Technology and Industrial, Mechanical, Electrical and Chemical Engineering, ICEVT 2015 and IMECE 2015*, pp. 253–257, Jun. 2016, doi: 10.1109/ICEVTIMECE.2015.7496684.

[25] K. Dutta, P. P. Puthra, and P. K. Das, "Constant torque angle controlled permanent magnet synchronous motor drive using hysteresis band current controller," *India International Conference on Power Electronics, IICPE*, vol. 2016-November, Jun. 2016, doi: 10.1109/IICPE.2016.8079400.

[26] R. F. Schiferl and T. A. Lipo, "Power Capability of Salient Pole Permanent Magnet Synchronous Motors in Variable Speed Drive Applications," *IEEE Trans Ind Appl*, vol. 26, no. 1, pp. 115–123, 1990, doi: 10.1109/28.52682.

[27] S. Morimoto, K. Hatanaka, Y. Tong, Y. Takeda, and T. Hirasa, “High performance servo drive system of salient pole permanent magnet synchronous motor,” 1992, pp. 463–468. doi: 10.1109/IAS.1991.178196.

[28] C. T. Pan and S. M. Sue, “A linear maximum torque per ampere control for IPMSM drives over full-speed range,” *IEEE Transactions on Energy Conversion*, vol. 20, no. 2, pp. 359–366, Jun. 2005, doi: 10.1109/TEC.2004.841517.

[29] R. S. Colby and D. W. Novotny, “Efficient operation of surface-mounted pm synchronous motors,” *IEEE Trans Ind Appl*, vol. IA-23, no. 6, pp. 1048–1054, 1987, doi: 10.1109/TIA.1987.4505028.

[30] C. Mademlis and N. Margaris, “Loss minimization in vector-controlled interior permanent-magnet synchronous motor drives,” *IEEE Transactions on Industrial Electronics*, vol. 49, no. 6, pp. 1344–1347, Dec. 2002, doi: 10.1109/TIE.2002.804990.

[31] J. Hang, H. Wu, S. Ding, Y. Huang, and W. Hua, “Improved Loss Minimization Control for IPMSM Using Equivalent Conversion Method,” *IEEE Trans Power Electron*, vol. 36, no. 2, pp. 1931–1940, Feb. 2021, doi: 10.1109/TPEL.2020.3012018.

[32] F. F. Bernal, A. Garefa-Cerrada, and R. Faure, “Loss-minimization control of synchronous machines with constant excitation,” in *PESC Record - IEEE Annual Power Electronics Specialists Conference*, 1998, vol. 1, pp. 132–138. doi: 10.1109/PESC.1998.701890.

[33] F. Fernández-Bernal, A. García-Cerrada, and R. Faure, “Model-based loss minimization for dc and ac vector-controlled motors including core saturation,”

IEEE Trans Ind Appl, vol. 36, no. 3, pp. 755–763, 2000, doi: 10.1109/28.845050.

[34] M. Cao, "Online loss minimization control of IPMSM for electric scooters," in *2010 International Power Electronics Conference - ECCE Asia -, IPEC 2010*, 2010, pp. 1388–1392. doi: 10.1109/IPEC.2010.5544580.

[35] Z. Biel, J. Vittek, and M. Hrkel, "Permanent magnet synchronous motor loss minimization control strategies," in *Proceedings of 9th International Conference, ELEKTRO 2012*, 2012, pp. 165–169. doi: 10.1109/ELEKTRO.2012.6225631.

[36] A. Acquaviva, E. A. Grunditz, S. Lundmark, and T. Thiringer, "Comparison of MTPA and minimum loss control for tooth coil winding PMSM Considering PM and inverter losses," in *2019 21st European Conference on Power Electronics and Applications, EPE 2019 ECCE Europe*, Sep. 2019. doi: 10.23919/EPE.2019.8914873.

[37] T. Bariša, D. Sumina, and M. Kutija, "Comparison of maximum torque per ampere and loss minimization control for the interior permanent magnet synchronous generator," in *2015 International Conference on Electrical Drives and Power Electronics, EDPE 2015 - Proceedings*, Nov. 2015, pp. 497–502. doi: 10.1109/EDPE.2015.7325344.

[38] C. C. Chan, R. Zhang, K. T. Chau, and J. Z. Jiang, "Optimal efficiency control of PM hybrid motor drives for electrical vehicles," in *PESC Record - IEEE Annual Power Electronics Specialists Conference*, 1997, vol. 1, pp. 363–368. doi: 10.1109/PESC.1997.616750.

[39] M. Abdesh Khan, M. Nasir Uddin, and M. Aziz Rahman, “A new loss minimization control of interior permanent magnet motor drives operating with a wavelet based speed controller,” in *Conference Record - IAS Annual Meeting (IEEE Industry Applications Society)*, 2011. doi: 10.1109/IAS.2011.6074337.

[40] M. N. Razavi, H. Abniki, and M. K. Zadeh, “An optimal control strategy for the IPM motor drives,” in *2009 IEEE Electrical Power and Energy Conference, EPEC 2009*, 2009. doi: 10.1109/EPEC.2009.5420367.

[41] W. Xie, X. Wang, F. Wang, W. Xu, R. Kennel, and D. Gerling, “Dynamic Loss Minimization of Finite Control Set-Model Predictive Torque Control for Electric Drive System,” *IEEE Trans Power Electron*, vol. 31, no. 1, pp. 849–860, Jan. 2016, doi: 10.1109/TPEL.2015.2410427.

[42] N. Yang, G. Luo, W. Liu, and K. Wang, “Interior permanent magnet synchronous motor control for electric vehicle using look-up table,” in *Conference Proceedings - 2012 IEEE 7th International Power Electronics and Motion Control Conference - ECCE Asia, IPEMC 2012*, 2012, vol. 2, pp. 1015–1019. doi: 10.1109/IPEMC.2012.6258940.

[43] E. W. Lee, C. H. Park, and J. bin Kim, “Real-time MTPA and field-weakening method for IPMSM in the full speed region,” in *2015 17th European Conference on Power Electronics and Applications, EPE-ECCE Europe 2015*, Oct. 2015. doi: 10.1109/EPE.2015.7309052.

[44] G. Gallegos-López, F. S. Gunawan, and J. E. Walters, “Optimum torque control of permanent-magnet ac machines in the field-weakened region,” in *IEEE Transactions on Industry Applications*, Jul. 2005, vol. 41, no. 4, pp. 1020–1028. doi: 10.1109/TIA.2005.851588.

[45] N. Bianchi, S. Bolognani, and M. Zigliotto, “High-performance PM synchronous motor drive for an electrical scooter,” *IEEE Trans Ind Appl*, vol. 37, no. 5, pp. 1348–1355, Sep. 2001, doi: 10.1109/28.952510.

[46] A. Consoli, G. Scarcella, G. Scelba, and A. Testa, “Steady-state and transient operation of IPMSMs under maximum-torque-per- ampere control,” *IEEE Trans Ind Appl*, vol. 46, no. 1, pp. 121–129, 2010, doi: 10.1109/TIA.2009.2036665.

[47] G. Kang, J. Lim, K. Nam, H. bin Ihm, and H. G. Kim, “A MTPA control scheme for an IPM synchronous motor considering magnet flux variation caused by temperature,” in *Conference Proceedings - IEEE Applied Power Electronics Conference and Exposition - APEC*, 2004, vol. 3, pp. 1617–1621. doi: 10.1109/APEC.2004.1296081.

[48] M. Cao, J. Egashira, and K. Kaneko, “High efficiency control of IPMSM for electric motorcycles,” in *2009 IEEE 6th International Power Electronics and Motion Control Conference, IPEMC ’09*, 2009, pp. 1893–1897. doi: 10.1109/IPEMC.2009.5157705.

[49] M. Cao and N. Hoshi, “Electrical loss minimization strategy for interior permanent magnet synchronous motor drives,” in *2010 IEEE Vehicle Power and Propulsion Conference, VPPC 2010*, 2010. doi: 10.1109/VPPC.2010.5729094.

[50] R. Ni, D. Xu, G. Wang, L. Ding, G. Zhang, and L. Qu, “Maximum Efficiency per Ampere Control of Permanent-Magnet Synchronous Machines,” *IEEE Transactions on Industrial Electronics*, vol. 62, no. 4, pp. 2135–2143, 2015, doi: 10.1109/TIE.2014.2354238.

[51] S. Y. Jung, J. Hong, and K. Nam, “Current minimizing torque control of the IPMSM using Ferrari’s method,” *IEEE Trans Power Electron*, vol. 28, no. 12, pp. 5603–5617, 2013, doi: 10.1109/TPEL.2013.2245920.

[52] B. Cheng and T. R. Tesch, “Torque feedforward control technique for permanent-magnet synchronous motors,” *IEEE Transactions on Industrial Electronics*, vol. 57, no. 3, pp. 969–974, Mar. 2010, doi: 10.1109/TIE.2009.2038951.

[53] B. Cheng and T. R. Tesch, “Torque feedforward control technique for Permanent Magnet synchronous motors,” in *IECON Proceedings (Industrial Electronics Conference)*, 2007, pp. 1055–1060. doi: 10.1109/IECON.2007.4460316.

[54] P. Mattavelli, L. Tubiana, and M. Zigliotto, “Torque-ripple reduction in PM synchronous motor drives using repetitive current control,” *IEEE Trans Power Electron*, vol. 20, no. 6, pp. 1423–1431, Nov. 2005, doi: 10.1109/TPEL.2005.857559.

[55] J. Lee, K. Nam, S. Choi, and S. Kwon, “Loss-minimizing control of PMSM with the use of polynomial approximations,” *IEEE Trans Power Electron*, vol. 24, no. 4, pp. 1071–1082, 2009, doi: 10.1109/TPEL.2008.2010518.

[56] Iec, “Rotating electrical machines-Part 4-1: Methods for determining electrically excited synchronous machine quantities from tests,” 2018. moz-extension://1f629494-d6da-4f3d-938a-7405fd7ae2b6/enhanced-reader.html?openApp&pdf=https%3A%2F%2Fwebstore.iec.ch%2Fpreview%2Finfo_iec60034-4-1%257Bed1.0%257Db.pdf (accessed Aug. 15, 2022).

[57] E. Machinery Committee of the IEEE Power and E. Society, *IEEE Guide for Test Procedures for Synchronous Machines Including Acceptance and Performance Testing and Parameter Determination for Dynamic Analysis IEEE Power and Energy Society Developed by the Electric Machinery Committee*. 2020. [Online]. Available: http://www.ieee.org/web/aboutus/whatis/policies/p9-26.html.

[58] "115A-1987 - IEEE Standard Procedures for Obtaining Synchronous Machine Parameters by Standstill Frequency Response Testing," 1987.

[59] P. J. Turner, A. B. J. Reece, and D. C. Macdonald, "The d.c. decay test for determning synchronous machine parameters: Measurement and simulation," *IEEE Transactions on Energy Conversion*, vol. 4, no. 4, pp. 616–623, 1989, doi: 10.1109/60.41720.

[60] F. Maurer, M. T. Xuan, and J. J. Simond, "Two novel methods for parameter identification of synchronous machine using DC-decay test with rotor in arbitrary position," in *Proceedings - 2016 22nd International Conference on Electrical Machines, ICEM 2016*, Nov. 2016, pp. 633–639. doi: 10.1109/ICELMACH.2016.7732592.

[61] B. Štumberger, B. Kreča, and B. Hribernik, "Determination of parameters of synchronous motor with permanent magnets from measurement of load conditions," *IEEE Transactions on Energy Conversion*, vol. 14, no. 4, pp. 1413–1416, 1999, doi: 10.1109/60.815082.

[62] P. V. V. Silva, E. C. Bortoni, and E. J. J. Rocha, "Identification of synchronous machines parameters using genetic algorithm and load rejection test," in *IEEE*

Power and Energy Society General Meeting, Jan. 2018, vol. 2018-January, pp. 1–5. doi: 10.1109/PESGM.2017.8274095.

[63] E. da Costa Bortoni, "Synchronous machines parameters identification using load rejection test data," in *IEEE International Electric Machines and Drives Conference Record, IEMDC*, 1997. doi: 10.1109/IEMDC.1997.604292.

[64] E. da C. Bortoni and J. A. Jardini, "A standstill frequency response method for large salient pole synchronous machines," *IEEE Transactions on Energy Conversion*, vol. 19, no. 4, pp. 687–691, Dec. 2004, doi: 10.1109/TEC.2004.832047.

[65] T. L. Vandoorn, F. M. de Belie, T. J. Vyncke, J. A. Melkebeek, and P. Lataire, "Generation of multisinusoidal test signals for the identification of synchronous-machine parameters by using a voltage-source inverter," *IEEE Transactions on Industrial Electronics*, vol. 57, no. 1, pp. 430–439, Jan. 2010, doi: 10.1109/TIE.2009.2031135.

[66] P. Guglielmi, M. Pastorelli, and A. Vagati, "Cross-saturation effects in IPM motors and related impact on sensorless control," *IEEE Trans Ind Appl*, vol. 42, no. 6, pp. 1516–1522, Nov. 2006, doi: 10.1109/TIA.2006.882646.

[67] S. A. Odhano, R. Bojoi, Ş. G. Roşu, and A. Tenconi, "Identification of the Magnetic Model of Permanent-Magnet Synchronous Machines Using DC-Biased Low-Frequency AC Signal Injection," *IEEE Trans Ind Appl*, vol. 51, no. 4, pp. 3208–3215, 2015, doi: 10.1109/TIA.2015.2413383.

[68] B. Štumberger, G. Štumberger, D. Dolinar, A. Hamler, and M. Trlep, "Evaluation of saturation and cross-magnetization effects in interior permanent magnet synchronous motor," in *Conference Record - IAS Annual Meeting*

(IEEE Industry Applications Society), 2001, vol. 4, pp. 2557–2562. doi: 10.1109/IAS.2001.955980.

[69] U. Schaible and B. Szabados, "Dynamic motor parameter identification for high speed flux weakening operation of brushless permanent magnet synchronous machines," *IEEE Transactions on Energy Conversion*, vol. 14, no. 3, pp. 486–492, 1999, doi: 10.1109/60.790901.

[70] A. M. El-Serafi and N. C. Kar, "Methods for determining the intermediate-axis saturation characteristics of salient-pole synchronous machines from the measured D-axis characteristics," *IEEE Transactions on Energy Conversion*, vol. 20, no. 1, pp. 88–97, Mar. 2005, doi: 10.1109/TEC.2004.841511.

[71] A. M. El-Serafi and N. C. Kar, "Methods for determining the q-axis saturation characteristics of salient-pole synchronous machines from the measured d-axis characteristics," *IEEE Transactions on Energy Conversion*, vol. 18, no. 1, pp. 80–86, 2003, doi: 10.1109/TEC.2002.808384.

[72] F. Wang, "A Nonlinear Saturation Model for Salient-Pole Synchronous Machines in High Performance Drive Applications," in *Conference Record - IAS Annual Meeting (IEEE Industry Applications Society)*, 2003, vol. 2, pp. 906–910. doi: 10.1109/IAS.2003.1257642.

[73] W. Jing and G. Tan, "Modeling of salient-pole synchronous motor considering saturation effect," in *ICCASM 2010 - 2010 International Conference on Computer Application and System Modeling, Proceedings*, 2010, vol. 3. doi: 10.1109/ICCASM.2010.5620132.

[74] N. Imai, S. Morimoto, M. Sanada, and Y. Takeda, "Influence of magnetic saturation on sensorless control for interior permanent-magnet synchronous

motors with concentrated windings," *IEEE Trans Ind Appl*, vol. 42, no. 5, pp. 1193–1200, Sep. 2006, doi: 10.1109/TIA.2006.880853.

[75] N. Imai, S. Morimoto, M. Sanada, and Y. Takeda, "Influence of PM flux variation and magnetic saturation on sensorless control for interior permanent magnet synchronous motors," in *Conference Record - IAS Annual Meeting (IEEE Industry Applications Society)*, 2005, vol. 3, pp. 1776–1783. doi: 10.1109/IAS.2005.1518687.

[76] S. Morimoto, T. Ueno, M. Sanada, A. Yamagiwa, Y. Takeda, and T. Hirasa, "Effects and compensation of magnetic saturation in permanent magnet synchronous motor drives," in *Conference Record - IAS Annual Meeting (IEEE Industry Applications Society)*, 1993, vol. 1, pp. 59–64. doi: 10.1109/IAS.1993.298904.

[77] S. Morimoto, M. Sanada, and Y. Takeda, "Effects and Compensation of Magnetic Saturation in Flux-Weakening Controlled Permanent Magnet Synchronous Motor Drives," *IEEE Trans Ind Appl*, vol. 30, no. 6, pp. 1632–1637, 1994, doi: 10.1109/TIA.1994.350318.

[78] G. Wang *et al.*, "Self-commissioning of permanent magnet synchronous machine drives at standstill considering inverter nonlinearities," *IEEE Trans Power Electron*, vol. 29, no. 12, pp. 6615–6627, 2014, doi: 10.1109/TPEL.2014.2306734.

[79] N. Urasaki, T. Senjyu, and K. Uezato, "A novel calculation method for iron loss resistance suitable in modeling permanent-magnet synchronous motors," *IEEE Transactions on Energy Conversion*, vol. 18, no. 1, pp. 41–47, Mar. 2003, doi: 10.1109/TEC.2002.808329.

[80] D. Zarko and T. Jercic, “Novel Empirical Model for Calculation of Core Losses in Permanent Magnet Machines,” *IEEE Transactions on Energy Conversion*, vol. 35, no. 1, pp. 248–259, Mar. 2020, doi: 10.1109/TEC.2019.2951944.

[81] L. Ma, M. Sanada, S. Morimoto, and Y. Takeda, “Prediction of iron loss in rotating machines with rotational loss included,” *IEEE Trans Magn*, vol. 39, no. 4 II, pp. 2036–2041, Jul. 2003, doi: 10.1109/TMAG.2003.812706.

[82] F. Fernandez-Bernal, A. Garcia-Cerrada, and R. Faure, “Determination of parameters in interior permanent magnet synchronous motors with iron losses without torque measurement,” in *Conference Record - IAS Annual Meeting (IEEE Industry Applications Society)*, 2000, vol. 1, pp. 409–415. doi: 10.1109/IAS.2000.881143.

[83] Y. Miao, H. Ge, M. Preindl, J. Ye, B. Cheng, and A. Emadi, “MTPA Fitting and Torque Estimation Technique Based on a New Flux-Linkage Model for Interior-Permanent-Magnet Synchronous Machines,” *IEEE Trans Ind Appl*, vol. 53, no. 6, pp. 5451–5460, Nov. 2017, doi: 10.1109/TIA.2017.2726980.

[84] W. Huang, Y. Zhang, X. Zhang, and G. Sun, “Accurate torque control of interior permanent magnet synchronous machine,” *IEEE Transactions on Energy Conversion*, vol. 29, no. 1, pp. 29–37, Mar. 2014, doi: 10.1109/TEC.2013.2290868.

[85] G. Pellegrino, B. Boazzo, and T. M. Jahns, “Magnetic Model Self-Identification for PM Synchronous Machine Drives,” *IEEE Trans Ind Appl*, vol. 51, no. 3, pp. 2246–2254, 2015, doi: 10.1109/TIA.2014.2365627.

[86] Q. Liu and K. Hameyer, “A fast online full parameter estimation of a PMSM with sinusoidal signal injection,” in *2015 IEEE Energy Conversion Congress*

and Exposition, ECCE 2015, Oct. 2015, pp. 4091–4096. doi: 10.1109/ECCE.2015.7310237.

[87] S. Morimoto, M. Sanada, and Y. Takeda, "Mechanical sensorless drives of IPMSM with online parameter identification," *IEEE Trans Ind Appl*, vol. 42, no. 5, pp. 1241–1248, Sep. 2006, doi: 10.1109/TIA.2006.880840.

[88] G. Feng, C. Lai, K. Mukherjee, and N. C. Kar, "Current Injection-Based Online Parameter and VSI Nonlinearity Estimation for PMSM Drives Using Current and Voltage DC Components," *IEEE Transactions on Transportation Electrification*, vol. 2, no. 2, pp. 119–128, Jun. 2016, doi: 10.1109/TTE.2016.2538180.

[89] Z. Li, G. Feng, C. Lai, D. Banerjee, W. Li, and N. C. Kar, "Current injection-based multi-parameter estimation for dual three-phase IPMSM considering VSI nonlinearity," *IEEE Transactions on Transportation Electrification*, vol. 5, no. 2, pp. 405–415, Jun. 2019, doi: 10.1109/TTE.2019.2913270.

[90] M. S. Rafaq, F. Mwasilu, J. Kim, H. H. Choi, and J. W. Jung, "Online Parameter Identification for Model-Based Sensorless Control of Interior Permanent Magnet Synchronous Machine," *IEEE Trans Power Electron*, vol. 32, no. 6, pp. 4631–4643, Jun. 2017, doi: 10.1109/TPEL.2016.2598731.

[91] D. Q. Dang, M. S. Rafaq, H. H. Choi, and J. W. Jung, "Online Parameter Estimation Technique for Adaptive Control Applications of Interior PM Synchronous Motor Drives," *IEEE Transactions on Industrial Electronics*, vol. 63, no. 3, pp. 1438–1449, Mar. 2016, doi: 10.1109/TIE.2015.2494534.

[92] Q. Liu and K. Hameyer, "High-Performance Adaptive Torque Control for an IPMSM with Real-Time MTPA Operation," *IEEE Transactions on Energy*

Conversion, vol. 32, no. 2, pp. 571–581, Jun. 2017, doi: 10.1109/TEC.2016.2633302.

[93] S. J. Kim *et al.*, "Torque ripple improvement for interior permanent magnet synchronous motor considering parameters with magnetic saturation," *IEEE Trans Magn*, vol. 45, no. 10, pp. 4720–4723, 2009, doi: 10.1109/TMAG.2009.2022053.

[94] H. Kim, J. Hartwig, and R. D. Lorenz, "Using on-line parameter estimation to improve efficiency of IPM machine drives," in *PESC Record - IEEE Annual Power Electronics Specialists Conference*, 2002, vol. 2, pp. 815–820. doi: 10.1109/PSEC.2002.1022554.

[95] P. Niazi, H. A. Toliyat, and A. Goodarzi, "Robust maximum torque per ampere (MTPA) control of PM-assisted SynRM for traction applications," *IEEE Trans Veh Technol*, vol. 56, no. 4 I, pp. 1538–1545, Jul. 2007, doi: 10.1109/TVT.2007.896974.

[96] X. Zhang and Z. Li, "Sliding-mode observer-based mechanical parameter estimation for permanent magnet synchronous motor," *IEEE Trans Power Electron*, vol. 31, no. 8, pp. 5732–5745, 2016, doi: 10.1109/TPEL.2015.2495183.

[97] Y. Zuo, J. Mei, X. Zhang, and C. H. T. Lee, "Simultaneous Identification of Multiple Mechanical Parameters in a Servo Drive System Using only One Speed," *IEEE Trans Power Electron*, vol. 36, no. 1, pp. 716–726, Jan. 2021, doi: 10.1109/TPEL.2020.3000656.

[98] M. S. Hossain and M. J. Hossain, "Performance analysis of a novel fuzzy logic and MTPA based speed control for IPMSM drive with variable d- and q-axis

inductances," in *ICCIT 2009 - Proceedings of 2009 12th International Conference on Computer and Information Technology*, 2009, pp. 361–366. doi: 10.1109/ICCIT.2009.5407264.

[99] F. J. Lin, Y. T. Liu, and W. A. Yu, "Power Perturbation Based MTPA with an Online Tuning Speed Controller for an IPMSM Drive System," *IEEE Transactions on Industrial Electronics*, vol. 65, no. 5, pp. 3677–3687, May 2018, doi: 10.1109/TIE.2017.2762634.

[100] H. Chaoui and P. Sicard, "Adaptive fuzzy logic control of permanent magnet synchronous machines with nonlinear friction," *IEEE Transactions on Industrial Electronics*, vol. 59, no. 2, pp. 1123–1133, Feb. 2012, doi: 10.1109/TIE.2011.2148678.

[101] M. N. Uddin and R. S. Rebeiro, "Online efficiency optimization of a fuzzy-logic-controller-based IPMSM drive," *IEEE Trans Ind Appl*, vol. 47, no. 2, pp. 1043–1050, Mar. 2011, doi: 10.1109/TIA.2010.2103293.

[102] S. Bolognani, R. Petrella, A. Prearo, and L. Sgarbossa, "Automatic tracking of MTPA trajectory in IPM motor drives based on AC current injection," *IEEE Trans Ind Appl*, vol. 47, no. 1, pp. 105–114, 2011, doi: 10.1109/TIA.2010.2090842.

[103] S. Kim, Y. D. Yoon, S. K. Sul, K. Ide, and K. Tomita, "Parameter independent maximum torque per ampere (MTPA) control of IPM machine based on signal injection," *Conference Proceedings - IEEE Applied Power Electronics Conference and Exposition - APEC*, no. 1, pp. 103–108, 2010, doi: 10.1109/APEC.2010.5433685.

[104] G. Liu, J. Wang, W. Zhao, and Q. Chen, “A Novel MTPA Control Strategy for IPMSM Drives by Space Vector Signal Injection,” *IEEE Transactions on Industrial Electronics*, vol. 64, no. 12, pp. 9243–9252, Dec. 2017, doi: 10.1109/TIE.2017.2711507.

[105] T. Sun, M. Koc, and J. Wang, “MTPA Control of IPMSM Drives Based on Virtual Signal Injection Considering Machine Parameter Variations,” *IEEE Transactions on Industrial Electronics*, vol. 65, no. 8, pp. 6089–6098, 2018, doi: 10.1109/TIE.2017.2784409.

[106] T. Sun, J. Wang, and X. Chen, “Maximum Torque per Ampere (MTPA) control for interior permanent magnet synchronous machine drives based on virtual signal injection,” *IEEE Trans Power Electron*, vol. 30, no. 9, pp. 5036–5045, 2015, doi: 10.1109/TPEL.2014.2365814.

[107] S. Kim, Y. D. Yoon, S. K. Sul, and K. Ide, “Maximum torque per ampere (MTPA) control of an IPM machine based on signal injection considering inductance saturation,” *IEEE Trans Power Electron*, vol. 28, no. 1, pp. 488–497, 2013, doi: 10.1109/TPEL.2012.2195203.

[108] C. Cavallaro, A. O. di Tommaso, R. Miceli, A. Raciti, G. R. Galluzzo, and M. Trapanese, “Efficiency enhancement of permanent-magnet synchronous motor drives by online loss minimization approaches,” *IEEE Transactions on Industrial Electronics*, vol. 52, no. 4, pp. 1153–1160, Aug. 2005, doi: 10.1109/TIE.2005.851595.

[109] F. Tinazzi and M. Zigliotto, “Torque Estimation in High-Efficency IPM Synchronous Motor Drives,” *IEEE Transactions on Energy Conversion*, vol. 30, no. 3, pp. 983–990, Sep. 2015, doi: 10.1109/TEC.2015.2408214.

[110] D. Anton, Y. K. Kim, S. J. Lee, and S. T. Lee, “Robust self-tuning MTPA algorithm for IPMSM drives,” *IECON Proceedings (Industrial Electronics Conference)*, pp. 1355–1360, 2008, doi: 10.1109/IECON.2008.4758151.

[111] L. Guo and L. Parsa, “Model reference adaptive control of five-phase IPM motors based on neural network,” *IEEE Transactions on Industrial Electronics*, vol. 59, no. 3, pp. 1500–1508, Mar. 2012, doi: 10.1109/TIE.2011.2163371.

[112] Y. A. R. I. Mohamed and E. F. El-Saadany, “A current control scheme with an adaptive internal model for robust current regulation and torque ripple minimization in PMSM vector drive,” in *Proceedings of IEEE International Electric Machines and Drives Conference, IEMDC 2007*, 2007, vol. 1, pp. 300–305. doi: 10.1109/IEMDC.2007.382683.

[113] H. H. Choi, N. T. T. Vu, and J. W. Jung, “Digital implementation of an adaptive speed regulator for a PMSM,” *IEEE Trans Power Electron*, vol. 26, no. 1, pp. 3–8, 2011, doi: 10.1109/TPEL.2010.2055890.

[114] G. Schoonhoven and M. Nasir Uddin, “MTPA-and FW-Based Robust Nonlinear Speed Control of IPMSM Drive Using Lyapunov Stability Criterion,” *IEEE Trans Ind Appl*, vol. 52, no. 5, pp. 4365–4374, Sep. 2016, doi: 10.1109/TIA.2016.2564941.

[115] J. Yu, P. Shi, S. Member, W. Dong, B. Chen, and C. Lin, “Brief Papers Permanent Magnet Synchronous Motors,” *IEEE Trans Neural Netw Learn Syst*, vol. 26, no. 3, pp. 640–645, 2015.

APPENDICES

Appendix A Matlab Code for Torque \Torque-angle with Saliency

```
clear all;
clc;
%% Definitions
np=2;%%Pole Pair
Is=5;%%Stator current amplitude
syms delta; %%Torque angle(the angle between q-axis and stator
current phasor)
pm_flux=0.1077;%% Permanent Magnet Flux
Ld=(8.72*10^-3);%%d-axis inductance
syms ro; %% the saliency coefficient
syms k; %% a coefficient to variate d -axis inductance
%% Plotting
delta=[-pi/6:pi/720:pi/3]; clf;
for ro=1:4;
k=1;
%Torque equation
T=(3/2)*np*Is.*cos(delta).*(pm_flux-0.5*Is*(1-
ro)*k*Ld.*sin(delta));
[T_max(ro), index] = max(T);
delta_degree=delta.*(180/pi);
delta_max(ro) = delta_degree(index);
% subplot(1,2,2)
plot(delta_degree,T,'linewidth',2),grid on
hold on
textstring = sprintf('(%.0f,%.2f)',delta_max(ro), T_max(ro));
text(delta_max(ro)-1, T_max(ro)+((-1)^ro)*(0.01), textstring,
'FontSize', 16);
end
hold on
scatter(delta_max,T_max,30,'filled');
legend('?=1','?=2','?=3','?=4','Tmax','fontsize',16),
xlabel('Torque angle(?r)','fontsize',16),
ylabel('Torque(Nm)','fontsize',16),xlim([-20 60]),ylim([1.1
2.2]);
```

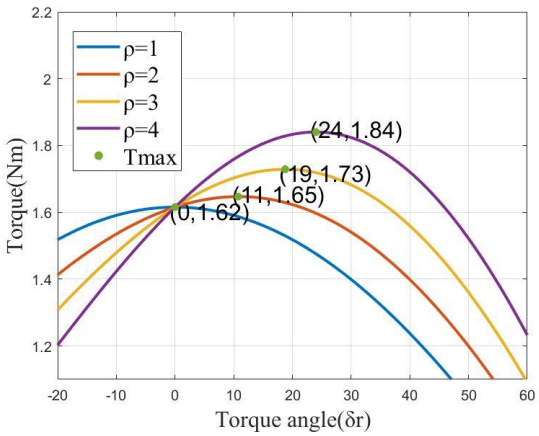

Appendix B MTPA Trajectory

```
clear all; clc;
%% Definitions
Rs=0.57;
np=2;%%Pole Pair
Im=8.46;%%Stator max current amplitude
Vm=50;%%Stator max voltage amplitude
Isrt=5;%%Stator rated current amplitude
wb=2400*(pi/30); %%base speed
pm_flux=0.1077;%% Permanent Magnet Flux
Ld=(8.72*10^-3);%%d-axis inductance
Lq=(22.78*10^-3);%%q-axis inductance
A=pm_flux/(2*(Lq-Ld));
iq=0:0.001:Im;
id=A-sqrt(A^2+iq.^2);
%%current limits
id1=-Im:0.001:Im;
iq1=sqrt(Im^2-id1.^2);
%%max Torque coordinates
idm=A/2-sqrt(A/4+((Im^2)/2));
iqm=sqrt(Im^2-idm^2);
%% voltage limits
Vom=Vm-Rs*Im;
ido=-Im:0.001:Im;
vqo=wb*pm_flux+wb*Ld.*ido;
vdo=-sqrt(Vom^2-vqo.^2);
iqo=-vdo/(wb*Lq);
%% plot
plot(id,iq,'r',id1,iq1,'b',ido,iqo,'linewidth',2),grid
on, hold on
legend('MTPA trajectory','Current Limit','Voltage
Limit','fontsize',16,'fontname','Times New Roman'),
xlabel('d-axis current-
idr(A)','fontsize',16,'fontname','Times New Roman'),
ylabel('q -axis current-
iqr(A)','fontsize',15,'fontname','Times New
Roman'),xlim([-9 9]),ylim([-0.5 11.5]);
```

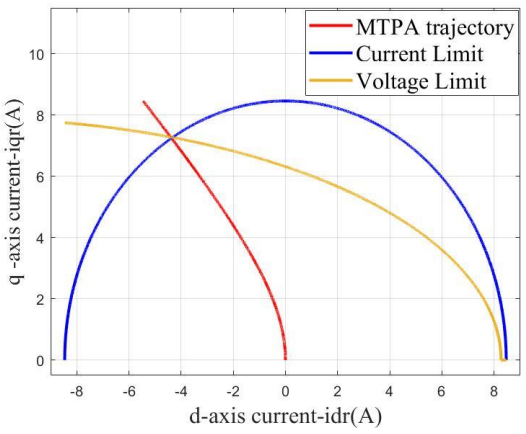

Appendix C Parameter Identification for PI Controllers

PI-controller of q-axis current

The expression for the q-axis current of IPMSM not accounting for the core loss is

$$L_q \frac{di_q}{dt} + R_S i_q = U_q - n_p \omega_R L_d i_d - n_p \omega_R \Psi_f$$

Introduce q-axes time constant $T_q = \frac{L_q}{R_S}$. Then the equation above transforms to the following view

$$T_q \frac{di_q}{dt} + i_q = \frac{1}{R_S}\left(U_q - n_p \omega_R L_d i_d - n_p \omega_R \Psi_f\right)$$

Denote $s = \frac{d}{dt}$ then

$$i_q = \frac{1/R_S}{T_q s + 1}\left(U_q - n_p \omega_R L_d i_d - n_p \omega_R \Psi_f\right)$$

In the control system the components $-n_p \omega_R L_d i_d - n_p \omega_R \Psi_f$ are compensated by the decoupling controller. Then the transfer function of the iq current open loop is

$$\frac{i_q(s)}{U_q(s)} = W_{iq}(s) = \frac{1/R_S}{T_q s + 1}$$

Select the PI iq current controller in the following view

$$W_{iqc}(s) = k_{des}\frac{T_q s + 1}{(1/R_S)s} = \frac{T_q s + 1}{s/(R_S k_{des})}$$

Where k_{des} is a desired gain of the controller.

Then the closed loop for the iq current is

$$W_{iqclosed} = \frac{W_{iqc}(s)W_{iq}(s)}{1 + W_{iqc}(s)W_{iq}(s)} = \frac{1}{W_{iqc}^{-1}(s)W_{iq}^{-1}(s) + 1} = \frac{1}{\frac{s/(R_S k_{des})}{T_q s + 1}\frac{T_q s + 1}{1/R_S} + 1} = \frac{1}{\frac{s}{k_{des}} + 1} = \frac{1}{T_{des} s + 1}$$

where T_{des} is a desired time constant.

So the closed iq loop should behave like an aperiodic transfer function.

For the researched motor

Lq=0.02278 H

Rs=0.57 Ohm

Then Tq=Lq/Rs=0.04 s. Assume Tdes=0.002 s.

Then

$$W_{iqc}(s) = k_{des}\frac{T_q s + 1}{(1/R_S)s} = k_{des}R_S\frac{T_q s + 1}{s} = k_{des}R_S T_q + \frac{k_{des}R_S}{s} = k_{piq} + k_{iiq}\frac{1}{s}$$

where the proportional and integral gains of the controller are

$$k_{piq} = k_{des}R_S T_q = \frac{1}{T_{des}}R_S T_q = \frac{1}{0.002}0.57 \cdot 0.04 = 11.4$$

$$k_{iiq} = k_{des} R_S = \frac{1}{T_{des}} R_S = \frac{1}{0.002} 0.57 = 285$$

PI-controller of d-axis current

The expression for the d-axis current of IPMSM not accounting for the core loss

$$L_d \frac{di_d}{dt} + R_S i_d = U_d + n_p \omega_R L_q i_q$$

Introduce d-axis time constant $T_d = \frac{L_d}{R_S}$. Then the equation above transforms to the following view

$$T_d \frac{di_d}{dt} + i_d = \frac{1}{R_S}\left(U_d + n_p \omega_R L_q i_q\right)$$

Denote $s = \frac{d}{dt}$ then $i_d = \frac{1/R_S}{T_d s + 1}\left(U_d + n_p \omega_R L_q i_q\right)$

In the control system the component $n_p \omega_R L_q i_q$ is compensated by the decoupling controller.

Then the transfer function of the id current open loop is

$$\frac{i_d(s)}{U_d(s)} = W_{id}(s) = \frac{1/R_S}{T_d s + 1}$$

Select the PI id current controller in the following view

$$W_{idc}(s) = k_{des} \frac{T_d s + 1}{(1/R_S)s}$$

Following the design procedure above, the proportional and the integral gains of the controller are

$$T_d = \frac{L_d}{R_S} = \frac{0.00872}{0.57} = 0.0153 s \cdot$$

$$k_{pid} = k_{des} R_S T_d = \frac{1}{T_{des}} R_S T_d = \frac{1}{0.002} 0.57 \cdot 0.0153 = 4.36.$$

$$k_{iid} = k_{des} R_S = \frac{1}{T_{des}} R_S = \frac{1}{0.002} 0.57 = 285.$$

PI-controller of the angular velocity

The motor shaft dynamics is described by the following differential equation

$$\frac{d\omega_R}{dt} = \frac{1}{J}\left(T_e - T_f - F\omega_R - T_m\right)$$

Where $T_e = f\left(i_d, i_q\right)$ is the electromagnetic torque, T_f is the static friction torque, F is the viscous friction torque gain and T_m is the load torque.

Assume F is small and negligible then

$$J \frac{d\omega_R}{dt} = T_e - T_f - T_m$$

Without the friction and load torque

$$J \frac{d\omega_R}{dt} = T_e$$

Denote $s = \frac{d}{dt}$ then

$$\omega_R = \frac{1}{Js} T_e .$$

The torque control can be approximated, based on the above optimised current loops, as an aperiodic transfer function. Then

$$\omega_R = \frac{1}{Js} \frac{1}{T_{des} s + 1} T_e^*$$

The corresponding transfer function ignoring the friction and load torque is

$$\frac{\omega_R(s)}{T_e^*(s)} = W_\omega(s) = \frac{1}{Js} \frac{1}{T_{des} s + 1}$$

$$W_{des\omega}(s) = \frac{4T_{des} s + 1}{4T_{des} s} \frac{1}{2T_{des} s \left(T_{des} s + 1 \right)}$$

Then the transfer function of the angular velocity controller is

$$W_{\omega c}(s) = \frac{W_{des\omega}(s)}{W_\omega(s)} = \frac{4T_{des} s + 1}{4T_{des} s} \frac{1}{2T_{des} s \left(T_{des} s + 1 \right)} \frac{Js}{1} \frac{T_{des} s + 1}{1} = J \frac{4T_{des} s + 1}{8T_{des} T_{des} s}$$

The proportional and integral gains of the PI controller above are.

$$k_{p\omega} = \frac{J}{2T_{des}} = \frac{0.004}{2 \cdot 0.002} = 1.$$

$$k_{i\omega} = \frac{J}{8T_{des} T_{des}} = \frac{0.004}{8 \cdot 0.002 \cdot 0.002} = 125 .$$

For zero d-axis current methods the torque Te=(3/2)*np*pm_flux*iq
The output of the velocity controller is iq reference and not torque reference.
Then a scaling must be added iq*=Te*/(1.5*np*pm_flux) in the d-axis method between the iq* and the output of the velocity controller!

Appendix D **ZDAC Control Approach in FOC Concept Accounting the Core Loss**

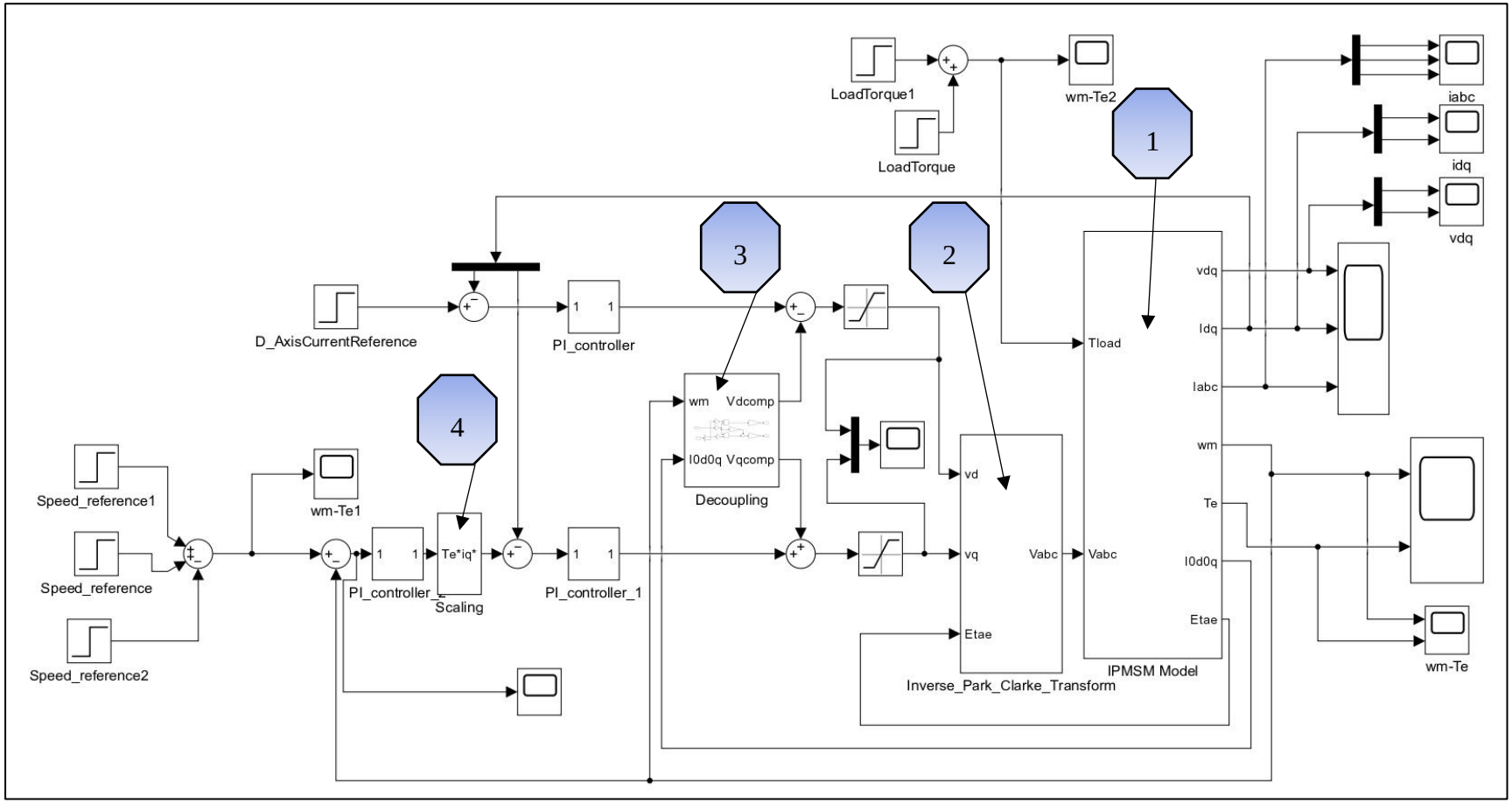

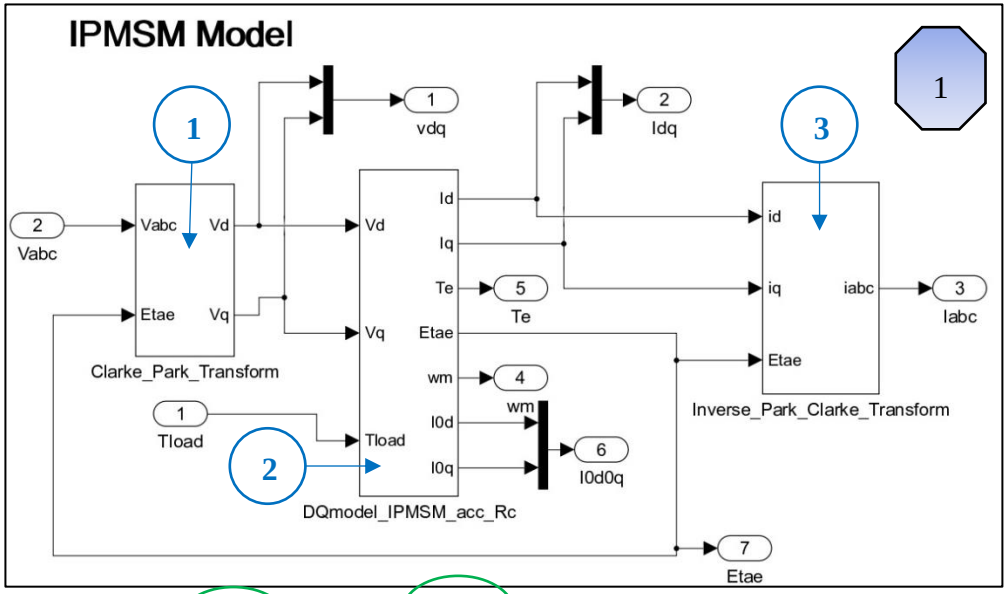
IPMSM Model
1
1
vdq
2
Idq
3
2
Vabc
Vabc
Vd
Etae
Vq
Clarke_Park_Transform
Vd
Vq
Tload
Tload
2
Id
Iq
Te
5
Te
Etae
wm
4
wm
I0d
I0q
6
I0d0q
DQmodel_IPMSM_acc_Rc
id
iq
Etae
iabc
3
Iabc
Inverse_Park_Clarke_Transform
7
Etae

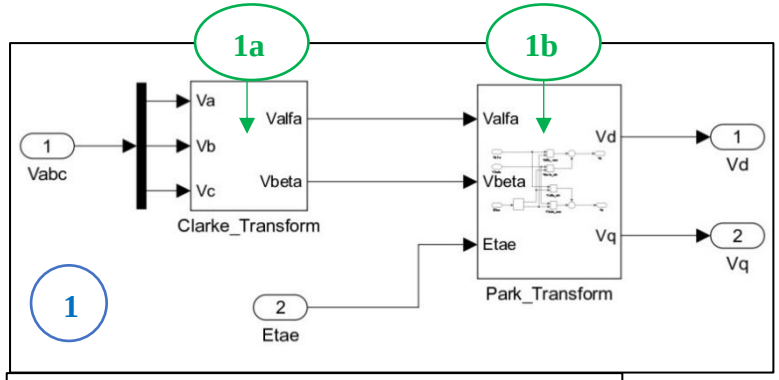
1a
1b
1
Vabc
Va
Vb
Vc
Valfa
Vbeta
Clarke_Transform
Valfa
Vbeta
Etae
Vd
Vq
Park_Transform
1
Vd
2
Vq
2
Etae
1

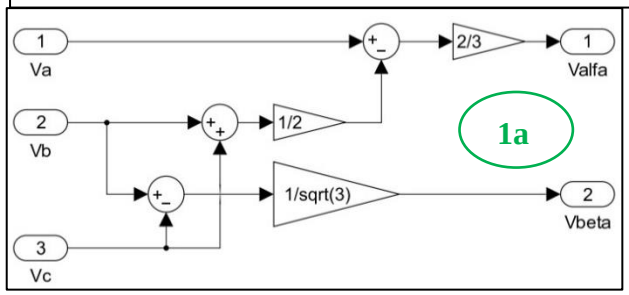
1
Va
2
Vb
3
Vc
2/3
1
Valfa
1/2
1/sqrt(3)
2
Vbeta
1a

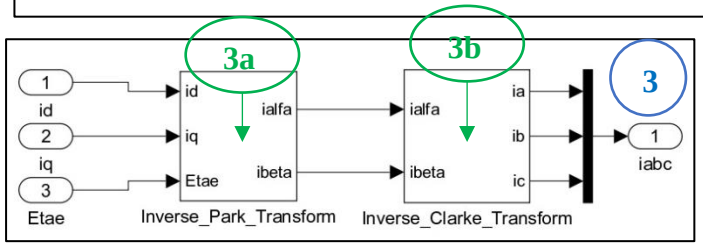
3a
3b
3
1
id
2
iq
3
Etae
id
iq
Etae
ialfa
ibeta
Inverse_Park_Transform
ialfa
ibeta
ia
ib
ic
Inverse_Clarke_Transform
1
iabc

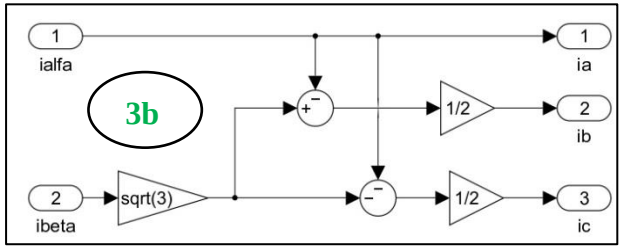
1
ialfa
3b
1
ia
1/2
2
ib
2
ibeta
sqrt(3)
1/2
3
ic

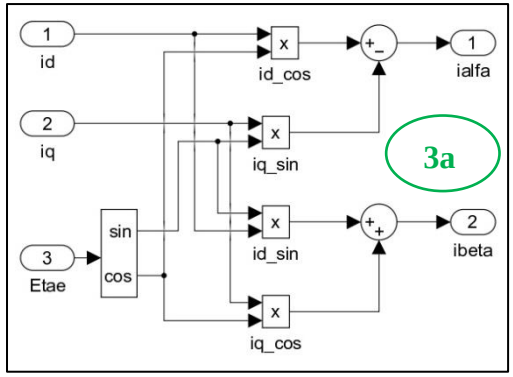
1
id
2
iq
3
Etae
sin
cos
x
id_cos
iq_sin
id_sin
iq_cos
1
ialfa
2
ibeta
3a

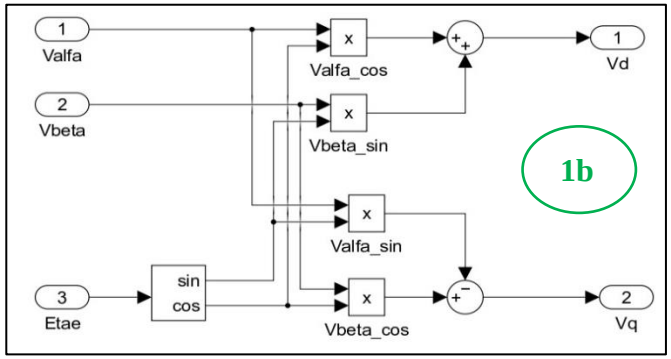
1
Valfa
2
Vbeta
3
Etae
sin
cos
x
Valfa_cos
Vbeta_sin
Valfa_sin
Vbeta_cos
1
Vd
2
Vq
1b

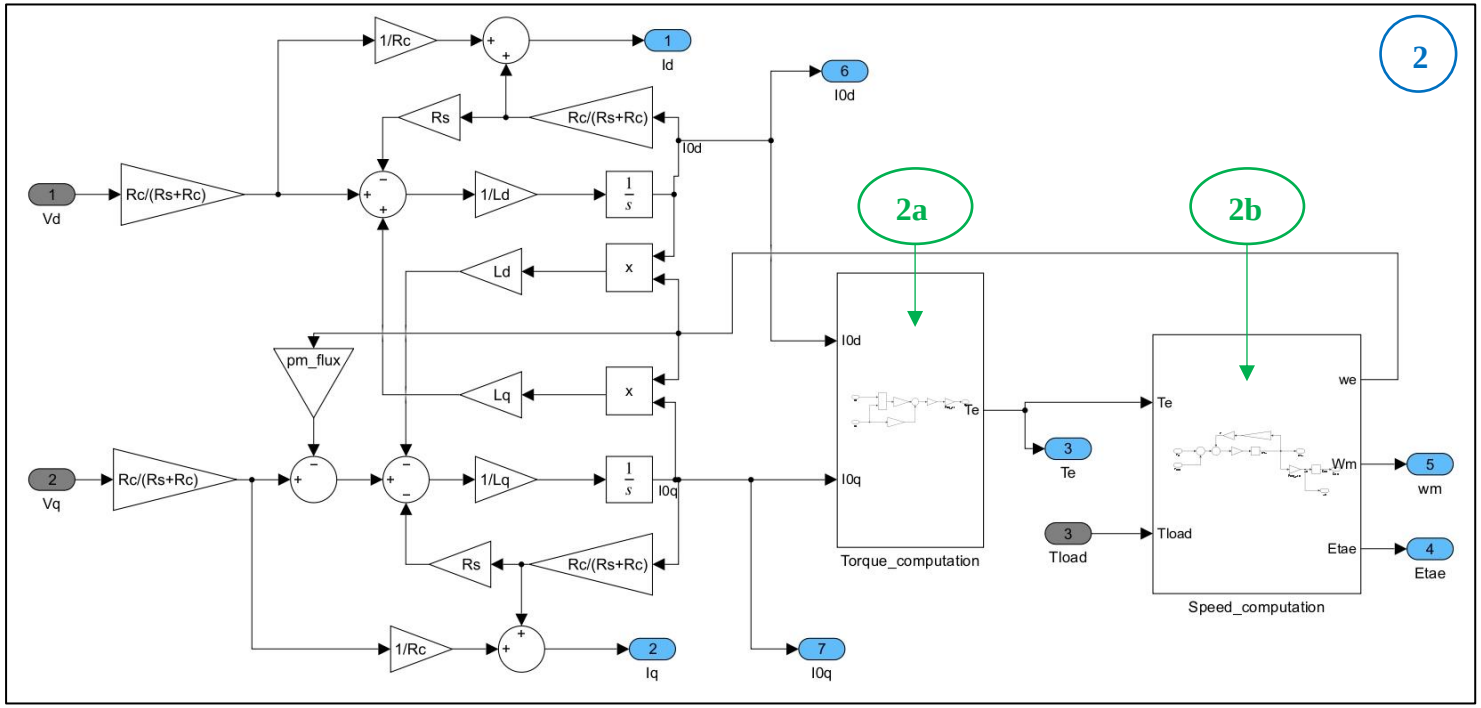
2
1/Rc
1
Id
6
I0d
Rs
Rc/(Rs+Rc)
I0d
1
Vd
Rc/(Rs+Rc)
1/Ld
Ld
x
2a
2b
pm_flux
Lq
x
I0d
Te
we
2
Vq
Rc/(Rs+Rc)
1/Lq
I0q
I0q
Te
3
Te
Wm
5
wm
Tload
3
Tload
Etae
4
Etae
Rs
Rc/(Rs+Rc)
Torque_computation
Speed_computation
1/Rc
2
Iq
7
I0q

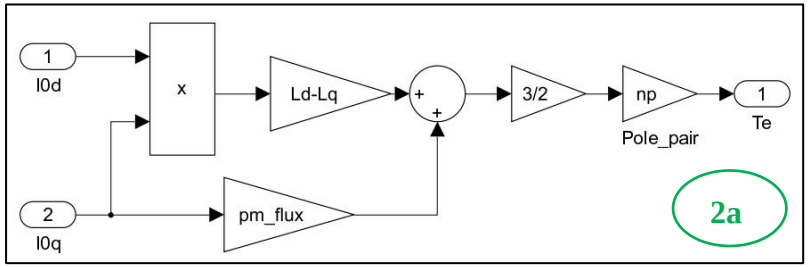
1
I0d
x
Ld-Lq
3/2
np
1
Te
Pole_pair
2
I0q
pm_flux
2a

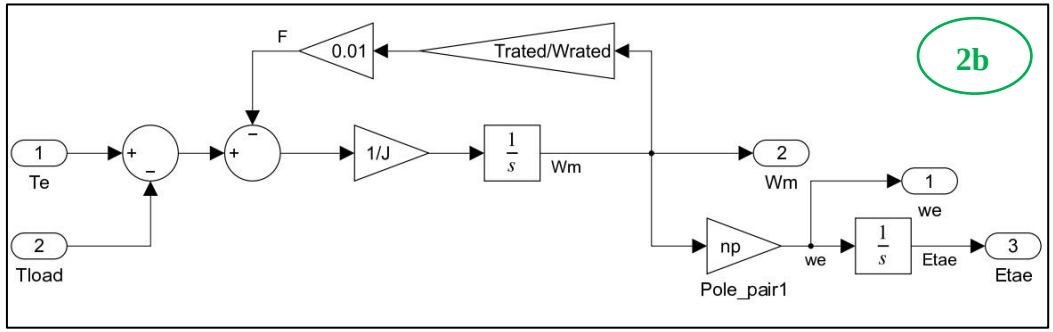
F
0.01
Trated/Wrated
2b
1
Te
1/J
Wm
2
Wm
1
we
2
Tload
np
we
Etae
3
Etae
Pole_pair1

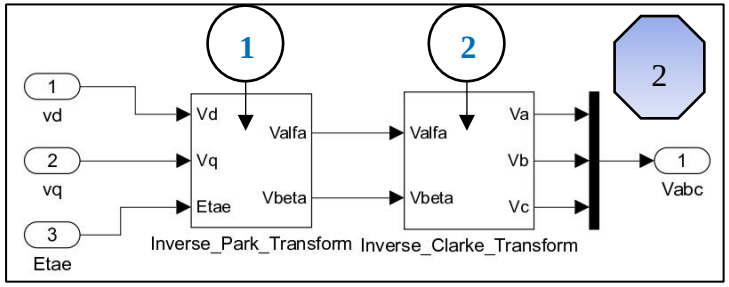
1
2
2
1
vd
2
vq
3
Etae
Vd
Vq
Etae
Valfa
Vbeta
Inverse_Park_Transform
Valfa
Vbeta
Va
Vb
Vc
Inverse_Clarke_Transform
1
Vabc

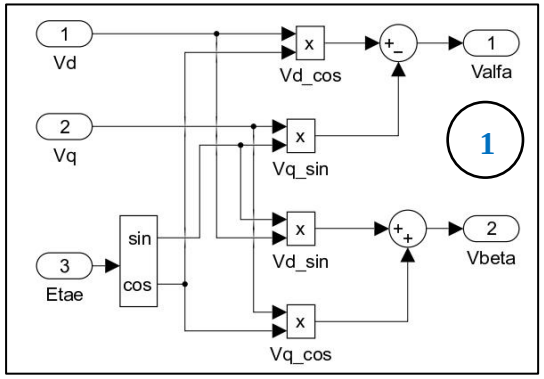
1
Vd
2
Vq
3
Etae
sin
cos
x
Vd_cos
x
Vq_sin
x
Vd_sin
x
Vq_cos
+
-
+
+
1
Valfa
2
Vbeta
1

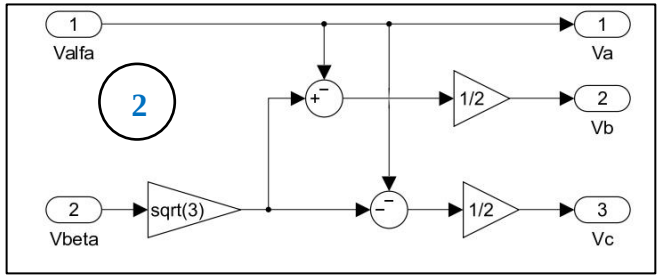
1
Valfa
2
2
Vbeta
sqrt(3)
+
-
-
1/2
1/2
1
Va
2
Vb
3
Vc

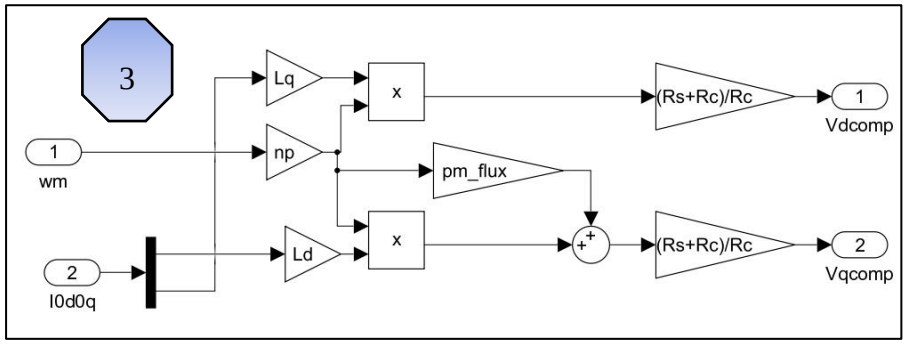
3
1
wm
2
I0d0q
Lq
np
Ld
x
x
pm_flux
+
+
(Rs+Rc)/Rc
(Rs+Rc)/Rc
1
Vdcomp
2
Vqcomp

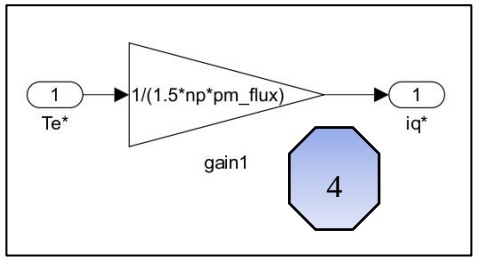
1
Te*
1/(1.5*np*pm_flux)
gain1
4
1
iq*

Appendix E Matlab Code for Power Loss Differentiation versus d-axis current with $P_1+P_2+P_3+P_4=0$

```
Te=1; Ld=0.00872; Lq=0.02278;
pm_flux=0.1077;
np=2; imax=20; i00d=-imax;
Rc=240; Rs=0.57; wm=100; beta=0.5;
i=0;
while (i00d<=imax)
    i=i+1;
    P1a=2*Lq*Te*wm*(Ld-Lq)/(3*Rc*(pm_flux+i00d*(Ld-
Lq))*(pm_flux+i00d*(Ld-Lq)))+1;
    P1b=i00d-2*Lq*Te*wm/(3*Rc*(pm_flux+i00d*(Ld-Lq)));
    P1=2*Rs*P1a*P1b;

    P2a=Ld*np*wm/Rc-2*Te*(Ld-Lq)/(3*np*(pm_flux+i00d*(Ld-
Lq))*(pm_flux+i00d*(Ld-Lq)));
    P2b=2*Te/(3*np*(pm_flux+i00d*(Ld-
Lq)))+np*wm*(pm_flux+Ld*i00d)/Rc;
    P2=2*Rs*P2a*P2b;

    P3=-8*beta*Lq*Lq*Te*Te*wm*wm*(Ld-
Lq)/(9*Rc*(pm_flux+i00d*(Ld-Lq))*(pm_flux+i00d*(Ld-
Lq))*(pm_flux+i00d*(Ld-Lq)));
    P4=2*beta*Ld*np*np*wm*wm*(pm_flux+Ld*i00d)/Rc;

    FF=P1+P2+P3+P4;
    %if (FF>0)  break; end
    FF_(i)=FF;
    id_(i)=i00d;
    i00d=i00d+0.01;
end
%icomputed=i00d
plot(id_,FF_);
```

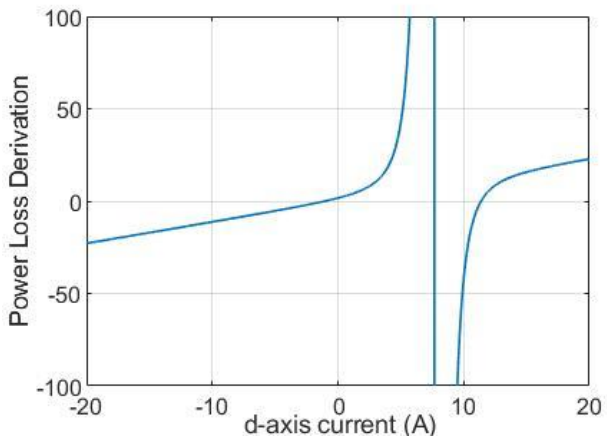

Appendix F Matlab Code for Power Loss Differentiation versus d-axis current with AB-T²C=0

```
Te=1;
Ld=0.00872;
Lq=0.02278;
pm_flux=0.1077;
np=2;
imax=100;
i00d=-imax;
Rc=240;
Rs=0.57;
wm=100;
beta=0.5;
i=0;
while (i00d<=imax)
    i=i+1;

A=1.5*1.5*np*np*(Rs*Rc*Rc*i00d+wm*wm*np*np*Ld*(Rs+Rc*beta
)*(Ld*i00d+pm_flux));
    B=(pm_flux+(Ld-Lq)*i00d)^3;
    C=(Rs*Rc*Rc+(Rs+Rc*beta)*(np*wm*Lq)*(np*wm*Lq))*(Ld-
Lq);
    FF=A*B-C*Te*Te;
    %if (FF>0)  break; end
    FF_(i)=FF;
    id_(i)=i00d;
    i00d=i00d+0.01;
end
%icomputed=i00d
plot(id_,FF_);
```

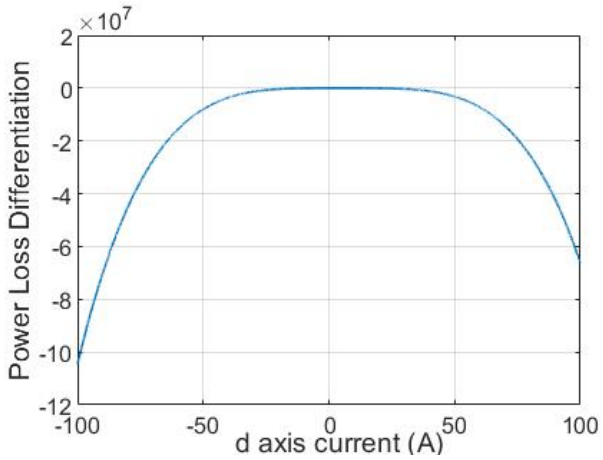

Appendix G **Combined MTPA/ME Control Approach in FOC Concept Accounting the Core Loss**

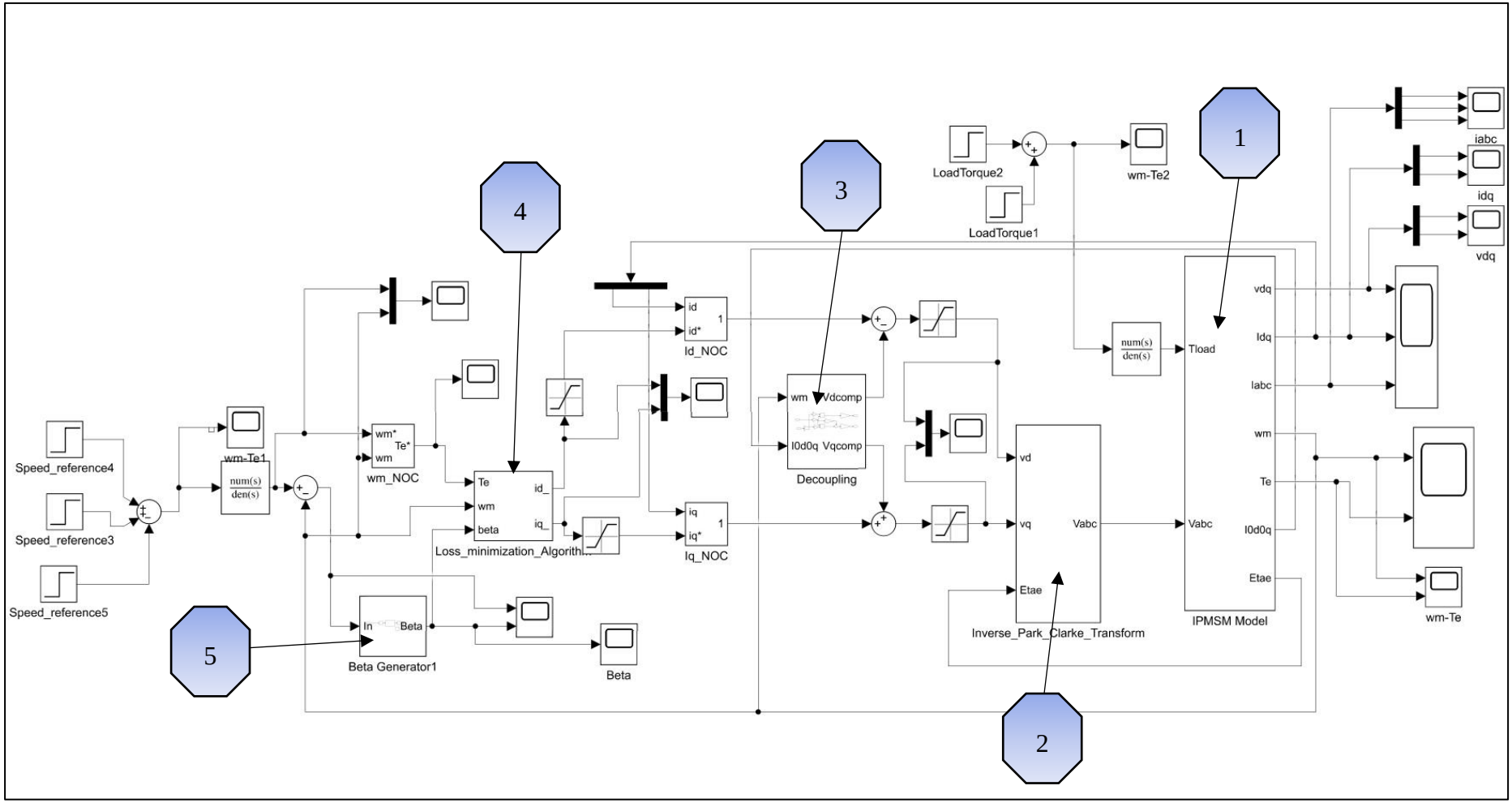

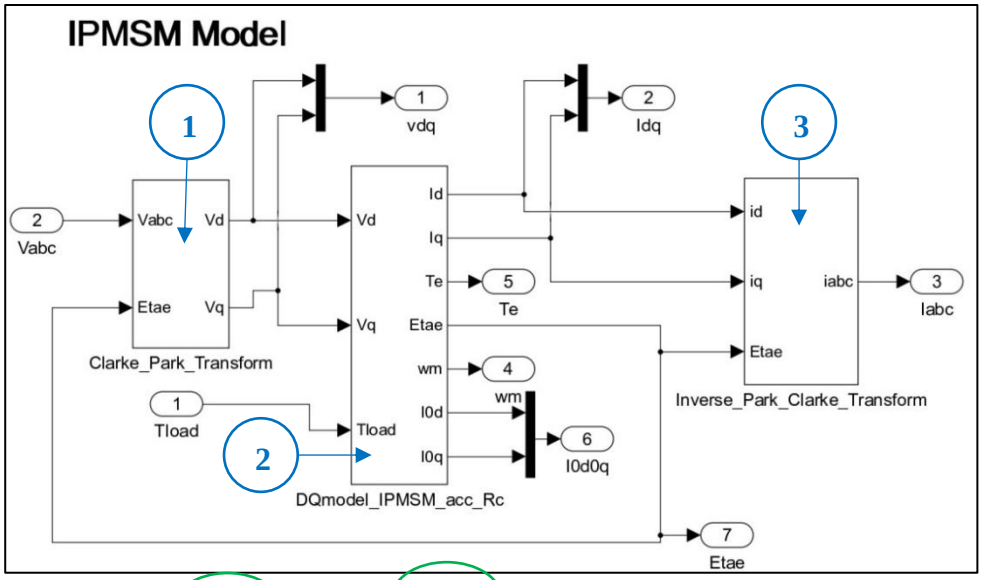
IPMSM Model
1
2
3
vdq
Idq
Vabc
Vd
Etae
Vq
Clarke_Park_Transform
Id
Iq
Te
Etae
wm
I0d
I0q
Tload
DQmodel_IPMSM_acc_Rc
id
iq
iabc
Inverse_Park_Clarke_Transform
Iabc
wm
I0d0q
Etae

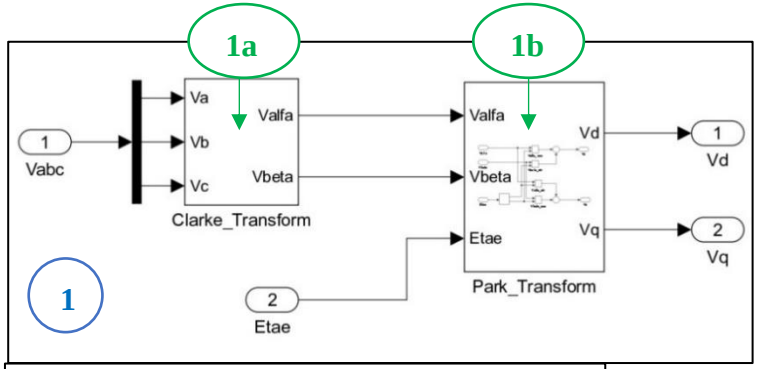
1a
1b
Va
Vb
Vc
Valfa
Vbeta
Clarke_Transform
Vabc
Valfa
Vbeta
Etae
Vd
Vq
Park_Transform
Vd
Vq
Etae
1

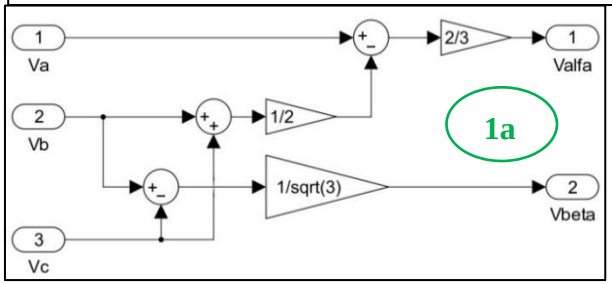
Va
Vb
Vc
2/3
1/2
1/sqrt(3)
Valfa
Vbeta
1a

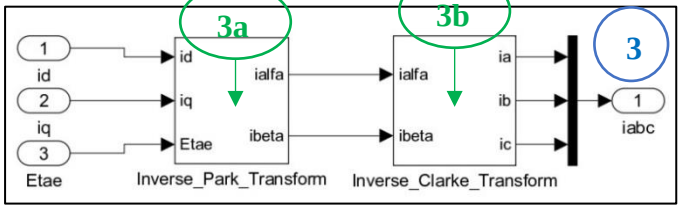
3a
3b
3
id
iq
Etae
ialfa
ibeta
Inverse_Park_Transform
ialfa
ibeta
ia
ib
ic
Inverse_Clarke_Transform
iabc

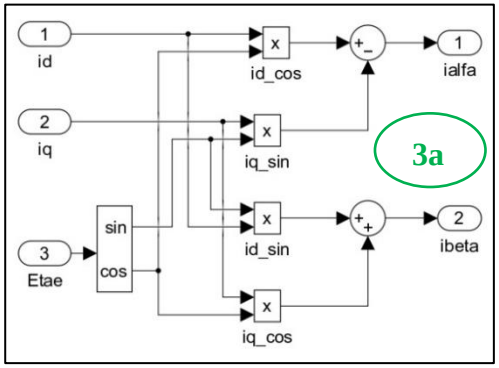
id
iq
Etae
id_cos
iq_sin
id_sin
iq_cos
sin
cos
ialfa
ibeta
3a

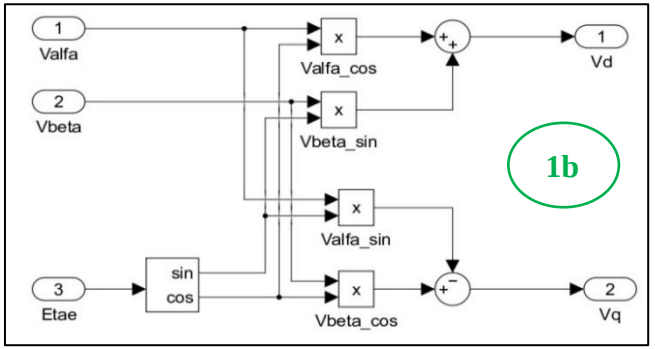
Valfa
Vbeta
Etae
Valfa_cos
Vbeta_sin
Valfa_sin
Vbeta_cos
sin
cos
Vd
Vq
1b

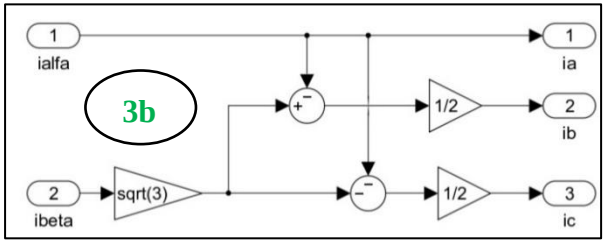
3b
ialfa
ibeta
sqrt(3)
1/2
1/2
ia
ib
ic

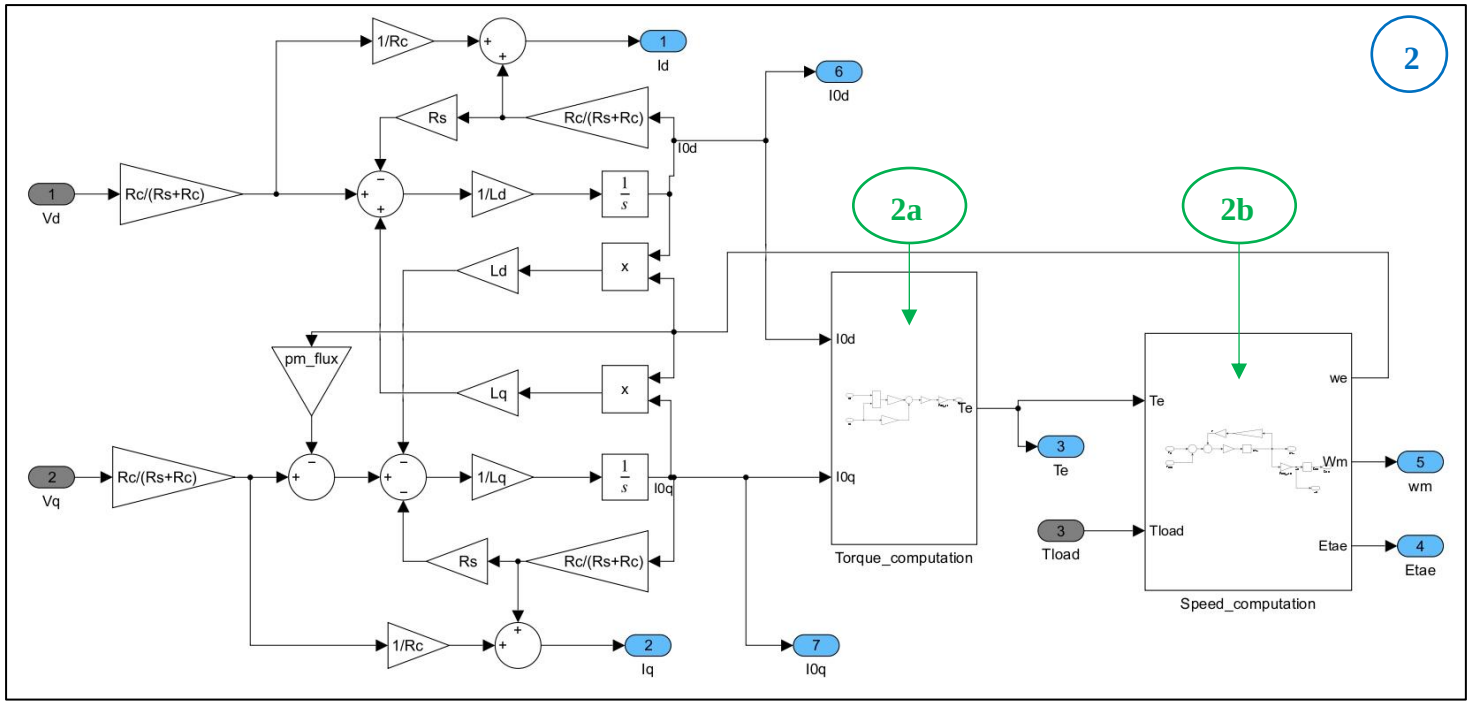
2
1/Rc
1
Id
6
I0d
Rs
Rc/(Rs+Rc)
I0d
1
Vd
Rc/(Rs+Rc)
1/Ld
Ld
x
2a
2b
pm_flux
Lq
x
I0d
Te
we
Te
3
Te
2
Vq
Rc/(Rs+Rc)
1/Lq
I0q
I0q
Wm
5
wm
3
Tload
Tload
Etae
4
Etae
Rs
Rc/(Rs+Rc)
Torque_computation
Speed_computation
1/Rc
2
Iq
7
I0q

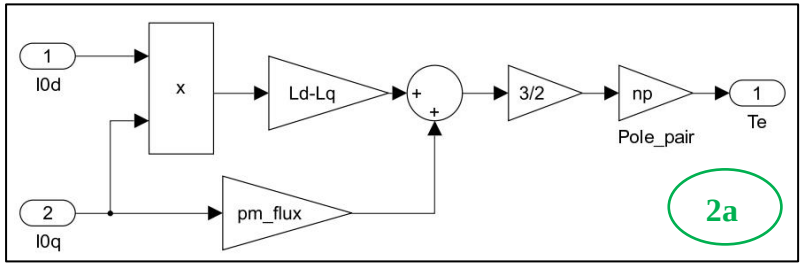
1
I0d
x
Ld-Lq
3/2
np
1
Te
Pole_pair
2
I0q
pm_flux
2a

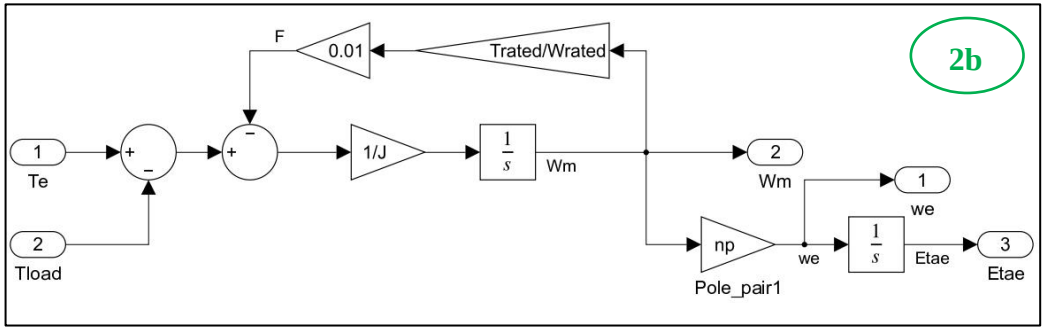
F
0.01
Trated/Wrated
2b
1
Te
1/J
Wm
2
Wm
1
we
2
Tload
np
we
Etae
3
Etae
Pole_pair1

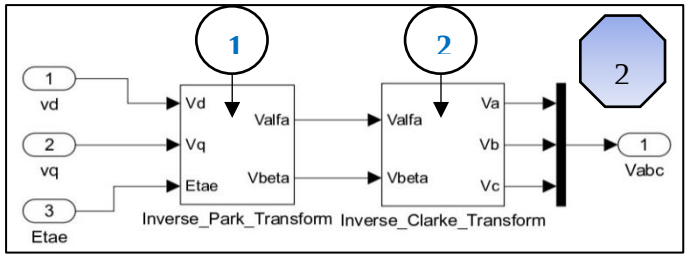
1
2
2
1
vd
2
vq
3
Etae
Vd
Vq
Etae
Valfa
Vbeta
Inverse_Park_Transform
Valfa
Vbeta
Va
Vb
Vc
Inverse_Clarke_Transform
1
Vabc

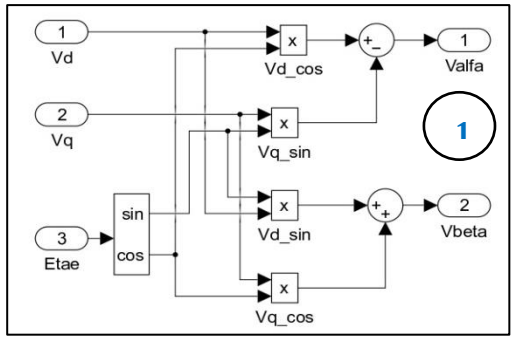
1
Vd
2
Vq
3
Etae
x
Vd_cos
+-
1
Valfa
x
Vq_sin
1
sin
cos
x
Vd_sin
++
2
Vbeta
x
Vq_cos

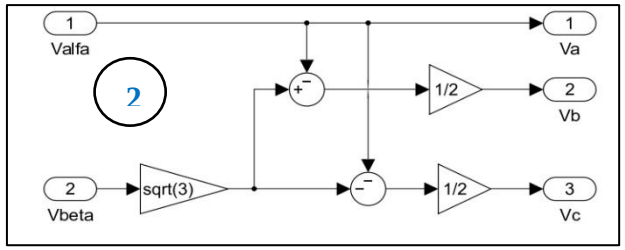
1
Valfa
2
2
Vbeta
sqrt(3)
1
Va
1/2
2
Vb
1/2
3
Vc

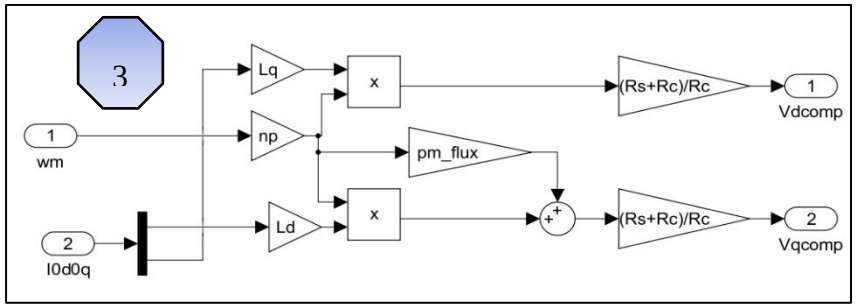
3
1
wm
2
I0d0q
Lq
np
Ld
x
pm_flux
x
(Rs+Rc)/Rc
1
Vdcomp
+
(Rs+Rc)/Rc
2
Vqcomp

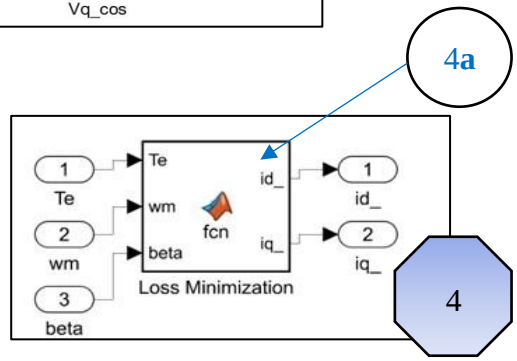
4a
1
Te
2
wm
3
beta
Te
wm
beta
fcn
id_
iq_
1
id_
2
iq_
Loss Minimization
4

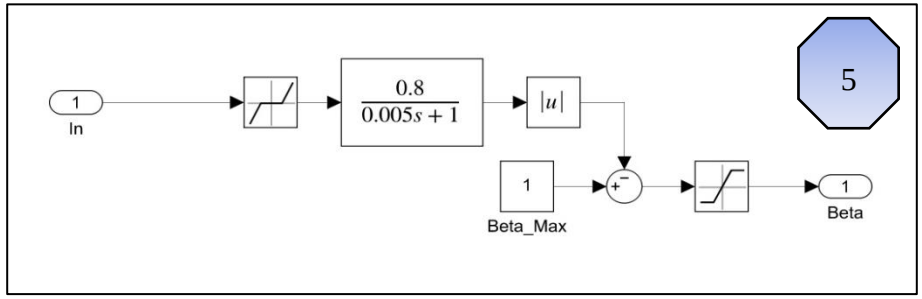
5
1
In
0.8
0.005s + 1
|u|
1
Beta_Max
1
Beta

Matlab Code in Block 4a

```
function [id_,iq_]=fcn(Te,wm,beta,np, Rs, Rc, Ld, Lq,
pm_flux)
imax=20;
i00d=-imax;
%See paper S. Amornwongpeeti, O. Kiselychnyk1, J. Wang,
C. Antaloae, M. Soumelidis, N. Shah,
%"A Combined MTPA and Maximum Efficiency Control Strategy
for IPMSM Motor Drive Systems,"
%https://ieeexplore.ieee.org/document/7841412, equation
(16)
%And my derivations in the file named
'Combined_derivations_for_Merve.docx'
while (i00d<=imax)
    %See final equations from the docx file

A=1.5*1.5*np*np*(Rs*Rc*Rc*i00d+wm*wm*np*np*Ld*(Rs+Rc*beta
)*(Ld*i00d+pm_flux));
    B=(pm_flux+(Ld-Lq)*i00d)^3;
    C=(Rs*Rc*Rc+(Rs+Rc*beta)*(np*wm*Lq)*(np*wm*Lq))*(Ld-
Lq);
    FF=A*B-C*Te*Te;
    if (FF>0)  break; end
    i00d=i00d+0.01;
end
i0d_=i00d;
%See paper Shigeo Morimoto, Yi Tong, Yoji Takeda, and
Takao Hirasa,
%"Loss Minimization Control of Permanent Magnet
Synchronous Motor Drives"
%IEEE TRANSACTIONS ON INDUSTRIAL ELECTRONICS, VOL. 41,
NO. 5, OCTOBER 1994
%From Torque Equation (7) in the paper above and scaled
by 3/2 which is neglected in the paper
i0q_=Te/(1.5*np*(pm_flux+(Ld-Lq)*i0d_));

%Current mapping equations (3) and (4) in the paper above
iq_=i0q_+(wm*np*(pm_flux+Ld*i0d_)/Rc);
id_=i0d_-(wm*np*Lq*i0q_/Rc);
```

```
%q-axis Current Controller Parameter Calculation
Lq=0.02278;
Rs=0.57;
%Regarding the state space equation  X'=AX+Bu+F
Tq01=Lq/Rs;
a1=-1/Tq01;
A=[0 1; 0 a1];
b1=1/(Tq01*Rs);
B=[0; b1];
% Q matrix is defined Regarding the simulation based
%observations
%The current limit in the simulations is defined as 10A
% R=c=1/(Umax)^2 is identified regarding the voltage
limit is Umax for d and q axes is limited to +/-150V,
alpha1=1/(0.05*10*0.05*10);
alpha2=1/(1.5*10*1.5*10);
Q=[alpha1 0;0 alpha2];
c=1/(150*150);
R=c;
%Computation of the controller gains k1 and k2 in eqn.
(4.28).which is
% u=-(b1/c)(k12x1+k22x2)=-(b1/c)k12x1-(b1/c)k22x2=-k1x1-k2x2
%Following equations are for calculations with matlab
%command lqr
[K,S,CLP]=lqr(A,B,Q,R);
k1=K(:,1)
k2=K(:,2)
%For the sake of double check
k22=(a1+sqrt(a1*a1+b1*b1/c*(2*sqrt(alpha1*c)/b1+alpha2)))
/(b1*b1/c);
k12=sqrt(alpha1*c)/b1;
%Computing k1 and k2 different methods
k1_=b1*k12/c
k2_=b1*k22/c
%It is seen that k1 and k1_ are identical and k2 and k2_
are identical
%It means the derivations are correct
 %Assuming that Rs=constant and due to magnetic
saturation and inaccurate measurements Lq can variate by
50%
%Then the new parameters in matrices A and B are
Tq02=0.5*Lq/Rs;
a2=-1/Tq02;
b2=1/(Tq02*Rs);

%For determining the controller parameters of the
nonlinear part
```

```
%Described by equation Error! Reference source not found.
,Error! Reference source not found. and
Error! Reference source not found.
k4=alpha1/(2*b2*k1);
k5=(alpha2+2*k4)/(2*(b2*k2-a2));
k6=b2*k4
k7=b2*k5
%Assume c1=c2=0.001 is identified by heuristic method,
thus the outputs of nonlinear and linear parts can be
comparable.
c1=0.001
c2=0.001
```

```
% d-axis Current Controller Parameters Calculation
Ld=0.00872;
Rs=0.57;
% Regarding the state space equation Ẋ = AX + Bu + F
Td01=Ld/Rs;
a1=-1/Td01;
A=[0 1; 0 a1];
b1=1/(Td01*Rs);
B=[0; b1];
%Q matrix is defined Regarding the simulation based
%observations
%The current limit in the simulations is defined as 10A
% R=c=1/(Umax)^2 is identified regarding the voltage
%limit is Umax for d and q axes is limited to +/-150V
alpha1=1/(0.05*10*0.05*10);
alpha2=1/(1.5*10*1.5*10);
Q=[alpha1 0;0 alpha2];
c=1/(150*150);
R=c;
% Computation of the controller gains k1 and k2 in eqn.
(4.28).which is
% u = -(b1/c)(k12 x1 + k22 x2) = -(b1/c) k12 x1 - (b1/c) k22 x2 = -k1 x1 - k2 x2
% Following equations are for calculations with matlab
%command lqr
[K,S,CLP]=lqr(A,B,Q,R);
k1=K(:,1)
k2=K(:,2)
%For the sake of double check
k22=(a1+sqrt(a1*a1+b1*b1/c*(2*sqrt(alpha1*c)/b1+alpha2)))
/(b1*b1/c);
k12=sqrt(alpha1*c)/b1;
%Computing k1 and k2 different methods
k1_=b1*k12/c
k2_=b1*k22/c
```

```
%It is seen that k1 and k1_ are identical and k2 and k2_
are identical
%It means the derivations are correct
 %Assuming that Rs=constant and due to magnetic
saturation and inaccurate measurements Lq can variate by
50%
%Then the new parameters in matrices A and B are
Td02=0.5*Ld/Rs;
a2=-1/Td02;
b2=1/(Td02*Rs);

%For determining the controller parameters of the
nonlinear part
%Described by equation Error! Reference source not found.
,Error! Reference source not found. and
Error! Reference source not found.
k4=alpha1/(2*b2*k1);
k5=(alpha2+2*k4)/(2*(b2*k2-a2));
k6=b2*k4
k7=b2*k5
%Assume c1=c2=0.001 is identified by heuristic method,
thus the outputs of nonlinear and linear parts can be
comparable.
c1=0.001
c2=0.001
```

```
% Velocity Controller Parameters Calculation
%The following parameters are taken from the Simulink
model
J=0.004;
Trated=1.67;
wrated=2000*pi/30;
F=0.01*Trated/wrated;
Tm01=J/F;
%Regarding that the inner loops, id and iq current loops,
%should provide significantly faster dynamics than the
%outer, velocity, loop. Ideally the developed torque
%should be equal to the reference torque T_e = T_e^* (the
%reference torque at the input of %MTPA or ML controller
%or output of the velocity controller %for the zero d-
%axis current method). In reality, a scaling parameter
%named k_T is introduced to provide T_e = k_T T_e^*.
kt01=1;

%Regarding the state space equation Xdot = AX + Bu + F
a1=-1/Tm01;
```

```
b1=kt01/(Tm01*F);
A=[0 1; 0 a1];
B=[0; b1];

%Q and R matrices are defined according to the current
%and voltage limits in the simulations for current
controller parameters. In this case, those are defined
with heuristic method.
alpha1=0.01/(0.0003*wrated*0.0003*wrated);
alpha2=0.01/(0.01*wrated*0.01*wrated);
Q=[alpha1 0;0 alpha2];
c=1/(3*Trated*3*Trated);
R=c;

% Computation of the controller gains k1 and k2 in eqn.
(4.28).which is
% u = -(b_1/c)(k_12 x_1 + k_22 x_2) = -(b_1/c) k_12 x_1 - (b_1/c) k_22 x_2 = -k_1 x_1 - k_2 x_2
% Following equations are for calculations with matlab
%command lqr
[K,S,CLP]=lqr(A,B,Q,R);
k1=K(:,1)
k2=K(:,2)

%For the sake of double check
k22=(a1+sqrt(a1*a1+b1*b1/c*(2*sqrt(alpha1*c)/b1+alpha2)))
/(b1*b1/c);
k12=sqrt(alpha1*c)/b1;
%Computing k1 and k2 different methods
k1_=b1*k12/c
k2_=b1*k22/c
%It is seen that k1 and k1_ are identical and k2 and k2_
are identical
%It means the derivations are correct
%Assuming that Rs=constant and due to magnetic saturation
%and inaccurate measurements Lq can variate by 50%
%Then the new parameters in matrices A and B are

%Assumming that F=constant and J can variate by 50% due
%to uncertainties or inaccurate measurements then
%The new parameters of matrices A and B are
Tm02=0.5*J/F;
kt02=kt01;
a2=-1/Tm02;
b2=kt02/(Tm02*F);
 %For determining the controller parameters of the
%nonlinear part
%Described by equation Error! Reference source not found.
,Error! Reference source not found. and
Error! Reference source not found.
```

```
k4=alpha1/(2*b2*k1);
k5=(alpha2+2*k4)/(2*(b2*k2-a2));
k6=b2*k4
k7=b2*k5
%Assume c1=c2=0.001 is identified by heuristic method,
thus the outputs of nonlinear and linear parts can be
comparable.
c1=0.01
c2=0.01
```

Appendix I Motor Specifications used in lab-based experiment rig

Motor specification				
No.	Parameter	Unit	Tirius JEM02	Ashwoods dual core
1	Maximum power	kW	30	29
2	Rated power	kW	12	10
3	Maximum torque	Nm	80	84
4	Rated torque	Nm	28	43
5	Maximum speed	rpm	10000	7500
6	Rated speed	rpm	3700	3250
7	Maximum DC voltage	VDC	600	600
8	Rated DC voltage	VDC	560	560
9	Maximum line voltage	V	600	600
10	Rated line voltage	V	400	400
11	Maximum current	A (rms)	80	80
12	Rated current	A (rms)	25	72,5
14	Rated frequency	Hz	308	216,6
15	Number of pole pairs	-	5	4
16	Winding connection	Star/ Delta	Star	Star
17	Phase-phase stator resistance	mΩ	280	42
18	Phase-phase stator inductance	mH	4,63	3,42
19	d-axis inductance	mH	1,62	3,52
20	q-axis inductance	mH	2,78	4,48
21	Back EMF constant	V/kprm	0,89	93,5
22	Torque constant	Nm/A	varies	1,3
23	Moment of inertia	kg.m^2	0,004	0,0263
24	Rotor PM flux linkage	Wb	0,109	0,181

Appendix J Publications

Energy Efficient and Transients Optimal IPMSM Drive for Electric Vehicles

Merve Öztekin, Oleh Kiselychnyk, Jihong Wang
Power and Control Systems Research Laboratory
The University of Warwick
merve.oztekin@warwick.ac.uk, O.Kiselychnyk@warwick.ac.uk, jihong.wang@warwick.ac.uk

***Abstract*—An energy efficient and transients optimal control for Interior Permanent Magnet Synchronous Motors is introduced based on the concept of the combined Maximum Torque per Ampere (MTPA) and total electric Loss Minimisation (LM) control approaches. The nonlinear optimal implicit equation of the combined MTPA/LM method is derived in a new compact form, the same as for the conventional LM approach. Then it is very simply applied to activate the MTPA control during transients for fast dynamics and the LM control during steady states for maximum efficiency. Compared to the existing similar approaches, it allows smooth transition between the methods with smaller number of equations simplifying required control coding and reducing the control algorithm execution time. Analytical results are supported by simulations and experimental results.**

Keywords—Permanent Magnet Motors, Variable Speed Drives, Trajectory Optimization, Electric Vehicles, Angular Velocity Control.

I. INTRODUCTION

As part of the targets of carbon emission reduction [1], electrification of road transport has been received great attention in last few decades. Interior Permanent Magnet Synchronous Motors (IPMSM) are widely utilised in Electric Vehicles (EVs) owing to their inherent features such as high-power density, high efficiency, compactness, large torque-current ratio, etc.

Conventional Field Oriented Control (FOC) concept transforms each motor electrical three-phase AC variable into equivalent two DC variables defined in a rotating *d*-*q* reference frame aligned with the IPMSM's rotor permanent magnet flux. Such approach allows to implement the control similarly to the DC motor control. It includes two stator currents in *d*- and *q*-axes closed loops with PI current controllers and a velocity closed loop with a PI controller which output is the reference of the *q*-axis current loop. Zero *d*-axis current (ZDAC) control strategy means that this current reference is all the time zero. It provides linear dependence of the motor torque on the *q*-axis current significantly simplifying the controllers design procedure and control implementation. Since the *d*-axis current diverges from zero value during transients, a decoupling algorithm is added to make these currents loops independent and improve the dynamic performance. However, the torque capability of IPMSM cannot be fully utilised in this case since the inherent reluctance torque is disregarded and the motor efficiency is far from the optimal value. Further improvement is achieved via setting a specific nonlinear relationship between the *d*- and *q*-axes stator current references which worsens the dynamic performance but allows two possible optimisations. The first, Maximum Torque Per Ampere (MTPA) control [2] allows to extract maximum possible torque for a given stator current rms (or amplitude) value. The second is the Loss Minimization (LM) control strategy [3] achieving maximum efficiency (ME) of the motor via minimising the total electric motor loss.

The influence of the stator *d*- and *q*-currents on the torque capability of IPMSM is investigated in [4]. It is shown that the magnetic saliency due to the buried magnets creates magnetic flux pathways with different permeances leading to the reluctance torque [4], [5] proportional to the product of the *d*- and *q*-axes currents. Then the total torque dependence on the *d*-axis stator current for a given amplitude has a maximum point. The corresponding optimal relationship between the *d*- and *q*-axes currents can be determined analytically in explicit view determining the MTPA control [2] or alternatively the optimal stator current vector angle as a function of the stator current amplitude can be determined [5]. To exclude influence of the motor parameters on the accuracy of the MTPA trajectories, automatic searching algorithms are used instead of the optimal equations based which significantly slows down the control. The process of the maximum searching is accelerated based on the online polynomial curve fitting proposed in [6]. In [7], the velocity regions, including ones with partial field weakening for higher velocities and lower torques, are defined were the MTPA implementation is possible. In general, all MTPA approaches provide faster transient response and minimisation of the motor copper loss.

The total electric loss in IPMSM consists mainly of two components: the copper loss and the iron loss. The iron loss is due to eddy currents, hysteresis [8] and the excess losses. They are accounted for in the IPMSM model using some empirical formulae [8] or as an equivalent iron loss constant resistance [3] or the iron loss resistance dependent on the motor velocity [9] which was justified using Bertotti iron loss formula and Finite Element Analysis. In all cases, the LM algorithm is based on the differentiation of the total electric loss function with respect to the *d*- or *q*-axis current with following equating the results to zero similarly as for the MTPA. However, this gives only implicit optimal relationship between the *d*- and *q*-axes currents [3] requiring the real time solution of the nonlinear optimal equation via iterations (slower algorithm compared to the MTPA).

In the EV applications the designers face a dilemma which control approach to be selected since there is a trade-off between faster dynamics and better efficiency varying during the corresponding driving cycles where the parameters of the motor are also subject to change influencing the control accuracy. The average efficiency or power loss over a driving cycle can be the selection criterion [10], [11] if the focus is on the energy saving. The efficiency difference between MTPA and LM approaches is presented in [12] during an overall driving cycle.

A compromising solution between the efficiency and faster dynamics is suggested in [13] where the control is switched between MTPA during transients and LM during steady states

introducing additional transients due to switching. A similar hybrid method based on the velocity error is proposed in [14] without using the switch to eliminate the switching disturbances. The MTPA trajectory is always kept activated and the difference between the optimal *d*-axis currents in MTPA and LM methods is added only during steady state operation. This complicates the implementation via real time computations for both approaches at the same time.

The presented paper is based on the previous results of the authors reported in [15], where so-called combined MTPA/ME control approach was introduced for IPMSMs. Compared to the solutions above there is no switching between these two techniques and only one nonlinear algebraic equation is to be solved online iteratively to determine the optimal current references. A special control parameter is introduced, limited between zero and one, allowing to move smoothly between MTPA and LM trajectories and to provide steady state operation with either MTPA or LM or combined (in-between MTPA and LM) optimal current reference curves. This allows additional optimisation procedures for EVs via regulation of this control parameter depending on the operation conditions. In the paper the control parameter was the ratio of the requested torque and its rated value which provided smooth transition from MTPA to LM while increasing the torque from zero to its rated value. The control parameter can be also considered as a function of State of Charge (SoC) of the battery feeding the drive. Moving from MTPA to LM with decreasing SoC may allow to save the energy and to increase the driving path. The presented paper extends the results obtained in [15]. It derives the optimisation nonlinear algebraic equation in a compact form similar to the standard LM optimisation equation from [3] allowing simpler coding, simpler possible upgrade from existing LM codes to the combined method and better understanding of the difference between the LM and combined approaches. The paper also shows the application of the combined approach to achieve the MTPA during transients and LM during the steady states and how simpler this approach is comparing to those from [13] and [14]. Instead of thinking what to use, MTPA or LM algorithms, there appears a new question of how to optimise their combination.

II. THE CONTROL CONCEPT

A. IPMSM Dynamics Modeling Accounting for Iron Loss

The dynamical model of IPMSM accounting for the iron loss is based on the equivalent circuits presented in Figure 1.

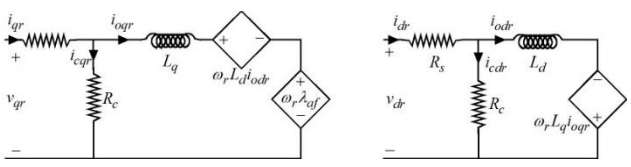

Figure 6.1. The equivalent circuit of IPMSM in *d*-*q* reference frame aligned with the rotor permanent magnet flux in *d*-axis

The following notation is used in the figure: v_{dr}, v_{qr} are the stator voltages in *d* and *q* axes, respectively, i_{dr}, i_{qr} are the stator currents, i_{cdr}, i_{cqr} are the corresponding iron loss currents, λ_{af} is the permanent magnet flux, R_S is the stator resistance, R_C is the iron loss resistance, L_d, L_q are the stator inductances in the corresponding axes, ω_r is the electrical angular frequency of the rotor. The equivalent circuits are described by the following two equations where p denotes the differentiation operation

$$\begin{bmatrix} v_{qr} \\ v_{dr} \end{bmatrix} = R_s \begin{bmatrix} i_{oqr} \\ i_{odr} \end{bmatrix} + \frac{R_s + R_c}{R_c} \left(\begin{bmatrix} L_q p & \omega_r L_d \\ -\omega_r L_q & L_d p \end{bmatrix} \begin{bmatrix} i_{oqr} \\ i_{odr} \end{bmatrix} + \begin{bmatrix} \omega_r \lambda_{af} \\ 0 \end{bmatrix} \right) \quad (1)$$

where $i_{odr} = i_{dr} - i_{cdr}$ and $i_{oqr} = i_{qr} - i_{cqr}$.

The electromagnetic torque is determined as [16], [17]

$$T_e = \frac{3}{2} n_p \left(\lambda_{af} i_{oqr} + \left(L_d - L_q \right) i_{odr} i_{oqr} \right) \quad (2)$$

where n_p is the number of pole pairs.

The dynamics of the motor's shaft is modelled according to the equation below [2]

$$T_e - T_l = J \frac{d\omega_m}{dt} + B\omega_m \quad (3)$$

where T_l denotes the load torque, J is the motor inertia, and ω_m is the mechanical velocity of the rotor, $\omega_m = \omega_e / n_p$ and B is the viscous friction coefficient.

B. MTPA Control Algorithm

The conventional MTPA control is designed ignoring the iron loss ($R_C = \infty$) then $i_{odr} = i_{dr}$ and $i_{oqr} = i_{qr}$. Differentiating the torque equation (2) with respect to i_{odr} and equating it zero gives the optimal relationship between the currents maximizing the torque for a given stator current amplitude

$$i_{dr} = \frac{\lambda_{af}}{2\left(L_q - L_d\right)} - \sqrt{\frac{\lambda_{af}^2}{4\left(L_q - L_d\right)^2} + i_{qr}^2} \; . \quad (4)$$

In the control algorithm $i_{qr} = i_{qr}^*$ is the reference of the *q*-axis current loop (the output signal of the PI velocity controller) and $i_{dr} = i_{dr}^*$ is computed in real time according to (4).

To decouple the i_{dr} and i_{qr} current loops the feed-forward voltage compensator is implemented depicted in Figure 6.2 [2].

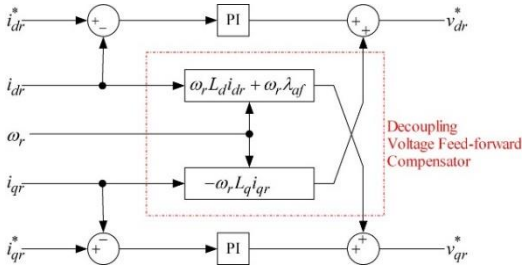

Figure 6.2. Feed-forward voltage compensator

C. Loss Minimization Algorithm

The total electrical loss W_e mainly consists of the copper loss and the iron loss as shown in (5). The stray losses are neglected [3].

$$W_e = W_{Cu} + W_{Fe}. \tag{5}$$

For a three-phase IPMSM, the copper loss W_{Cu} and the iron loss W_{Fe} are determined as in (6).

$$W_{Cu} = \frac{3}{2} R_s (i_{qr}^2 + i_{dr}^2)$$
$$W_{Fe} = \frac{3}{2} R_c (i_{cqr}^2 + i_{cdr}^2) \tag{6}$$

Based on Figure 6.1, equations (6) are transformed to the following view

$$W_{Cu} = \frac{3}{2} R_s \left(\left(i_{odr} - \frac{\omega_r L_q i_{oqr}}{R_c} \right)^2 + \left(i_{oqr} + \frac{\omega_r \left(\lambda_{af} + L_d i_{odr} \right)}{R_c} \right)^2 \right)$$

$$W_{Fe} = \frac{3}{2} \left(\frac{\omega_r^2 (L_q i_{oqr})^2}{R_c} + \frac{\omega_r^2 \left(\lambda_{af} + L_d i_{odr} \right)^2}{R_c} \right)$$

The conventional LM trajectory equation is attained via differentiation of the total electrical loss in (5) with respect to the i_{odr} current and equating it to zero, $dW_e / di_{odr} = 0$. It results in a polynomial equation of third order with respect to i_{odr} [3].

$$AB = T_e^2 C \tag{7}$$

where

$$A = \left(9 n_p^2 / 4 \right) \left(R_s R_c^{\,2} i_{odr} + \omega_r^2 L_d \left(R_s + R_c \right) \left(L_d i_{odr} + \lambda_{af} \right) \right),$$

$$B = \left(\lambda_{af} + (L_d - L_q) i_{odr} \right)^3,$$

$$C = \left(R_s R_c^{\,2} + (R_s + R_c)(\omega_r L_q)^2 \right) (L_d - L_q).$$

During LM control, the requested torque T_e^* is the output signal of the PI velocity controller. The i_{odr}^* reference value is computed in real time via iterative solution of (7) with $T_e = T_e^*$. Then i_{oqr}^* is computed using (2). Finally, i_{odr}^* and i_{oqr}^* are mapped into i_{dr}^* and i_{qr}^*. Please note that LM control current trajectory depends on ω_r and R_c. The feed-forward voltage compensation shown in Figure 6.2. Feed-forward voltage compensatorcan still be used but the currents i_{odr} and i_{oqr} must be used instead of i_{dr} and i_{qr}.

D. Combined MTPA/LM Algorithm

Introduce the fictitious electrical power loss defined as below [15]

$$W_f = W_{Cu} + \beta W_{Fe}, \tag{8}$$

where β is the control parameter and $0 \le \beta \le 1$.

Eliminating i_{oqr} from (8) with following differentiating equation (8) with respect to i_{odr} and equating it to zero, $dW_f / di_{odr} = 0$, yields the same polynomial equation (7) where B is the same but A and C are updated as follows

$$A = \left(9 n_p^2 / 4 \right) \left(R_s R_c^{\,2} i_{odr} + \omega_r^{\,2} L_d \left(R_s + \beta R_c \right) \left(L_d i_{odr} + \lambda_{af} \right) \right) \tag{9}$$

$$C = \left(R_s R_c^{\,2} + \left(R_s + \beta R_c \right) \left(\omega_r L_q \right)^2 \right) \left(L_d - L_q \right) \tag{10}$$

The obtained nonlinear optimal equation for the combined MTPA/LM technique is the same as for the conventional LM but with the modified R_c value only in two places. The obtained form is very convenient for upgrading existing LM control systems and more compact compared to one in [15] for coding new systems. Please note that if $\beta = 0$ then $W_f = W_{Cu}$ and the solution of (7) with (9) and (10) gives the MTPA optimal currents trajectory which is close but a bit different from (4) since it still accounts for R_c and ω_r. If $\beta = 1$ then $W_f = W_e$ and the solution yields the LM optimal currents trajectory which is identical to the conventional case. Changing β in real time in the range from zero to one allows to create optimal currents trajectories in-between the LM and MTPA optimal currents curve and to formulate β optimisation goal depending on operating conditions.

E. Steady-State LM and Dynamical MTPA Hybrid Algorithm Implementation

The block diagram for β computation is shown in Fig. 3. During the transients there is a dynamical velocity error $\omega_m^* - \omega_m$. The error is amplified, and the abs value is taken with following subtraction from one. Since the amplification gain is quite high and the output signal is saturated between zero and one then during transients $\beta = 0$ and the MTPA is implemented. During the steady states due to the PI velocity controller $\omega_m^* = \omega_m$ and $\beta = 1$. During transients there are also short periods when $0 \le \beta \le 1$ and β changes smoothly due to the I-part of the controller providing smooth transitions between the two control approaches. The duration of these periods can be adjusted via proper selection of the gain value. Compared to the solution in [13] the switching is avoided. In the presented method, only one nonlinear optimal equation is solved in real time iteratively instead of the similar equation plus another nonlinear equation for MTPA and their combining [14] which simplifies the implementation and reduces the whole algorithm execution time.

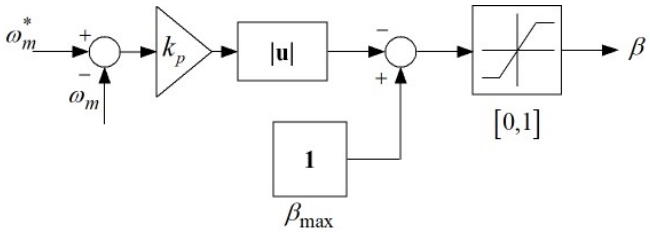

Figure 6.3. Decision algorithm in β Generator

Therefore, MTPA control provides faster dynamic response for acceleration or deceleration demand during velocity changes, while LM control ensures less energy consumption during steady state operation for efficient battery

management. The block diagram of the whole control system is depicted in Figure 6.4 where θ_m is the angular position of the rotor, i_a and i_b are the stator currents in phases *a* and *b*, V_{dc} is the input DC voltage of the inverter. The feed-forward voltage compensator is used as well but it is not shown for simplicity of the block diagram figure.

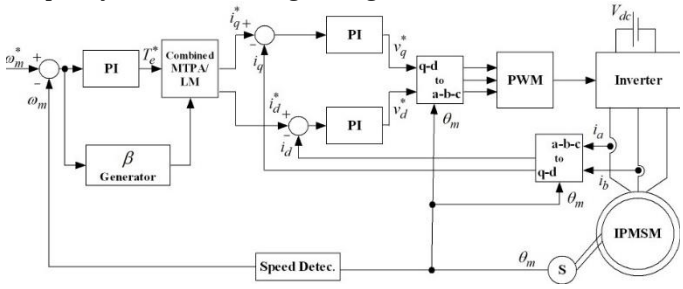

Figure 6.4. The proposed control structure

III. SIMULATION RESULTS

The proposed control structure in Figure 6.4 is investigated in simulations using Simulink excluding PWM generation. The IPMSM parameters [2], [3] and specifications are presented in Table 6.1. The proportional *kp* and integral *ki* gains of the corresponding PI controllers are specified in Table 6.2.

The profiles of the angular velocity reference and the load torque are shown in Figure 6.5.a. The corresponding angular velocity and torque transients are presented in Figure 6.5.b. Please note that there exist regions with linear angular velocity increase or decrease caused by the saturation of the output signal of the velocity controller. The acceleration and deceleration happen under the constant torque applied to the motor shaft. Figure 6.5.c depicts *a*-, *b*-, and *c*-phase currents, and *d*- and *q*-axis stator currents as well. Responding to the angular velocity error variations, β parameter changes smoothly in-between 0 and 1 (see Figure 6.5.d). It converges to 1 during steady state operation ensuring LM control. Therefore, the control algorithm optimises the motor efficiency and optimum DC power consumption is provided. Otherwise, during transients including the linear velocity increase/decrease, β coefficient is set to zero and MTPA control algorithm is activated which leads to better acceleration or deceleration performance.

Table 6.1. IPMSM Specifications and Parameters

Rated Torque T_{rt} (Nm)	1.67
Rated Current I_{rt} (A)	5
Rated Velocity n_{rt} (rpm)	2000
Rated Voltage V_{rt} (V)	97
DC link Voltage V_{dc} (V)	150
R_s (Ω)	0.57
R_c (Ω)	240
L_q (mH)	22.78
L_d (mH)	8.72
λ_{af} (Wb)	0.1077
n_p	2

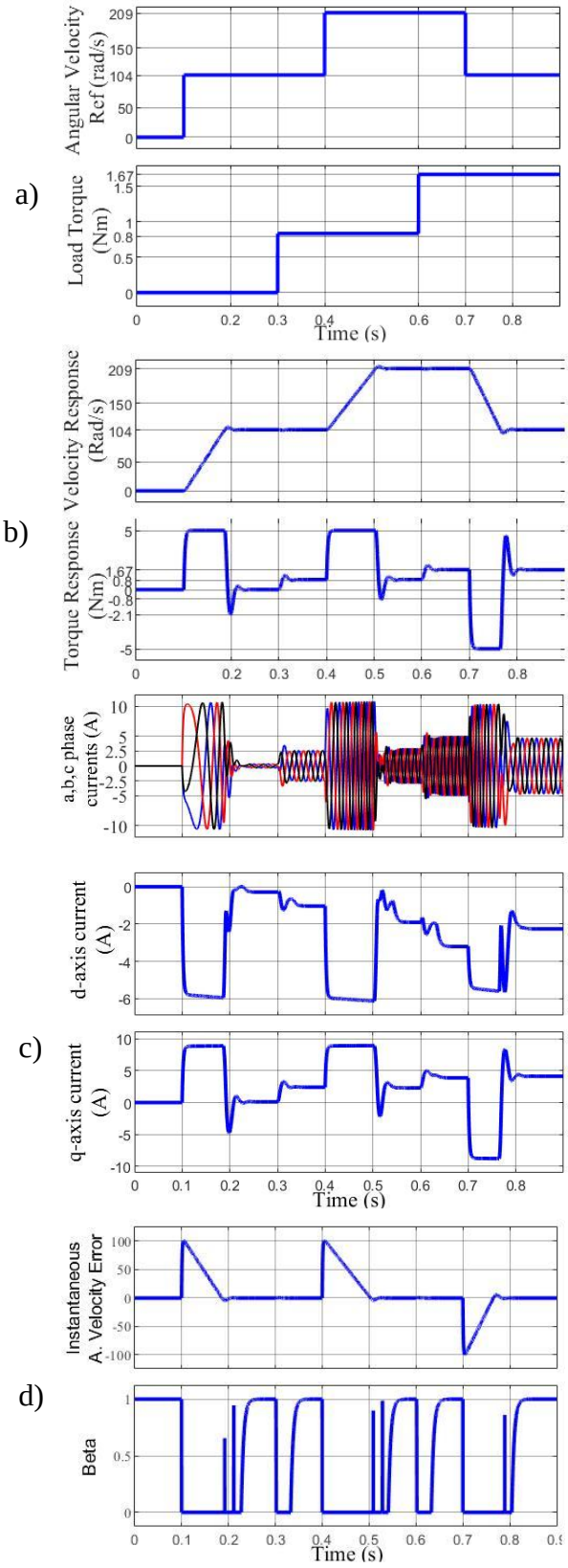

Figure 6.5. Simulation results a) Angular velocity reference and load torque b) Angular velocity and torque response c) *a*-, *b*-, *c*-phase and *d*-, *q*-axis currents d) Instantaneous angular velocity error and β

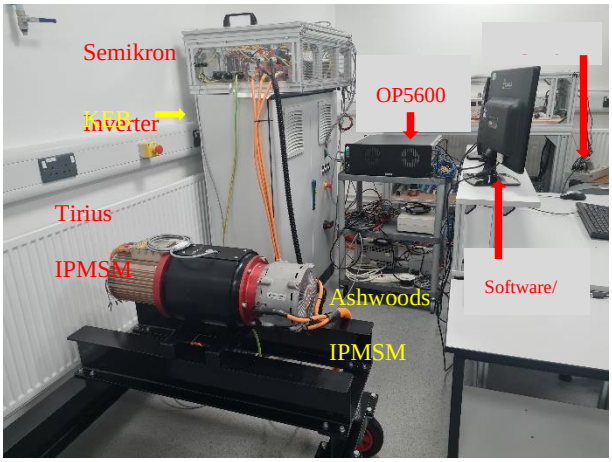

Figure 6.6. Experimental Rig

The experiments are carried out on a laboratory-installed test rig shown in Figure 6.6. The test rig consists of an under-test motor (Tirius IPMSM, three-phase, 5 pole pairs, 12kW, 28 Nm, 3700 rpm, 560 Vdc), an under-test drive (Semikron 3 power modules based three-phase IGBT inverter with 600 VDC), Real Time Simulators (dSPACE DS1104 and OPAL-RT OP5600 HIL), a load motor (Ashwoods IPMSM, three-phase, 4 pole pairs, 10kW, 43Nm, 3250 rpm, 560 Vdc), a load motor drive (KEB COMBIVERT F5 AC motor controller and drive unit, 30kW, 305-500V, 2-16kHz), resolver and power supply units. The parameters of the PI controllers are given in Table 3. The data attained from experimental test rig is denoised with Symlet-4 Wavelet filter.

Figs. 7 and 8 show some auxiliary experimental results obtained for the MTPA and LM control algorithms for the no load motor start following by the gradual loading and unloading using 2 Nm load torque steps and helping to understand the possible advantage of the combining. As it is expected the LM algorithm provides less torque compared to the MTPA algorithm in steady states. As it can be noted from the figures, the MTPA algorithm slightly reduces the transient time caused by the 2 Nm load torque step increase, compared to the LM case.

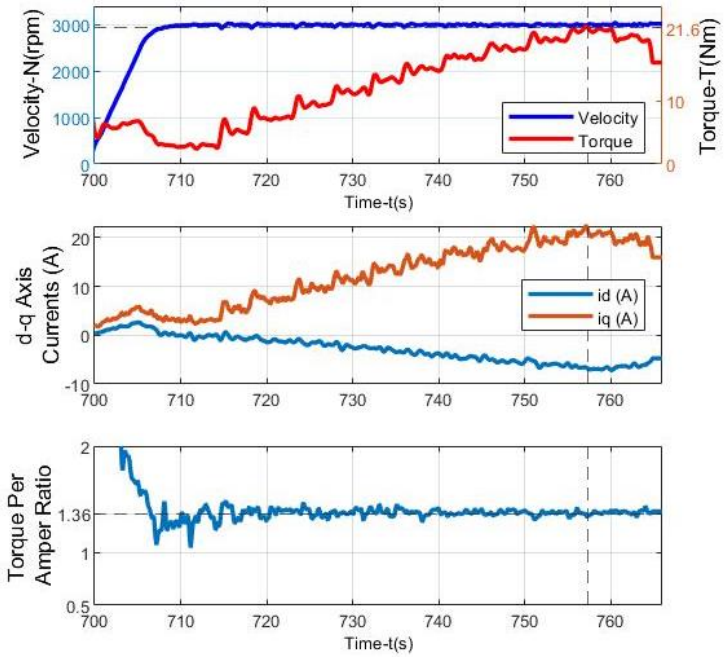

Figure 6.7. MTPA Control
a) Torque, Velocity
b) d-q axes currents
c) Torque per Ampere Ratio

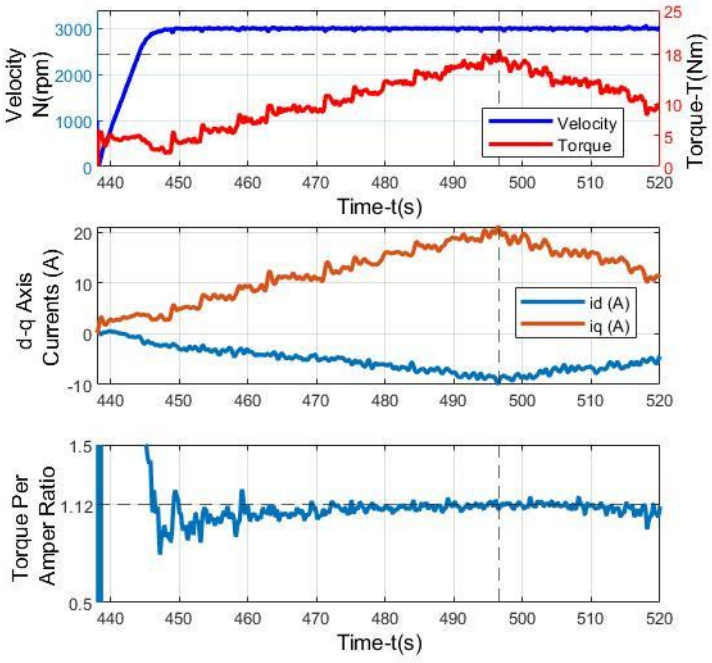

Figure 6.8. ME Control
a) Torque, Velocity
b) d-q axes currents
c) Torque Per Ampere Ratio

V. CONCLUSION

The paper succeeds in derivation of the implicit nonlinear optimal algebraic equation allowing to implement the combined MTPA/LM control technique of the IPMSM based on the concept of the fictitious electric power loss, in the same view as for the conventional LM method. This simplifies modification of the standard LM coding into the MTPA/LM coding or implementation of new systems compared to the existing approach. The application of the designed combined approach makes very simple the implementation of the system with the MTPA control during transients for faster dynamics and with LM control during steady states for maximum efficiency. It allows to provide smooth transition between the control methods due to combining instead of switching and to reduce the control algorithm execution time due to reducing the number of equations compared to the existing hybrid methods.

VI. Appendix

Table 6.2. The Controller Parameters in Simulations

		ω_m Controller	i_d Controller	i_q Controller
PI	*ki*	125	285	285
	kp	1	4.36	11.4
	Sat	5	150	150

Gain coefficient k_p for β Generator is defined as 100.

Table 6.3. Controllers' gains for experiments

		i_d Controller	i_q Controller	ω_m Controller
PI	k_i	8	8	1.2
	k_p	6	6	0.2

VII. REFERENCES

[1] F. Knobloch, S. V. Hanssen, A. Lam, H. Pollitt, P. Salas, M. A. J. Huijbregts and J. F. Mercure, "Net Emission Reductions from electric cars and heat pumps in 59 world regions over time," *Nature Sustainability*, vol. 3, no. 6, pp. 437-447, 2020.

[2] S. Morimoto, M. Sanada and Y. Takeda, "Wide-speed operation of interior permanent magnet synchronous motors with high-performance current regulator," *IEEE Trans. on Ind. App.*, vol. 30, no. 4, pp. 920 - 926, Jul/Aug 1994.

[3] S. Morimoto, Y. Tong, Y. Takeda and T. Hirasa, "Loss minimization control of permanent magnet synchronous motor drives," *Industrial Electronics, IEEE Transactions*, vol. 41, no. 5, pp. 511-517, 1994.

[4] T. M. Jahns, G. B. Kliman and T. W. Neumann, "Interior Permanent-Magnet Synchronous Motors for Adjustable-Speed Drives," *IEEE Trans. on Inds. Apps.*, Vols. IA-22, no. 4, pp. 738-747, 1986.

[5] S. Morimoto and K. Hatanaka, "Design and control system of inverter-driven permanent magnet synchronous motors for high torque operation," *IEEE Trans. on Inds. Apps.*, vol. 29, no. 6, pp. 1150 - 1155, 1993.

[6] G. Feng, C. Lai and Y. Han, "Fast Maximum Torque Per Ampere (MTPA) Angle Detection for Interior PMSMs Using Online Polynomial Curve Fitting," *IEEE Trans on Power Electronics*, vol. 37, no. 2, pp. 2045 - 2056, 2022.

[7] C.-T. Pan and S.-M. Sue, "A Linear Maximum Torque Per Ampere Control for IPMSM Drives Over Full-Speed Range," *IEEE Trans. on Energy Conversion*, vol. 20, no. 2, pp. 359 - 366, 2005.

[8] C. Mademlis and N. Margaris, "Loss Minimization in Vector-Controlled Interior Permanent-Magnet Synchronous Motor Drives," *IEEE Trans. on Industrial Electronic*, vol. 49, no. 6, pp. 1344-1347, 2002.

[9] R. Ni, D. Xu, G. Wang, L. Ding, G. Zhang and L. Qu, "Maximum Efficiency Per Ampere Control of Permanent-Magnet Synchronous Machines," *IEEE Trans. on Industr. Apps.*, vol. 62, no. 4, pp. 2135 - 2143, 2015.

[10] Q. Li, T. Fan, X. Wen, Y. Li, Z. Wang and J. Guo, "Design optimization of interior permanent magnet sychronous machines for traction application over a given driving cycle," in *IECON 2017 - 43rd Annual Conference of the IEEE Industrial Electronics Society*, Beijing, China, 29 Oct.-1 Nov. 2017.

[11] P. H. Nguyen, E. Hoang and M. Gabsi, "Performance Synthesis of Permanent-Magnet Synchronous Machines During the Driving Cycle of a Hybrid Electric Vehicle," *IEEE Trans. on Vehicular technology*, vol. 60, no. 5, pp. 1991-1998, 2011.

[12] A. Acquaviva, E. G. Arfa, S. Lundmark and T. Thiringer, "Comparison of MTPA and Minimum Loss Control for Tooth Coil Winding PMSM Considering PM and Inverter Losses," in *2019 21st European Conference on Power Electronics and Applications (EPE '19 ECCE Europe)*, Genova,Italy, 3-5 Sept. 2019.

[13] M. Nabavi Razavi, H. Abniki and M. Karbalaye Zadeh , "An Optimal Control Strategy for the IPM Motor Drives," in *2009 IEEE Electrical Power & Energy Conference (EPEC)*, Montreal, 22-23 Oct. 2009.

[14] M. A. Khan, M. N. Uddin and M. A. Rahman, "A new loss minimization control of interior permanent magnet motor drives operating with a wavelet based speed controller," in *2011 IEEE Industry Applications Society Annual Meeting*, Orlando, FL, USA, 2011.

[15] S. Amornwongpeeti, O. Kiselychnyk, J. Wang, C. Antaloae, M. Soumelidis and N. Shah, "A Combined MTPA and Maximum Efficiency Control Strategy for IPMSM Motor Drive Systems," in *2016 International Conference on Electrical Systems for Aircraft, Railway, Ship Propulsion and Road Vehicles & International Transportation Electrification Conference (ESARS-ITEC)*, Toulus, 2-4 November 2016.

[16] R. Krishnan, Permanent Magnet Synchronous and Brushless DC Motor Drives, Boca Raton: CRC Press,Taylor and Francis Group, 2010.

[17] S. V. Zadeh, Control of Permanent Magnet Synchronous Motors, New York: Oxford University Press, 2018.

Nonlinear Optimal Control for Interior Permanent Magnet Synchronous Motor Drives

Merve Öztekin, Oleh Kiselychnyk, *Member, IEEE* and Jihong Wang, *Senior Member, IEEE*

***Abstract*— A concept of nonlinear optimal control is introduced for IPMSM drives. The control configuration remains the same as for the conventional control with three PI controllers for the *d* and *q* axes currents and velocity, but these controllers are replaced by corresponding nonlinear optimal controllers. The proposed controllers include linear (with Linear Quadratic Regulator - LQR) parts and nonlinear optimal parts emulating the automatic adjustment of the LQR gains based on operating conditions. The nonlinear parts are designed based on Krasovskiy's optimality criterion leading to an explicit solution of the control design problem. The proposed controller possesses some robustness properties which is explored in simulations. Compared to conventional system, it allows to reduce velocity overshoot and torque oscillations without extending the transient times. The control concept is validated using a test rig.**

***Index Terms*—Control Engineering, Nonlinear Control Systems, Permanent Magnet Motors, Machine Vector Control, PI Control, Feedback, Velocity Control, Control Nonlinearities, Stability, Optimal Control, Optimization methods, Cost Function, Robust Control**

I. INTRODUCTION

Interior Permanent Magnet Synchronous Motors (IPMSM) found wide industrial applications due to their inherent features such as high-power density, high efficiency, compactness, large torque-current ratio, etc. [18], [17]. Field Oriented Control (FOC) of these motors in the reference frame aligned with the rotor magnetic flux became a standard for the IPMSM drives manufactured and used in industry. It was originally developed for zero *d*-axis stator current control approach and with added *d* and *q* axes control decoupling which leads to the control system with three PI-controllers for velocity, *d* and *q* axes stator currents. Attenuation of the controllers' parameters is straightforward since the *d* and *q* axes subsystems are linear and independent and the motor parameters are assumed constant and known.

Further improvement of the FOC of the IPMSM is achieved via minimization of the total motor electrical losses [19] (Maximum Efficiency Control), via minimization of only motor copper losses [2] (Maximum Torque per Ampere Control) or via smart combining of both methods based on operating conditions [15]. In all three cases a static nonlinearity is introduced into the control system coupling the *d* and *q* axes subsystems again. Then the parameters of the PI-controllers are adjusted iteratively via simulations or experiments to provide necessary control quality in the entire velocity regulation range [20]. In case actual motor's parameters differ from the measured or estimated values the iterative simulations and experiments can be used as well. Certainly, the controllers' adjustments can be stored in look-up tables [3] and extracted accordingly. However, it is a solution for a specific motor and its implementation is very time consuming. Model Reference Adaptive velocity controller can be implemented [21] forcing the velocity to track a reference signal and thus in some way solving the problem of the introduced minimization nonlinearities and parameters inaccuracy. However, it makes the control slower.

In [22] a pseudo-linearization is applied to the IPMSM motor allowing to design a Linear Quadratic Regulator (LQR) of velocity, including integral component but without efficiency or torque per ampere ratio optimization. Although LQR controller possess some robustness properties, still for the wide range control the LQR gains should be updated. Besides they should be very accurately determined to decouple the mechanical and electrical subsystems of the motor. In [23] an optimal torque controller is designed via introducing a nonlinear disturbance observer. The additional torque loop copes with the parameters' nonlinearities (efficiency and torque/current ratio is not considered) but it makes control more complicated and estimated torque accuracy dependent.

This paper proposes a nonlinear optimal control of the IPMSM which replaces three ordinary PI controllers by corresponding nonlinear optimal controllers in the *d* and *q* axes current loops and in the velocity loop. Each nonlinear optimal controller is designed based on an LQR controller with integral component obtained for specific loop. The gains of the LQR controller are considered as new control actions and using Krasovskiy's criterion [24] explicit nonlinear formulae are derived allowing to update the gains based on the state coordinates. The linear (LQR) part of the controller is designed for a specific operating point and in fact it is a PI-controller with optimal parameters. The nonlinear part optimizes the system's dynamics when the operating point is different from the designed one. This approach allows easy to cope with introduced optimization nonlinearities and parameters' inaccuracies. The configuration of the system is the same as the standard system so the industrial drives might be updated with only insignificant software update.

This paper is organized as follows: Section II explains the Nonlinear Optimal (NO) control concept and the design procedure. Comparison of simulation results for the system with conventional PI and NO controllers is presented in Section III. The experimental validation of the suggested system is presented in Section IV. Finally, the conclusions are drawn.

*Research supported with YLSY foundation By Turkish Education Ministry.

Merve Öztekin, Oleh Kiselychnyk and Jihong Wang are with the Power and Control Systems Research Laboratory, University of Warwick, West Midlands, CV4 7AL UK, (e-mail: Merve.Oztekin@warwick.ac.uk, O.Kiselychnyk@warwick.ac.uk, Jihong.Wang@warwick.ac.uk).

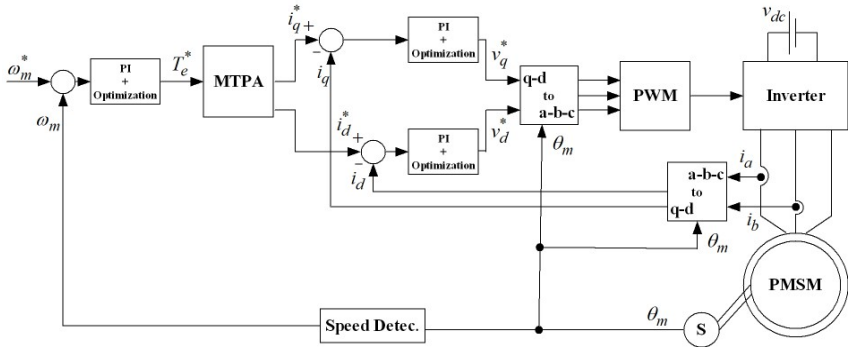

Figure 6.9. The Nonlinear Optimal Control Structure of IPMSM with MTPA algorithm

II. NONLINEAR OPTIMAL CONTROL CONCEPT

Figure 6.9 depicts the control structure of IPMSM with MTPA regulation based on the suggested NO control concept. The structure is the same as in conventional control systems of IPMSM, for example in [2]. However, three PI controllers are replaced by corresponding three NO controllers which are designed based on the same optimization procedure. In Figure 1, ω_m denotes the mechanical velocity, θ_m is the mechanical angle of the shaft measured by sensor S, T_e is the electromagnetic torque, i_d and i_q are the *d* and *q* axes stator currents, i_a and i_b are the stator currents in phases *a* and *b*, v_d and v_q are the *d* and *q* axes stator voltages, V_{dc} is the DC link voltage, the subscript '*' denotes the corresponding reference values.

The block diagrams of three NO controllers are identical (the parameters are different) and they include a linear (LQR) part and a nonlinear part (Figure 2), where X_2 denotes the input signal of the controller and X_1 is its time integral. During simulations and experiment the output of the controller is saturated at certain level and the output of the integrator is saturated at this level divided by K_1. Since X_2 is dynamical error then the linear part implements an optimal PI controller.

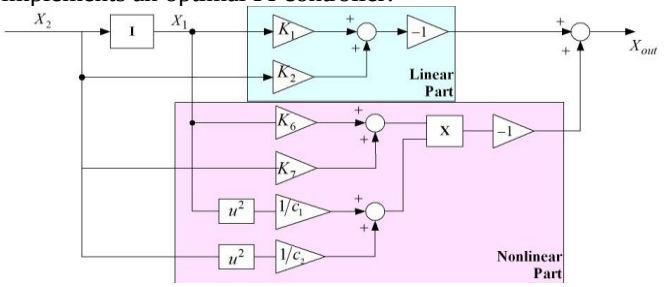

Figure 6.10. Block diagram of the NO Controller

A. LQR based Linear Part Design

The LQR design for *d* and *q* axes current loops is done independently. The LQR design for the velocity loop is done assuming no dynamics in the current loops, $T_e = T_e^*$. In all three cases the corresponding controlled subsystem model is represented in the view below

$$\dot{\mathbf{X}} = \mathbf{A}\mathbf{X} + \mathbf{B}u + \mathbf{F} \qquad (1)$$

where, **X** is the vector of subsystem's state variables, u is the corresponding control input and **F** denotes the vector of disturbances.

Each subsystem (1) is of second order. It contains a linearized differential equation describing the dynamics of the deviations of i_d or i_q or ω_m with respect to an arbitrary steady state and the dynamics of their integrals, necessary while designing LQR with an integral action.

The linearized equations are derived from IPMSM dynamic model in the reference frame aligned with the rotor permanent magnet flux linkage vector as

$$\begin{cases} T_d\left(di_d/dt\right)+i_d=\left(v_d+n_p\omega_m L_q i_q\right)/R_s \\ T_q\left(di_q/dt\right)+i_q=\left(v_q-n_p\omega_m L_d i_d-n_p\omega_m\lambda_{af}\right)/R_s \\ T_m\left(d\omega_m/dt\right)+\omega_m=\left(T_e-T_f-T_l\right)/B \end{cases} \qquad (2)$$

where, $T_{d,q}=L_{d,q}/R_s$, $T_m=J/B$ are time constant, R_s is the stator resistance, L_d, L_q are *d* and *q* axes inductances, respectively, J is the motor inertia, B is the viscous friction torque gain, n_p denotes the number of pole pairs, λ_{af} is the permanent magnet flux linkage, T_f is the static friction torque, T_l is the load torque.

In actual IPMSMs, L_d, L_q are current-dependent, due to the magnetic saturation. Since the modelling is done for the deviations from the steady state values, these parameters are assumed constant during the controllers' design, but they are different for different operating points. Similarly, the inertia J is taken constant during the design but it can be different for different operating points. Therefore, all three time constants in (2) are changing with the change of the operating point. Voltages $n_p\omega_m L_q i_q$ and $n_p\omega_m\lambda_{af}+n_p\omega_m L_d i_d$ are regarded as disturbances.

The time integrals of the dynamical errors are defined as

$$\begin{cases} i_{ind,q}=\int\left(i_{d,q}-i_{d,q}^*\right)dt \\ \omega_{in}=\int\left(\omega_m-\omega_m^*\right)dt \end{cases} \qquad (3)$$

Consider the state coordinates as a sum of steady state values and corresponding small deviations: $i_{d,q} = i_{d,q01} + \delta i_{d,q}$, $\omega_m = \omega_{m01} + \delta\omega_m$, $i_{ind,q} = i_{ind,q01} + \delta i_{ind,q}$, $\omega_{in} = \omega_{in01} + \delta\omega_{in}$ where the index '01' denotes corresponding steady state values and δ denotes deviations. Similarly, for control actions, disturbances and parameters: $v_{d,q} = v_{d,q01} + \delta v_{d,q}$, $L_{d,q} = L_{d,q01} + \delta L_{d,q}$, $T_e = T_{e01} + \delta T_e$, $T_f = T_{f01} + \delta T_f$, $T_l = T_{l01} + \delta T_l$. Substituting the definitions above into (2) and (3) with following subtracting the corresponding steady state equations and neglecting the second order small values gives three second order linearized models (1) which controllers are designed independently. Please note that for the current subsystems $\delta\omega_m = 0$ and for the velocity subsystem $T_e = T_e^*$. In all three cases, the deviations of the time constants due to the parameters' changes are neglected in the final linearized equations due to their multiplication by small variables' deviation.

The details of model (1) for the three cases are given below

$$\mathbf{X} = \begin{bmatrix} x_1 & x_2 \end{bmatrix}^T = \begin{cases} \begin{bmatrix} \delta i_{ind} & \delta i_d \end{bmatrix}^T \\ \begin{bmatrix} \delta i_{inq} & \delta i_q \end{bmatrix}^T \\ \begin{bmatrix} \delta\omega_{in} & \delta\omega_m \end{bmatrix}^T \end{cases}, u = \begin{cases} \delta v_d \\ \delta v_q \\ \delta T_e^* \end{cases} \quad (4)$$

$$\mathbf{A} = \begin{bmatrix} 0 & 1 \\ 0 & a_1 \end{bmatrix}, \mathbf{B} = \begin{bmatrix} 0 & b_1 \end{bmatrix}^T \rightarrow a_1 = \begin{cases} -1/T_{d01} \\ -1/T_{q01} \\ -1/T_{m01} \end{cases}, b_1 = \begin{cases} 1/(T_{d01}R_s) \\ 1/(T_{q01}R_s) \\ 1/(T_{m01}B) \end{cases} \quad (5)$$

$$\mathbf{F} = \begin{cases} \begin{bmatrix} -\delta i_d^* & n_p\omega_{m01}\left(L_{q01}\delta i_q + i_{q01}\delta L_q\right)/\left(T_{d01}R_s\right) \end{bmatrix}^T \\ \begin{bmatrix} -\delta i_q^* & -n_p\omega_{m01}\left(L_{d01}\delta i_d + i_{d01}\delta L_d\right)/\left(T_{q01}R_s\right) \end{bmatrix}^T \\ \begin{bmatrix} -\delta\omega_m^* & \left(-\delta T_f - \delta T_m\right)/\left(T_{m01}B\right) \end{bmatrix}^T \end{cases} \quad (6)$$

Please note that in steady states $i_{d,q01} = i_{d,q}^*$ then $x_2 = \delta i_{d,q} = i_{d,q} - i_{d,q}^*$ and $x_1 = \int\left(i_{d,q} - i_{d,q}^*\right)dt$, respectively. For the velocity control, $\omega_{m01} = \omega_m^*$ then $x_2 = \delta\omega_m = \omega_m - \omega_m^*$ and $x_1 = \int\left(\omega_m - \omega_m^*\right)dt$.

The cost function for system (1) leading to the LQR controller is selected in the following view

$$\min_u J = \int_0^\infty \left(\alpha_1 x_1^2 + \alpha_2 x_2^2 + cu^2\right)dt \quad (7)$$

where α_1, α_2 and c are positive weighting constants.

Following the standard procedure based on functional Bellman equation, Hamilton-Jacobi-Bellman equation in closed form, assuming a quadratic form of the Lyapunov function and solving the algebraic Riccati equation gives the following equation of the each LQR controller as

$$u = -\left(b_1/c\right)k_{12}x_1 - \left(b_1/c\right)k_{22}x_2 = -k_1x_1 - k_2x_2 \quad (8)$$

where, $k_{22} = \left(a_1 + \sqrt{a_1^2 + b_1^2\left(2\sqrt{\alpha_1 c}/b_1 + \alpha_2\right)/c}\right)/\left(b_1^2/c\right)$ and $k_{12} = \sqrt{\alpha_1 c}/b_1$

The values of the gains can also be obtained numerically using 'lqr' command in Matlab.

B. Nonlinear Optimal Control Part Design

The controller above is the LQR controller designed for the system linearized within a specific operating point. Once the operating point changes it is necessary to update the gains of the controller k_1 and k_2. To avoid using a look-up table, an alternative approach is proposed below based on measured coordinates.

Assume that the gain coefficients k_1, k_2 in (8) are obtained for possible maximum values of time constants, $|a_1| = |a_{1\min}|, |b_1| = |b_{1\min}|$ in (5). For possible minimum values of time constants, a_1 is replaced by a_2, $|a_2| = |a_{2\max}|$, and b_1 is replaced by b_2, $|b_2| = |b_{2\max}|$. Then

$$\mathbf{A} = \begin{bmatrix} 0 & 1 \\ 0 & a_2 \end{bmatrix}, \mathbf{B} = \begin{bmatrix} 0 & b_2 \end{bmatrix}^T \rightarrow a_2 = \begin{cases} -1/T_{d02} \\ -1/T_{q02} \\ -1/T_{m02} \end{cases}, b_2 = \begin{cases} 1/(T_{d02}R_s) \\ 1/(T_{q02}R_s) \\ 1/(T_{m02}B) \end{cases} \quad (9)$$

For the operating point '02' the LQR controller is similar as in (8) but with different parameters denoted by the prime sign

$$u' = -\left(b_2/c\right)k'_{12}x_1 - \left(b_2/c\right)k'_{22}x_2 = -k'_1x_1 - k'_2x_2 \quad (10)$$

For $T_{d,q,m0\min} \le T_{d,q,m0} \le T_{d,q,m0\max}$, the gains of the controller should be adjusted between k_i and k_i'. Then for an arbitrary time constant within the allowed range the controller is represented as

$$u' = -\left(k'_1x_1 + k'_2x_2\right) = -\left(\left(k_1 + \delta k_1\right)x_1 + \left(k_2 + \delta k_2\right)x_2\right) \quad (11)$$

where δk_1, δk_2 are new control inputs and equations for their update are to be derived based on optimal control theory.

Substitute (11) into (1). Then the description of the control system for an arbitrary steady state not accounting for disturbances is as follows

$$\begin{aligned} \dot{x}_1 &= x_2 \\ \dot{x}_2 &= a_2x_2 + b_2u = a_2x_2 - b_2\left(k_1x_1 + k_2x_2 + \delta k_1x_1 + \delta k_2x_2\right) \end{aligned} \quad (12)$$

The criterion of the generalized work of A.A. Krasovskiy used for the cost minimization as

$$\min_{\delta k_1, \delta k_2} J = \int_0^\infty \begin{pmatrix} \alpha_1x_1^2 + \alpha_2x_2^2 + c_1\delta k_1^2 + c_2\delta k_2^2 \\ +\left(b_2^2/4c_1\right)\left(x_1\left(\partial V/\partial x_2\right)\right)^2 + \left(b_2^2/4c_2\right)\left(x_2\left(\partial V/\partial x_2\right)\right)^2 \end{pmatrix} dt \quad (13)$$

where, first four terms are similar as for the LQR design, the last two terms are added to obtain an explicit control solution and c_1, c_2 are positive weighting constants.

The same procedure as for the LQR design with Lyapunov function as a quadratic form gives the nonlinear optimal controls as

$$\begin{aligned} \delta k_1 &= \left(b_2/c_1\right)x_1\left(k_4x_1 + k_5x_2\right) \\ \delta k_2 &= \left(b_2/c_2\right)x_2\left(k_4x_1 + k_5x_2\right) \end{aligned} \quad (14)$$

where $k_4 = \left(\alpha_1/2b_2k_1\right)$, $k_5 = \left(\alpha_2 + 2k_4\right)/\left(2\left(b_2k_2 - a_2\right)\right)$.

Finally, based on (11) and (14) the NO controller can be represented in the following view (as shown in Figure 2)

$$\begin{aligned} u' &= -\left(k_1x_1 + k_2x_2 + \left(k_6x_1 + k_7x_2\right)\left(\left(x_1^2/c_1\right) + \left(x_2^2/c_1\right)\right)\right) \\ &\rightarrow k_6 = k_4b_2, k_7 = k_5b_2 \end{aligned} \quad (15)$$

The designed controller includes the linear (LQR) part which is a PI-controller with optimal parameters and the nonlinear optimal part which emulates the adjustments of k_1 and k_2 based on the operating conditions.

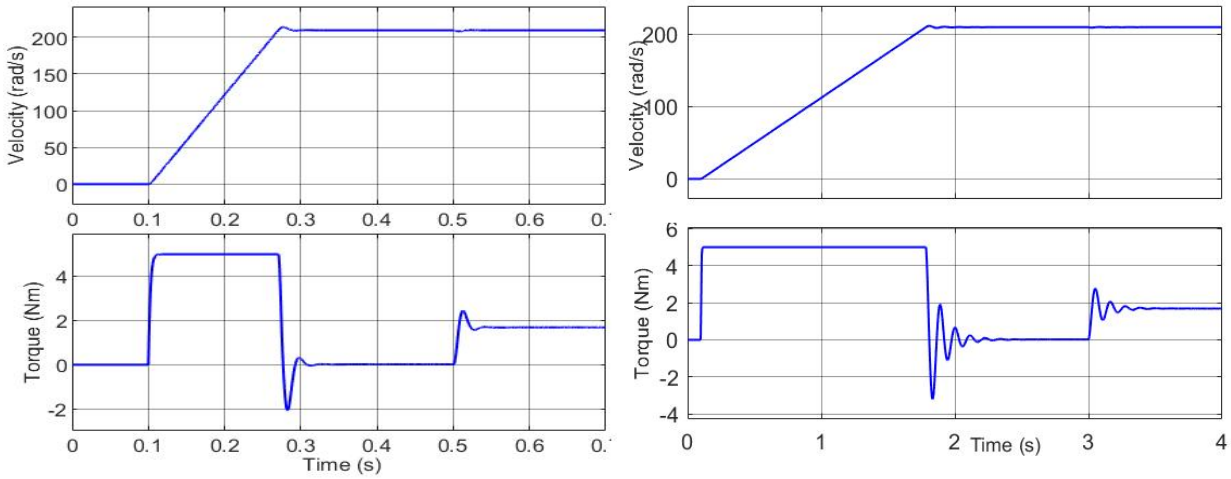

Figure 6.11. Torque and velocity response of FOC with MTPA with PI Controllers a) for Moment of Inertia J=0.004 kg.m² b) for Moment of Inertia J=0.04 kg.m²

III. SIMULATION RESULTS

In this section, the simulation results for FOC with MTPA Approach for IPMSMs are investigated with both conventional PI (in Figure 6.11) and NO controllers (in Figure 6.12) The parameters and specifications of simulated IPMSM [3] are shown in Table 6.5. The controllers are tuned with the gain parameters shown in Table 6.6.

In simulations, the reference velocity is linearly increased to the rated value (2000 rpm) starting at 0.1 s and without load. After the system reaches the reference velocity, the load torque is applied as the rated torque value $T_{lrated} = 1,67$ Nm.

The simulations are performed with the moment of inertia J=(0.004, 0.04) kgm² values for both PI and NO controllers. As expected, the conventional method is more sensitive to the variations of moment of inertia than the proposed method. Please note that the initial start happens when both NO and PI velocity controllers are saturated, so the difference will be not seen. The above conclusions are made based on the start region where there is no saturation (when the velocity is close to the reference value and there is overshoot) and the region corresponding to the step load applying. The oscillations seen in Figure 6.11b are because of the increased inertia.

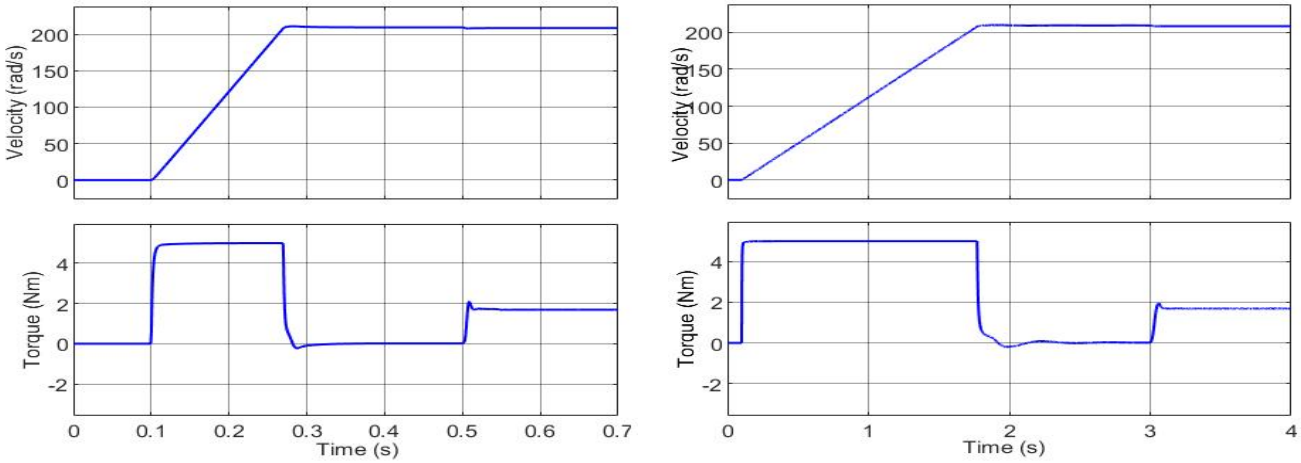

Figure 6.12. Torque and velocity response of FOC under MTPA with NO Controllers a) for Moment of Inertia J=0.004 kg.m² b) for Moment of Inertia J=0.04 kg.m²

IV. EXPERIMENTAL RESULTS

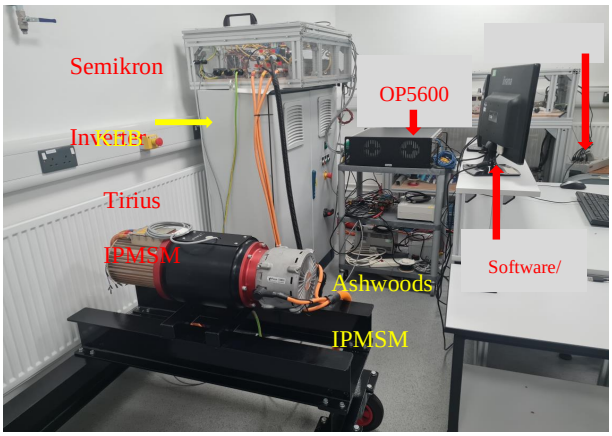

Figure 6.14. Experimental Rig

The experimental verification is carried out on a laboratory-installed test rig shown in Figure 6.14, which is designed for testing IPMSM drives for novel optimal control approaches. The test rig consists of an under-test motor (Tirius IPMSM, three-phase, 4 pole, 12kW, 28 Nm, 3700 rpm, 560 Vdc), an under-test drive (Semikron 3 power modules based three-phase IGBT inverter with 600 VDC), Real Time Simulators (dSPACE DS1104 and OPAL-RT OP5600 HIL), a load motor (Ashwoods IPMSM, three-phase, 4 pole, 10kW,43Nm, 3250 rpm 560 Vdc), a load motor drive (KEB COMBIVERT F5 AC motor controller and drive unit, 30kW, 305-500V,2-16kHz), resolver and Power Supply Units.

In Figure 6.13, the experimental results of the proposed NO Control Method are shown. In Figure 6.13a, no load start-up performance to 2000 rpm followed by gradually step increasing torque demand is demonstrated. The oscillations happening in speed curve for each torque shift are reasonable. Figure 6.13b shows *d*, *q*-axes current variations for the same pattern as in Figure 6.13a. Due to MTPA control characteristic, *d*-axis current increases in negative direction as torque demand increases. Thus, the reluctance torque contributes more to torque response. Therefore, the proposed NO control approach can be implemented with MTPA control.

In Figure 6.15 torque and speed oscillations seen during torque shifts between 4 to 8 Nm. Table 6.4 shows specified gain coefficients of the controllers for the under-test motor.

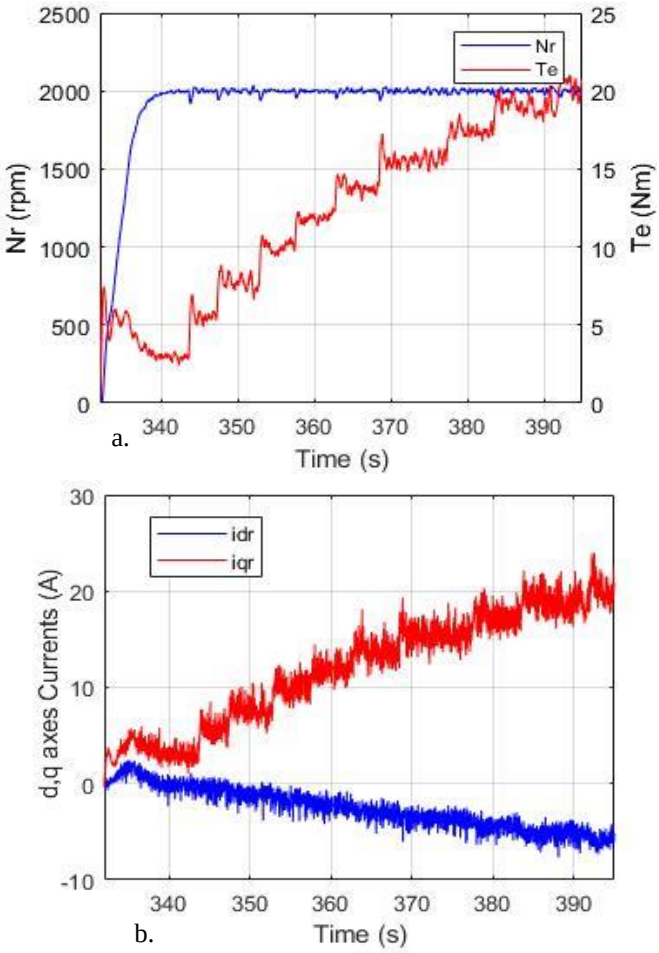

Figure 6.13. Experimental Data a.) Torque and Speed Response

b.) *d*, *q* axes currents

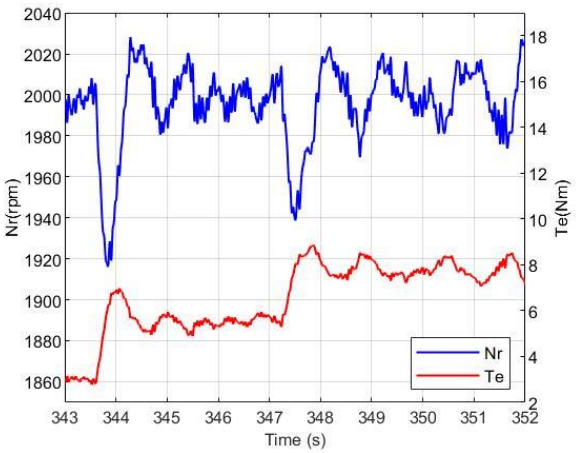

Figure 6.15. Experimental Data Zoom-in View of Figure 6.13a

Te=4-8 Nm Nr=2000 rpm

CONCLUSION

This paper presents a nonlinear optimal control method for IPMSM drives. The IPMSM control configuration remains the same as for conventional drives with three PI controllers for *d* and *q* axes currents and velocity, but the controllers are replaced by the corresponding nonlinear optimal controllers. The proposed controllers include the linear part designed as conventional LQR controllers (PI controllers with optimal parameters) and a nonlinear optimal part. The linear part is designed for a specific operating point whereas the nonlinear part is designed using the Krasovskiy's optimality criterion and emulates the automatic adjustments of the LQR gains according to different operating conditions. The description of the controllers is obtained in the explicit view providing easy upgrade of the conventional drives and their tuning. The proposed control possess some robustness properties with respect to parameters variations which was shown in simulation. The experimental validation of the concept is presented as well.

V. APPENDIX

Table 6.4 Gain Coefficients of Controllers for Test-rig

		i_d Controller	i_q Controller	ω_m Controller
NO	K1	8	8	1,2
	K2	6	6	0,2
	K6	0,4	0,8	0,12
	K7	0,3	0,6	0,02
	C1	15,6	15,6	694,45
	C2	27	27	25000
	Sat	35	175	29,167

Table 6.5 The Parameters of Interior Permanent Magnet Synchronous Motor Used in Simulations

Rated Torque T_{rt} (Nm)	1.67
Rated Current I_{rt} (A)	5
Rated Speed W_{rt} (rpm)	2000
Rated Voltage V_{rt} (V)	97
DC link Voltage V_{dc} (V)	150
R_s (Ω)	0.57
L_q (mH)	22.78
L_d (mH)	8.72
λ_{af} (Wb)	0.1077
n_p	2

Table 6.6 Gain Coefficients of Controllers for Simulation

		i_d Controller	i_q Controller	ω_m Controller
PI	ki	125	285	285
	kp	1	4.36	4.36
NO	K1	300	300	7,9737
	K2	9,7041	10,1067	0,3478
	K6	0,0067	0.0067	0.1588
	K7	2,19e-04	2,15e-4	0,0042
	C1	0.001	0.001	0.01
	C2	0.001	0.001	0.01
	Sat	10	10	0.05

VI. REFERENCES

[1] R. Krishnan, Permanent Magnet Synchronous and Brushless DC MOtor Drives, Boca Raton: CRC Press, 2010.

[2] S. V. Zadeh, Control of Permanent Magnet Synchronous Motors, New York: Oxford University Press, 2018.

[3] C. Mademlis, I. Kioskeridis and N. Margari, "Optimal efficiency Control Strategy for Interior Permanent Magnet Synchronous Motor Drives," *IEEE Trans on Energy Conversion*, vol. 19, no. 4, pp. 715-723, 2004 .

[4] S. Morimoto, M. Sanada and Y. Takeda, "Wide-speed operation of interior permanent magnet synchronous motors with high-performance current regulator," *IEEE Trans. on Ind. App.*, vol. 30, no. 4, pp. 920 - 926, Jul/Aug 1994.

[5] S. Amornwongpeeti, O. Kiselychnyk, J. Wang, C. Antaloae, M. Soumelidis and N. Shah, "A Combined MTPA and Maximum Efficiency Control Strategy for IPMSM Motor Drive Systems," in *2016 International Conference on Electrical Systems for Aircraft, Railway, Ship Propulsion and Road Vehicles & International Transportation Electrification Conference (ESARS-ITEC)*, Toulus, 2-4 November 2016.

[6] N. Urasaki and T. Senjyu, "A Novel Calculation Method for Iron Loss Resistance Suitable in Modeling Permanent-Magnet Synchronous Motors," *IEEE Trans. On Energy Conversion*, vol. 18, no. 1, pp. 41-47, 2003.

[7] S. Morimoto, Y. Tong, Y. Takeda and T. Hirasa, "Loss minimization control of permanent magnet synchronous motor drives," *Industrial Electronics, IEEE Transactions*, vol. 41, no. 5, pp. 511-517, 1994.

[8] O. C. Kivac and S. B. Ozturk , "Sensorless PMSM Drive Based on Stator Feedforward Voltage Estimation Improved with MRAS Multiparameter Estimation," *IEEE/ASME Trans. on Mechatronics*, vol. 23, no. 3, pp. 1326-1337, 2018.

[9] K.-T. Chang, T.-S. Low and T.-H. Lee, "An Optimal Speed Controller for Permanent-Magnet Synchronous Motor Drives," *IEEE Trans. On Industrial Electronics*, vol. 41, no. 5, pp. 503-510, 1994.

[10] T. Shi and Z. Zhou, "Linear Quadratic Regulator Control for PMSM Drive Systems Using Nonlinear Disturbance Observer," *IEEE Trans. on Power Electronics*, vol. 35, no. 5, pp. 5093-5101, 2020.

[11] V. F. Kudin, O. I. Kiselycnyk and J. Kolancny, "Suboptimal Astatic two-band System for Automatic Speed Control of a DC motor with independent excitation," *Russian Electrical Engineering C/C of Elektrotekhnika*, vol. 77, no. 11, pp. 1-7, 2006.